The associations between pathological pathways in the progression of Alzheimer's disease

Tharick Ali Pascoal

Integrated Program in Neuroscience

McGill University, Montreal

December 2018

A thesis proposal submitted to McGill University in partial fulfillment of the requirements of the degree of **Doctor of Philosophy**

Table of Contents

Abstract

Alzheimer's disease (AD) is pathologically characterized by the progressive brain accumulation of amyloid-β and tau proteins and neuronal degeneration. Yet, the complex interplay between these pathological processes and dementia is poorly understood. In fact, the development of *in vivo* biomarkers has significantly advanced our understanding of AD progression. The most accepted biomarker model of disease progression supports brain amyloid-β as the key trigger of sequential downstream events leading to tau hyperphosphorylation and neuronal degeneration, which in turn leads to dementia. However, the presence of amyloid-β deposition in the brain of numerous cognitively stable individuals and the lack of strong association between amyloid-β and neurodegeneration or cognitive decline in AD patients have been used to question the key role of amyloid-β in the pathogenesis of AD. Since all of the above pathologies are highly linked to AD but are not independently sufficient to determine dementia, it is reasonable to assume that synergistic interactions between these pathological pathways determine the vulnerability to dementia. Recently, it has been proposed that the progressive accumulation of multiple brain pathologies imposes neuroepigenetic modifications through class I histone deacetylases (HDACs I) abnormalities determining brain tissue vulnerability. Thus, it is possible that the biological mechanism by which brain pathologies interact to drive AD relies on dysregulations of the brain's epigenetic landscape. This thesis, composed of two main parts, describes six studies using positron emission tomography and cerebrospinal fluid biomarkers. In part one, we tested the hypothesis that, phenomenologically, synergistic interactions between pathologies better explain AD progression than the traditional sequential disease model. Part two tested the hypothesis that, mechanistically, epigenetic abnormalities imposed on brain tissues by the coexistence of pathologies are the biological links between pathological interactions and the progression of the

disease. Firstly, we showed that the synergistic interactions between, rather than independent or sequential effects of, amyloid-β, tau, and neurodegeneration determine AD progression. Also, we identified the existence of biomarker thresholds associated with the triggering of these interactions and their usefulness in selecting individuals that are more likely to progress, for the enrichment of clinical trial populations. Secondly, we showed that epigenetic dysregulations link brain pathologies and AD symptoms. Specifically, we found that HDACs I reduction underscores the biological mechanism by which amyloid-β and tau interact to drive neurodegeneration and cognitive symptoms in AD. Together, these findings have broadened our understanding of the associations between pathological pathways in AD and how these pathways interact to determine dementia.

Résumé

La maladie d'Alzheimer (MA) est pathologiquement caractérisée par l'accumulation progressive de β-amyloïde et de protéines tau ainsi que par la dégénérescence neuronale. Cependant, le lien complexe entre ces processus pathologiques et la démence est peu compris. En fait, le développement de marqueurs biologiques *in vivo* a considérablement aidé à la compréhension de la progression de la MA. Le modèle de marqueur biologique de la progression de la maladie le plus accepté soutient que β-amyloïde est l'élément déclencheur d'une suite d'évènements menant à l'hyperphosphorylation de tau et à la dégénérescence neuronale, provoquant ensuite la démence. Néanmoins, la présence de dépôt de β-amyloïde dans le cerveau de nombreux individus cognitivement stables et le manque d'élaboration d'un lien réel entre β-amyloïde et la dégénérescence neuronale, ou le déclin cognitif chez les patients atteints de la MA, a été souligné afin de remettre en cause le rôle-clé de β-amyloïde dans la pathogenèse de la MA. Étant donné

que toutes les pathologies précédemment mentionnées sont fortement liées à la MA mais ne suffisent pas à causer une démence, il est raisonnable de supposer que les interactions synergiques entre ces voies pathologiques provoquent une vulnérabilité face à la démence. Récemment, il a été supposé que l'accumulation progressive de multiples pathologies cérébrales provoque des modifications neuroépigénétiques à travers des anormalités de l'histone désacétylase de catégorie I (HDAC I) qui déterminent la vulnérabilité du tissu cérébral. Par conséquent, il est possible que le mécanisme biologique par lequel les pathologies cérébrales interagissent avant de mener à la MA repose sur des dérèglements de l'épigénétique cérébral. Cette thèse, composée de deux grandes parties, décrit six études qui utilisent la tomographie à émission de positons et les biomarqueurs du liquide encéphalo-rachidien. Dans la première partie, nous avons testé l'hypothèse que, phénoménologiquement, les interactions synergiques expliquent mieux la progression de la MA que le modèle séquentiel traditionnel de la maladie. La seconde partie teste l'hypothèse que, mécaniquement, les anormalités épigénétiques imposées au tissu cérébral par la coexistence de pathologies sont le lien biologique entre les interactions pathologiques et la progression de la maladie. Premièrement, nous avons montré que, plutôt que des effets indépendants ou séquentiels, l'interaction synergique entre β-amyloïde, tau et la dégénérescence neuronale déterminent la progression de la MA. De plus, nous avons identifié l'existence de seuils de biomarqueurs associés au déclenchement de ces interactions ainsi que leur utilité dans la sélection d'individus, plus susceptibles de progresser, aidant ainsi à l'enrichissement des populations des essais cliniques. Deuxièmement, nous avons montré que les dérèglements epigénétiques associent les pathologies cérébrales et les symptômes de la MA. Plus précisément, nous avons trouvé que la réduction d'HDACs I souligne le mécanisme biologique par lequel β-amyloïde et tau interagissent afin de conduire à la dégénérescence neuronale et aux

symptômes cognitifs dans la MA. Ensemble, ces découvertes ont élargi notre compréhension des associations entre les voies pathologiques dans la MA, et comment ces mêmes voies pathologiques interagissent pour causer la démence.

Acknowledgements

I would like to express my sincere gratitude to my supervisor **Dr**. **Pedro Rosa-Neto**, who introduced me to research, for many insightful discussions, for passing on knowledge, and for giving me freedom in my work but challenging my way of thinking. Thank you for sharing with me your passion for science and for having played such a central role in my career.

Also, I was also fortunate enough to have the guidance of **Dr. Serge Gauthier**, who contributed to my career as a clinician and scientist with his deep knowledge in these two fields. I would also like to thank **Dr. Gassan Massarweh** and **Dr. Jean-Paul Soucy** for the opportunity to work together and supporting our research.

This research would not have been possible without the assistance of all members of the MCSA and TNL lab, which built the foundations for the data analysis, patients' recruitment, data collection, etc.: **Sulantha Mathotaarachchi, Monica Shin, Andréa Lessa Benedet, Min Su Peter Kang, Joseph Therriault, Seqian Wang, Mira Chamoun, Arturo Aliaga, Silvana Aguzzi**, **Tamar Tatigian, and Guylaine Gagne.** In special to **Sara Mohaddes**, a very special "thanks" for being supportive since the early days in the lab. It has been a pleasure and an honor to work with all of you. I would like to extend my gratitude to PREVENT-AD, Alzheimer Society of Canada, and Canadian Consortium on Neurodegeneration in Aging for the scholarship

support. Also, the work carried out in this thesis would not have been possible without the support of the Canadian Institutes of Health Research, Alzheimer's Association, Fonds de Recherche du Québec – Santé, Weston Brain Institute, Alzheimer's Disease Neuroimaging Initiative, Cerveau Technologies, and the several collaborators described in each chapter.

Finally, I would like to dedicate my biggest "thanks" to my family because I could not have done this without you. To my mom **Fátima Duarte Ali** and my father **Leonir Luiz Pascoal**, I do not have enough words to thank you for all the things you have done for me. No matter where we are, "home" is always being with you.

Preface

This thesis contains eight chapters. Chapter 1 is a review of the current background literature relevant to subsequent chapters. Chapters 2 to 5 describe the associations between amyloid-β, tau, and neurodegeneration as determinants of clinicopathological progression in AD. Chapter 6 characterize a new PET tracer, while Chapter 7 describes the interplay between the aforementioned pathologies and epigenetics. Chapters 2, 3, and 4 were published in Molecular Psychiatry, The European Journal of Nuclear Medicine and Molecular Imaging, and Alzheimer's and Dementia, respectively. The papers associated with Chapters 5 and 7 are under review, and the paper in Chapter 6 was published in Alzheimer's Research & Therapy. Chapter 8 is a summary, discussion, future and concluding remarks of findings described from Chapters 2 to 7. Also, we provide links between papers at the beginning of chapters.

This thesis is based on the following original papers:

Chapter 2. Pascoal TA, Mathotaarachchi S, Mohades S, Benedet AL, Chung CO, Shin M, Wang S, Beaudry T, Kang MS, Soucy JP, Labbe A, Gauthier S, Rosa-Neto P. Amyloid-β and hyperphosphorylated tau synergy drives metabolic decline in preclinical Alzheimer's disease. Mol Psychiatry. 2017 Feb;22(2):306-311. PubMed PMID: 27021814; PubMed Central PMCID: PMC5262471.

Chapter 3. Pascoal TA, Mathotaarachchi S, Shin M, Park AY, Mohades S, Benedet AL, Kang MS, Massarweh G, Soucy JP, Gauthier S, Rosa-Neto P. Amyloid and tau signatures of brain metabolic decline in preclinical Alzheimer's disease. Eur J Nucl Med Mol Imaging. 2018 Jun;45(6):1021-1030. PubMed PMID: 29396637; PubMed Central PMCID: PMC5915512.

Chapter 4. Pascoal TA, Mathotaarachchi S, Shin M, Benedet AL, Mohades S, Wang S, Beaudry T, Kang MS, Soucy JP, Labbe A, Gauthier S, Rosa-Neto P. Synergistic interaction between amyloid and tau predicts the progression to dementia. Alzheimers Dement. 2017 Jun;13(6):644-653. PubMed PMID: 28024995.

Chapter 5. Pascoal TA, Mathotaarachchi S, Kang MS, Mohaddes S, Shin M, Park AY, Parent M, Benedet A, Chamoun M, Therriault J, Hwang H, Cuello AC, Misic B, Soucy JP, Aston JAD, Gauthier S, and Rosa-Neto P. Aβ-induced vulnerability propagates via the brain's default mode network (Under review).

Chapter 6. Pascoal TA, Shin M, Kang MS, Chamoun M, Chartrand D, Mathotaarachchi S, Bennacef I, Therriault J, Ng KP, Hopewell R, Bouhachi R, Hsiao HH, Benedet AL, Soucy JP, Massarweh G, Gauthier S, Rosa-Neto P. In vivo quantification of neurofibrillary tangles with [^{18}F]MK-6240. Alzheimers Res Ther. 2018 Jul 31;10(1):74. PubMed PMID: 30064520; PubMed Central PMCID: PMC6069775.

Chapter 7. Pascoal TA, Chamoun M, Lax E, Wey HY, Shin M, Ng KP, Kang MS, Mathotaarachchi S, Benedet AL, Therriault J, Schroeder FA, DuBois JM, Hightower BG, Gilbert TM, Zürcher NR, Wang C, Hopewell R, Chakravarty M, Savard M, Thomas E, Mohaddes S, Farzin S, Salaciak A, Tullo S, Cuello AC, Soucy JP, Massarweh G, Hwang H, Kobayashi E, Hyman BT, Dickerson BC, Szyf M, Gauthier S, Hooker JM, and Rosa-Neto P. Class I HDAC reduction links amyloid and tau with dementia in living patients with Alzheimer's disease (Under Review).

Contribution of authors

Chapter 2. T.A.P. and P.R-N. conceived the study as well as analyzed and interpreted the data. T.A.P., S.M., S.M., A.L.B., C.C.O., M.S., S.W., T.B., and M.S.K. processed the imaging data. A.L. assisted with the data statistical analysis. T.A.P. and P.R.-N. prepared the figures, the table, and drafted the manuscript with input from J.P.S. and S.G. All authors approved the final version of the manuscript.

Chapter 3. T.A.P., S.G., and P.R-N. performed the conception of the study. T.A.P., S.M., M.S., A.L.B., S.M., and M.S.K. performed the processing and the quality control of the image data.

T.A.P., S.M., and P.R-N. analyzed and interpreted the data. A.Y.P. assisted in the statistical analysis. T.A.P., M.S., J.P.S., S.G., and P.R-N. prepared figures, table, and drafted the manuscript.

Chapter 4. T.A.P. and P.R-N. performed the conception of the study, analysis, and interpretation of the data. T.A.P., S.M., A.L.B., S.M., S.W., T.B., and M.S.K. processed the imaging data. A.L. assisted with the data statistical analysis. T.A.P. and P.R.-N. prepared the figures, the tables, and drafted the manuscript with input from J.P.S. and S.G. All authors revised the final version of the manuscript.

Chapter 5. T.A.P., S.G., and P.R-N. performed the conception of the study and interpreted the data. T.A.P., S.M., A.L.B., S.M., M.S.K., M.C., and J.T. performed the processing, analysis, and quality control of the image data. M.S.K., M.J.P., and M.S. performed the acquisition of the animal data. A.C.C. developed the transgenic rat model. B.M. assisted in the metabolic network analysis. A.Y.P., J.A.D.A., and H.H. assisted in the statistical analysis. T.A.P., J.P.S., A.C.C., S.G., and P.R-N. prepared the figures, the table, and drafted the manuscript. All author revised the final manuscript draft.

Chapter 6. T.A.P., I.B, S.G., and P.R-N. performed the conception of the study. R.B. and G.M. performed radiochemistry production and revised the manuscript. M.S., M.S.K., M.C., D.C., J.T., K.P.N., R.B., H.H., and A.L.B. participated in the acquisition process of the PET data and revised the manuscript. T.A.P. and S.M. performed the processing and the quality control of the

image data. T.A.P., S.G., and P.R-N. performed the statistical analysis and interpreted the data. T.A.P., J.P.S., S.G., and P.R-N. prepared the figures, the table, and drafted the manuscript.

Chapter 7. T.A.P., F.A.S., S.G., J.M.H., and P.R-N. conceived the study. T.A.P. and P.R.-N. prepared the figures, the table and drafted the manuscript with input from H-Y.W., S.G., and J.M.H. T.A.P., M.C., H-Y.W, M.S., K.P.N., M.S.K., S.M., A.L.B, J.T., F.A.S., J.M.D., B.G.H., T.M.G., N.R.Z., C.W., M.C. M.S., E.T., S.M., S.F., A.S., S.T., E.K., B.T.H., B.C.D., J.M.H., and P.R.-N. participated in the acquisitions, processing, quality control, and/or interpretation of the *in vivo* data. E.L. and M.S. performed *in vitro* proteins quantification. R.H., J.P.S., and G.M. worked in the radiochemistry production of the tracers. A.C.C. developed the McGill-R-Thy1-APP rat model. H.H. assisted with the data statistical analysis. All authors revised and approved the final manuscript draft.

Contribution to original knowledge

The original scientific contributions in this thesis include:

Chapter 2. We showed that a synergistic interaction between amyloid-β and tau determines hypometabolism in preclinical AD. This was the first study showing interactions between AD-related biomarkers using exclusively continuous measurements without assuming thresholds for abnormality or artificial dichotomization techniques.

Chapter 3. We proposed the concept of thresholds responsible for triggering the synergy between amyloid-β and tau. We suggested the use of these thresholds as a tangible framework to

identify individuals with the highest likelihood of disease progression. Also, this was the first study performing a voxel-wise sample size calculation, which consists of a new alternative to increase the statistical power of clinical trial designs.

Chapter 4. Complementing the findings from Chapters 2 and 3, we demonstrated for the first time that the synergistic interaction between amyloid-β and tau is also a determinant of the clinical progression from MCI to AD dementia. This was the first study conducting voxel-wise logistic regression using PET.

Chapter 5. We showed that a synergy between amyloid-β and neurodegeneration is associated with the clinical progression to dementia. Moreover, we suggested for the first time that amyloid-β leads to hypometabolism in distant regions that are functionally connected, rather than in the same brain region.

Chapter 6. We conducted the first human evaluation of the novel tau PET tracer [^{18}F]MK-6240 using full kinetic modeling and long scan acquisition duration. The methodological approaches validated in this work are currently being used by other research groups worldwide.

Chapter 7. We performed the first study measuring brain epigenetics in living patients. We proposed that HDACs I reduction links the interactive effect of amyloid-β and tau with AD progression. We suggested HDACs I reduction as a novel therapeutic target for AD.

List of abbreviations

ACC	Anterior cingulate cortex
AD	Alzheimer's disease
ADAS-Cog	Alzheimer's disease Assessment Scale-Cognitive Subscale
ADNI	Alzheimer's Disease Neuroimaging Initiative
AIC	Akaike information criterion
ANCOVA	Analysis of covariance
APOE	Apolipoprotein E
APP	Amyloid Precursor Protein
Aβ	Amyloid-β
BIC	Bayesian information criterion
BP	Binding potential
CDR	Clinical dementia rating
CERAD	Consortium to Establish a Registry for Alzheimer Disease
CFI	Comparative fit index
CI	Confidence interval
CN	Cognitively normal
CSF	Cerebrospinal fluid
CV	Coefficient of variation
DMN	Default mode network
DNA	Deoxyribonucleic acid
DSM	Diagnostic and Statistical Manual of Mental Disorders
DVR	Distribution volume ratio

[^{18}F]FDG	[^{18}F]Fluorodeoxyglucose
FDR	False discovery rate
FWER	Family-wise error rate
HDAC	Histone deacetylase
HRRT	Siemens High Resolution Research Tomograph
ICC	Intraclass correlation coefficient
IWG	International Working Group
LM	The Logical Memory subtest of the Wechsler Memory Scale
MAPT	Microtubule-associated protein tau
MCI	Mild cognitive impairment
MCSA	McGill University Research Centre for Studies in Aging
MGH	Massachusetts General Hospital
MINC	Medical Image NetCDF software
MMSE	Mini-mental state examination
MNI	Montreal Neurological Institute
MO	Monoamine oxidase
MRI	Magnetic resonance imaging
MTL	Medial temporal lobe
MWM	Morris Water Maze
ND	Non-displaceable
NIA-AA	National Institute on Aging and the Alzheimer's Association
NIH	National Institutes of Health
NINCDS-ADRDA	National Institute of Neurological and Communicative Disorders and

	Stroke and the Alzheimer's Disease and Related Disorders Association
NPS	Neuropsychological test scores
OSEM	Ordered-Subsets Expectation Maximization
PC	Probability of correctness
PCC	Posterior cingulate cortex
PET	Positron emission tomography
[^{11}C]PIB	[^{11}C]Pittsburgh compound B
P-tau	Phosphorylated tau
RMSEA	Root mean square error of approximation
RNA	Ribonucleic acid
ROC	Receiver operating characteristic curve
ROI	Region-of-interest
SD	Standard deviation
SE	Standard error of the mean
SEM	Structured equation model
SNAP	Suspected Non-AD Pathophysiology
SRMR	Standardized root mean square residual
SRTM	Simplified reference tissue model
SUVR	Standardized uptake value ratio
T-CM	Tissue compartment model
TMT	Trail Making Test
V_T	Volume of distribution

List of Tables

List of Figures

Chapter 1: General Introduction

1.1 The discovery of "a peculiar disease of the cerebral cortex"

Dr. Alois Alzheimer met his most notorious patient, Auguste Deter, in November 1901, at the mental asylum of Frankfurt (Burns *et al.*, 2002). According to Auguste's family, she had been developing progressive personality changes in the months prior to her admission, first showing an intense sense of jealousy toward her husband, followed by disorientation, memory impairment, and reading and writing difficulties (Burns *et al.*, 2002). During the hospitalization, she experienced a rapid worsening of symptoms, developing loss of higher mental functions and severe hallucinations (Perusini, 1909). Over time, Auguste Deter developed into a state of total apathy and, after four and a half years of symptoms, she died as a result of sepsis caused by an infected decubitus ulcer (Perusini, 1909, Burns *et al.*, 2002). In 1906, at a meeting of the Society of German Alienists, Dr. Alois Alzheimer described "a peculiar disease of the cerebral cortex" based on the neuropathological and clinical characteristics of Auguste Deter (Cipriani *et al.*, 2011). The neuropathological description showed brain atrophy and two other microscopic abnormalities, the miliary foci on the silver-staining (later described as amyloid-β plaques) and bundles of fibrils (later described as neurofibrillary tangles) (Alzheimer, 1911). In his presentation, Dr. Alois Alzheimer made the important assumption that the neuropathological changes mentioned above were directly related to the clinical symptoms of Auguste Deter (Maurer *et al.*, 1997). In fact, in the late nineteenth and early twentieth centuries, simple distinctions such as the difference between mental illness and dementia were a major theme of controversy in medical science (Boller and Forbes, 1998). Indeed, when identified, dementia was considered a state of mind from senile decay (Boller and Forbes, 1998). Therefore, Dr. Alois Alzheimer pioneering work, linking clinical symptoms with neuropathological abnormalities,

marked the beginning of the Alzheimer's disease (AD) research and provided the fundamental framework for the current models of disease progression (Cipriani *et al.*, 2011, Jack *et al.*, 2013).

1.2 The clinical spectrum of Alzheimer's disease

The clinical progression of AD is invariably linked to typical postmortem neuropathological features, such as extracellular deposition of amyloid-β protein in plaques, intracellular inclusions of tau protein in the form of neurofibrillary tangles, and neuronal degeneration (Braak and Braak, 1995, Braak and Braak, 1997). This clinical progression is insidious and characterized by a latent and a prodromal phase followed by dementia symptoms (Jack *et al.*, 2009). The fact that amyloid-β plaques, neurofibrillary tangles, and neurodegeneration, have been detected in non-demented individuals indicates that the AD pathophysiology begins before the onset of dementia (Braak, 1991, Thal *et al.*, 2002). In this regard, mild cognitive impairment (MCI) has been identified as a prodromal phase of AD (Kayed *et al.*, 2003, Albert *et al.*, 2011), and preclinical AD has been defined as cognitively normal persons with abnormal AD biomarkers (Sperling *et al.*, 2014, Dubois *et al.*, 2016)

1.2.1 Alzheimer's disease dementia

Dementia is a clinical syndrome characterized by difficulties in cognitive functions, such as memory, executive abilities, and language, which affect the patient's ability to perform activities of daily living (Association and Association, 2000). In 2016, the World Health Organization indicated that approximately 47 million people worldwide suffered from some form of dementia. In 2050, it is projected that 131 million people will suffer from dementia due to the aging of the populations (Prince *et al.*, 2016). Recently, the World Health Organization has suggested that

dementia should be considered a global public health priority because of its immense social and economic costs (Organization, 2012).

AD is the most common cause of dementia, accounting for 60-70% of all cases (Masters *et al.*, 2006, 2018). In 1984, the National Institute of Neurological and Communicative Disorders and Stroke and the Alzheimer's Disease and Related Disorders Association (NINCDS-ADRDA) working groups proposed the first criteria for AD dementia (McKhann *et al.*, 1984). According to these criteria, progressive decline in memory is the earliest and most prominent cognitive feature of most individuals with AD dementia, in association with the decline of at least one of the other cognitive functions in absence of other disorders that could justify cognitive deficits. These characteristics were used to define a clinical diagnosis of probable AD, which together with pathological evidence from brain biopsy or autopsy establish a definitive diagnosis of AD dementia (McKhann *et al.*, 1984).

Over the last few years, different working groups have revised the NINCDS-ADRDA criteria in order to incorporate clinical and biological advances from the literature. Despite several similarities with the NINCDS-ADRDA criteria, the updated criteria proposed by the Diagnostic and Statistical Manual of Mental Disorders (DSM) (Association and Association, 2000), the International Working Group (IWG) (Dubois *et al.*, 2007, Dubois *et al.*, 2014), and the National Institute on Aging and the Alzheimer's Association (NIA-AA) (McKhann *et al.*, 2011) groups suggest importance advances such as the recognition of nonamnestic presentations of AD and the importance of defining activities of daily living impairment for the diagnosis of dementia (Guy M. McKhanna, 2011). In addition, some of these groups proposed to incorporate disease

biomarkers in the criteria. The IWG criteria for probable AD, for example, require cognitive deficits and the abnormality of at least one biomarker supportive of AD, such as brain atrophy, amyloid-β, and tau (Dubois *et al.*, 2007, Dubois *et al.*, 2014).

1.2.2 Mild cognitive impairment

MCI is a clinical entity associated with a heterogeneous group of disorders that course with cognitive deterioration (DeCarli, 2003, Gauthier *et al.*, 2006). MCIs are capable of independently performing daily living activities, despite of the presence of a quantifiable cognitive decline (Gauthier *et al.*, 2006, Albert *et al.*, 2011). This clinical definition has been widely used by healthcare providers and researchers who do not have access to disease biomarkers (Albert *et al.*, 2011). More recently, the research criteria, incorporating neuroimaging and cerebrospinal fluid (CSF), were created to define MCI individuals more likely to be on an AD pathway (Albert *et al.*, 2011). In these criteria, MCI due to AD is defined in four levels of certainty depending on the presence of AD biomarkers, and the MCIs that are most likely to be on an AD pathway are those with abnormal biomarkers of amyloid-β and tau pathology/neuronal injury (Albert *et al.*, 2011).

1.2.3 Preclinical Alzheimer's disease

The concept of preclinical AD emerged from early histopathological observations that found AD pathology in the brain of cognitively normal (CN) individuals (Hubbard *et al.*, 1990). With the advance of *in vivo* biomarkers of AD, this concept evolved, and different classifications were proposed based on the presence of AD biomarkers in living CN individuals. The NIA-AA working group conceptualized preclinical AD in three stages: Stage 1, CN with evidence of

amyloid-β pathology; Stage 2, CN with evidence of amyloid-β pathology plus neurodegeneration; Stage 3, CN with evidence of amyloid-β pathology, neurodegeneration, and subtle cognitive decline (Sperling *et al.*, 2011). Subsequently, Jack and colleagues suggested a Stage 0 to describe CN individuals with the absence of biomarker abnormalities and Suspected Non-AD Pathophysiology (SNAP), which include CN individuals with neurodegeneration evidenced by biomarkers without amyloid-β pathology (Jack *et al.*, 2012). Recently, the IWG suggested saving the term "preclinical AD" for CN individuals with amyloid-β plus tau biomarkers abnormality, whereas CN individuals with only one abnormal biomarker (amyloid-β or tau) would be defined as "at risk for AD" (Dubois *et al.*, 2016).

1.3 Alzheimer's disease pathology

AD pathology is typically characterized by the cerebral accumulation of amyloid-β plaques, neurofibrillary tangles, and downstream events such as neurodegeneration (Hardy and Allsop, 1991, Hardy and Higgins, 1992, Jack *et al.*, 2013).

1.3.1 Amyloid-β pathology

Amyloid-β plaques are extracellular deposits of amyloid-β aggregates generated by an abnormal cleavage of the Amyloid Precursor Protein (APP) by a β- and γ-secretase (Chow *et al.*, 2010). In the healthy brain, APP has been associated with the regulation of neuronal structure and synaptic function (Tyan *et al.*, 2012). APP may be cleaved either in 40 (amyloid-β_{1-40}) or 42 (amyloid-β_{1-42}) residues (Jarrett *et al.*, 1993). Although amyloid-β_{1-40} differs from amyloid-β_{1-42} only in two residues, the latter shows greater aggregation and neurotoxicity (Nguyen *et al.*, 2016). The brain distribution of amyloid-β pathology follows typical patterns during the course of AD. According

to Braak and Braak (Figure 1-1), amyloid-β deposits can be found first in the basal neocortex (stage A), followed by virtually all neocortical regions and the hippocampus (stage B), extending to the sensorimotor cortex in the latest stage (stage C) (Braak and Braak, 1991). On the other hand, Thal et al. propose that amyloid-β deposition progresses in five phases involving, first, exclusively the neocortex (phase 1), followed by the entorhinal and hippocampal cortices (phase 2), the striatum and diencephalon nuclei (phase 3), certain brainstem nuclei (phase 4), and, finally, the cerebellum and the remaining brainstem nuclei (phase 5) (Thal *et al.*, 2002). Notably, these postmortem studies show brain amyloid-β pathology in CN individuals with a distribution similar to that observed in AD dementia patients, suggesting that amyloid-β is not a sufficient condition to determine dementia (Hof *et al.*, 1992, Schmitt *et al.*, 2000, Morris and Price, 2001, Knopman *et al.*, 2003).

1.3.2 Tau pathology

The microtubule-associated protein tau (MAPT) plays an essential role in stabilizing microtubule structure (Vingtdeux *et al.*, 2012). The MAPT gene on chromosome 17 encodes six different isoforms of the tau protein that present either three (3R) or four (4R) microtubule-binding domains (Liu and Gong, 2008, Vingtdeux *et al.*, 2012). Both types of isoforms, 3R and 4R, undergo abnormal hyperphosphorylation in AD, which leads to the formation of insoluble intracellular aggregates, named paired helical filaments (Vingtdeux *et al.*, 2012). Paired helical filaments are the main constituents of neurofibrillary tangles, which are implicated in the pathogenesis of AD (Selkoe, 1991). In AD, neurofibrillary tangles accumulation has been suggested to begin in transentorhinal regions (stages I/II), followed by limbic (stage III/IV) and neocortical regions (stages V/VI) (Figure 1-1) (Braak and Braak, 1991). In these studies, tau

aggregates have been reported in the brain of non-demented individuals in limbic, transentorhinal, and basal temporal strictures (Braak and Braak, 1991, Hof *et al.*, 1992, Bouras *et al.*, 1993, Sonnen *et al.*, 2011), suggesting that tau pathology alone is also not a sufficient condition to determine dementia.

Figure 1-1. Pathological evolution of amyloid□β and tau in Alzheimer's disease.

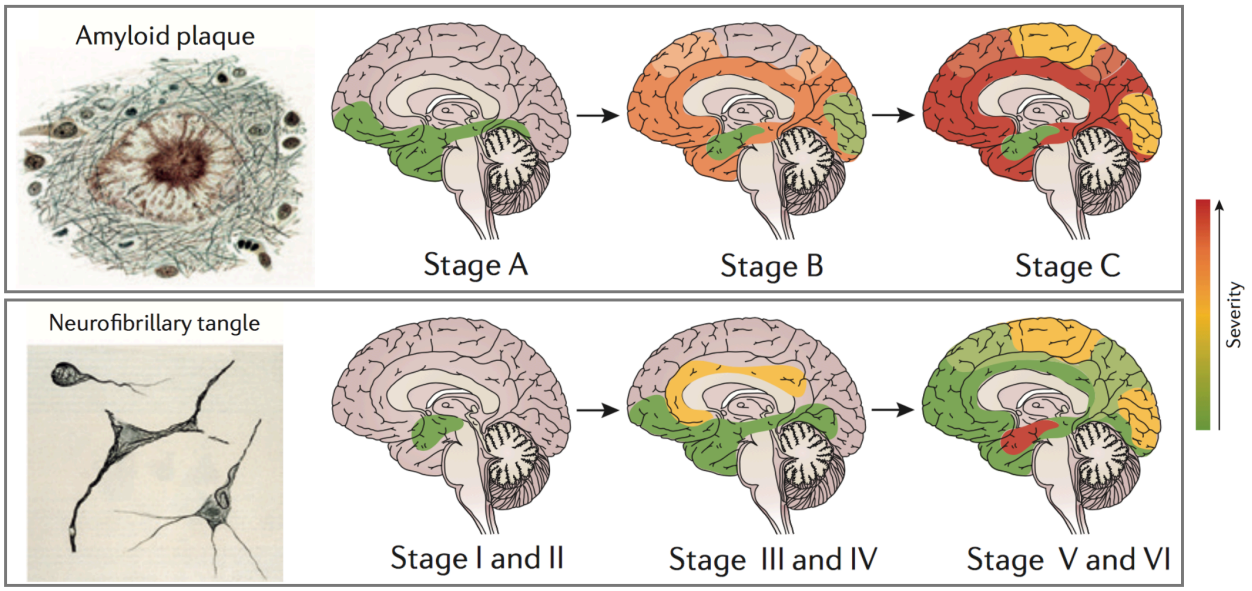

Typical progression of amyloid-β plaques and neurofibrillary tangles in AD proposed by Braak and Braak. Adapted from Masters, *et al.* (Masters *et al.*, 2015).

1.3.3 Neurodegeneration

Neurodegeneration refers to the pathophysiological processes associated with progressive loss of neuronal structure and function (Selkoe, 1991). The presence of brain degeneration is closely related to cognitive decline in patients with AD (Jack *et al.*, 2013). However, it is important to mention that neurodegeneration may be found in several other pathological processes and cognitively normal aging (Wilson *et al.*, 2010, Wyss-Coray, 2016). In AD, neurodegeneration

occurs in allocortical and neocortical regions (Hubbard and Anderson, 1985, West *et al.*, 1994, Gomez-Isla *et al.*, 1996, Reddy *et al.*, 2005).

1.3.4 Other key pathophysiological processes

Several other pathophysiological processes have been associated with AD, such as cerebrovascular diseases and neuroinflammation (Gauthier *et al.*, 2018). A growing body of literature suggests a direct link between AD pathology and cerebrovascular disease (Beach *et al.*, 2007, Yarchoan *et al.*, 2012). These studies report that these two brain pathologies share many risk factors, such as the APOE ε4 allele, which is a genetic risk factor for AD (Kim *et al.*, 2009) and is independently associated with increased cerebrovascular load (Schilling *et al.*, 2013). Also, studies show that vascular risk factors can predict the clinical progression from MCI to AD dementia (Li *et al.*, 2011, Bergland *et al.*, 2017). Indeed, it has been suggested that small vessel diseases play a central role in the pathogenesis of AD (Lee *et al.*, 2016). Similarly, neuroinflammation has been often associated with AD (Heneka *et al.*, 2015). Neuropathological studies have reported reactive microglia in the brain of AD patients (Akiyama *et al.*, 2000, Eikelenboom *et al.*, 2010), which is related to an inflammatory brain state and is correlated with neurofibrillary tangles and amyloid-β plaques (DiPatre *et al.*, 1997, Bamberger *et al.*, 2003, Mandrekar *et al.*, 2009). Although strong evidence links microglial activation with AD pathology, it remains to be clarified whether this association is protective or deleterious to patients (Boche and Nicoll, 2008, De Strooper and Karran, 2016).

1.3.5 Epigenetic modifications

Recently, epigenetic modifications have been found to be associated with the progression of

chronic conditions (Egger *et al.*, 2004, Feinberg, 2007). Although there is no consensus on the definition of epigenetics, a widely accepted definition suggests that epigenetic mechanisms, such as Deoxyribonucleic acid (DNA) methylation and histone modifications, encompass a range of processes capable of imposing changes in gene expression without altering the DNA nucleotide sequence (Levenson and Sweatt, 2005). Among different epigenetic regulators, histone acetylation has been the most frequently associated with AD in recent studies (Graff *et al.*, 2012, Graff and Tsai, 2013) and is one of the most understood epigenetic modifications associated with memory (Guan *et al.*, 2009, Stefanko *et al.*, 2009, Bousiges *et al.*, 2010, Kim *et al.*, 2012, Malvaez *et al.*, 2013, Lopez-Atalaya and Barco, 2014). Histone acetylation is a post-translational modification that consists of adding an acetyl group to the N-terminal tail of histones, which can lead to changes in gene transcription (Graff and Tsai, 2013). This process is modulated by the equilibrium of two antagonistic groups of enzymes, histone acetyltransferases and histone deacetylases (HDACs) (Grunstein, 1997, Verdone *et al.*, 2006). Pharmacological manipulations of histone acetylation using HDACs inhibitors have been found to improve long-term memory in mice (Bredy and Barad, 2008, Haettig *et al.*, 2011, Mahan *et al.*, 2012, Ganai *et al.*, 2015). In addition, previous studies also associated histone acetylation with memory reconsolidation through hippocampus and amygdala (Lubin and Sweatt, 2007, Maddox and Schafe, 2011). Recently, studies have focused on class I HDACs (HDACs I) (isoforms 1-3) as a key epigenetic element associated with AD (Wei *et al.*, 2017). They show HDACs I increase in several animal models of AD and postmortem tissue (Graff *et al.*, 2012, Yamakawa *et al.*, 2017, Zhu *et al.*, 2017, Mahady *et al.*, 2018). Some of these studies have linked the increase of HDAC1 with tau pathology and the increase of HDAC2 and 3 with amyloid-β pathology (Bie *et al.*, 2014, Zhu *et al.*, 2017, Mahady *et al.*, 2018). Also, in line with these findings, analysis of postmortem AD

brain tissue shows elevated HDAC2 levels in the hippocampus and entorhinal cortex (Braak stages I-II), suggesting the existence of HDACs I dysregulation in early disease stages (Graff *et al.*, 2012). Overall, these studies suggest that elevated levels of HDACs I play a role in the pathophysiology of AD.

1.3.6 Neuropathological criteria

To date, the definitive diagnosis of AD is obtained only with histopathological examination. The most recent neuropathological diagnostic of AD proposed by NIA-AA (Hyman *et al.*, 2012) is based on the staging of amyloid-β plaques (Thal *et al.*, 2002) and neurofibrillary tangles (Braak and Braak, 1991), as well as neuritic plaque load (Mirra *et al.*, 1991).

1.4 *In vivo* biomarkers

Biomarkers are objective measures that indicate a physiological or pathological process (Biomarkers Definitions Working, 2001). In AD, the most recognized groups of biomarkers are those derived from CSF and neuroimaging.

1.4.1 *In vivo* biomarkers of brain amyloid-β pathology

The presence of brain amyloid-β deposition can be evaluated *in vivo* from the concentrations of amyloid-β species in the CSF as well as directly from the brain using positron emission tomography (PET) (Motter *et al.*, 1995, Blennow and Vanmechelen, 2003, Klunk *et al.*, 2004, Hansson *et al.*, 2006, Bacskai *et al.*, 2007, Ikonomovic *et al.*, 2008).

CSF observations suggest that amyloid-β_{1-42}, rather than amyloid-β_{1-40}, is highly correlated with brain amyloid-β plaques (Iwatsubo *et al.*, 1994, Yarchoan *et al.*, 2012). Subsequently, several studies have found abnormally reduced CSF levels of amyloid-β_{1-42} in AD patients and that these levels are related to AD progression (Motter *et al.*, 1995, Blennow and Vanmechelen, 2003, Hansson *et al.*, 2006). Since brain amyloid-β accumulation leads to a decrease in available CSF amyloid-β (Kester *et al.*, 2009), CSF amyloid-β values correlate inversely with brain plaques in postmortem and PET studies (Strozyk *et al.*, 2003, Fagan *et al.*, 2006, Fagan *et al.*, 2009, Tapiola *et al.*, 2009).

The cerebral imaging of amyloid-β plaques offers a unique opportunity to detect regional patterns of amyloid-β deposition *in vivo*, which is its most important advantage over other techniques with non-spatial resolution, such as CSF (Tosun *et al.*, 2011). [^{11}C]Pittsburgh compound B ([^{11}C]PIB), the first high-affinity radiotracer for amyloid-β plaques, shows increased cortical uptake in AD patients compared to CN and a regional uptake consistent with postmortem descriptions of amyloid-β plaques in AD patients (Klunk *et al.*, 2004, Bacskai *et al.*, 2007, Ikonomovic *et al.*, 2008). However, the short half-life of [^{11}C] (~20 min) prevented the dissemination of amyloid-β PET imaging beyond centers with radiochemical facilities. Subsequently, with the development of [^{18}F]-labeled radiotracers with a longer half-life (~110 min), such as [^{18}F]florbetapir, [^{18}F]florbetaben, [^{18}F]flutemetamol, and [^{18}F]AZD4694, a broader dissemination of amyloid-β PET became possible (Nelissen *et al.*, 2009, Jagust, 2010, Cselenyi *et al.*, 2012, Newberg *et al.*, 2012, Sabri *et al.*, 2015). These [^{18}F]-labeled markers showed results highly comparable to those found with [^{11}C]PIB (Rowe *et al.*, 2013, Hatashita *et al.*, 2014, Landau *et al.*, 2015). These studies suggest that PET constitutes a reliable marker for the

in vivo detection of amyloid-β (Jack *et al.*, 2009), particularly for brain deposits of fibrillar amyloid-β peptides in the form of plaques (Ikonomovic *et al.*, 2008). In concordance with postmortem observation, PET studies have shown amyloid-β deposition in approximately 30% of CN elderly and 60% of MCIs with a distribution similar to that observed in patients with AD dementia, encompassing frontal, temporal, inferior parietal, and anterior and posterior cingulate cortices (Figure 1-2) (Hof *et al.*, 1992, Schmitt *et al.*, 2000, Morris and Price, 2001, Knopman *et al.*, 2003, Forsberg *et al.*, 2008, Okello *et al.*, 2009, Jagust *et al.*, 2010). Moreover, amyloid-β biomarkers have limitations in predicting the clinical progression of AD (Jagust, 2016, Walsh and Selkoe, 2016). In fact, brain amyloid-β levels measured *in vivo* or postmortem tissue show low association with cognition (Terry *et al.*, 1991, Snowdon *et al.*, 1996, Riley *et al.*, 2005, Bennett *et al.*, 2006, Savva *et al.*, 2009). Thus, these studies support the idea that amyloid-β pathology alone is an insufficient condition to determine dementia (Braak and Braak, 1997, Petersen *et al.*, 2006).

1.4.2 *In vivo* biomarkers of brain neurofibrillary tangles

Neurofibrillary tangles can be assessed *in vivo* from CSF concentrations of phosphorylated tau (p-tau) protein and directly from the brain using PET (Blennow *et al.*, 2010, Skillback *et al.*, 2015, Jack *et al.*, 2016, Pascoal *et al.*, 2017).

Since the discovery that neurofibrillary tangles are composed of abnormally hyperphosphorylated tau (Grundke-Iqbal *et al.*, 1986), CSF p-tau assays have been developed and validated. Although tau can ben phosphorylated at various sites, most studies assay phosphorylated tau at threonine 181 or 231 (Kohnken *et al.*, 2000, Vanmechelen *et al.*, 2000).

Postmortem studies show that CSF p-tau correlates with neocortical neurofibrillary tangles (Tapiola *et al.*, 1997, Buerger *et al.*, 2006), and *in vivo* observations show that p-tau levels are abnormally increased in AD patients and are correlated with disease progression (Tapiola *et al.*, 1997, Jack *et al.*, 2016).

In vivo quantification of neurofibrillary tangles represents a new frontier in AD research. Several radiotracers were proposed as candidates to measure tangles *in vivo*, such as [^{18}F]AV-1451, [^{18}F]THK5117, [^{18}F]THK5317, [^{18}F]THK5351, and [^{11}C]PBB3 (Chien *et al.*, 2013, Xia *et al.*, 2013, Hashimoto *et al.*, 2014, Harada *et al.*, 2015, Stepanov *et al.*, 2017). Validation studies showed that these tracers have abnormal cortical uptake in MCI and AD patients and that this uptake is consistent with the Braak staging (Johnson *et al.*, 2016, Schwarz *et al.*, 2016, Betthauser *et al.*, 2017, Kim *et al.*, 2017). Similar to what has been described in postmortem observation(Braak and Braak, 1991), tau abnormalities have been reported in the brains of non-demented living individuals, supporting the idea that tau tangles alone is insufficient to lead to AD dementia (Figure 1-2) (Johnson *et al.*, 2016, Schwarz *et al.*, 2016, Betthauser *et al.*, 2017, Kim *et al.*, 2017). However, subsequent *in vivo* and *in vitro* observations suggest that other pathophysiological processes heavily influence the cortical signal of the aforementioned first-generation tau tracers. For instance, monoamine oxidase B (MAO-B) has been shown to affect the uptake of [^{18}F]THK5351 in typical AD-relate brain regions (Ng *et al.*, 2017), whereas MAO-A and α-synuclein may affect the uptakes of [^{18}F]AV-1451 and [^{11}C]PBB3, respectively (Hostetler *et al.*, 2016, Koga *et al.*, 2017). Recently, second-generation tau tracers were developed with the objective of presenting higher affinity and selectivity for tangles than the first-generation tracers. In early observations, these agents (e.g., [^{18}F]MK-6240,

[^{18}F]RO6958948, [^{18}F]PI2620) showed promising results with an uptake pattern consistent with the one reported by Braak as well as apparent higher affinity and selectivity for tangles than the first-generation tracers (Pascoal *et al.*, 2018, Villemagne *et al.*, 2018, Wong *et al.*, 2018).

1.4.3 *In vivo* biomarkers of neurodegeneration

Biomarkers of neurodegeneration provide information about neuronal damage (Jack *et al.*, 2009, Jack *et al.*, 2013). Although CSF p-tau and total tau levels are highly associated, CSF total tau is proposed to better reflect neuronal degeneration, rather than neurofibrillary tangles (Albert *et al.*, 2011, Blennow and Zetterberg, 2015, Jack *et al.*, 2016). Magnetic resonance imaging (MRI) is the most widely used neurodegeneration biomarker (Shimizu *et al.*, 2018). Brain volume measured with MRI showed to be closely related to neuronal counts in autopsy studies (Jack *et al.*, 2002). Brain atrophy is a common finding in AD patients and usually manifests first in the medial temporal lobe (Scahill *et al.*, 2002). Brain measurements of glucose metabolism using [^{18}F]Fluorodeoxyglucose ([^{18}F]FDG) PET are postulated to provide information on neuronal function (Raichle and Mintun, 2006, Jack *et al.*, 2009). Age-related [^{18}F]FDG hypometabolism has been reported in the dorsolateral and ventromedial frontal cortices (de Leon *et al.*, 1987, Leenders *et al.*, 1990, Moeller *et al.*, 1996), whereas hypometabolism in regions comprising the brain's default mode network (DMN) is highly associated with AD progression (Buckner *et al.*, 2005, Sperling *et al.*, 2009, Landau *et al.*, 2012, Mosconi, 2013). The visual assessment of [^{18}F]FDG uptake has shown to improve the clinical diagnosis of AD (Jagust *et al.*, 2007).

Figure 1-2. Representative individual showing abnormalities in biomarkers of amyloid-β, tau, and neurodegeneration.

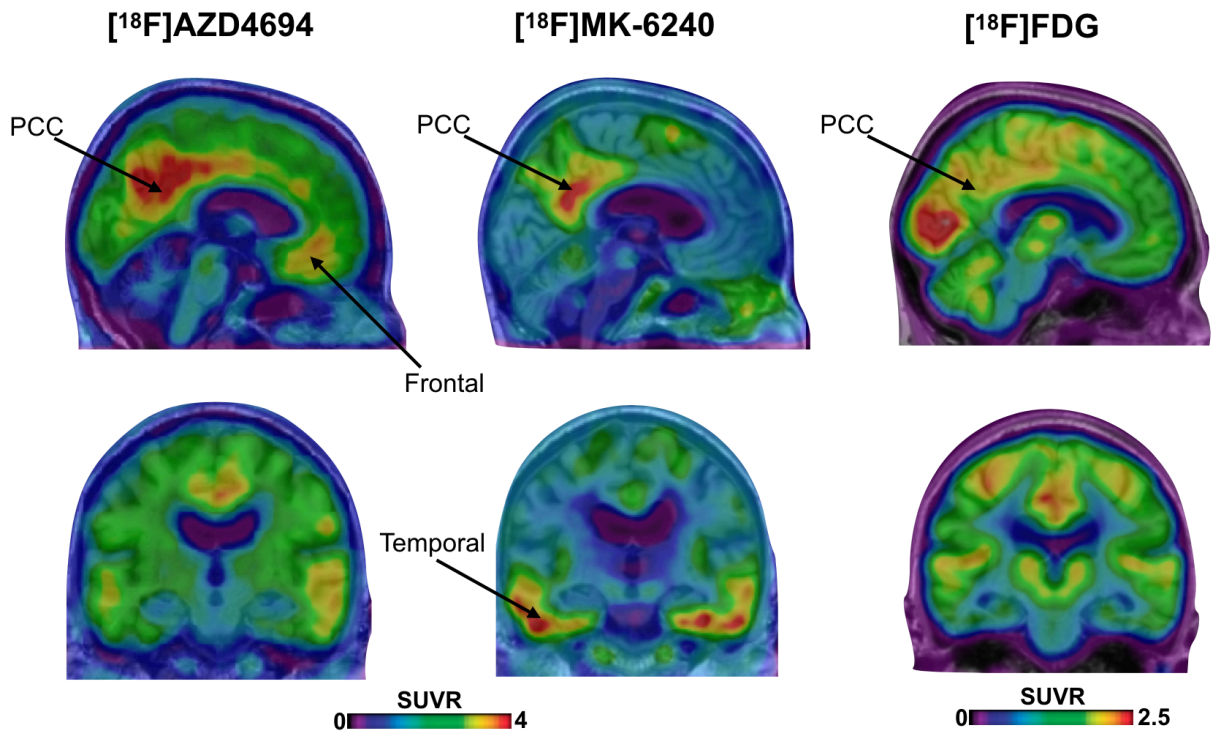

The figure shows a representative CN individual showing amyloid-β ([^{18}F]AZD4694), tau ([^{18}F]MK-6240), and neurodegeneration ([^{18}F]FDG) biomarkers abnormality. The participant shows high amyloid-β load in the precuneus, PCC, and frontal lobe, high tau tangles load in PCC and temporal lobe, and mild to moderate hypometabolism in the precuneus and PCC cortices.

1.4.4 *In vivo* brain biomarker of epigenetics

Very recently, *in vivo* quantification of brain epigenetics has become possible with the development of the HDACs I selective PET tracer [^{11}C]Martinostat (Wey *et al.*, 2015, Wey *et al.*, 2016). In contrast to fluid-based markers, [^{11}C]Martinostat provides direct epigenetic measures in brain tissue, allowing for the first time to establish direct associations between brain epigenetic modifications, pathophysiological processes, and cognitive symptoms. [^{11}C]Martinostat allows whole brain quantification of HDAC I isoforms 1, 2, and, 3, which are mostly related to the transcription regulation of genes associated with neuroplasticity and

cognition (Guan *et al.*, 2009, Wey *et al.*, 2016). Indeed, pharmacological doses of [^{11}C]Martinostat have been shown to induce changes in expression of genes linked to neuroplasticity (e.g., brain-derived neurotrophic factor and synaptophysin) and neurodegeneration (e.g., progranulin), as well as changes in histone acetylation (Wey *et al.*, 2016). In healthy volunteers, [^{11}C]Martinostat showed high uptake in neocortex and low uptake in white matter and hippocampus (Wey *et al.*, 2016).

1.5 Animal models of Alzheimer's disease

Animal models expressing autosomal dominant human mutations are particularly useful for studying the dynamic changes of AD biomarkers in controlled environments (Gotz and Ittner, 2008). Studies using these models offer less genetic and environmental variability than human studies; therefore, they provide an important tool for investigating a specific hypothesis with less interference of confounding factors (Gotz *et al.*, 2004, Gotz and Ittner, 2008). Most of the transgenic models of AD are mice (Gotz and Ittner, 2008) since few rat models expressing amyloid-β have been successfully developed to date (Zimmer *et al.*, 2014). Rats have a larger brain compared to mice, which is an important advantage, particularly for *in vivo* studies using techniques with low spatial resolution, such as PET (Zimmer *et al.*, 2014). In this regard, the McGill-R-Thy1-APP rat expressing human APP with Swedish double (K670N and M671L(Mullan *et al.*, 1992)) and Indiana (V717F(Murrell *et al.*, 1991)) mutations was developed (Leon *et al.*, 2010). McGill-R-Thy1-APP rats present amyloid-β accumulation (Parent *et al.*, 2017) but do not form neurofibrillary tangles (Do Carmo and Cuello, 2013). In contrast, TgF344-AD rats with Presenilin-1 and APP mutations (Cohen *et al.*, 2013, Munoz-Moreno *et*

al., 2018) develop amyloid-β pathology and downstream neurofibrillary tangles (Cohen *et al.*, 2013, Munoz-Moreno *et al.*, 2018).

1.6 Hypothetical models of Alzheimer's disease progression

1.6.1 Amyloid hypothesis

The most accepted hypothesis describing AD progression, the so-called "amyloid-β hypothesis", predicts that amyloid-β triggers all subsequent pathological manifestations associated with AD (Hardy and Selkoe, 2002). This hypothesis was based on phenomenological observations, such as the fact that the APP gene is located on chromosome 21(Kang *et al.*, 1987) and that aged Down syndrome patients, a condition caused by a trisomy of chromosome 21, develop AD pathophysiology (Olson and Shaw, 1969). In this model, increased toxic forms of amyloid-β lead to tau hyperphosphorylation and consequently to its aggregation in the form of neurofibrillary tangles. Subsequently, an imbalance of amyloid-β production and clearance determines neuronal cell death, resulting in cognitive decline and eventually dementia.

1.6.2 Biomarkers models of Alzheimer's disease progression

1.6.2.1 Sequential model

Based on the amyloid-β hypothesis, Jack and colleagues proposed a biomarkers cascade model for AD progression (Jack *et al.*, 2013). This model suggests that amyloid-β triggers a cascade of sequential downstream events leading to neurofibrillary tangles formation, neuronal degeneration, and cognitive decline. In this model, amyloid-β deposition reaches a plateau early on in the disease process; therefore, the subsequent disease progression is defined by the severity of tau pathology and neuronal degeneration. Thus, in this model, dementia symptoms do not

result from a direct influence of amyloid-β; it is the tau pathology and neurodegeneration that drive cognitive decline (Figure 1-3).

1.6.2.2 Alternative models

Since a purely sequential model of AD progression failed to explain numerous findings in the biomarker literature, such as the presence of tau pathology and neurodegeneration in cognitively normal individuals, even before amyloid-β in some brain regions (Braak and Braak, 1991, Hof *et al.*, 1992, Bouras *et al.*, 1993, Sonnen *et al.*, 2011), several adaptations of the canonical model have been recently proposed. For instance, Figure 1-4 demonstrates several variations of the sequential model and suggests the possibility of parallel pathophysiological effects between amyloid-β and tau on disease progression, which suggest amyloid-β and tau as two independent upstream processes that in a parallel lead to AD progression. In Figure 1-5, an alternative model suggests that amyloid-β may facilitate the spreading of tau from the medial temporal lobe over neocortical structures, which in turn leads to synaptic loss and dementia (Sperling *et al.*, 2014).

Figure 1-3. Hypothetical model of Alzheimer's disease dynamic biomarkers.

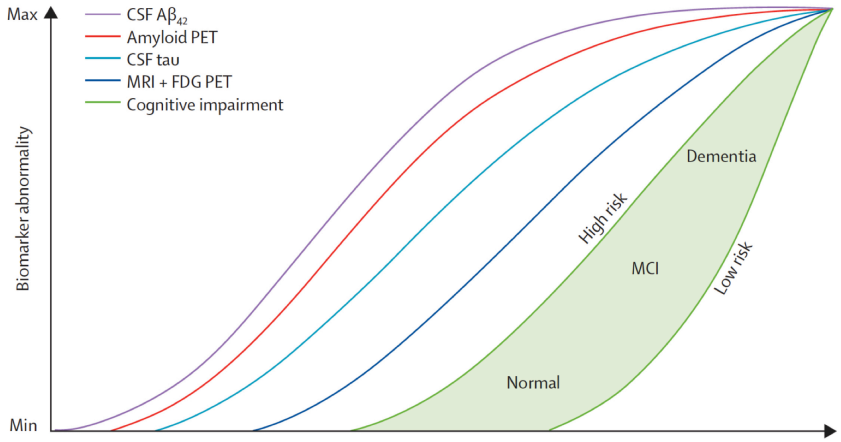

The curves show a chronological order of biomarkers progression that begins with amyloid-β (Aβ) deposition (purple and red). This induces acceleration of tauopathy (light blue), followed by neurodegeneration (FDG PET and MRI, dark blue), and finally, cognitive impairment (green). Adapted from Jack, *et al.* (Jack *et al.*, 2013).

Figure 1-4. Hypothetical models linking amyloid-β, tau, and neurodegeneration with cognitive decline.

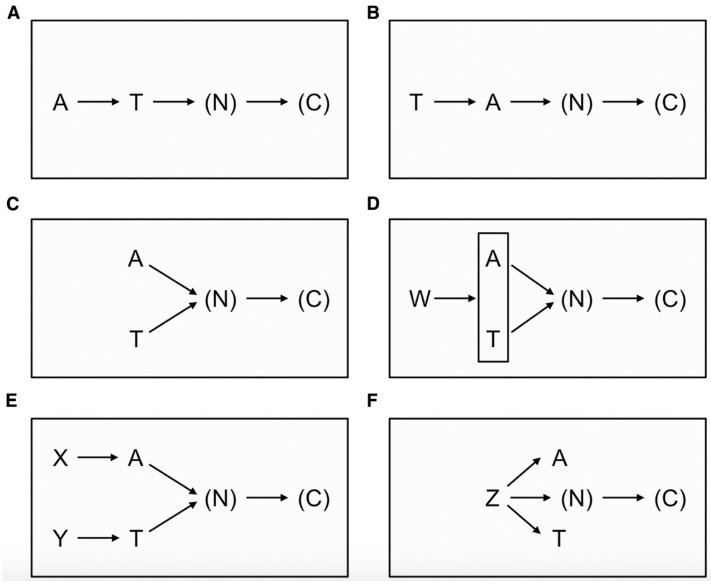

The figure summarizes possible mechanistic pathways of amyloid-β (A), tau (T), and neurodegeneration (N) leading to cognitive decline (C). Amyloid-β and tau may arise simultaneously due to a common upstream pathologic process (W) or may be induced by two independent upstream pathologic processes (X and Y). Also, amyloid-β, tau, and neurodegeneration may be induced by a common pathological process (Z). Adapted from Jack, *et al.* (Jack *et al.*, 2018).

Figure 1-5. Hypothetical model showing an interplay between amyloid-β and tau in the progression of Alzheimer's disease.

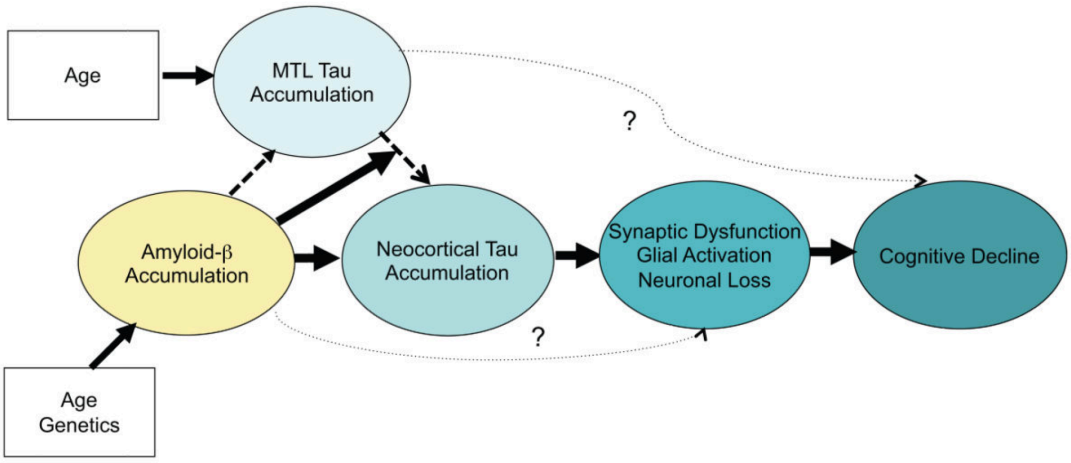

Amyloid-β accumulation triggers the spread of tau pathology from the medial temporal lobe (MTL) over the neocortex. Adapted from Sperling, *at al.* (Sperling *et al.*, 2014).

1.6.3 Synergistic model

A possible alternative explanation that is able to integrate some of the models mentioned above is that amyloid-β, tau, and neurodegeneration arise, at least partially, independently and, at some point, synergistic interact to determine dementia (Duyckaerts, 2011, Pascoal *et al.*, 2017). In the context of AD, the presence of a synergistic model would suggest that the effects of amyloid-β, tau, and neurodegeneration on disease progression, taken together, is higher than the sum of their separate effects at the same pathological levels. In the context of regression analysis, an interaction occurs when a simultaneous influence of two or more independent predictors affect the dependent outcome, whereas a synergistic interaction refers to the situation where the interactive effect between independent predictors is higher than the sum of their separated effects (Slinker, 1998) (Figure 1-6).

Figure 1-6. Schematic representation of the synergistic interaction

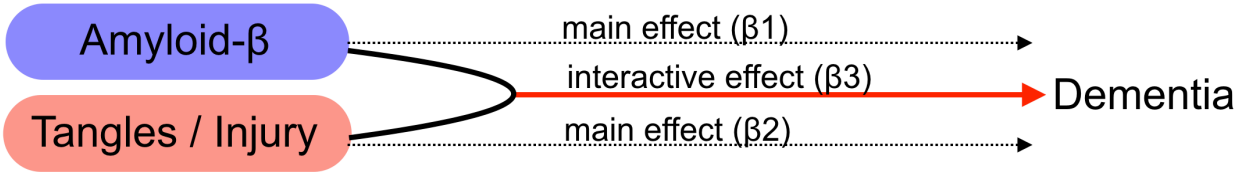

β3 represents the interactive effect between amyloid-β and neurofibrillary tangles or neuronal injury associated with the development of dementia symptoms.

1.7 Rationale and Objectives

AD is the main cause of dementia but does not have an effective treatment. There is growing recognition that the best strategy for achieving more effective disease-modifying therapies for AD is to better understand the complex pathophysiological associations that occur during the disease process, which are still poorly known. Although the leading theory suggests that amyloid-β triggers downstream events leading to dementia, the presence of amyloid-β in the brains of cognitively stable individuals and the loose correlation between amyloid-β and downstream events challenge the accuracy of this model (Hof *et al.*, 1992, Schmitt *et al.*, 2000, Morris and Price, 2001, Knopman *et al.*, 2003). Therefore, the overarching goal of this thesis was to use multimodal neuroimaging and fluid markers to provide new insights into the interplay between amyloid-β, tau, neurodegeneration, and epigenetics as a determinant of AD progression.

Toward this goal, we designed 6 studies with the following specific objectives. In Chapters 2-4, we evaluated individuals from the Alzheimer's Disease Neuroimaging Initiative (ADNI) dataset to define whether the synergistic interaction between, rather than the sequential or additive effects of, amyloid-β and tau is associated with 2-year disease progression. To start, we sought to determine whether this synergy determines metabolic decline in preclinical AD (**Chapter 2**).

The objective of **Chapter 3** was to investigate the existence of biomarker thresholds associated with the triggering of the aforementioned synergy. **Chapter 4** was conceived to test whether this synergy is responsible for the clinical progression from MCI to dementia. In **Chapter 5**, we used ADNI dataset and transgenic rats to study the associations between amyloid-β and neurodegeneration (without the influence of tau pathology) with the clinical progression of AD dementia. The next study (**Chapter 6**) was designed to validate, methodologically and clinically, a new tau PET tracer for use in Chapter 7. Finally, in **Chapter 7**, we brain imaged individuals across the AD spectrum using amyloid-β, tau, degeneration, and epigenetic biomarkers, as well as evaluated postmortem brain tissue to investigate the role of epigenetic abnormalities in the interplay between the AD pathophysiological processes.

Chapter 2: Amyloid-β and hyperphosphorylated tau synergy drives metabolic decline in preclinical Alzheimer's disease

Tharick A. Pascoal MD [1], Sulantha Mathotaarachchi BSc [1], Sara Mohades BSc [1], Andrea L. Benedet MSc [1,2], Chang-Oh Chung MD [1], Monica Shin BSc [1], Seqian Wang BSc [1], Tom Beaudry BSc [1], Min Su Kang BSc [1], Jean-Paul Soucy MD, PhD [3], Aurelie Labbe PhD [4,5,6], Serge Gauthier MD [7], and Pedro Rosa-Neto MD, PhD [1,3,7,8] for the Alzheimer's Disease Neuroimaging Initiative*

[1]Translational Neuroimaging Laboratory, The McGill University Research Centre for Studies in Aging, Montreal, Canada [2]CAPES Foundation, Ministry of Education of Brazil, Brasília, Brazil [3] Montreal Neurological Institute, Montreal, Canada [4]Douglas Hospital Research Centre, McGill University, Montreal, Canada [5]Department of Epidemiology, Biostatistics & Occupational Health, McGill University, Montreal, Canada [6]Douglas Mental Health University Institute, Verdun, QC, Canada Department of Psychiatry, McGill University Faculty of Medicine, Montreal, QC, Canada [7]Alzheimer's Disease Research Unit, The McGill University Research Centre for Studies in Aging, Montreal, McGill University, Montreal, Canada [8]Department of Neurology and Neurosurgery, McGill University, Montreal, Canada.

Published in Molecular Psychiatry. 2017 Feb;22(2):306-311 (PMID: 27021814).

2.1 Preface

Although the vast majority of previous studies have focused on either amyloid-β or tau as independent predictors of AD progression (Buerger *et al.*, 2005, Ossenkoppele *et al.*, 2014), a theoretical framework proposes that both proteinopathies arise independently but synergistically potentiate downstream neurodegeneration (Duyckaerts, 2011, Sperling *et al.*, 2014). In fact, recent studies have supported this idea showing that tau modulates the associations between brain amyloid-β and atrophy in preclinical AD (Desikan *et al.*, 2012, Fortea *et al.*, 2014, Sperling *et al.*, 2014), while animal models have demonstrated an interactive effect between amyloid-β and tau peptides, leading to synaptic and neuronal damages (Ittner and Gotz, 2011). Hence, it is plausible to propose that a synergy between amyloid-β and tau is the key element involved in the subsequent metabolic decline in preclinical AD. In Chapter 2, we tested - for the first time - whether the synergistic interaction between, rather than the independent or sequential effects of, amyloid-β PET and CSF p-tau is associated with a 2-year metabolic decline in a population of CN persons.

2.2 Abstract

This study was designed to test the interaction between amyloid-β and tau proteins as a determinant of metabolic decline in preclinical Alzheimer's disease. We assessed 120 cognitively normal individuals with [^{18}F]florbetapir positron emission tomography and cerebrospinal fluid measurements at baseline as well as [^{18}F]fluorodeoxyglucose positron emission tomography at baseline and at 24 months. A voxel-based interaction model was built to test the associations between continuous measurements of cerebrospinal fluid biomarkers, [^{18}F]florbetapir and [^{18}F]fluorodeoxyglucose standardized uptake value ratios. We found that the synergistic interaction between [^{18}F]florbetapir standardized uptake value ratio and cerebrospinal

fluid phosphorylated tau measurements, rather than the sum of their independent effects, was associated with a 24-month metabolic decline in basal and mesial temporal, orbitofrontal, and anterior and posterior cingulate cortices ($p<0.001$). In contrast, interactions using cerebrospinal fluid amyloid-β_{1-42} and total tau biomarkers did not associate with metabolic decline over a time frame of 24 months. The interaction found in this study further support the framework that amyloid-β and hyperphosphorylated tau aggregates synergistically interact to cause downstream Alzheimer's disease neurodegeneration. In fact, the regions displaying the metabolic decline reported here were confined to brain networks affected early by amyloid-β plaques and neurofibrillary tangles. Preventive clinical trials may benefit from using a combination of amyloid-β positron emission tomography and phosphorylated tau biomarkers to enrich study populations of cognitively normal subjects with a high probability of disease progression in studies using [^{18}F]fluorodeoxyglucose as a biomarker of efficacy.

2.3 Introduction

Alzheimer's disease (AD) clinically develops in the context of presymptomatic, mild cognitive impairment and dementia stages and can be quantified in vivo via imaging and fluid biomarkers (Jack *et al.*, 2013). AD pathophysiological process has been modelled as a cascade of progressive neuropathological events initiated by amyloidosis followed by hyperphosphorylated tau accumulation and subsequent structural, functional and cognitive declines (Hardy and Selkoe, 2002, Jack *et al.*, 2013). Recent longitudinal studies have shown that the coexistence of upstream events of the AD cascade predicts downstream structural and functional declines (Jack *et al.*, 2014). For example, Knopman and colleagues have reported that faster structural and metabolic declines are observed in those individuals with abnormal baseline amyloid-β load and

metabolism or hippocampal volume (Knopman *et al.*, 2013). Furthermore, studies conducted in cognitively normal individuals revealed amnestic and non amnestic cognitive declines in individuals with co-occurrence of abnormal amyloid-β load and cerebrospinal fluid (CSF) tau pathology, brain atrophy or hypometabolism (Knopman *et al.*, 2012, Roe *et al.*, 2013, Vos *et al.*, 2013, Mormino *et al.*, 2014).

A conceptual framework proposes that amyloid-β and tau pathologies synergistically potentiates subsequent downstream neurodegeneration (Duyckaerts, 2011). This synergistic framework challenges previous AD pathophysiological theories emphasising amyloid-β or tau pathologies as the major driving forces of disease progression, the so-called baptist and tauist perspectives, respectively (Trojanowski, 2002). In fact, a cross-sectional study conducted in cognitive normal individuals suggested brain atrophy of temporoparietal and occipital cortices as a function of the interaction between abnormal CSF amyloid-$\beta_{1\text{-}42}$ and phosphorylated tau (p-tau) biomarker status (Fortea *et al.*, 2014). Similarly, the deleterious associations between CSF amyloid-$\beta_{1\text{-}42}$ and brain structure or cognition are dependent on the presence of abnormal CSF p-tau levels (Desikan *et al.*, 2011, Desikan *et al.*, 2012). In fact, data supporting molecular synergistic interactions between amyloid-β and tau peptides, leading to downstream toxicity, have been described in the recent animal model literature (Ittner and Gotz, 2011, Chabrier *et al.*, 2014, Khan *et al.*, 2014).

[^{18}F]Fluorodeoxyglucose ([^{18}F]FDG) positron emission tomography (PET) is one of the most important biomarkers in AD research and clinical practice. [^{18}F]FDG abnormalities reflecting focal cerebral hypometabolism constitute a well-validated and sensitive biomarker associated with AD pathophysiology, with potential applications in following disease progression and

assessing the efficacy of disease-modifying interventions (Jagust *et al.*, 2007). Although brain metabolism is vulnerable to AD pathophysiology, the relationship between amyloid-β and tau pathologies as determinants of brain hypometabolism is still unclear. Few longitudinal imaging studies have supported a link, albeit a modest one, between amyloid-β or tau pathology and metabolic decline (Ossenkoppele *et al.*, 2012, Dowling *et al.*, 2015). Although the pathogenic synergism between brain amyloidosis and tau pathology has been postulated as a determinant of AD progression, no previous study so far has tested whether the interactions between amyloid-β and tau pathologies are associated with developing brain hypometabolism.

Here, in a longitudinal study of cognitively normal elderly individuals, we test the hypothesis that [^{18}F]FDG metabolic decline depends on the interaction between, rather than the independent effects of, amyloid-β and tau biomarkers.

2.4 Subjects and Methods

Database description and study participants

Data used in the preparation of this article were obtained from the Alzheimer's Disease Neuroimaging Initiative (ADNI) database (adni.loni.usc.edu). The ADNI was launched in 2003 as a public-private partnership, led by Principal Investigator Michael W. Weiner, MD. The primary goal of ADNI has been to test whether serial magnetic resonance imaging (MRI), PET, other biological markers, and clinical and neuropsychological assessment can be combined to measure the progression of mild cognitive impairment and early AD.

For the present study, we selected cognitively normal subjects who had undergone baseline lumbar puncture and [^{18}F]florbetapir PET imaging, as well as both baseline and 24-month follow-up visits for the [^{18}F]FDG PET. The operational definition of cognitively normal individuals adopted in this study was a mini–mental state examination score of 24 or higher, a clinical dementia rating 0, and absence of any neuropsychiatric diagnosis including mild cognitive impairment and dementia. The inclusion/exclusion criteria adopted by the ADNI are described in detail at www.adni-info.org [accessed January 2016].

CSF analyses

CSF amyloid-$\beta_{1\text{-}42}$, tau phosphorylated at threonine 181 and total tau were quantified using the multiplex xMAP Luminex platform (Luminex Corp, Austin, TX) with INNO-BIA AlzBio3 (Innogenetics) immunoassay kit-based reagents. The CSF biomarker data sets used in this study were obtained from the ADNI files "UPENNBIOMK5-8.csv", and all the biomarkers values for each individual were selected from the same file. Further details of ADNI methods for CSF acquisition and CSF measurement can be found at www.adni-info.org [accessed January 2016].

MRI/PET methods

ADNI MRI and PET standard acquisition protocols are detailed elsewhere (http://adni.loni.usc.edu/methods; accessed January 2016). Imaging analysis methods are summarized in Figure 2-1. T1-weighted MRI images were corrected for field distortions and subsequently processed using the CIVET image-processing pipeline. In summary, images underwent non-uniformity correction, followed by brain masking and segmentation using the Brain Extraction based on nonlocal Segmentation Technique (Eskildsen *et al.*, 2012). Images

were subsequently co-registered using a nine-parameter affine transformation and non-linearly spatially normalized to the MNI 152 reference template. PET images were blurred with a volumetric Gaussian kernel with a full-width half maximum of 8 mm. Subsequently, linear co-registration and non-linear spatial normalization to the MNI 152 template space were performed using the transformation derived from the semiautomatic PET/T1-MRI transformation and anatomical MRI registration for each subject. Voxel-wise, standardized uptake value ratio (SUVR) maps were then generated for [^{18}F]florbetapir using the cerebellum grey matter and the global white matter as reference regions. [^{18}F]FDG SUVR images were generated using the pons as a reference region. A global SUVR value for each subject was estimated from the precuneus as well as from the prefrontal, orbitofrontal, parietal, temporal, anterior and posterior cingulate cortices. Individual [^{18}F]FDG SUVR values were obtained from the region of interest, tailored by voxel-based statistical clusters.

Statistical methods

Statistical analyses were performed using the R Statistical Software Package version 3.0.2 with the RMINC library. RMINC is an imaging package that allows image files in the MINC format to be analysed within the R statistical environment (http://www.r-project.org/; accessed January 2016). The primary endpoint on this study was the rate of metabolic decline defined as:

$$\Delta\%[^{18}\mathrm{F}]FDG = \left(\frac{\text{SUVR Follow up} - \text{SUVR Baseline}}{\text{SUVR Baseline}}\right) * \frac{1}{\Delta\text{Time}} * 100$$

The biomarkers were analyzed using z-scores. Simple linear regression models evaluated the effects of global [^{18}F]florbetapir SUVR or CSF p-tau as single regressors on Δ%[^{18}F]FDG. The

voxel-based interaction model described below was built to test whether main and interactive effects between global [^{18}F]florbetapir SUVR and CSF p-tau are associated with metabolic decline.

$$\Delta\%[^{18}\mathrm{F}]FDG = \beta 0 + \beta 1([^{18}\mathrm{F}]Florbetapir) + \beta_2(p-tau) + \beta_3([^{18}\mathrm{F}]Florbetapir * p-tau) + covariates + error$$

To ensure that our results were not due to issues related to voxel-based analysis, we then isolated the clusters, averaged the SUVRs, and performed the same analysis for each cluster using the averaged SUVRs as the outcomes. The model was adjusted for age, gender and *APOE ε4* status. The statistical parametric maps presented in this study were corrected for multiple testing. Statistical significance was defined using a false discovery rate with a threshold of $p<0.001$.

2.5 Results

Demographics and key sample characteristics are summarized in Table 1. The effects of [^{18}F]florbetapir SUVR or CSF p-tau as single regressors on metabolic decline were not significant in our population. Voxel-based analysis revealed that longitudinal [^{18}F]FDG SUVR decline on basal and mesial temporal, orbitofrontal, anterior and posterior cingulate cortices was driven by the synergistic interaction between [^{18}F]florbetapir SUVR and CSF p-tau measurements (Figure 2-2). While the interaction term was significant (β3), the main effects of [^{18}F]florbetapir SUVR (β1) or CSF p-tau (β2) on 24 months metabolic decline were not significant using our voxel-based regression model.

Subsequently, we examined the interaction between [^{18}F]florbetapir SUVR and CSF p-tau on Δ%[^{18}F]FDG SUVR in the regions revealed by the voxel-based analysis using an averaged SUVR value for each regions of interest. The effect of the interaction on metabolic decline was higher in mesiobasal temporal (slope-coefficient (β3)=−4.42, SE=1.16, p<0.0001) and orbitofrontal (slope-coefficient (β3)=−4.12, SE=1.4, p=0.0002), followed by anterior (slope-coefficient (β3)=−2.77, SE=0.73, p=0.0001) and posterior cingulate (slope-coefficient (β3)=−1.78, SE=0.75, p=0.0009) clusters. The main effects of [^{18}F]florbetapir SUVR or CSF p-tau on metabolic decline were not significant in each of the regions of interest evaluated. This interaction was absent in other brain regions such as the occipital lobe (slope-coefficient (β3)=0.46, SE=1.03, p=0.65) or precuneus (slope-coefficient (β3)=1.18, SE=0.73, p=0.14). Importantly, the interaction between [^{18}F]florbetapir SUVR and CSF p-tau as a function of declines in [^{18}F]FDG was not observed using global [^{18}F]FDG SUVR measurements (slope-coefficient (β3)=−0.51, SE=0.59, p=0.36).

Interestingly, the average global [^{18}F]FDG SUVR decline in our population was 1.6% (95% CI : 0.6% - 2.5%), whereas within the cluster revealed by the interaction analysis in basal and mesial temporal, orbitofrontal, anterior and posterior cingulate cortices the average metabolic decline was 6.1% (95% CI : 4.7% - 6.9%) over 24 months (see Supplementary Figure 1).

In our study population, [^{18}F]florbetapir SUVR was highly correlated with CSF amyloid-β_{1-42} (Spearman's rho=0.68, p<0.0001), while CSF p-tau was highly correlated with CSF total tau (Spearman's rho=0.70, p<0.0001). However, alternative models showed that [^{18}F]FDG SUVR decline was not associated with the interaction between CSF amyloid-β_{1-42} with total tau or p-

tau. Furthermore, [^{18}F]FDG SUVR decline was not associated with the interaction between CSF total tau and [^{18}F]florbetapir SUVR. Similarly, interactions using CSF amyloid-β_{1-42} or total tau biomarkers were not significant in the mesiobasal temporal, orbitofrontal, anterior and posterior cingulate clusters.

Notably, longitudinal brain hypometabolism was independent of APOE ε4 status or its interactions with CSF p-tau (slope-coefficient (β3)=−0.47, SE=1.40, p=0.74), CSF total tau (slope-coefficient (β3)=0.56, SE=1.37, p=0.69), CSF amyloid-β_{1-42} (slope-coefficient (β3)=−0.70, SE=1.26, p=0.58) or [^{18}F]florbetapir SUVR (slope-coefficient (β3)=0.48, SE=1.31, p=0.72).

2.6 Discussion

The present study shows that the synergism between, rather than the sum of independent effects of, continuous brain amyloid-β deposition and p-tau biomarkers drives the rate of metabolic decline in AD related regions in a cognitively normal elderly population. We further found that the interaction between brain amyloid-β deposition and total tau biomarkers did not predict metabolic decline.

The synergistic interaction between brain amyloid-β deposition and CSF p-tau biomarkers concentrations found in our study has to be carefully interpreted from the pathophysiological perspective. In the statistical model proposed, in terms of such interaction within the study population, the density of the brain amyloid-β deposition and CSF concentrations of p-tau synergistically amplify the severity of the subsequent brain hypometabolism. As such,

individuals with the highest baseline concentrations of [^{18}F]florbetapir SUVR and p-tau had the highest rate of metabolic decline in AD related regions over a time frame of 24 months. One might claim that this interaction supports the conceptual framework that amyloid-β and hyperphosphorylated tau aggregates synergistically, rather than independently, potentiate downstream neurodegeneration (Mesulam, 1999, Small and Duff, 2008, Duyckaerts, 2011). The combined effect between amyloid-β and hyperphosphorylated tau has been supported by animal model literature (Ittner *et al.*, 2010). For example, p-tau potentiates amyloid-β induced neurotoxicity (Quintanilla *et al.*, 2014) and molecular interactions between amyloid-β and p-tau have shown to amplify synaptic and neuronal damage in AD (Manczak and Reddy, 2013). Indeed, deleterious interactions between peptide aggregates have already been described in other proteinopathies such as Lewy body disease (alpha-synuclein) (Clinton *et al.*, 2010) and frontal temporal lobar degeneration (TDP-43 inclusions) (Wang *et al.*, 2014).

Fast metabolic decline in mesial temporal regions is not considered part of the normal aging process (Kuhl *et al.*, 1984, Moeller *et al.*, 1996). Indeed, the mesial temporal metabolic decline found in the present study is consistent with the idea that mesial temporal hypometabolism may be an early metabolic abnormality linked to the AD pathophysiological process (Mosconi *et al.*, 2009, Lowe *et al.*, 2014). Furthermore, the hypometabolic areas reported here converge to the brain circuits that are affected early by neurofibrillary tangles and amyloid-β plaques (Braak and Braak, 1991, Delacourte *et al.*, 1999, Thal *et al.*, 2002). Such convergence between metabolic and neuropathological abnormalities in limbic regions further supports a synergism between amyloid-β and tau pathologies leading to hypometabolism. Recently, a hypothetical model in which the interaction between amyloid-β and tau aggregates potentiates mesial temporal synaptic

dysfunction in the preclinical stages of AD has been suggested (Sperling *et al.*, 2014). One may claim that brain amyloid-β measurements represent a proxy of oligomeric amyloid-β (Lesne *et al.*, 2013). As such, the deleterious effects of amyloidosis reported here might be mediated by amyloid-β oligomers rather than fibrillar conformations.

In addition to recent findings supporting the claim that the synergism between brain amyloidosis and neurodegeneration is associated with AD progression (Knopman *et al.*, 2013, Jack *et al.*, 2014), here we demonstrate that [^{18}F]florbetapir PET rather than CSF amyloid-β_{1-42} – and CSF p-tau rather than total tau – better predict mesial temporal metabolic decline. The motivation to explore these effects using amyloid-PET in our study is derived from its close association with Aβ plaques load (Ikonomovic *et al.*, 2008), whereas CSF total tau and p-tau may provide additional information regarding neurodegeneration and neurofibrillary tangles load, respectively (Blennow *et al.*, 2010, Skillback *et al.*, 2015). Therefore, our results support the concept that the interaction between brain amyloid-β plaques and neurofibrillary tangles drives downstream neurodegeneration in early disease stages. Additionally, the better prediction obtained with CSF p-tau as compared with total tau might be explained by the possible higher specificity of p-tau to AD pathophysiology. While high concentrations of p-tau better characterize the AD pathological process (Hampel *et al.*, 2010), abnormal CSF total tau may be found in several brain disorders associated with axonal death and neuronal loss (Brandt *et al.*, 2005). Indeed, two previous studies conducted in ADNI participants also found that CSF p-tau, but not total tau, modulates the link between amyloid-β pathology and brain atrophy or cognitive decline (Desikan *et al.*, 2011, Desikan *et al.*, 2012). Although CSF amyloid-β_{1-42} is considered an effective biomarker for representing disease status, direct measurements of brain amyloid-β deposition, as measured with

amyloid-PET imaging, might be more strongly associated with eminent disease progression in early AD stages (Leuzy *et al.*, 2015, Mattsson *et al.*, 2015). Alternatively, the lack of association of CSF total tau and CSF amyloid-β_{1-42} with metabolic decline may be due to the characteristics of the participants of the study population or the CSF assay.

Clinical insights can be derived from the present results. For example, the combination of abnormalities of CSF p-tau and amyloid-PET biomarkers might serve as a strategy for population enrichment, while [^{18}F]FDG PET may serve as a biomarker of efficacy in disease-modifying clinical trials that focus on individuals in the preclinical stages of AD.

The major methodological strength of the present results constitutes the use of continuous variables in our statistical analysis. In fact, biomarkers are naturally continuous measurements and dichotomization techniques such as establishment of abnormalities thresholds have been constantly debated (Villeneuve *et al.*, 2015) and might not be ideal way to evaluate a disease with a continuous spectrum as Alzheimer's disease. Another strength in our analysis was the conservative multiple comparison correction threshold using a significance level of 0.001 to interpret the data, which helped to avoid false positives results. To the best of our knowledge, this is the first study showing the synergism between amyloidosis and neurodegeneration without assuming a threshold for biomarker abnormalities or artificial dichotomization techniques.

Methodological aspects limit the interpretation and external validity of the present results. It is important to mention that ADNI participants are highly educated; therefore mechanisms of brain and cognitive reserve may play a role in the [^{18}F]FDG PET outcomes reported here (Stern,

2012). The study population is composed of a group of individuals who accepted to participate in a study focusing on AD. Therefore, our population may be a self-selected group of individuals who worry about cognition. It would be highly desirable to replicate these results in a larger population-based cohort. The observations reported here are purely phenomenological and do not intend to prove a biological synergy between amyloidosis and tau pathology. Our statistical model might have captured a sequence of events involving amyloid-β aggregation, and subsequent tau phosphorylation and metabolic decline. Certainly, molecular biology approaches involving cell cultures and in vivo studies combining long-term sequential imaging of amyloid-β, tau and brain metabolism in animal models and in humans could better assess a causal relation between these pathological proteins and brain metabolic decline. We presented the PET data without correcting for partial volume effects. Although partial volume correction had an impact on our SUVR values, this effect did not translate into significant differences in our final results. Previous studies suggest that hypometabolism is more related to *APOE ε4* status than to amyloid-β accumulation (Jagust *et al.*, 2012). Interestingly, we found no interactive effects between *APOE ε4* status and tau biomarkers leading to hypometabolism. However, despite recent evidence suggesting no effect of APOE ε4 status in the metabolism of AD related brain regions in preclinical individuals (Lowe *et al.*, 2014), one should be cautious regarding the influence of APOE ε4 in the present results due to our relatively small sample size to detect genetic influences in early disease stages.

In conclusion, the proposed interaction between amyloid-β and tau supports the idea of a more integrative model of AD, although it does not explicitly refute the baptist or tauist perspectives.

2.7 Tables and Figures

Table 2-1. Demographics and key sample characteristics.

Characteristics	Values
Number of subjects	120
Age, mean, years (SD)	74.9 (6.7)
Males, n (%)	63 (52)
Education, mean (years) (SD)	16.5 (2.6)
MMSE, mean (SD)	29.1 (1.2)
APOE ε4 carriers, n (%)	30 (25)
Follow-up, months, mean (SD)	24.1 (1.7)
CSF p-tau, mean pg/ml (SD)	35.7 (16.5)
CSF total tau, mean pg/ml (SD)	71.9 (34.2)
CSF amyloid-β_{1-42}, mean pg/ml (SD)	199.4 (51.5)
[^{18}F]Florbetapir, mean SUVR (SD)	1.14 (0.14)

CSF=cerebrospinal fluid; MMSE=mini-mental state examination; p-tau=phosphorylated tau; SD=standard deviation; SUVR=standardized uptake value ratio.

Figure 2-1. Summary of image analysis methods.

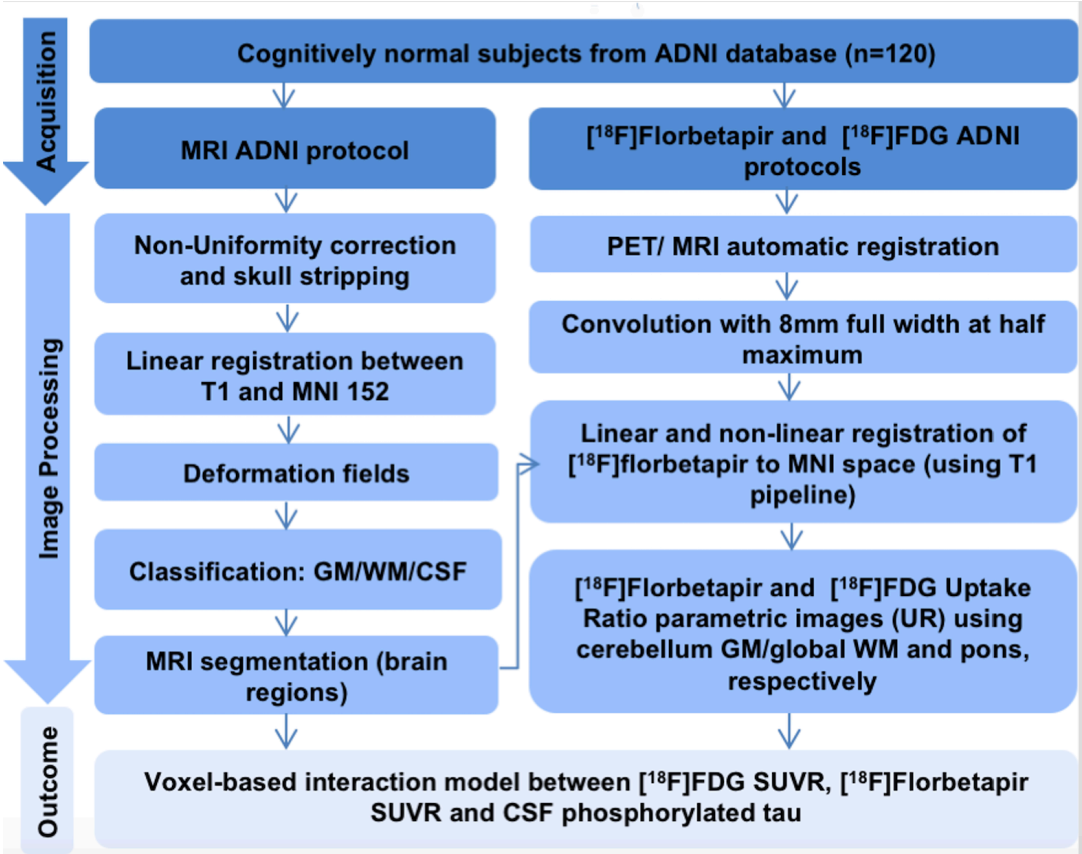

Figure 2-2. Synergistic effect between [^{18}F]florbetapir SUVR and CSF p-tau drives [^{18}F]FDG uptake decline in limbic regions.

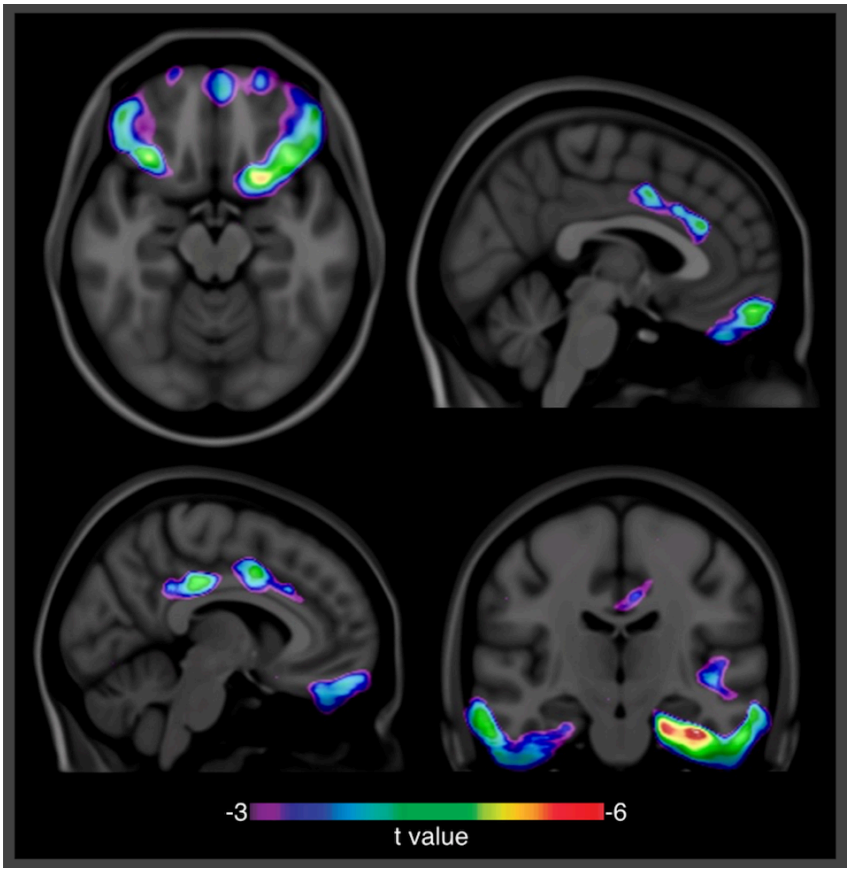

Statistical parametric maps, after correcting for multiple comparisons (false discovery rate corrected at $p<0.001$), overlaid in a structural MRI scan, reveal areas in which 24-month [^{18}F]FDG uptake decline occurs as a function of the interaction between baseline [^{18}F]florbetapir SUVR and CSF p-tau measurements. Significant interactive effects were observed in the basal and mesial temporal, orbitofrontal, and anterior and posterior cingulate cortices. The analysis was corrected for age, gender and *APOE ε4* status.

2.8 Acknowledgments

This work was supported by the Canadian Institutes of Health Research (CIHR) [MOP-11-51-31], the Alan Tiffin Foundation, the Alzheimer's Association [NIRG-12-92090, NIRP-12-259245], the Fonds de Recherche du Québec – Santé, and the PREVENT-AD Research Group. Data collection and sharing for this project was funded by the ADNI (National Institutes of

Health Grant U01 AG024904) and DOD ADNI (Department of Defense award number W81XWH-12-2-0012). ADNI is funded by the National Institute on Aging, the National Institute of Biomedical Imaging and Bioengineering, and through generous contributions from the following: AbbVie, Alzheimer's Association; Alzheimer's Drug Discovery Foundation; Araclon Biotech; BioClinica, Inc.; Biogen; Bristol-Myers Squibb Company; CereSpir, Inc.; Eisai Inc.; Elan Pharmaceuticals, Inc.; Eli Lilly and Company; EuroImmun; F. Hoffmann-La Roche Ltd and its affiliated company Genentech, Inc.; Fujirebio; GE Healthcare; IXICO Ltd.; Janssen Alzheimer Immunotherapy Research & Development, LLC.; Johnson & Johnson Pharmaceutical Research & Development LLC.; Lumosity; Lundbeck; Merck & Co., Inc.; Meso Scale Diagnostics, LLC.; NeuroRx Research; Neurotrack Technologies; Novartis Pharmaceuticals Corporation; Pfizer Inc.; Piramal Imaging; Servier; Takeda Pharmaceutical Company; and Transition Therapeutics. The Canadian Institutes of Health Research is providing funds to support ADNI clinical sites in Canada. Private sector contributions are facilitated by the Foundation for the National Institutes of Health (www.fnih.org). The grantee organization is the Northern California Institute for Research and Education, and the study is coordinated by the Alzheimer's Disease Cooperative Study at the University of California, San Diego. ADNI data are disseminated by the Laboratory for Neuro Imaging at the University of Southern California.

2.9 Supplementary Material

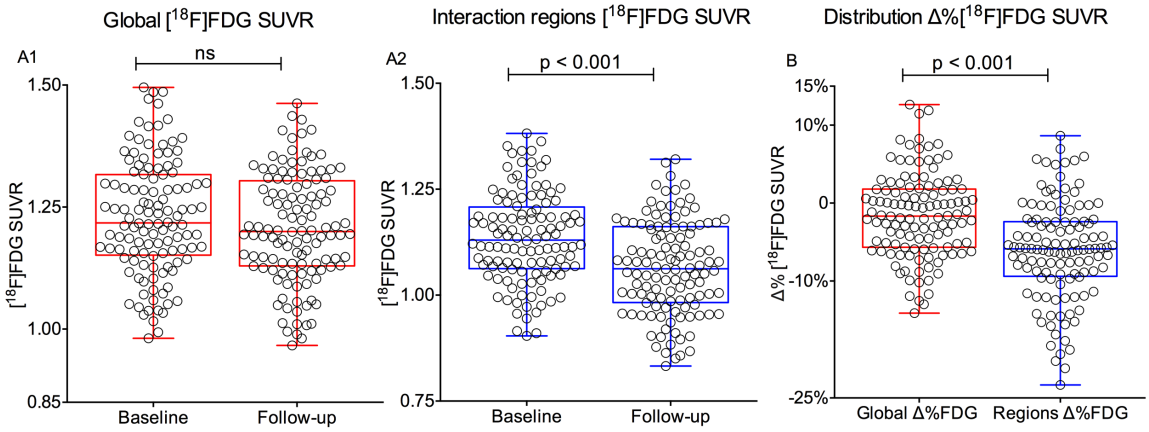

Supplementary Figure 1. The highest rates of [^{18}F]FDG decline were found in regions where the interaction between [^{18}F]florbetapir SUVR and CSF p-tau was determinant to the metabolic decline. In the box and whisker plots, the lower and upper boundaries show the 25th and 75th percentiles, respectively, whereas the horizontal line shows the median. *P* values indicate the values assessed with paired t-test between baseline and 24-month follow-up visits. A1) The dots represent the global [^{18}F]FDG standardized uptake value ratio (SUVR) values for each subject. A2) The dots represent the [^{18}F]FDG SUVR values inside the clusters revealed by the interaction analysis in basal and mesial temporal, orbitofrontal and anterior and posterior cingulate cortices for each subject. B) The dots represent percentage of difference between baseline and 24-month follow-up visits using global [^{18}F]FDG SUVR values (red) and the regions revealed by the interaction analysis (blue) for each subject.

2.10 References

Blennow K, Hampel H, Weiner M, Zetterberg H. Cerebrospinal fluid and plasma biomarkers in Alzheimer disease. Nature reviews Neurology. 2010;6(3):131-44.

Braak H, Braak E. Neuropathological stageing of Alzheimer-related changes. Acta neuropathologica. 1991;82(4):239-59.

Brandt R, Hundelt M, Shahani N. Tau alteration and neuronal degeneration in tauopathies: mechanisms and models. Biochimica et biophysica acta. 2005;1739(2-3):331-54.

Buerger K, Ewers M, Andreasen N, Zinkowski R, Ishiguro K, Vanmechelen E, et al. Phosphorylated tau predicts rate of cognitive decline in MCI subjects: a comparative CSF study. Neurology. 2005;65(9):1502-3.

Chabrier MA, Cheng D, Castello NA, Green KN, LaFerla FM. Synergistic effects of amyloid-beta and wild-type human tau on dendritic spine loss in a floxed double transgenic model of Alzheimer's disease. Neurobiology of disease. 2014;64:107-17.

Clinton LK, Blurton-Jones M, Myczek K, Trojanowski JQ, LaFerla FM. Synergistic Interactions between Abeta, tau, and alpha-synuclein: acceleration of neuropathology and cognitive decline. The Journal of neuroscience : the official journal of the Society for Neuroscience. 2010;30(21):7281-9.

Delacourte A, David JP, Sergeant N, Buee L, Wattez A, Vermersch P, et al. The biochemical pathway of neurofibrillary degeneration in aging and Alzheimer's disease. Neurology. 1999;52(6):1158-65.

Desikan RS, McEvoy LK, Thompson WK, Holland D, Brewer JB, Aisen PS, et al. Amyloid-beta--associated clinical decline occurs only in the presence of elevated P-tau. Archives of neurology. 2012;69(6):709-13.

Desikan RS, McEvoy LK, Thompson WK, Holland D, Roddey JC, Blennow K, et al. Amyloid-beta associated volume loss occurs only in the presence of phospho-tau. Annals of neurology. 2011;70(4):657-61.

Dowling NM, Johnson SC, Gleason CE, Jagust WJ, Alzheimer's Disease Neuroimaging I. The mediational effects of FDG hypometabolism on the association between cerebrospinal fluid biomarkers and neurocognitive function. NeuroImage. 2015;105:357-68.

Duyckaerts C. Tau pathology in children and young adults: can you still be unconditionally baptist? Acta neuropathologica. 2011;121(2):145-7.

Eskildsen SF, Coupe P, Fonov V, Manjon JV, Leung KK, Guizard N, et al. BEaST: brain extraction based on nonlocal segmentation technique. NeuroImage. 2012;59(3):2362-73.

Fortea J, Vilaplana E, Alcolea D, Carmona-Iragui M, Sanchez-Saudinos MB, Sala I, et al. Cerebrospinal fluid beta-amyloid and phospho-tau biomarker interactions affecting brain structure in preclinical Alzheimer disease. Annals of neurology. 2014;76(2):223-30.

Hampel H, Blennow K, Shaw LM, Hoessler YC, Zetterberg H, Trojanowski JQ. Total and phosphorylated tau protein as biological markers of Alzheimer's disease. Experimental gerontology. 2010;45(1):30-40.

Hardy J, Selkoe DJ. The amyloid hypothesis of Alzheimer's disease: progress and problems on the road to therapeutics. Science. 2002;297(5580):353-6.

Ikonomovic MD, Klunk WE, Abrahamson EE, Mathis CA, Price JC, Tsopelas ND, et al. Post-mortem correlates of in vivo PiB-PET amyloid imaging in a typical case of Alzheimer's disease. Brain. 2008;131(Pt 6):1630-45.

Ittner LM, Gotz J. Amyloid-beta and tau--a toxic pas de deux in Alzheimer's disease. Nat Rev Neurosci. 2011;12(2):65-72.

Ittner LM, Ke YD, Delerue F, Bi M, Gladbach A, van Eersel J, et al. Dendritic function of tau mediates amyloid-beta toxicity in Alzheimer's disease mouse models. Cell. 2010;142(3):387-97.

Jack CR, Jr., Knopman DS, Jagust WJ, Petersen RC, Weiner MW, Aisen PS, et al. Tracking pathophysiological processes in Alzheimer's disease: an updated hypothetical model of dynamic biomarkers. The Lancet Neurology. 2013;12(2):207-16.

Jack CR, Jr., Wiste HJ, Knopman DS, Vemuri P, Mielke MM, Weigand SD, et al. Rates of beta-amyloid accumulation are independent of hippocampal neurodegeneration. Neurology. 2014;82(18):1605-12.

Jagust W, Reed B, Mungas D, Ellis W, Decarli C. What does fluorodeoxyglucose PET imaging add to a clinical diagnosis of dementia? Neurology. 2007;69(9):871-7.

Jagust WJ, Landau SM, Alzheimer's Disease Neuroimaging I. Apolipoprotein E, not fibrillar beta-amyloid, reduces cerebral glucose metabolism in normal aging. The Journal of neuroscience : the official journal of the Society for Neuroscience. 2012;32(50):18227-33.

Khan UA, Liu L, Provenzano FA, Berman DE, Profaci CP, Sloan R, et al. Molecular drivers and cortical spread of lateral entorhinal cortex dysfunction in preclinical Alzheimer's disease. Nature neuroscience. 2014;17(2):304-11.

Knopman DS, Jack CR, Jr., Wiste HJ, Weigand SD, Vemuri P, Lowe V, et al. Short-term clinical outcomes for stages of NIA-AA preclinical Alzheimer disease. Neurology. 2012;78(20):1576-82.

Knopman DS, Jack CR, Jr., Wiste HJ, Weigand SD, Vemuri P, Lowe VJ, et al. Selective worsening of brain injury biomarker abnormalities in cognitively normal elderly persons with beta-amyloidosis. JAMA neurology. 2013;70(8):1030-8.

Kuhl DE, Metter EJ, Riege WH, Hawkins RA. The effect of normal aging on patterns of local cerebral glucose utilization. Annals of neurology. 1984;15 Suppl:S133-7.

Lesne SE, Sherman MA, Grant M, Kuskowski M, Schneider JA, Bennett DA, et al. Brain amyloid-beta oligomers in ageing and Alzheimer's disease. Brain : a journal of neurology. 2013;136(Pt 5):1383-98.

Leuzy A, Carter SF, Chiotis K, Almkvist O, Wall A, Nordberg A. Concordance and Diagnostic Accuracy of [11C]PIB PET and Cerebrospinal Fluid Biomarkers in a Sample of Patients with Mild Cognitive Impairment and Alzheimer's Disease. Journal of Alzheimer's disease : JAD. 2015;45(4):1077-88.

Lowe VJ, Weigand SD, Senjem ML, Vemuri P, Jordan L, Kantarci K, et al. Association of hypometabolism and amyloid levels in aging, normal subjects. Neurology. 2014;82(22):1959-67.

Manczak M, Reddy PH. Abnormal interaction of oligomeric amyloid-beta with phosphorylated tau: implications to synaptic dysfunction and neuronal damage. Journal of Alzheimer's disease : JAD. 2013;36(2):285-95.

Mattsson N, Insel PS, Donohue M, Landau S, Jagust WJ, Shaw LM, et al. Independent information from cerebrospinal fluid amyloid-beta and florbetapir imaging in Alzheimer's disease. Brain : a journal of neurology. 2015;138(Pt 3):772-83.

Mesulam MM. Neuroplasticity failure in Alzheimer's disease: bridging the gap between plaques and tangles. Neuron. 1999;24(3):521-9.

Moeller JR, Ishikawa T, Dhawan V, Spetsieris P, Mandel F, Alexander GE, et al. The metabolic topography of normal aging. Journal of cerebral blood flow and metabolism : official journal of the International Society of Cerebral Blood Flow and Metabolism. 1996;16(3):385-98.

Mormino EC, Betensky RA, Hedden T, Schultz AP, Amariglio RE, Rentz DM, et al. Synergistic effect of beta-amyloid and neurodegeneration on cognitive decline in clinically normal individuals. JAMA neurology. 2014;71(11):1379-85.

Mosconi L, Mistur R, Switalski R, Brys M, Glodzik L, Rich K, et al. Declining brain glucose metabolism in normal individuals with a maternal history of Alzheimer disease. Neurology. 2009;72(6):513-20.

Ossenkoppele R, Tolboom N, Foster-Dingley JC, Adriaanse SF, Boellaard R, Yaqub M, et al. Longitudinal imaging of Alzheimer pathology using [11C]PIB, [18F]FDDNP and [18F]FDG PET. European journal of nuclear medicine and molecular imaging. 2012;39(6):990-1000.

Ossenkoppele R, van der Flier WM, Verfaillie SC, Vrenken H, Versteeg A, van Schijndel RA, et al. Long-term effects of amyloid, hypometabolism, and atrophy on neuropsychological functions. Neurology. 2014;82(20):1768-75.

Quintanilla RA, von Bernhardi R, Godoy JA, Inestrosa NC, Johnson GV. Phosphorylated tau potentiates Abeta-induced mitochondrial damage in mature neurons. Neurobiology of disease. 2014;71:260-9.

Roe CM, Fagan AM, Grant EA, Hassenstab J, Moulder KL, Maue Dreyfus D, et al. Amyloid imaging and CSF biomarkers in predicting cognitive impairment up to 7.5 years later. Neurology. 2013;80(19):1784-91.

Skillback T, Farahmand BY, Rosen C, Mattsson N, Nagga K, Kilander L, et al. Cerebrospinal fluid tau and amyloid-beta1-42 in patients with dementia. Brain : a journal of neurology. 2015;138(Pt 9):2716-31.

Small SA, Duff K. Linking Abeta and tau in late-onset Alzheimer's disease: a dual pathway hypothesis. Neuron. 2008;60(4):534-42.

Sperling R, Mormino E, Johnson K. The evolution of preclinical Alzheimer's disease: implications for prevention trials. Neuron. 2014;84(3):608-22.

Stern Y. Cognitive reserve in ageing and Alzheimer's disease. The Lancet Neurology. 2012;11(11):1006-12.

Thal DR, Rub U, Orantes M, Braak H. Phases of A beta-deposition in the human brain and its relevance for the development of AD. Neurology. 2002;58(12):1791-800.

Trojanowski JQ. Tauists, Baptists, Syners, Apostates, and new data. Annals of neurology. 2002;52(3):263-5.

Villeneuve S, Rabinovici GD, Cohn-Sheehy BI, Madison C, Ayakta N, Ghosh PM, et al. Existing Pittsburgh Compound-B positron emission tomography thresholds are too high: statistical and pathological evaluation. Brain : a journal of neurology. 2015.

Vos SJ, Xiong C, Visser PJ, Jasielec MS, Hassenstab J, Grant EA, et al. Preclinical Alzheimer's disease and its outcome: a longitudinal cohort study. The Lancet Neurology. 2013;12(10):957-65.

Wang J, Yan K, Wu ZQ, Zheng CY, Xu RX, Chen LH, et al. TDP-43 interaction with the intracellular domain of amyloid precursor protein induces p53-associated apoptosis. Neuroscience letters. 2014;569:131-6.

Chapter 3: Amyloid and tau signatures of brain metabolic decline in preclinical Alzheimer's disease

Tharick A. Pascoal MD[1], Sulantha Mathotaarachchi MSc[1], Monica Shin MSc[1], Ah Yeon Park, PhD[2], Sara Mohades BSc[1], Andrea L. Benedet MSc[1], Min Su Kang BSc[1], Gassan Massarweh[3], Jean-Paul Soucy MD, MSc[3,4], Serge Gauthier MD, FRCPC[5], and Pedro Rosa-Neto MD, PhD[1,3,,5,6] for the Alzheimer's Disease Neuroimaging Initiative*

[1]Translational Neuroimaging Laboratory, The McGill University Research Centre for Studies in Aging, Montreal, Canada.[2] Statistical laboratory, University of Cambridge, Cambridge, UK. [3]Montreal Neurological Institute, Montreal, Canada. [4]PERFORM Centre, Concordia University, Montreal, Canada. [5]Alzheimer's Disease Research Unit, The McGill University Research Centre for Studies in Aging, Douglas Hospital, McGill University, Montreal, Canada. [6]Department of Neurology and Neurosurgery, McGill University, Montreal, Canada.

Published in The European Journal of Nuclear Medicine and Molecular Imaging. 2018 Jun;45(6):1021-1030 (PMID: 29396637).

3.1 Preface

We placed a special focus on better understanding the progression of CN individuals in the previous chapter because this population is known to present minimal rates of AD-related progression over typical clinical trial periods. This lack of disease-related progression imposes several methodological limitations to test the emerging anti-amyloid or anti-tau therapies in these individuals. Specifically, we demonstrated in the previous chapter that a synergistic interaction between amyloid-β and tau drives metabolic decline over 2 years in CN individuals. These results support a model where amyloid-β and tau arise independently, but when these pathologies reach certain pathological levels, they synergistically interact to determine disease progression. This suggests the existence of amyloid-β and tau pathological thresholds associated with the triggering of this synergy. Likely, these thresholds may provide a better framework for the enrichment of clinical trial populations with CN individuals at the imminence of progression as compared to standard thresholds that indicate only the presence of brain pathologies. Therefore, in Chapter 3, we studied the amyloid-β and tau pathological thresholds associated with triggering their synergy in order to provide a tangible framework to be used in clinical trials focusing on CN individuals.

3.2 Abstract

Purpose: We aimed to determine the amyloid (Aβ) and tau biomarker levels associated with imminent Alzheimer's disease (AD) - related metabolic decline in cognitively normal individuals.

Methods: A threshold analysis was performed in 120 cognitively normal elderly individuals by modelling 2-year declines in brain glucose metabolism measured with [^{18}F]fluorodeoxyglucose ([^{18}F]FDG) as a function of [^{18}F]florbetapir Aβ positron emission tomography (PET) and cerebrospinal fluid phosphorylated-tau biomarker thresholds. Additionally, using a novel

analytical framework capable to perform voxel-wise power calculations, we determined the sample sizes needed to test an estimated 25% drug effect with 80% of power on changes in [^{18}F]FDG uptake over 2 years.

Results: We found that the combination of a [^{18}F]florbetapir standardized uptake value ratio and phosphorylated-tau levels more than one standard deviation higher than their respective thresholds for biomarker abnormality was the best predictor of metabolic decline in preclinical AD. Moreover, we found that a clinical trial using these thresholds would require as little as 100 individuals for testing a 25% drug effect on AD-related metabolic decline over 2 years.

Conclusions: These results highlight the new concept of combined Aβ and tau thresholds predictive of imminent neurodegeneration as an alternative framework with a high statistical power for testing the effect of disease-modifying therapies in [^{18}F]FDG decline over a typical 2-year clinical trial period in preclinical AD.

3.3 Introduction

The preclinical stages of Alzheimer's disease (AD) have become the main focus of therapeutic clinical trials given the assumption that better outcomes can be achieved with changes in the course of the disease before cognitive symptoms (Sperling *et al.*, 2014, Dubois *et al.*, 2016). The International Working Group and the American Alzheimer's Association have recently characterized preclinical AD as the combination of amyloid-β and tau abnormalities in cognitively normal persons(Dubois *et al.*, 2016). Although these individuals have shown greater rates of disease progression than cognitively normal biomarker negative ones, most of them remain stable

over typical clinical trials periods (Holland *et al.*, 2012, Dubois *et al.*, 2016). Therefore, a critical next step proposed by the working groups was to identify, among the preclinical individuals, those with the highest likelihood of disease progression within time frames acceptable for clinical trial designs due to the financial, medical, and ethical considerations (Dubois *et al.*, 2016).

Its slow rate of change makes the use of cognition as the primary outcome of clinical trials using preclinical AD individuals difficult because it imposes prohibitively high sample sizes and long follow-ups (Gauthier *et al.*, 2016). Hence, surrogate measurements of disease progression using established biomarkers of neurodegeneration might provide a useful alternative for such trials(Sperling *et al.*, 2011). In fact, few studies have tested changes in structural magnetic resonance imaging (MRI) as a possible surrogate marker for preclinical AD clinical trials. For example, a recent observation in ADNI has suggested prohibitively large sample size estimates to test changes in structural MRI in preclinical AD individuals enriched using Aβ and tau biomarkers (Holland *et al.*, 2012). In this regard, changes in [^{18}F]fluorodeoxyglucose ([^{18}F]FDG) uptake have been suggested with applications in following disease progression and monitoring therapeutic effects (Edison *et al.*, 2007, Jagust *et al.*, 2007, Fouquet *et al.*, 2009, Bruck *et al.*, 2013, Morbelli *et al.*, 2017, Torosyan *et al.*, 2017). Indeed, [^{18}F]FDG positron emission tomography (PET) is one of the most important biomarkers of AD with applications in the research and clinical settings. However, the characteristics of [^{18}F]FDG as a surrogate variable for preclinical AD clinical trials are scarcely known.

In fact, an inclusion criteria with cognitively normal individuals harboring amyloid-β, tau, and abnormal [^{18}F]FDG uptake could be argued as an interesting strategy for these trials, since they

have a higher probability of developing further neurodegeneration and cognitive symptoms (Dubois *et al.*, 2016). However, it is reasonable to suggest that the absence of baseline neurodegeneration might offer a more favourable pathophysiological scenario for preventive therapies aiming to mitigate disease progression (Sperling *et al.*, 2014).

Recent literature has proposed that Aβ and tau pathologies may arise independently and, at some pathophysiological point, synergistically potentiate imminent neurodegeneration in preclinical AD (Duyckaerts, 2011, Sperling *et al.*, 2014, Pascoal *et al.*, 2016, Pascoal *et al.*, 2016). Notably, this framework infers the existence of thresholds for Aβ and tau pathologies associated with the triggering of their deleterious synergy on neurodegeneration. However, the fact that the majority of the preclinical individuals, Aβ positive plus tau positive, remain pathophysiological stable over long periods suggests that these thresholds are greater than their respective individual thresholds for biomarker abnormality(Dubois *et al.*, 2016). Thus, the determination of the, Aβ and tau, biomarker thresholds associated with imminent neurodegeneration might provide complementary information on preclinical individuals destined to develop AD-related progression.

Here, we tested the hypothesis that the combination of optimized amyloid-β and tau thresholds predictive of neurodegeneration might provide an alternative framework with a high statistical power for testing the efficacy of the emerging disease-modifying therapies. This framework has the potential to select preclinical individuals on the verge of AD-related progression, considering metabolic changes as indices of neurological decline.

3.4 Subjects and Methods

Participants

Data used in the preparation of this article were obtained from the Alzheimer's Disease Neuroimaging Initiative (ADNI) database (adni.loni.usc.edu). The ADNI was launched in 2003 as a public-private partnership, led by Principal Investigator Michael W. Weiner, MD. The primary goal of ADNI has been to test whether serial MRI, PET, other biological markers, and clinical and neuropsychological assessment can be combined to measure the progression of mild cognitive impairment and early Alzheimer's disease. For the present analysis, we selected 120 cognitively normal ADNI participants who underwent cerebrospinal fluid (CSF) phosphorylated-tau (p-tau) and [^{18}F]florbetapir PET at the same baseline visit, as well as [^{18}F]FDG PET at the baseline and at the 2-year follow-up visit.

CSF analysis

CSF p-tau and CSF Aβ were quantified with INNO-BIA AlzBio3 immunoassay using the multiplex xMAP Luminex platform (Luminex Corp, TX). The CSF data used in the analysis were selected from the ADNI files "UPENNBIOMK5-8.csv", and all the values for each subject were obtained from the same file. The standard threshold for p-tau abnormality was based on ADNI published value (>23pg/ml) (Shaw *et al.*, 2009, Toledo *et al.*, 2013). Further details of methods for CSF acquisition and quantification can be found at www.adni-info.org.

MRI/PET

MRI and PET acquisitions followed the ADNI protocols (http://adni.loni.usc.edu/methods). The MRI T1-weighted images underwent non-uniformity correction, brain masking, and segmentation using the Brain Extraction based on nonlocal Segmentation Technique (Eskildsen *et al.*, 2012).

Then, T1-weighted images were processed using the CIVET image-processing pipeline and registered using a nine-parameter affine transformation and non-linearly spatially normalized to the MNI 152 template (Zijdenbos *et al.*, 2002). PET images were smoothed using a volumetric Gaussian kernel with a full-width half maximum of 8 mm. Subsequently, linear registration and nonlinear normalization to the MNI 152 template were performed with the linear and nonlinear transformation derived from the automatic PET to MRI transformation and the individuals anatomical MRI co-registration. [^{18}F]Florbetapir and [^{18}F]FDG standardized uptake value ratio (SUVR) maps were generated using the cerebellum grey matter and the pons as reference regions, respectively(Pascoal *et al.*, 2016). Global PET SUVR values for each subject were estimated from the precuneus, prefrontal, orbitofrontal, parietal, temporal, and cingulate cortices. In our pipeline, 30% of controls were amyloid-β positive using a standard [^{18}F]florbetapir SUVR threshold of 1.15, which is consistent with ADNI publications (Joshi *et al.*, 2012, Landau *et al.*, 2012). Further details regarding our imaging-processing pipeline can be found elsewhere (Pascoal *et al.*, 2016, Pascoal *et al.*, 2016).

Statistical methods

Threshold analysis

We determined the thresholds predictive of metabolic decline by modeling Δ[^{18}F]FDG ($\left(\frac{\text{SUVR Follow up}-\text{SUVR Baseline}}{\text{SUVR Baseline}}\right) * \frac{100}{\Delta\text{Time}}$) as a function of baseline [^{18}F]florbetapir and p-tau thresholds in regions-of-interest. The regions were segmented using the coordinates in the MNI ICBM atlas(Mazziotta *et al.*, 2001), and the threshold analysis was performed using the GraphPad Prism 6.0 software. R-squared and F-test served as the basis of the goodness-of-fit, while the Akaike information criterion (AIC) compared linear and non-linear functions. The non-linear

associations were assumed as sigmoidal, based on literature(Jack *et al.*, 2013), and formulated as follows:

$$Y = a + \left(\frac{b}{1 + \mathrm{e}^{\frac{-(X-c)}{d}}} \right)$$

In this equation, Y is the $\Delta[^{18}\mathrm{F}]$FDG, X is the biomarker threshold, and *a, b, c*, and *d* are the parameters of the fitting, where *a* corresponds to the lower asymptote of the $\Delta[^{18}\mathrm{F}]$FDG at the unit of Y, *b* corresponds to the total change in $\Delta[^{18}\mathrm{F}]$FDG as a function of biomarkers (value between the lower and the upper asymptote) at the unit of Y, *c* is the $\Delta[^{18}\mathrm{F}]$FDG at the inflection point of the curve at the unit of X, and *d* represents the curve steepness. The biomarkers threshold of imminent metabolic decline was defined as the value where the curvatures changed sign (X(*c*)). This point was assumed as the magnitude that needs to be reached by the biomarker for the determination of a significant 2-year metabolic decline.

Group comparison analysis

Group comparisons were performed with analysis of covariance (ANCOVA) using R Statistical Software Package version 3.1 to test for significant differences in metabolic decline between biomarker groups and also in demographic differences between biomarker groups for continuous variables, whereas a chi-square was performed for the categorical ones. The *P* values are presented after correction for multiple comparisons testing using Bonferroni at a significance level of 0.05, and differences in metabolic decline among the biomarker groups were further adjusted for age, gender, education, and *APOEε4* carriage status.

Voxel-wise sample size calculation

A voxel-wise power analysis was performed using MATLAB 15a software with a novel analytical tool adapted to assess the sample size necessary for a clinical trial testing for a drug effect on Δ[^{18}F]FDG at every brain voxel (Mathotaarachchi *et al.*, 2016). To the best of our knowledge, this is the first PET study performing voxel-wise power calculations. The sample calculations estimated the number of subjects required to detect 25% slowing in Δ[^{18}F]FDG for a hypothetical disease-modifying therapy versus placebo with 80% of power at a 5% level (Leung *et al.*, 2010, Grill *et al.*, 2013). The analysis was performed with a well describe formula across the biomarker groups (Benjamini and Hochberg, 1995, Fox *et al.*, 2000, Leung *et al.*, 2010, Grill *et al.*, 2013).

$$\text{sample size (voxel (x, y, z))} = (\partial + \delta)^2 * \frac{2\sigma^2}{(\Delta\mu * \beta)^2}$$

We used ∂=0.842 to power at 80 %, δ=1.96 to test a significance of 5%; $\Delta\mu$ is the average percentage of change in the signal intensity of [^{18}F]FDG; β is the drug effect of 0.25 to reflect the difference in [^{18}F]FDG uptake between drug and placebo groups; σ is the standard deviation (SD) of [^{18}F]FDG changes, and (x, y, z) is each voxel coordinate. Importantly, the parametric images show the regions with a significant metabolic decline over 2 years after correction for multiple comparisons testing using a false discovery rate at $P < 0.001$.

3.5 Results

Threshold analysis

A sigmoidal-shaped curve was the best fit to represent the decline in [^{18}F]FDG over 2 years as a function of [^{18}F]florbetapir thresholds in the mediobasal temporal (R^2=0.98; AIC of 11.83 with

probability of correctness (PC) of 96.57% versus 3.43% for the linear model), orbitofrontal (R^2=0.97; AIC=17.11; PC=99.98%), anterior (R^2=0.97; AIC=1.86; PC=71.68%), and posterior cingulate (R^2=0.97; AIC=6.43; PC=96.13%) cortices. Based on the inflexion point of the preferred sigmoidal model, a curve-fitting threshold analysis on averaged clusters (R^2=0.98; AIC=5.26; PC=93.28%) revealed the optimal [^{18}F]florbetapir threshold predictive of imminent metabolic decline to be at 1.228 (95%CI 1.205–1.253; 1 SD higher than the standard threshold) (Figure 3-1A,B) (Supplementary table 1). Interestingly, although [^{18}F]florbetapir SUVR was highly correlated with CSF Aβ (Spearman's rho=0.68, $P < 0$ .0001), CSF Aβ thresholds did not significantly model the declines in [^{18}F]FDG uptake in the aforementioned regions in our population.

A sigmoidal-shaped curve was the best fit to represent declines in [^{18}F]FDG as a function of p-tau thresholds in the mesiobasal temporal (R^2=0.97; AIC=7.53; PC=97.74%), orbitofrontal (R^2=0.96; AIC=7.88; PC=98%), anterior cingulate (R^2=0.98; AIC=23, PC>99%), posterior cingulate (R^2=0.94; AIC=5.15, PC>96%), and averaged clusters (R^2=0.94; AIC=8; PC=98.23%). Curve-fitting threshold analysis on averaged clusters revealed an inflexion point of 45 pg/ml (95%CI 43.72–47.9; 1.3 SD higher than the standard threshold) (Figure 3-1C, D) (Supplementary table 1).

In addition, we plotted Δ[^{18}F]FDG inside clusters in [^{18}F]florbetapir positive plus p-tau positive groups segregated by using all possible combinations of thresholds for both biomarkers (n=14,400). The 3D plot further supported that preclinical AD individuals defined using progressively higher biomarker thresholds, with both biomarkers levels greater than the thresholds of imminent metabolic decline, had progressively higher rates of Δ[^{18}F]FDG hypometabolism (Figure 3-2).

Group comparison analysis

Applying the new criteria for preclinical AD with standard thresholds(Dubois *et al.*, 2016), out of 120 individuals, 24 (20%) were biomarker negative, 63 (53%) were at risk for AD (only one biomarker abnormality), while 33 (27%) were preclinical AD with both Aβ plus p-tau abnormalities. Using the proposed combination of [^{18}F]florbetapir (SUVR>1.228) and CSF p-tau (>45 pg/ml) thresholds predictive of imminent metabolic decline, out of 33 preclinical individuals 17 (14%) had both biomarkers above thresholds. Importantly, voxel-wise comparison revealed that all the aforementioned biomarker groups did not have any significant difference in [^{18}F]FDG uptake from each other at the baseline visit. Demographics and key sample characteristics of the individuals of population across biomarker groups are summarized in Table 3-1.

ANCOVA in averaged regions further confirmed that individuals with [^{18}F]florbetapir plus p-tau levels above the aforementioned thresholds drove the rate of [^{18}F]FDG decline in the mediobasal temporal, orbitofrontal, anterior, and posterior cingulate cortices in our population (Figure 3-3). The biomarker groups did not present any difference from each other in baseline [^{18}F]FDG uptake inside the averaged regions-of-interest. Interestingly, in the precuneus and the occipital lobe, there were no significant differences in the decline in [^{18}F]FDG uptake across the biomarker groups.

Voxel-wise sample size calculation

A voxel-wise power analysis – free of anatomical assumptions - further confirmed that individuals with both biomarkers above the proposed thresholds offer the best alternative for population enrichment of therapeutic trials using changes in voxel-wise [^{18}F]FDG over 2 years as a surrogate variable, requiring as little as 50 individuals per trial arm in large clusters in the orbitofrontal,

anterior and posterior cingulate, mediobasal and lateral temporal cortices (Figure 3-4).

Additionally, to ensure that the results of our voxel-wise power calculation were not due to any issues related to the voxel-wise approach, we averaged the SUVR values inside segregated regions and performed the same analyses for each region using these averaged SUVRs as the outcome (Supplementary table 2). Using averaged Δ[^{18}F]FDG in the mediobasal temporal cortex as surrogate, a study enriched with the combination of the proposed thresholds ([^{18}F]florbetapir SUVR>1.228 and p-tau >45 pg/ml) would require 87 preclinical AD individuals per trial arm for testing a 25% drug effect (80% of power at a 5% level) over 2 years. On the other hand, a clinical trial using the concept of preclinical AD with standard thresholds ([^{18}F]florbetapir SUVR>1.15 and p-tau >23 pg/ml) would require 416 individuals per arm, whereas a trial with not enrichment strategy would require 738 individuals per arm.

3.6 Discussion

In summary, our results suggest that the Aβ and tau thresholds associated with imminent AD-related metabolic decline in preclinical AD are higher than their respective thresholds of biomarker abnormality. In addition, we showed that an inclusion criterion based on these thresholds and the use of voxel-wise changes in [^{18}F]FDG as a surrogate constitute an alternative framework with a high statistical power for a 2-year long clinical trials in preclinical AD.

Overall, we propose here the new concept of amyloid-β and tau thresholds of imminent neurodegeneration as a valuable asset for the enrichment of clinical trials with preclinical individuals with a high probability of developing AD-related neurodegeneration within short time

frames. Specifically, we demonstrated that a 2-year long clinical trial using brain Aβ plus CSF p-tau thresholds more than one standard deviation higher than their standard values for enrichment and regional [^{18}F]FDG as a surrogate would require as little as 100 cognitively normal individuals for testing a hypothetical 25% drug effect. These results contrast with a recent study performed in ADNI preclinical AD individuals defined as Aβ positive plus tau positive which found that a clinical trial would require more than 2,000 individuals for testing a hypothetical 25% drug effect with 80% of power on 2-year changes in cognition or structural MRI (Holland *et al.*, 2012). It is important to emphasize that the thresholds proposed here are based on dynamic biomarker changes and indicate metabolic decline over short time frames, rather than the presence or absence of pathological proteinopathies, which is best assessed with post-mortem correlations (Villeneuve *et al.*, 2015). It is also important to mention that in our understanding the term "biomarker abnormality" refers to the presence of brain pathology and should be defined by the thresholds that better associate with post-mortem studies. Within the biomarker abnormality spectrum, we suggest the existence of thresholds of imminent disease progression, which will select among the individual with biomarker abnormality the ones with the highest probability of progression to a given outcome.

Since the proposed model optimizes neurodegeneration as a function of amyloid-β and tau levels, we may argue that this model has immediate applicability to provide a framework with a high statistical power for the emerging anti-tau and anti-amyloid therapies. Interestingly, the highest rates of metabolic decline presented by the preclinical AD individuals were found in the limbic structures within the cingulate, orbitofrontal, medial and basal temporal cortices. Importantly, this pattern of metabolic dysfunction is not considered part of the normal aging (Kuhl *et al.*, 1984,

Moeller *et al.*, 1996). In fact, metabolic decline in limbic structures has been proposed as an early abnormality associated with AD (Mosconi *et al.*, 2009, Lowe *et al.*, 2014). In addition, the fact that this brain circuit is affected by tangles or plaques (Kuhl *et al.*, 1984, Moeller *et al.*, 1996), rather than by the normal aging process (Braak and Braak, 1991, Delacourte *et al.*, 1999, Thal *et al.*, 2002), further supports the notion that cognitive normal subjects with these baseline biomarker signatures are on the AD pathway. Interestingly, in contrast with [^{18}F]florbetapir, CSF Aβ levels failed in modeling imminent metabolic decline in our population, which is in line with previous observation showing that Aβ PET better depicts metabolic decline as compared to CSF Aβ in this preclinical AD population (Pascoal *et al.*, 2016). Although CSF Aβ well-represents the disease status, brain fibrillar Aβ deposition seems to be better associated with imminent disease progression (Mattsson *et al.*, 2015, Pascoal *et al.*, 2016).

Declines in [^{18}F]FDG as a function of the hallmark AD proteins were best described by a sigmoidal rather than a linear association. This pattern of relationship is consistent with the most accepted models of AD progression(Jack *et al.*, 2013), which assume "ceiling effects" of amyloid-β and tau. Therefore, our results further emphasize that this "ceiling effect" should be considered in studies testing the relationship between these proteinopathies and downstream neurodegeneration. For example, studies using linear functions for testing the association between proteins and brain hypometabolism in AD patients might not find any correlation(Furst *et al.*, 2012), since it is likely that most of demented patients have already reached the plateau of the relationship.

Methodological aspects limit the external validity of the present results. Our population is

composed of self-selected individuals and might not represent the general elderly cognitively normal population. Therefore, it would be highly desirable to replicate our results in a larger population-based study. However, it is important to mention that the use of a conservative multiple comparison correction thresholds at 0.001 helped to avoid false positives results in our analysis. It is also important to emphasize that change in cognition is always the most desirable outcome for a therapeutic clinical trial aiming to mitigate AD progression. However, due to the methodological limitations for the use of cognition in preclinical AD and the advance of *in vivo* biomarkers, the increase of our understanding regarding to the use of brain imaging as surrogate is the paramount importance. Importantly, preclinical AD individuals in this study are referred to as those with normal cognition but Aβ and tau abnormalities rather than those who will certainly develop dementia over time. The 2-year follow-up is not sufficient to derive definite conclusions regarding the clinical progression from cognitively normal to dementia. Partial volume correction did not translate into differences in our final results; therefore, we presented the PET data without corrections for volume effects. Biomarker thresholds are invariably subject to idiosyncrasies and as such might change slightly depending on the analytical method. However, according to our results, it is expected that biomarker levels predictive of rapid metabolic decline would be at least 1 SD higher than the threshold for the presence of brain pathology in an elderly cognitively normal population. Notably, it is expected that the thresholds associated with imminent disease progression will be invariably higher than the ones used to determine an abnormal biomarker status. It is important to mention that the use of a hypothetical drug effect of 25% used in our analysis was same as the one used in previous AD literature (Fox *et al.*, 2000, Leung *et al.*, 2010, Holland *et al.*, 2012, Grill *et al.*, 2013). Although study enrichment with two biomarker modalities might potentially have a high economical cost, it is important to emphasize that an increasingly large number of observational studies performing multiple biomarkers for Aβ and tau have

already been proposed to serve as a screening tool to select individuals for therapeutic trials. Despite the lack of current effective disease-modify therapy available for AD, the promising recent results of anti-Aβ drugs such as Aducanumab suggest the need for sensitive frameworks to detect disease progression in the near future.

To conclude, our results highlight that Aβ and tau biomarker thresholds associated with imminent neurodegeneration are higher than their respective thresholds for abnormality. In addition, the determination of these thresholds may provide complementary information for selecting preclinical AD individuals that most likely will pathophysiologically progress over time frames compatible with clinical trials.

3.7 Tables and Figures

Table 3-1. Demographics and key characteristics of the population across biomaker groups.

Characteristic	Biomarkers negative	At risk for AD	Preclinical AD bellow thresholds	Preclinical AD above thresholds	*P* value
No. (n)	24	63	16	17	
Age, mean (years) (SD)	75.1 (7.4)	73.9 (6.1)	74.9 (6.2)	78.6 (5.1)	0.37
Male, No. (%)	14 (58)	35 (55)	7 (44)	7 (42)	0.3
Education, mean (years) (SD)	17.7 (2.5)	16.3 (2.9)	15.6 (2.4)	16.7 (2.5)	0.6
MMSE baseline, mean (SD)	29.1 (1.4)	29.2(0.96)	28.9 (0.97)	29 (0.92)	0.81
MMSE follow-up, mean (SD)	29 (1.6)	29 (1.1)	28.4 (1.9)	28.6 (1.3)	0.27
APOE ε4 carriage, no. (%)	1 (4)	17 (27)	6 (38)	6 (35)	0.06
P-tau, mean (pg/ml) (SD)	9.3 (2.9)	35.8(14.8)*	36.5 (8.9)*	56.4 (15.8)*	< 0.001
[^{18}F]Florbetapir, mean (SUVR) (SD)	1 (0.03)	1.12 (1)*	1.25 (0.08)*	1.35 (0.07)*	< 0.001
Follow-up, mean (months) (SD)	24.3 (0.98)	23.8 (0.9)	24.1 (1.8)	24 (0.7)	0.53
	Diagnostic at follow-up visit, no. (%)				
Cognitively normal, No. (%)	22 (91)	55 (87.5)	14 (88)	12 (71)	—
MCI, No. (%)	2 (9)	7 (11)	2 (12)	5 (29)	0.2
Dementia, No. (%)	0	1 (1.5)	0	0	—

P values indicate the values assessed with analyses of variance (ANCOVA) for each variable except gender, *APOE ε4*, and diagnostic at follow-up, where a chi-square test was performed. *Post-hoc analysis provided significant differences from the biomarkers negative group. AD =

Alzheimer's disease; MCI = mild cognitive impairment; MMSE = mini-mental state examination; p-tau = phosphorylated tau; SD = standard deviation; SUVR = standardized uptake value ratio.

Figure 3-1. Aβ and tau thresholds associated with imminent metabolic decline are higher than their standard thresholds for biomarker abnormality.

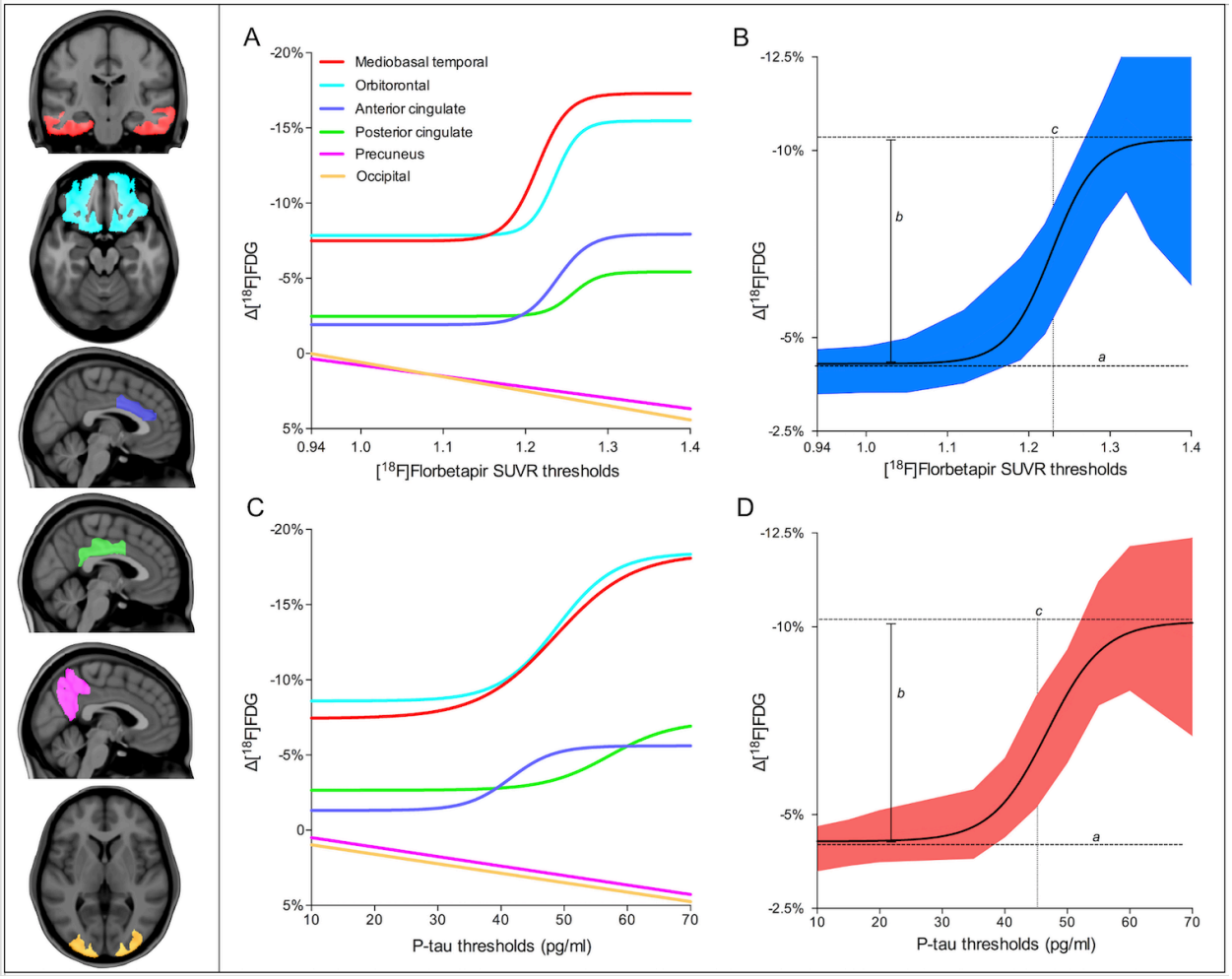

Curves represent changes in [^{18}F]FDG uptake over 2 years within anatomically segregated clusters as a function of baseline [^{18}F]florbetapir SUVR and CSF p-tau thresholds. (**A**) As a function of [^{18}F]florbetapir thresholds, [^{18}F]FDG decline fitted a sigmoidal-shaped curve in the mediobasal temporal (R^2=0.98), orbitofrontal (R^2=0.97), and anterior (R^2=0.97) and posterior cingulate (R^2 = 0.97) cortices. (**B**) In the average clusters, the inflexion point of [^{18}F]FDG decline was at [^{18}F]florbetapir SUVR of 1.228 (R^2 = 0.98; 95% CI 1.205 – 1.253). (**C**) As a function of CSF p-tau thresholds, [^{18}F]FDG decline fitted a sigmoidal-shaped curve in the mesiobasal temporal (R^2=0.97), orbitofrontal (R^2=0.96), and anterior (R^2=0.98) and posterior cingulate (R^2=0.94) cortices. (**D**) The inflexion point of the sigmoidal curve in the averaged clusters was a CSF p-tau of 45 pg/ml (95% CI 43.72 – 47.9). Notably, clusters in the precuneus or occipital lobe did not have any linear or sigmoidal association with biomarker thresholds. In the curves, *a*

corresponds to the lower asymptote, *b* corresponds the total change in Δ[^{18}F]FDG, while *c* is the Δ[^{18}F]FDG at the inflexion point of the curve.

Figure 3-2. Preclinical AD groups defined with progressively higher Aβ and tau thresholds, with both biomarker levels greater than the ones of imminent metabolic decline, had progressively higher rates of [^{18}F]FDG hypometabolism.

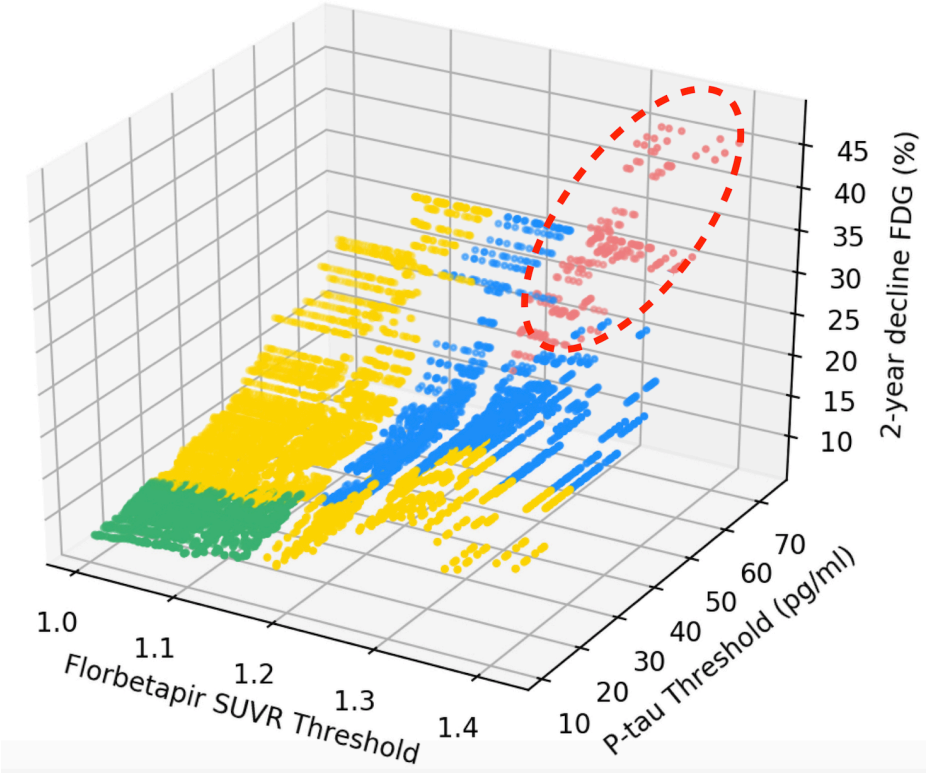

The dots in the 3D plot represent the mean of metabolic decline in clusters over 2 years in Aβ positive plus p-tau positive groups segregated by using all possible combinations (n=14,400) of threshold values for [^{18}F]florbetapir SUVR and CSF p-tau. The groups, segregated using both biomarker thresholds lower than the standard values (green), only one biomarker threshold higher than the standard thresholds (yellow), or both biomarker thresholds higher than the standard values with at least one lower than the thresholds (blue) of imminent metabolic decline did not have a significant 2-year decline in [^{18}F]FDG uptake. On the other hand, Aβ positive plus p-tau positive groups segregated by using both thresholds equal to or higher than the proposed thresholds showed progressively higher rates of metabolic decline with the progressive increase of the biomarker threshold values (red).

Figure 3-3. Preclinical AD individuals segregated using the optimized Aβ and tau thresholds drove the rate of 2-year AD-related metabolic decline in the cognitively normal population.

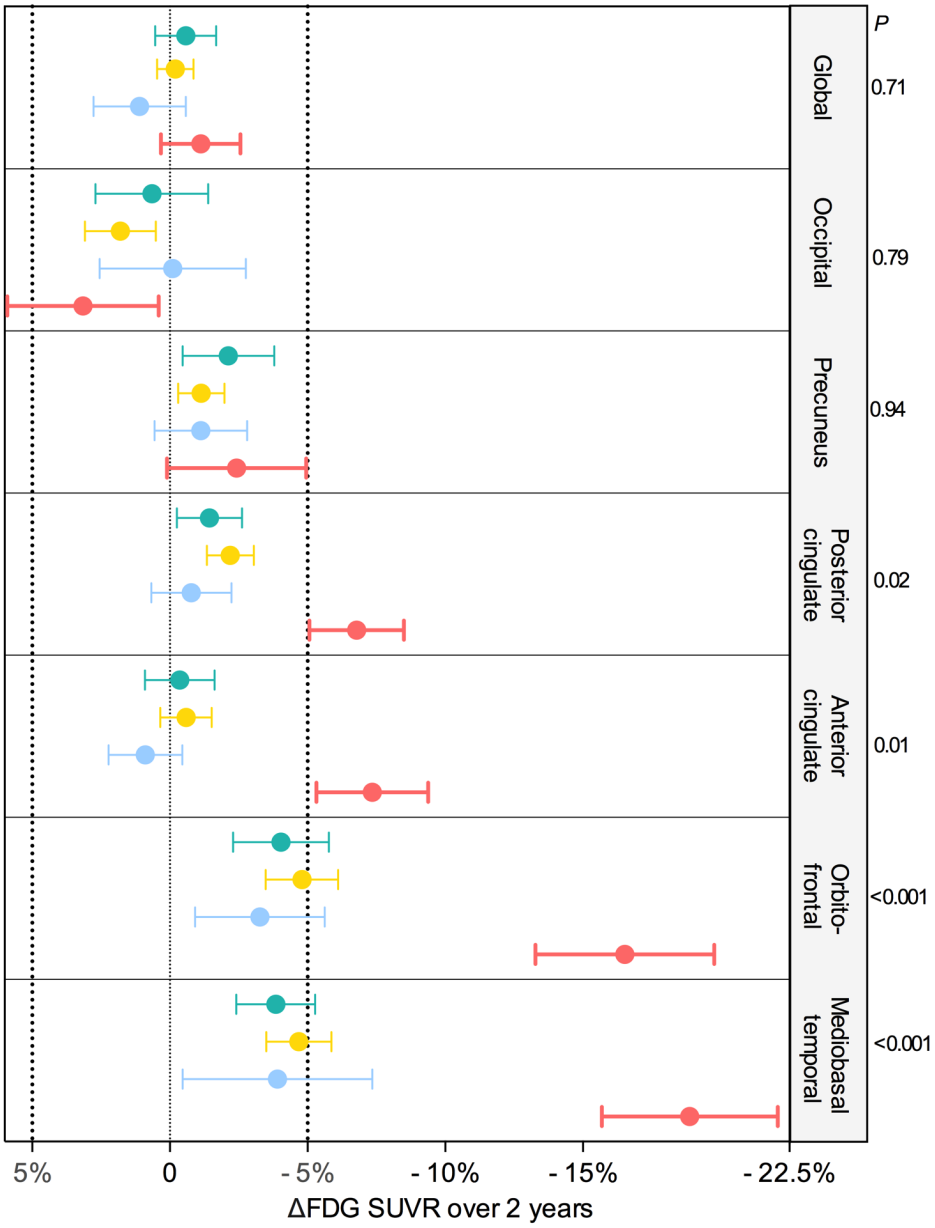

ANCOVA confirmed that preclinical AD individuals defined with the combination of optimized thresholds for [^{18}F]florbetapir (SUVR>1.23) and p-tau (>45 pg/ml) biomarkers (n=17, red) drove the 2-year rate of [^{18}F]FDG uptake decline in the mediobasal temporal, orbitofrontal, and cingulate cortices in our cognitively normal population. It is important to emphasise that preclinical AD individuals with at least one of the biomarkers below the aforementioned thresholds (n=16, blue) had declines in [^{18}F]FDG not different from biomarkers negative (n=24, green) and at risk for AD (n=63, yellow) groups. The analyses were adjusted for age, gender, *APOE ε4* carriage status, and *Bonferroni* corrected at a significance level of 0.05.

Figure 3-4. Voxel-wise power analysis confirmed that preclinical AD defined with the thresholds predictive of imminent metabolic decline offers a robust framework with a high statistical power for the population enrichment of clinical trials using regional Δ[^{18}F]FDG as a surrogate variable.

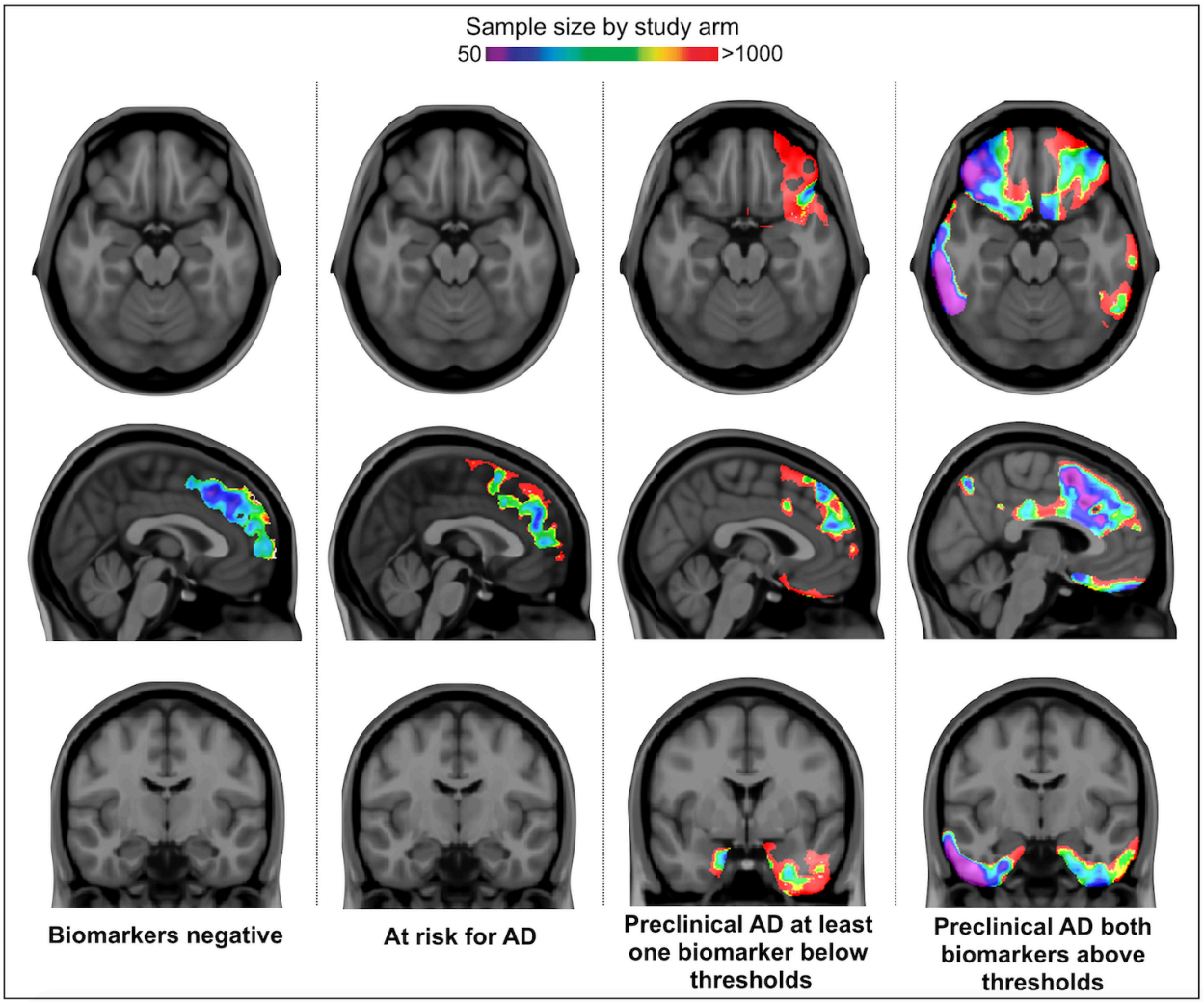

The parametric maps represent the voxel-wise sample size calculation, overlaid in a structural MRI scan, in the regions with a significant decline in [^{18}F]FDG uptake in each biomarker group after the multiple comparison correction (false discovery rate at $P < 0.001$). The maps confirmed that individuals with both biomarkers above the threshold of imminent metabolic decline provided the best framework to test a 25% drug effect on changes in [^{18}F]FDG, requiring a sample as small as 50 individuals per trial arm in large clusters in mediobasal temporal, cingulate, and orbitofrontal cortices.

3.8 Acknowledgements

This work was supported by the Canadian Institutes of Health Research (CIHR; MOP-11-51-31), the Alan Tiffin Foundation, the Alzheimer's Association (NIRG-12- 92090, NIRP-12-259245), Prevent-AD scholarship (T.A.P.), Fonds de Recherche du Québec – Santé (FRQS; Chercheur Boursier, P.R-N.), S.G. and P.R-N. are members of the CIHR-CCNA Canadian Consortium of Neurodegeneration in Aging. Data collection and sharing for this project was funded by the Alzheimer's Disease Neuroimaging Initiative (ADNI; National Institutes of Health Grant U01 AG024904) and DOD ADNI (Department of Defense award number W81XWH-12-2-0012). ADNI is funded by the National Institute on Aging, the National Institute of Biomedical Imaging and Bioengineering and through generous contributions from the following: AbbVie, Alzheimer's Association; Alzheimer's Drug Discovery Foundation; Araclon Biotech; BioClinica; Biogen; Bristol–Myers Squibb Company; CereSpir; Eisai Inc.; Elan Pharmaceuticals; Eli Lilly and Company; EuroImmun; F. Hoffmann-La Roche and its affiliated company Genentech; Fujirebio; GE Healthcare; IXICO; Janssen Alzheimer Immunotherapy Research & Development; Johnson & Johnson Pharmaceutical Research & Development; Lumosity; Lundbeck; Merck; Meso Scale Diagnostics; NeuroRx Research; Neurotrack Technologies; Novartis Pharmaceuticals Corporation; Pfizer; Piramal Imaging; Servier; Takeda Pharmaceutical Company; and Transition Therapeutics. The Canadian Institutes of Health Research is providing funds to support ADNI clinical sites in Canada. Private sector contributions are facilitated by the Foundation for the National Institutes of Health (www.fnih.org). The grantee organization is the Northern California Institute for Research and Education, and the study is coordinated by the Alzheimer's Disease Cooperative Study at the University of California, San Diego. ADNI data are disseminated by the Laboratory for Neuro Imaging at the University of Southern California.

3.9 Supplementary Material

Supplementary Table 1. [^{18}F]FDG uptake decline as a function of baseline [18F]florbetapir SUVR and CSF p-tau thresholds best fitted a sigmoidal function in AD-related regions.

[^{18}F]Florbetapir SUVR						
Δ[^{18}F]FDG	Probability of correctness (%)		R^2		AIC	*P* value
	Linear	Sigmoid	Linear	Sigmoid		
Mediobasal temporal	3.43	96.57	0.85	0.98	11.83	<0.001
Orbitofrontal	0.02	99.98	0.77	0.97	17.11	<0.001
Anterior Cingulate	28.32	71.68	0.62	0.97	1.857	<0.001
Posterior Cingulate	3.87	96.13	0.83	0.94	6.432	<0.001

CSF p-tau						
Δ[^{18}F]FDG	Probability of correctness (%)		R^2		AIC	*P* value
	Linear	Sigmoid	Linear	Sigmoid		
Mediobasal temporal	2.26	97.74	0.89	0.97	7.531	<0.001
Orbitofrontal	2	98	0.86	0.96	7.885	<0.001
Anterior Cingulate	0.6	99.4	0.87	0.98	23	<0.001
Posterior Cingulate	3.8	96.2	0.77	0.94	5.15	<0.001

Sigmoidal model was the better fit for mediobasal temporal, orbitofrontal, anterior and posterior cingulate cortices when compared with the linear analyses. No linear or sigmoidal functions significantly fitted in the precuneus and occipital cortices. AIC=Akaike information criterion; CSF=cerebrospinal fluid, FDG=fluorodeoxyglucose, p-tau=phosphorylated tau, SUVR=standardized uptake value ratio.

Supplementary table 2. Required sample sizes per arm for a 2-year clinical trial using changes in [^{18}F]FDG SUVR uptake in averaged regions-of-interest as a surrogate variable.

Enrichment strategy	Mediobasal temporal	Orbito-frontal	Posterior cingulate	Anterior cingulate	Global
None	738	987	2300	7330	*No decline
Aβ+	567	1162	1739	4150	*No decline
P-tau+	605	761	1728	5965	*No decline
Aβ+/ p-tau+	416	724	1356	2232	*No decline
Aβ+/ p-tau+ (above thresholds)	87	369	581	542	4520

Aβ=amyloid-β, FDG=fluorodeoxyglucose, p-tau=phosphorylated tau, SUVR=standardized uptake value ratio. * No decline in mean [^{18}F]FDG uptake over 2 years follow-up.

3.10 References

Benjamini Y, Hochberg Y. Controlling the false discovery rate: a practical and powerful approach to multiple testing. Journal of the royal statistical society Series B (Methodological). 1995:289-300.

Braak H, Braak E. Neuropathological stageing of Alzheimer-related changes. Acta neuropathologica. 1991;82(4):239-59.

Bruck A, Virta JR, Koivunen J, Koikkalainen J, Scheinin NM, Helenius H, et al. [11C]PIB, [18F]FDG and MR imaging in patients with mild cognitive impairment. European journal of nuclear medicine and molecular imaging. 2013;40(10):1567-72.

Delacourte A, David JP, Sergeant N, Buee L, Wattez A, Vermersch P, et al. The biochemical pathway of neurofibrillary degeneration in aging and Alzheimer's disease. Neurology. 1999;52(6):1158-65.

Dubois B, Hampel H, Feldman HH, Scheltens P, Aisen P, Andrieu S, et al. Preclinical Alzheimer's disease: Definition, natural history, and diagnostic criteria. Alzheimer's & dementia : the journal of the Alzheimer's Association. 2016;12(3):292-323.

Duyckaerts C. Tau pathology in children and young adults: can you still be unconditionally baptist? Acta neuropathologica. 2011;121(2):145-7.

Edison P, Archer HA, Hinz R, Hammers A, Pavese N, Tai YF, et al. Amyloid, hypometabolism, and cognition in Alzheimer disease: an [11C]PIB and [18F]FDG PET study. Neurology. 2007;68(7):501-8.

Eskildsen SF, Coupe P, Fonov V, Manjon JV, Leung KK, Guizard N, et al. BEaST: brain extraction based on nonlocal segmentation technique. NeuroImage. 2012;59(3):2362-73.

Fouquet M, Desgranges B, Landeau B, Duchesnay E, Mezenge F, de la Sayette V, et al. Longitudinal brain metabolic changes from amnestic mild cognitive impairment to Alzheimer's disease. Brain : a journal of neurology. 2009;132(Pt 8):2058-67.

Fox NC, Cousens S, Scahill R, Harvey RJ, Rossor MN. Using serial registered brain magnetic resonance imaging to measure disease progression in Alzheimer disease: power calculations and estimates of sample size to detect treatment effects. Archives of neurology. 2000;57(3):339-44.

Furst AJ, Rabinovici GD, Rostomian AH, Steed T, Alkalay A, Racine C, et al. Cognition, glucose metabolism and amyloid burden in Alzheimer's disease. Neurobiology of aging. 2012;33(2):215-25.

Gauthier S, Albert M, Fox N, Goedert M, Kivipelto M, Mestre-Ferrandiz J, et al. Why has therapy development for dementia failed in the last two decades? Alzheimer's & dementia : the journal of the Alzheimer's Association. 2016;12(1):60-4.

Grill JD, Di L, Lu PH, Lee C, Ringman J, Apostolova LG, et al. Estimating sample sizes for predementia Alzheimer's trials based on the Alzheimer's Disease Neuroimaging Initiative. Neurobiology of aging. 2013;34(1):62-72.

Holland D, McEvoy LK, Desikan RS, Dale AM, Alzheimer's Disease Neuroimaging I. Enrichment and stratification for predementia Alzheimer disease clinical trials. PloS one. 2012;7(10):e47739.

Jack CR, Jr., Knopman DS, Jagust WJ, Petersen RC, Weiner MW, Aisen PS, et al. Tracking pathophysiological processes in Alzheimer's disease: an updated hypothetical model of dynamic biomarkers. The Lancet Neurology. 2013;12(2):207-16.

Jagust W, Reed B, Mungas D, Ellis W, Decarli C. What does fluorodeoxyglucose PET imaging add to a clinical diagnosis of dementia? Neurology. 2007;69(9):871-7.

Joshi AD, Pontecorvo MJ, Clark CM, Carpenter AP, Jennings DL, Sadowsky CH, et al. Performance characteristics of amyloid PET with florbetapir F 18 in patients with alzheimer's disease and cognitively normal subjects. Journal of nuclear medicine : official publication, Society of Nuclear Medicine. 2012;53(3):378-84.

Kuhl DE, Metter EJ, Riege WH, Hawkins RA. The effect of normal aging on patterns of local cerebral glucose utilization. Annals of neurology. 1984;15 Suppl:S133-7.

Landau SM, Mintun MA, Joshi AD, Koeppe RA, Petersen RC, Aisen PS, et al. Amyloid deposition, hypometabolism, and longitudinal cognitive decline. Annals of neurology. 2012;72(4):578-86.

Leung KK, Clarkson MJ, Bartlett JW, Clegg S, Jack CR, Jr., Weiner MW, et al. Robust atrophy rate measurement in Alzheimer's disease using multi-site serial MRI: tissue-specific intensity normalization and parameter selection. NeuroImage. 2010;50(2):516-23.

Lowe VJ, Weigand SD, Senjem ML, Vemuri P, Jordan L, Kantarci K, et al. Association of hypometabolism and amyloid levels in aging, normal subjects. Neurology. 2014;82(22):1959-67.

Mathotaarachchi S, Wang S, Shin M, Pascoal TA, Benedet AL, Kang MS, et al. VoxelStats: A MATLAB Package for Multi-Modal Voxel-Wise Brain Image Analysis. Front Neuroinform. 2016;10:20.

Mattsson N, Insel PS, Donohue M, Landau S, Jagust WJ, Shaw LM, et al. Independent information from cerebrospinal fluid amyloid-beta and florbetapir imaging in Alzheimer's disease. Brain : a journal of neurology. 2015;138(Pt 3):772-83.

Mazziotta J, Toga A, Evans A, Fox P, Lancaster J, Zilles K, et al. A probabilistic atlas and reference system for the human brain: International Consortium for Brain Mapping (ICBM). Philos Trans R Soc Lond B Biol Sci. 2001;356(1412):1293-322.

Moeller JR, Ishikawa T, Dhawan V, Spetsieris P, Mandel F, Alexander GE, et al. The metabolic topography of normal aging. Journal of cerebral blood flow and metabolism : official journal of the International Society of Cerebral Blood Flow and Metabolism. 1996;16(3):385-98.

Morbelli S, Bauckneht M, Arnaldi D, Picco A, Pardini M, Brugnolo A, et al. 18F-FDG PET diagnostic and prognostic patterns do not overlap in Alzheimer's disease (AD) patients at the mild cognitive impairment (MCI) stage. European journal of nuclear medicine and molecular imaging. 2017.

Mosconi L, Mistur R, Switalski R, Brys M, Glodzik L, Rich K, et al. Declining brain glucose metabolism in normal individuals with a maternal history of Alzheimer disease. Neurology. 2009;72(6):513-20.

Pascoal TA, Mathotaarachchi S, Mohades S, Benedet AL, Chung CO, Shin M, et al. Amyloid-beta and hyperphosphorylated tau synergy drives metabolic decline in preclinical Alzheimer's disease. Mol Psychiatry. 2016.

Pascoal TA, Mathotaarachchi S, Shin M, Benedet AL, Mohades S, Wang S, et al. Synergistic interaction between amyloid and tau predicts the progression to dementia. Alzheimer's & dementia : the journal of the Alzheimer's Association. 2016.

Shaw LM, Vanderstichele H, Knapik-Czajka M, Clark CM, Aisen PS, Petersen RC, et al. Cerebrospinal fluid biomarker signature in Alzheimer's disease neuroimaging initiative subjects. Annals of neurology. 2009;65(4):403-13.

Sperling R, Mormino E, Johnson K. The evolution of preclinical Alzheimer's disease: implications for prevention trials. Neuron. 2014;84(3):608-22.

Sperling RA, Aisen PS, Beckett LA, Bennett DA, Craft S, Fagan AM, et al. Toward defining the preclinical stages of Alzheimer's disease: recommendations from the National Institute on Aging-Alzheimer's Association workgroups on diagnostic guidelines for Alzheimer's disease. Alzheimer's & dementia : the journal of the Alzheimer's Association. 2011;7(3):280-92.

Thal DR, Rub U, Orantes M, Braak H. Phases of A beta-deposition in the human brain and its relevance for the development of AD. Neurology. 2002;58(12):1791-800.

Toledo JB, Xie SX, Trojanowski JQ, Shaw LM. Longitudinal change in CSF Tau and Abeta biomarkers for up to 48 months in ADNI. Acta neuropathologica. 2013;126(5):659-70.

Torosyan N, Mason K, Dahlbom M, Silverman DHS, Alzheimer'sDisease Neuroimaging I. Value of FDG-PET scans of non-demented patients in predicting rates of future cognitive and functional decline. European journal of nuclear medicine and molecular imaging. 2017;44(8):1355-63.

Villeneuve S, Rabinovici GD, Cohn-Sheehy BI, Madison C, Ayakta N, Ghosh PM, et al. Existing Pittsburgh Compound-B positron emission tomography thresholds are too high: statistical and pathological evaluation. Brain : a journal of neurology. 2015.

Zijdenbos AP, Forghani R, Evans AC. Automatic "pipeline" analysis of 3-D MRI data for clinical trials: application to multiple sclerosis. IEEE Trans Med Imaging. 2002;21(10):1280-91.

Chapter 4: Synergistic interaction between amyloid-β and tau predicts the progression to dementia

Tharick A. Pascoal MD [1], Sulantha Mathotaarachchi MSc [1], Monica Shin MSc [1], Andrea L. Benedet MSc [1,2], Sara Mohades BSc [1], Seqian Wang MSc [1], Tom Beaudry BSc [1], Min Su Kang BSc [1], Jean-Paul Soucy MD, PhD [3], Aurelie Labbe PhD [4,5], Serge Gauthier MD [6], and Pedro Rosa-Neto MD, PhD [1,3,6,7]* for the Alzheimer's disease Neuroimaging Initiative. [#]

[1]Translational Neuroimaging Laboratory, The McGill University Research Centre for Studies in Aging, Montreal, Canada. [2]CAPES Foundation, Ministry of Education of Brazil, Brasília, Brazil. [3]Montreal Neurological Institute, Montreal, Canada. [4]Douglas Hospital Research Centre, McGill University, Montreal, Canada. [5]Department of Epidemiology, Biostatistics & Occupational Health, McGill University, Montreal, Canada. [6]AD Research Unit, The McGill University Research Centre for Studies in Aging, Montreal, McGill University, Montreal, Canada. [7]Department of Neurology and Neurosurgery, McGill University, Montreal, Canada.

Published in Alzheimer's & Dementia. 2017 Jun;13(6):644-653. (PMID: 28024995).

4.1 Preface

In the two previous chapters, we assessed the synergy between amyloid-β and tau as a determinant of pathophysiological changes in CN individuals. A remaining question, however, is whether this synergy is a key element of the patients' progression to dementia. This is particularly important because it links amyloid-β to dementia symptoms through its synergy with tau, which challenges current models of AD progression suggesting that amyloid-β is not directly related to cognitive decline. Thus, in Chapter 4, we tested whether the synergy between amyloid-β and tau is also associated with the clinical progression from MCI to dementia.

4.2 Abstract

Introduction: Recent literature proposes that amyloid-β and phosphorylated tau (p-tau) synergism accelerates biomarker abnormalities in controls. Yet, it remains to be answered whether this synergism is the driving force behind Alzheimer's disease (AD) dementia.

Methods: We stratified 314 mild cognitive impairment individuals using [^{18}F]florbetapir positron emission tomography amyloid-β imaging and cerebrospinal fluid p-tau. Regression and voxel-based logistic regression models with interaction terms evaluated 2-year changes in cognition and clinical status as a function of baseline biomarkers.

Results: We found that the synergism between [^{18}F]florbetapir and p-tau, rather than their additive effects, was associated with the cognitive decline and progression to AD. Furthermore, voxel-based analysis revealed that temporal and inferior parietal were the regions where the synergism determined an increased likelihood of developing AD.

Discussion: Together, the present results support that progression to AD dementia is driven by the synergistic rather than a mere additive effect between amyloid-β and p-tau proteins.

4.3 Introduction

Alzheimer's disease (AD) is characterized by the progressive accumulation of extracellular amyloid-β (Aβ) plaques, intracellular inclusions of hyperphosphorylated tau in tangles and neuronal degeneration(Jack *et al.*, 2013). The most widely accepted model of AD progression proposes a cascade of neuropathological events in which abnormal levels of Aβ, neurofibrillary tangles and neurodegeneration precede dementia(Jack *et al.*, 2013). The idea of pathophysiological progression was incorporated by the National Institute on Aging and the Alzheimer's Association criterion for predementia phase of AD, which recognizes that the coexistence of abnormal Aβ and neurodegeneration biomarkers better identify mild cognitive impairment (MCI) patients who will progress to dementia (Albert *et al.*, 2011). This notion has been supported by recent observations demonstrating that MCI Aβ+ individuals with neurodegenerative changes, measured by brain hypometabolism or atrophy, have higher rates of neuropsychological decline as compared with MCI biomarker negative participants (Petersen *et al.*, 2013, Caroli *et al.*, 2015, Wisse *et al.*, 2015). Yet, a key question that remains unanswered is whether the highest rate of progression to dementia in MCI Aβ+ individuals with downstream cascade abnormalities, are due to a synergistic effect between the coexistent brain pathologies or simply the sum of their deleterious effects. This question is particularly important in the context of the two hallmark proteinopathies underlying AD (Selkoe, 2005). Whereas Aβ and phosphorylated tau (p-tau) proteins well characterize AD pathophysiology, brain hypometabolism or atrophy may be found in several other brain disorders associated with

neuronal loss (Albert *et al.*, 2011, Blennow and Zetterberg, 2015).

Given the emphasis of the current literature on the combination of Aβ and neuronal degeneration biomarkers (Petersen *et al.*, 2013, Caroli *et al.*, 2015, Knopman *et al.*, 2015, Wisse *et al.*, 2015), the clinical fate of MCI patients with abnormal Aβ plus p-tau proteins is scarcely known. The importance of characterizing the synergistic effect between Aβ and p-tau on the development of dementia goes beyond the understanding of the mechanisms of disease progression. Determination of such synergism has immediate implications for the population enrichment of clinical trials testing anti-amyloid or anti-tau therapy. For example, if Aβ and p-tau synergistically determine dementia, the enrichment of clinical trial populations with carriers of both pathologies would increase the rate of clinical progression without loss of therapeutic effectiveness. Conversely, if Aβ and p-tau simply add their deleterious effects on cognitive decline, carriers of both pathologies would lead to a reduced therapeutic effectiveness of an intervention targeting only one of these proteinopathies, given the residual effect of the untreated protein on the clinical course of the disease.

Although several studies have shown that Aβ and p-tau independently predict disease progression (Buerger *et al.*, 2005, Ossenkoppele *et al.*, 2014), a hypothetical framework proposes that both proteinopathies synergistically potentiate downstream neurodegeneration (Duyckaerts, 2011). The presence of such a synergism would suggest that the effect of Aβ and p-tau on the progression of AD taken together is greater than the sum of their separate effects at the same level. In fact, recent findings from our laboratory support this framework showing that the synergistic effect between brain Aβ and p-tau rather than neurodegeneration drives AD related

metabolic decline in a cognitively normal population (Pascoal *et al.*, 2016). Similarly, in vivo studies conducted in controls have suggested that p-tau modulates the link between Aβ and brain atrophy or behavioural changes (Desikan *et al.*, 2012, Fortea *et al.*, 2014, Sperling *et al.*, 2014), while animal model literature has demonstrated a synergistic effect between Aβ and p-tau peptides, leading to downstream synaptic and neuronal dysfunctions(Ittner and Gotz, 2011)

Here, in a longitudinal analysis conducted in amnestic MCI individuals, we tested the hypothesis that the synergism between Aβ aggregation and tau hyperphosphorylation determines progression from amnestic MCI to AD dementia.

4.4 Materials and Methods

Database description and study participants

Data used in the preparation of this article were obtained from the Alzheimer's disease Neuroimaging Initiative (ADNI) database. ADNI was launched in 2003 as a public-private partnership, led by Principal Investigator Michael W. Weiner, MD. The primary goal of ADNI has been to test whether serial magnetic resonance imaging (MRI), positron emission tomography (PET), cerebrospinal fluid (CSF), and clinical assessment can be combined to measure the progression of MCI and early AD.

For the present study, we selected 314 ADNI-GO/2 participants meeting the criteria for single-domain or multi-domain amnestic MCI, who underwent lumbar puncture and [^{18}F]florbetapir PET imaging at baseline as well as neuropsychological assessments at both baseline and at a 2-year follow-up. The eligibility criteria for selecting MCI were participants who had a mini-

mental state examination (MMSE) score equal to or greater than 24, a clinical dementia rating of 0.5, subjective and objective memory loss, and absence of other neuropsychiatric disorders (Petersen, 2003). (Further information about the inclusion/exclusion criteria may be found at www.adni-info.org[accessed September 2016].)

CSF analyses

The multiplex xMAP Luminex platform (Luminex Corp, Austin, TX) was used to quantify p-tau at threonine 181 using INNO-BIA AlzBio3 immunoassay kit-based reagents (Innogenetics, Ghent, Belgium). All of the CSF p-tau data used in this study were obtained from the ADNI files 'UPENNBIOMK5-8.csv'. The data were statistically rescaled based on the baseline assay analysis that was used to define the CSF p-tau threshold (Olsson *et al.*, 2005). We considered a subject positive for tau hyperphosphorylation if the CSF p-tau value was above the ADNI published threshold (>23pg/ml) (Shaw *et al.*, 2009, Toledo *et al.*, 2013) (Further details can be found at www.adni-info.org[accessed September 2016].)

MRI/PET methods

The schematic representation of the image analysis methods is presented in Figure 4-1. The [^{18}F]florbetapir standardized uptake value ratio (SUVR) was obtained using the cerebellum grey matter and global white matter as reference regions. A global [^{18}F]florbetapir standardized uptake value ratio (SUVR) standardized uptake value ratio value for each subject was estimated by averaging the precuneus, prefrontal, orbitofrontal, parietal, temporal, anterior, and posterior cingulate cortices. The cutoff value was established based on the 10th percentile of the [18F]florbetapir SUVR distribution of the ADNI AD population (n = 90), which corresponds to

90% sensitivity for a diagnosis of AD. This approach was based on previous publications that performed similar types of analyses in individuals segregated by Aβ and neurodegeneration biomarkers (Petersen *et al.*, 2013, Caroli *et al.*, 2015, Wisse *et al.*, 2015). Using this approach, individuals were considered positive for Aβ deposition if [^{18}F]florbetapir SUVR>1.12. Finally, grey matter density was computed at every voxel using voxel-based morphometry (Details about ADNI image acquisitions may be found at www.adni-info.org[accessed September 2016].)

Cognitive measurements

The Logical Memory subtest of the Wechsler Memory Scale was used to assess immediate recall memory (LMI) and 30 min delayed recall memory (LM30). Psychomotor speed processing was assessed with the Trail Making Test part A (TMT-A). The performance of participants on the Trail Making Test part B (TMT-B) was assessed to examine executive function. Category Fluency animals was used to evaluate language. To assess the global cognitive performance, we used MMSE and Alzheimer's disease Assessment Scale-Cognitive Subscale (ADAS-Cog) scores. For TMT-A and B tests, and ADAS-Cog higher scores indicate poorer performance (Details about tests acquisition may be found at www.adni-info.org[accessed September 2016].)

Biomarker-based stratification of participants

For analysis purposes, we divided the 314 MCI participants into four biomarker groups using the above described [^{18}F]florbetapir and p-tau thresholds. At baseline, out of 314 individuals, 47 (15%) were biomarker negative (Aβ−/p-tau−), 37 (12%) had only abnormal [^{18}F]florbetapir (Aβ+/p-tau−), 62 (20%) had only abnormal p-tau (Aβ−/p-tau+), and 168 (53%) showed abnormal [^{18}F]florbetapir and p-tau (Aβ+/p-tau+).

Statistical methods

The statistical analyses were performed using the R Statistical Software Package version 3.1.2 with RMINC library (http://www.r-project.org/;accessed September 2016). Neuropsychological test scores (NPS) were analysed using z-scores anchored in normative data obtained from the ADNI cognitively normal controls (n = 162). Controls had a MMSE of 24 or greater, a CDR of 0, had no neuropsychiatric diagnosis including MCI and dementia, and performed the same protocols for data collection as the studied MCI population. All analyses involving neuropsychological measurements were repeated for each of the seven neuropsychological tests at baseline as well as for longitudinal changes between baseline and follow-up, where cognitive progression was measured using the difference between z-scores.

Analysis of covariance (ANCOVA) was performed to test for significant differences between groups (coded as a factor with four levels) on neuropsychological functions. *P* values were corrected for multiple comparisons using Bonferroni, and a significance level of 0.05 was used to interpret the results. Post-hoc analysis provided significant differences between groups.

In order to evaluate the synergistic effect between Aβ and p-tau on neuropsychological changes, ANCOVA models were fitted using both biomarkers as main effects as well as an interaction term between biomarkers.

$$\Delta NPS = \beta_0 + \beta_1(florbetapir\ status) + \beta_2\ (ptau\ status) + \beta_3\ (florbetapir\ status * ptau\ status) + covariates + error$$

To evaluate if Aβ and p-tau values predict cognitive changes across biomarker groups, a stratified linear regression analysis was performed in each of the four biomarker groups using change in test as the outcome and biomarker levels as the main covariate. Another model was fitted to evaluate if the effect of biomarker levels on cognitive changes differed significantly between the biomarker groups by adding in the model a main effect for biomarker groups, as well as an interaction term between biomarker groups and biomarker levels.

$$\Delta NPS = \beta_0 + \beta_1(florbetapir\ SUVR\ or\ ptau\ continuous) + \beta_2(biomarker\ groups) + \beta_3(florbetapir\ SUVR\ or\ ptau\ continuous * biomarker\ groups) + covariates + error$$

Subsequently, to characterize the effects of abnormal Aβ and p-tau status on the clinical progression to dementia, a logistic regression analysis was performed using progression as the outcome, biomarker status as the two main effects, and an interaction term between biomarkers.

Voxel-based logistic regression analysis

Furthermore, in order to identify the brain regions susceptible to the synergism between Aβ and p-tau, a voxel-based logistic regression model was built to test the interactive and main effects between CSF p-tau status and [^{18}F]florbetapir SUVR at every brain voxel on the likelihood of developing dementia (Mathotaarachchi *et al.*, 2016), assuming the probability of progression as $\hat{p}, (\text{progression} = 1)$.

$$log\left(\frac{\hat{p}}{1-\hat{p}}\right) = \beta_0 + \beta_1(florbetapir\ SUVR) + \beta_2(ptau\ status) + \beta_3(florbetapir\ SUVR * ptau\ status) + covariates + error$$

The voxel-based statistical parametric maps were corrected for multiple testing. Statistical significance was defined using a Random Field Theory at a threshold of $P < 0.001$(Worsley, 2003). We further adjusted the voxel-based model for the grey matter density at every voxel in order to correct our results for grey matter atrophy effects(Mathotaarachchi *et al.*, 2016).

All analyses were adjusted for age, gender, years of formal education, *APOE ε4* status and baseline neuropsychological scores (only for models involving longitudinal changes), varying intervals between cognitive assessments were also considered in the models.

4.5 Results

Demographics and key population characteristics are summarized in Table 4-1. The biomarker groups did not differ in age, gender, or years of education. The proportion of *APOE ε4* carriers was higher in Aβ+/p-tau+ (63%) than in the other three groups (24%)($P < 0.001$).

Synergistic effect between Aβ and p-tau predicts the rate of cognitive decline in MCI individuals

ANCOVA models revealed that the Aβ+/p-tau+ group had the worst baseline score and the highest rate of decline in most of the neuropsychological tests when compared with all other biomarker groups (Fig. 4-2). Interestingly, the baseline and longitudinal cognitive performances of the Aβ+/p-tau− and Aβ−/p-tau+ groups were similar to those of the biomarker negative group (Fig. 4-2). Notably, our regression models confirmed that the synergistic interaction, rather than

the sum of individual contributions of Aβ+ and p-tau+ status, determined worse baseline performance or higher rate of impairment over time on the MMSE, ADAS-Cog, LMI, LM30, and TMT-B for the Aβ+/p-tau+ group ($P < 0.05$).

Aβ and p-tau values predict cognitive decline only among MCI Aβ+/p-tau+ individuals

Stratified regression analysis revealed that high [^{18}F]florbetapir SUVR values predicted poorer longitudinal performance in all neuropsychological tests in Aβ+/p-tau+ group (Table 4-2). By contrast, [^{18}F]florbetapir SUVR values did not predict longitudinal changes on any of the tests in biomarker negative, Aβ+/p-tau− and Aβ−/p-tau+ groups, or in models evaluating these three groups together. Interaction models between [^{18}F]florbetapir SUVR values and biomarker groups confirmed that the prediction slope of [^{18}F]florbetapir SUVR was significantly higher in Aβ+/p-tau+ as compared to the other biomarker groups in all neuropsychological tests (MMSE, $P = 0.002$; ADAS-Cog, $P = 0.001$; LMI, $P = 0.04$; LM30, $P < 0.0001$; TMT-A, $P = 0.03$; TMT-B, $P = 0.04$; Category Fluency, $P = 0.03$).

Stratified regression analysis revealed that high CSF p-tau continuous values predicted worse scores in MMSE, ADAS-Cog, LMI and LM30 only in the Aβ+/p-tau+ group (Table 4-2). Interaction models between CSF p-tau values and the biomarker groups showed that the effects of CSF p-tau values in predicting declines in LMI and LM30 were significantly higher in Aβ+/p-tau+ when compared with other biomarker groups ($P < 0.01$).

Synergistic effect between Aβ and p-tau predicts progression from MCI to AD

Although Aβ+ and p-tau+ status independently predicted dementia ($P < 0.05$), a significant

interaction term with no significant main effects between Aβ and p-tau status on progression to dementia revealed that Aβ+/p-tau+ individuals showed a rate of progression greater than the sum of the independent contributions of Aβ+ and p-tau+ ($P < 0.05$).

Further, a multivariate logistic regression revealed that the presence of Aβ+/p-tau+ was the strongest factor associated with developing dementia with a 14.1-fold (95% CI 5.7-38, $P < 0.0001$) increase in likelihood of progression. *APOE ε4* status (OR = 5.7, 95% CI 3.1-12, $P < 0.0001$) also predicted likely progression to dementia. Furthermore, [^{18}F]florbetapir SUVR values (OR = 2.0, 95% CI 1.31-3.1, $P = 0.001$) and CSF p-tau values (OR = 1.47, 95% CI 1.14-1.96, $P = 0.004$) predicted dementia exclusively in Aβ+/p-tau+ group.

The overall progression rate to probable AD dementia of this study was 19% over 2 years. Among Aβ−/p-tau−, Aβ+/p-tau−, Aβ−/p-tau+, and Aβ+/p-tau+ participants, the progression rate was 4%, 3%, 3%, and 32%, respectively (Fig. 4-3). Out of 59 participants who converted to dementia, 54 (92%) were Aβ+/p-tau+ at baseline.

Synergistic effect between Aβ and p-tau in temporoparietal regions predicts progression from MCI to AD

Voxel-based logistic regression analysis revealed that lateral and basal temporal and inferior parietal cortices are the brain regions where the synergistic effect between [^{18}F]florbetapir SUVR and CSF p-tau determined the increased likelihood of progression from amnestic MCI to AD dementia over a 2-year period (Fig. 4-4).

4.6 Discussion

In this study, we found that amnestic MCI Aβ+/p-tau+ individuals had the highest rate of cognitive decline and progression to dementia, as compared to all other biomarker groups. Remarkably, our regression models confirmed that a synergistic rather than additive effect between Aβ and p-tau determined greater cognitive decline and clinical progression in amnestic MCI Aβ+/p-tau+. Furthermore, we found that only among amnestic MCI Aβ+/p-tau+ individuals did the baseline values of Aβ and p-tau biomarkers predict cognitive and clinical impairments. Finally, a voxel-based analysis revealed that the temporal and inferior parietal cortices were the brain regions vulnerable to the synergism between Aβ and p-tau peptides.

Overall, our results suggest the synergism between Aβ and p-tau as an important element involved in the progression from amnestic MCI to AD dementia. This finding extends previous studies conducted in cognitively normal persons demonstrating that the synergism between Aβ and p-tau determines functional and structural abnormalities(Desikan *et al.*, 2012, Fortea *et al.*, 2014, Sperling *et al.*, 2014, Pascoal *et al.*, 2016). Interestingly, the temporal and inferior parietal cortices described here as the structural substrates in which the Aβ and p-tau synergistic effect conferred an increased likelihood of clinical progression, are well known as vulnerable brain regions in patients who progressed from MCI to dementia(Schroeter *et al.*, 2009). Indeed, the synergistic effect between Aβ and p-tau reported here is well supported by molecular studies describing synaptic and neuronal damages as consequences of the synergistic interactions between Aβ and tau peptides (Vossel *et al.*, 2010, Ittner and Gotz, 2011, Vossel *et al.*, 2015).

This study revealed that the link between Aβ levels and progression to AD dementia depends on

the p-tau status. This finding sheds light on the literature showing conflicting results reporting the association between Aβ and cognition. Although the majority of studies describe a modest association in early disease stages (Edison *et al.*, 2007, Villemagne *et al.*, 2011, Chetelat *et al.*, 2012, Landau *et al.*, 2012, Kemppainen *et al.*, 2014), others suggest that Aβ levels strongly predict cognitive decline in populations with a high probability to present p-tau abnormalities (Desikan *et al.*, 2012, Ossenkoppele *et al.*, 2014). Interestingly, Aβ levels fail to predict time-to-progression to dementia in MCI Aβ+ individuals with evidences of brain hypometabolism or atrophy (Caroli *et al.*, 2015). One might claim that Aβ levels represent an important predictor of forthcoming dementia, particularly in predementia persons with p-tau abnormalities (Albert *et al.*, 2011).

Suspected non-Alzheimer disease pathophysiology (SNAP) has emerged as an important concept referring to patients showing a biomarker signature of neurodegeneration without Aβ abnormalities (Jack *et al.*, 2016). As the concept of SNAP arises in our study as the group of MCI Aβ−/p-tau+ individuals (Jack *et al.*, 2016), we would like to comment on the clinical progression of this population. Previous studies have demonstrated that in SNAP MCI, characterized by the presence of neuronal degeneration evidenced by brain hypometabolism or atrophy, the rate of cognitive decline is higher than in MCI individuals who are biomarker negative and comparable to MCI carriers of Aβ plus neurodegeneration (Petersen *et al.*, 2013, Caroli *et al.*, 2015, Wisse *et al.*, 2015). In contrast, we demonstrate here that SNAP MCI Aβ−/p-tau+ subjects clinically progress at a rate similar to that of MCI subjects who are biomarker negative. This reduced rate of progression of our SNAP MCI Aβ−/p-tau+ population may be explained by the fact that CSF p-tau reflects neurofibrillary tangles pathology rather than

neuronal degeneration (Blennow and Zetterberg, 2015). Importantly, the clinical stability of MCI Aβ−/p-tau+ participants supports the synergism between Aβ and p-tau pathologies as a key element triggering AD dementia (Duyckaerts, 2011, Sperling *et al.*, 2014). The reduced rate of clinical progression of our SNAP MCI Aβ−/p-tau+ group as compared to that observed in previous studies may be due to the presence of a significant proportion of MCI individuals who are in the early clinical stages of MCI in the ADNI-GO/2 cohort (Aisen *et al.*, 2010, Beckett *et al.*, 2015). This is consistent with studies on cognitively normal individuals showing that SNAP progresses at a rate similar to that of biomarker negative subjects (Jack *et al.*, 2012, Vos *et al.*, 2013). Furthermore, it is possible that the cognitive decline observed in SNAP MCI in previous studies, defined by less specific biomarkers for AD such as brain hypometabolism or atrophy, was driven by other pathophysiological processes such as TDP-43, alpha-synuclein inclusions, and hippocampal sclerosis (Nelson *et al.*, 2011, Ishii, 2014). Together, these results support that SNAP MCI individuals characterized by the presence of p-tau pathology, different from those with SNAP MCI defined by neuronal degeneration biomarkers, clinically progress at rates comparable to those seen in MCI biomarker negative individuals.

This study has some methodological limitations. Biomarkers provide naturally continuous measurements; therefore, thresholds are invariably subject to conceptual and analytical idiosyncrasies and may change depending on the method of analysis utilized. However, the use of regression models with continuous biomarker values helped prevent our results from being driven by the use of more liberal or more conservative biomarker threshold. Additionally, we assessed the synergy between Aβ and p-tau across all brain voxels. To the best of our knowledge, this is the first study conducting a voxel-based logistic regression analysis to

evaluate progression to dementia using Aβ PET imaging. Importantly, our results showing the synergism between amyloid-β and p-tau leading to downstream clinical progression do not exclude the possibility that these two proteinopathies might arise sequentially (e.g. amyloid-β triggering the spreading of tau over the neocortex early on in the pathophysiological progression (Sperling *et al.*, 2014)). Certainly, cell cultures and in vivo studies with long-term imaging of amyloid-β and p-tau in animal models and in humans could better investigate causal and temporal relationships between these proteins. It is also important to mention that the observations reported here do not to prove a biological synergy between Aβ and p-tau proteins. Our overall progression rate to dementia was 19% over 2 years. Previous studies conducted in memory clinic cohorts have reported progression rate in MCI of up to 59% over 2 years (Koivunen *et al.*, 2011). This might be explained by the fact that the ADNI-GO/2 inclusion criteria include MCI individuals in a less advanced disease stage as compared to these cohorts(Beckett *et al.*, 2015). In fact, our findings are similar to a recent study involving MCI ADNI-GO/2 participants that reported an overall progression rate of 15% over 1.6 years (Schreiber *et al.*, 2015). Finally, regarding the population included in this analysis, it is important to emphasize that it represents a select group of amnestic MCI persons motivated to participate in a dementia study. As such, for reasons related to the study inclusion criteria and self-selection bias(Spix *et al.*, 2015), these individuals may not represent the general MCI population. Therefore, it would be highly desirable to replicate our findings on a population-based cohort.

From a clinical perspective, if replicated, such a synergism has important implications in understanding the dynamics of progression to dementia. For example, the clinical stability of nondemented persons with biomarker abnormalities described in numerous cohorts (Braak and

Braak, 1991, Morris and Price, 2001), could be explained by the absence of convergence of the Aβ and p-tau pathways, postulated here to be crucial for imminent clinical progression in amnestic MCI. In addition, the combination of abnormal amyloid-PET and CSF p-tau biomarkers may represent a valuable strategy for the enrichment of amnestic MCI populations with individuals having a high probability of developing AD dementia in therapeutic clinical trials targeting Aβ or tau aggregates.

From a therapeutic perspective, one can derive important predictions from the existence of a synergistic interaction between Aβ and p-tau in AD. For example, one can predict that therapeutic interventions targeting either Aβ or p-tau pathology might similarly mitigate AD progression. Furthermore, the same synergistic model implies better effectiveness of a combined therapeutic approach targeting both, Aβ and p-tau, pathological pathways. However, it is important to mention that the synergism between pathological pathways might not always translate into synergistic effects of multiple treatments. Importantly, this model should be supported by further studies combining long-term sequential biomarker and clinical observations.

In conclusion, our results support the synergism between Aβ and tau pathologies as a driving force behind the clinical progression to AD dementia.

4.7 Tables and Figures

Table 4-1. Demographics and key characteristics of the amnestic MCI population.

Characteristics	Aβ−/p-tau−	Aβ+/p-tau−	Aβ−/p-tau+	Aβ+/p-tau+	*P*
No.	47	37	62	168	
Age, y, mean (SD)	71 (7.6)	70.2 (7.2)	71 (8.1)	72.6 (7.1)	0.16
Male, no. (%)	31 (66)	17 (46)	33 (54)	87 (52)	0.34
***APOE ε4*, no. (%)**	9 (19)	11 (30)	15 (24)	105 (63) [a,b,c]	<0.0001
Education, y, mean (SD)	17.1 (2.2)	15.6 (2.4)	16.3 (2.7)	16.4 (2.6)	0.05
[^{18}F]Florbetapir, mean SUVR (SD)	1.07 (0.04)	1.18 (0.07) [a,c]	1.05 (0.05)	1.34 (0.11) [a,b,c]	<0.0001
CSF p-tau, mean pg/ml (SD)	18.5 (3.9)	17.4 (4)	37 (12.8) [a,b]	53.5 (24.1) [a,b,c]	<0.0001
Diagnostic at follow-up, no. (%)					
CN	2 (4)	3 (8)	1 (2)	6 (4)	0.45
MCI	43 (92)	33 (89)	59 (95)	108 (64)	—
Dementia	2 (4)	1 (3)	2 (3)	54 (32) [a,b,c]	<0.0001

P values indicate the values assessed with analyses of variance for each variable except gender, *APOE ε4*, and diagnostic at follow-up, where a contingency chi-square was performed. Post-hoc analysis provided significant differences between groups: [a] from Aβ−/p-tau−; [b] from Aβ+/p-tau−; [c] from Aβ−/p-tau+. MCI = mild cognitive impairment; p-tau = phosphorylated tau; SUVR = standardized uptake value ratio.

Table 4-2. Predictive biomarker effects on neuropsychological functions in amnestic MCI participants according biomarker groups.

Tests	Aβ−/p-tau−		Aβ+/p-tau−		Aβ−/p-tau+		Aβ+/p-tau+	
	Aβ	p-tau	Aβ	p-tau	Aβ	p-tau	Aβ	p-tau
MMSE (SE)	0.23 (1.07)	−0.34 (0.95)	−0.16 (0.53)	0.96 (1.26)	0.83 (0.61)	−0.5 (0.3)	−1.16 (0.25)**	−0.36 (0.15)*
ADAS-cog (SE)	−1.49 (1.87)	2 (2.08)	−0.04 (0.97)	1.87 (2.3)	−0.39 (0.94)	0.82 (0.42)	0.99 (0.45)*	0.52 (0.26)*
LMI (SE)	2.5 (2.24)	−4.1 (2.5)	0.3 (0.98)	−0.79 (2.55)	1.6 (1.28)	0.1 (0.67)	−1.39 (0.32)**	−0.68 (0.19)**
LM30 (SE)	0.42 (2.77)	−6.9 (3)	2 (1.19)	−2.5 (2.9)	1.7 (1.37)	−0.43 (0.65)	−1.30 (0.39)**	−0.79 (0.23)**
TMT-A (SE)	5.6 (8.2)	4.2 (9.2)	−11.7 (5.9)	−8.9 (14)	−3.7 (3.78)	1.5 (1.88)	5.30 (1.6)*	1.11 (1.04)
TMT-B (SE)	6.2 (21.4)	36 (23)	−11.45 (15.5)	−17 (36)	18.33 (17.58)	−3.5 (8.5)	16.62 (5.9)*	4.95 (3.75)
Category Fluency (SE)	−3.33 (2.2)	−6.14 (2.5)	1.73 (1.26)	−1.6 (3.08)	−0.93 (1.57)	0.29 (0.76)	−2.25 (0.48)**	−0.52 (0.24)

The results are presented in change (slope-coefficient) of neuropsychological test score per standard deviation of baseline biomarker. For the Alzheimer's Disease Assessment Scale-Cognitive Subscale (ADAS-cog), Trail Making Test part A (TMT-A) and B (TMT-B) greater values reflect worse cognition. The models were adjusted for age, gender, years of education, *APOE ε4* status, baseline test score, and Bonferroni-corrected for multiple comparisons. It is important to emphasise that [^{18}F]florbetapir and p-tau values did not significantly predict longitudinal cognition in biomarker negative, Aβ+/p-tau− and Aβ−/p-tau+ individuals. LMI = Logical Memory immediate recall; LM30 = Logical Memory 30 min delayed recall; MMSE = mini-mental state examination; p-tau = phosphorylated tau. Significance at $^{*}P < 0.05$; $^{**}P < 0.001$.

Figure 4-1. Schematic representation of the image analysis methods.

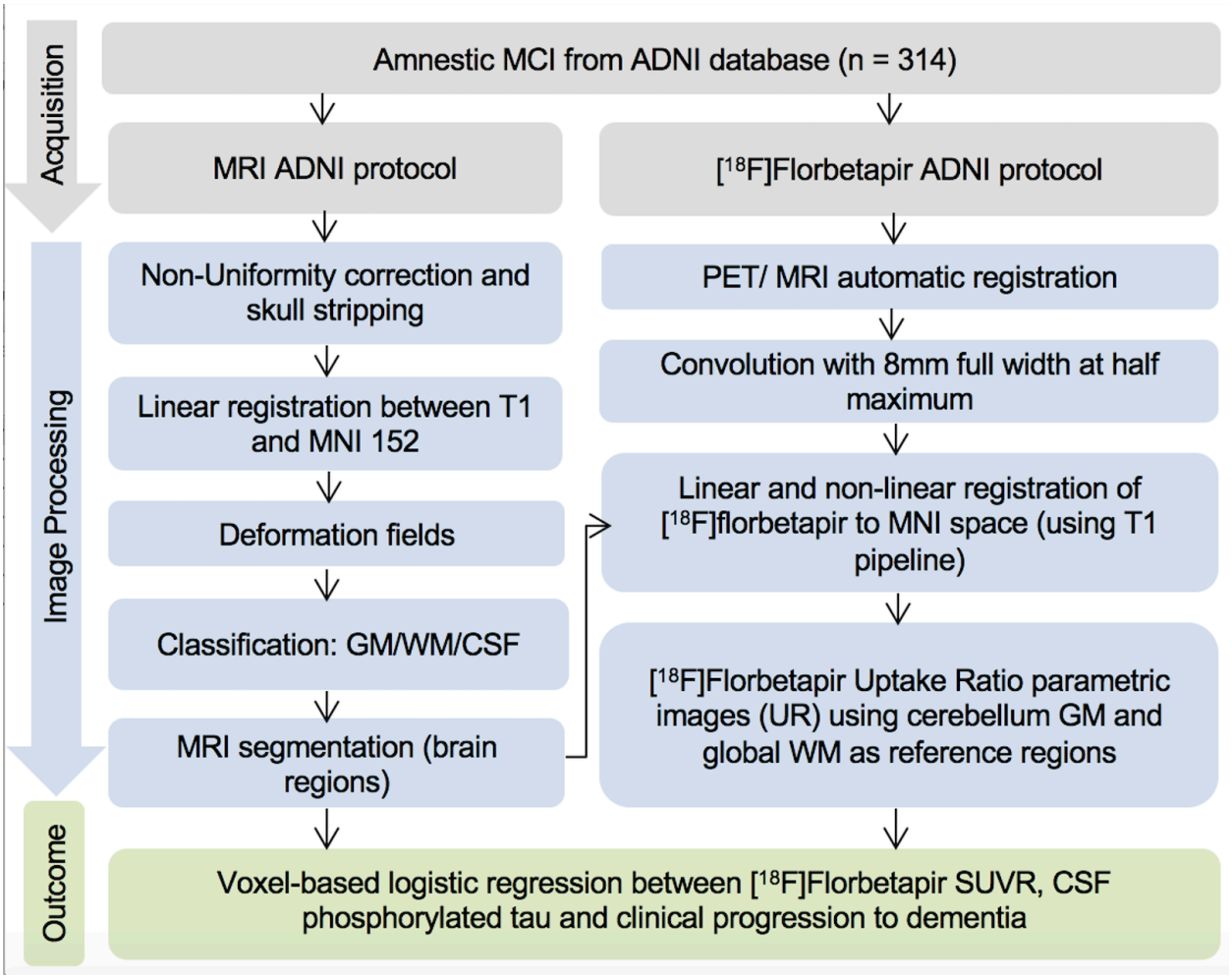

Figure 4-2. The amnestic MCI Aβ+/p-tau+ individuals present the lowest baseline scores and the highest rate of decline in most neuropsychological functions.

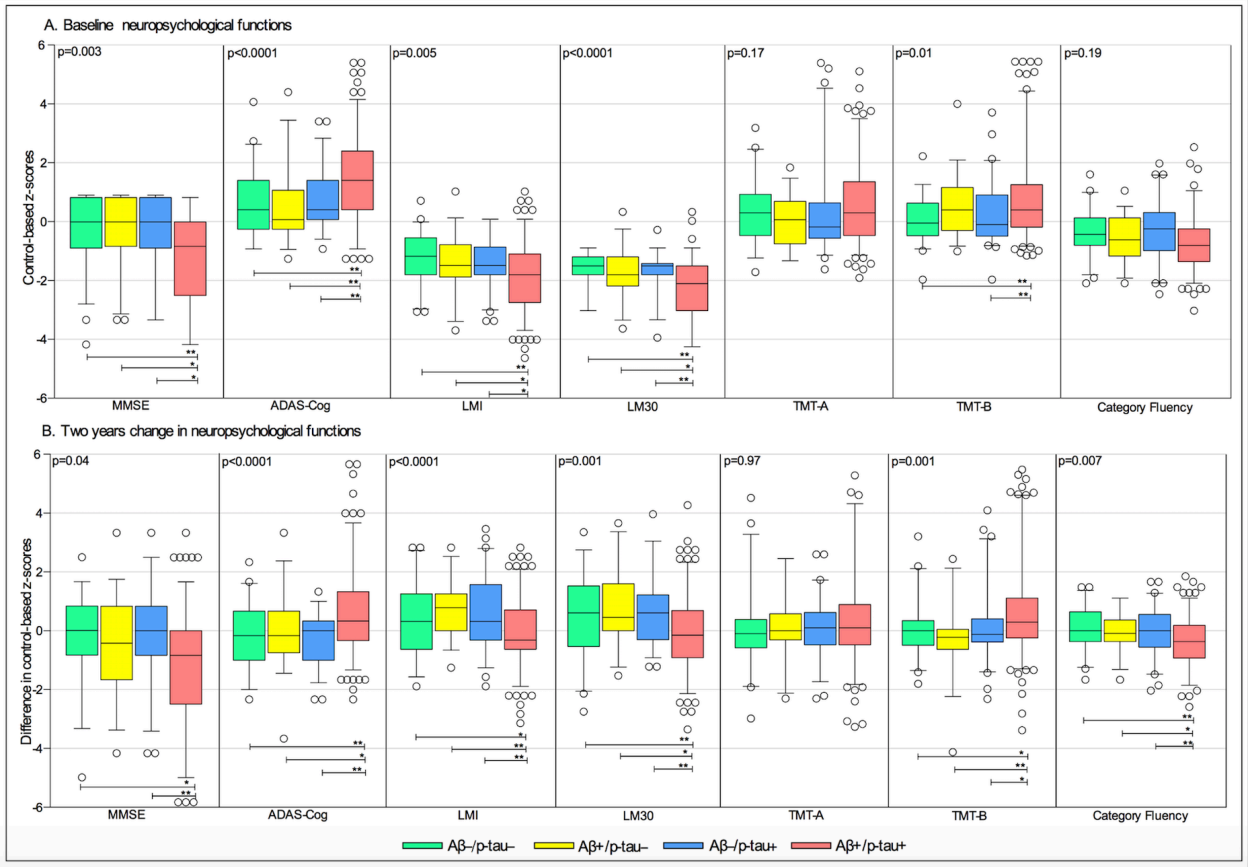

The values are presented in z-scores anchored in normative data of a cognitively normal population. In the box and whisker plots, the lower and upper boundaries show the 25th and 75th percentiles, respectively, whereas the horizontal line shows the median. The dots represent mild cognitive impairment (MCI) individuals less than the fifth or higher than the 95th percentile. Bonferroni-corrected *P* values for multiple comparisons indicate the values assessed with analyses of covariance adjusted for age, gender, years of education, APOE ε4 status and baseline neuropsychological test score for longitudinal analysis. Post-hoc multiple comparison analysis provided significant differences between biomarker groups for each neuropsychological test at $*P < 0.05$ and $**P < 0.001$. (A) At baseline, the Aβ+/p-tau+ group presented the lowest baseline scores in mini-mental state examination (MMSE), Alzheimer's Disease Assessment Scale-Cognitive Subscale (ADAS-Cog), logical memory immediate recall (LMI) and 30 min delayed recall (LM30). The Aβ+/p-tau+ group showed worse performance in the Trail Making Test part B (TMT-B) than the Aβ−/p-tau− and Aβ−/p-tau+ groups. (B) The Aβ+/p-tau+ group presented the highest longitudinal impairment in all neuropsychological tests except TMT-A and MMSE. Aβ+/p-tau+ group showed higher decline in MMSE than Aβ−/p-tau− and Aβ−/p-tau+ groups. Notably, Aβ−/p-tau−, Aβ+/p-tau−, and Aβ−/p-tau+ groups did not differ from each other in any baseline or longitudinal cognitive performance.

Figure 4-3. Aβ+/p-tau+ individuals drove the rate of progression to dementia over 2 years in the amnestic MCI population.

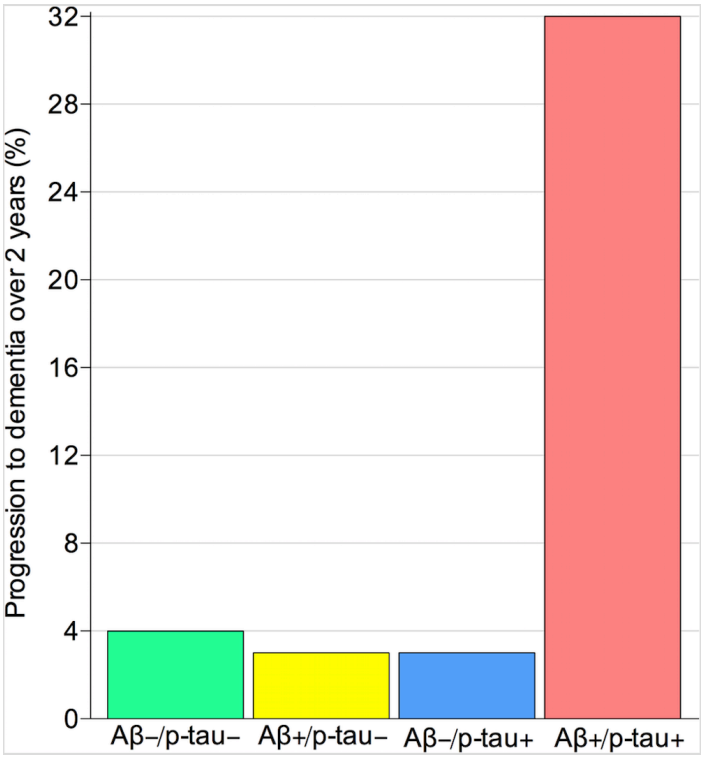

Figure 4-4. Synergistic effect between [^{18}F]florbetapir SUVR and CSF p-tau in temporal and inferior parietal cortices predicts progression to dementia.

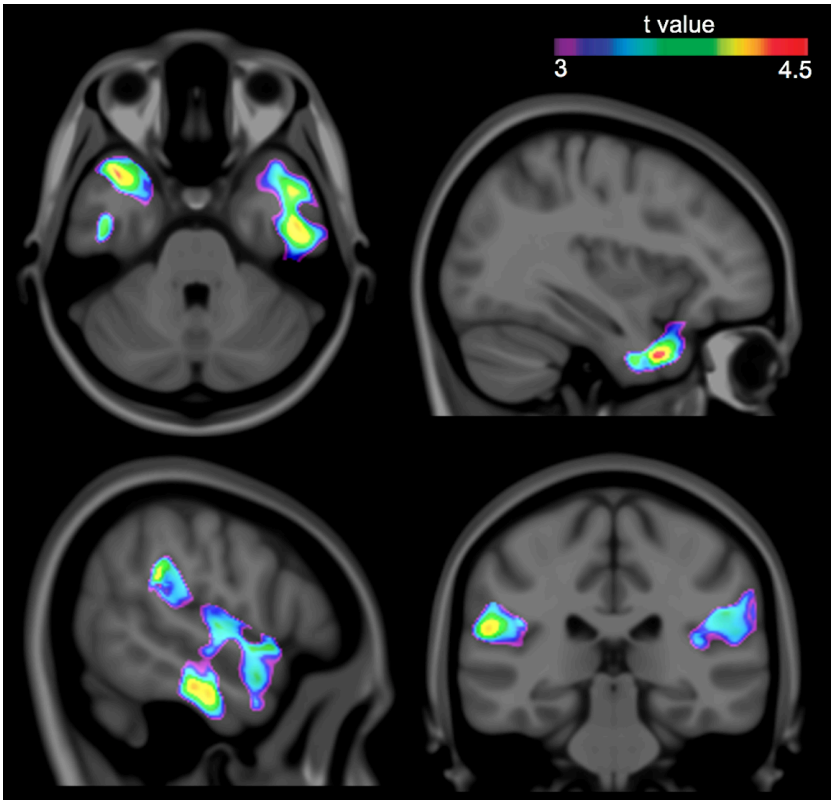

T-statistical parametric map, after correcting for multiple comparisons (Random Field Theory at $P < 0.001$), overlaid in a structural magnetic resonance scan revealed that lateral and basal temporal and inferior parietal cortices were the brain regions where the synergism between [^{18}F]florbetapir standardized uptake value ratio (SUVR) and cerebrospinal fluid (CSF) phosphorylated tau (p-tau) status was associated with an increased likelihood of progression to Alzheimer's disease (AD) dementia over 2 years.

4.8 Acknowledgements

This work was supported by the Canadian Institutes of Health Research (CIHR; MOP-11-51-31), the Alan Tiffin Foundation, the Alzheimer's Association (NIRG-12- 92090, NIRP-12-259245), Prevent-AD scholarship (TAP), Fonds de Recherche du Québec – Santé (FRQS; Chercheur Boursier, PR-N), S.G. and P.R-N. are members of the CIHR-CCNA Canadian Consortium of Neurodegeneration in Aging. Data collection and sharing for this project was funded by the

ADNI (National Institutes of Health Grant U01 AG024904) and DOD ADNI (Department of Defense award number W81XWH-12-2-0012). ADNI is funded by the National Institute on Aging, the National Institute of Biomedical Imaging and Bioengineering, and through generous contributions from the following: AbbVie, Alzheimer's Association; Alzheimer's Drug Discovery Foundation; Araclon Biotech; BioClinica, Inc.; Biogen; Bristol-Myers Squibb Company; CereSpir, Inc.; Eisai Inc.; Elan Pharmaceuticals, Inc.; Eli Lilly and Company; EuroImmun; F. Hoffmann-La Roche Ltd and its affiliated company Genentech, Inc.; Fujirebio; GE Healthcare; IXICO Ltd.; Janssen Alzheimer Immunotherapy Research & Development, LLC.; Johnson & Johnson Pharmaceutical Research & Development LLC.; Lumosity; Lundbeck; Merck & Co., Inc.; Meso Scale Diagnostics, LLC.; NeuroRx Research; Neurotrack Technologies; Novartis Pharmaceuticals Corporation; Pfizer Inc.; Piramal Imaging; Servier; Takeda Pharmaceutical Company; and Transition Therapeutics. The Canadian Institutes of Health Research also provides funds to support ADNI clinical sites in Canada. Private sector contributions are facilitated by the Foundation for the National Institutes of Health (www.fnih.org). The grantee organization is the Northern California Institute for Research and Education, and the study is coordinated by the AD Cooperative Study at the University of California, San Diego. ADNI data were disseminated by the Laboratory for Neuro Imaging at the University of Southern California.

4.9 References

Aisen PS, Petersen RC, Donohue MC, Gamst A, Raman R, Thomas RG, et al. Clinical Core of the Alzheimer's Disease Neuroimaging Initiative: progress and plans. Alzheimer's & dementia : the journal of the Alzheimer's Association. 2010;6(3):239-46.

Albert MS, DeKosky ST, Dickson D, Dubois B, Feldman HH, Fox NC, et al. The diagnosis of mild cognitive impairment due to Alzheimer's disease: recommendations from the National Institute on Aging-Alzheimer's Association workgroups on diagnostic guidelines for Alzheimer's disease. Alzheimer's & dementia : the journal of the Alzheimer's Association. 2011;7(3):270-9.

Beckett LA, Donohue MC, Wang C, Aisen P, Harvey DJ, Saito N, et al. The Alzheimer's Disease Neuroimaging Initiative phase 2: Increasing the length, breadth, and depth of our understanding. Alzheimer's & dementia : the journal of the Alzheimer's Association. 2015;11(7):823-31.

Blennow K, Zetterberg H. Understanding biomarkers of neurodegeneration: Ultrasensitive detection techniques pave the way for mechanistic understanding. Nature medicine. 2015;21(3):217-9.

Braak H, Braak E. Neuropathological stageing of Alzheimer-related changes. Acta neuropathologica. 1991;82(4):239-59.

Buerger K, Ewers M, Andreasen N, Zinkowski R, Ishiguro K, Vanmechelen E, et al. Phosphorylated tau predicts rate of cognitive decline in MCI subjects: a comparative CSF study. Neurology. 2005;65(9):1502-3.

Caroli A, Prestia A, Galluzzi S, Ferrari C, van der Flier WM, Ossenkoppele R, et al. Mild cognitive impairment with suspected nonamyloid pathology (SNAP): Prediction of progression. Neurology. 2015;84(5):508-15.

Chetelat G, Villemagne VL, Pike KE, Ellis KA, Ames D, Masters CL, et al. Relationship between memory performance and beta-amyloid deposition at different stages of Alzheimer's disease. Neuro-degenerative diseases. 2012;10(1-4):141-4.

Desikan RS, McEvoy LK, Thompson WK, Holland D, Brewer JB, Aisen PS, et al. Amyloid-beta--associated clinical decline occurs only in the presence of elevated P-tau. Archives of neurology. 2012;69(6):709-13.

Duyckaerts C. Tau pathology in children and young adults: can you still be unconditionally baptist? Acta neuropathologica. 2011;121(2):145-7.

Edison P, Archer HA, Hinz R, Hammers A, Pavese N, Tai YF, et al. Amyloid, hypometabolism, and cognition in Alzheimer disease: an [11C]PIB and [18F]FDG PET study. Neurology. 2007;68(7):501-8.

Fortea J, Vilaplana E, Alcolea D, Carmona-Iragui M, Sanchez-Saudinos MB, Sala I, et al. Cerebrospinal fluid beta-amyloid and phospho-tau biomarker interactions affecting brain structure in preclinical Alzheimer disease. Annals of neurology. 2014;76(2):223-30.

Ishii K. PET approaches for diagnosis of dementia. AJNR Am J Neuroradiol. 2014;35(11):2030-8.

Ittner LM, Gotz J. Amyloid-beta and tau--a toxic pas de deux in Alzheimer's disease. Nat Rev Neurosci. 2011;12(2):65-72.

Jack CR, Jr., Knopman DS, Chetelat G, Dickson D, Fagan AM, Frisoni GB, et al. Suspected non-Alzheimer disease pathophysiology - concept and controversy. Nature reviews Neurology. 2016;12(2):117-24.

Jack CR, Jr., Knopman DS, Jagust WJ, Petersen RC, Weiner MW, Aisen PS, et al. Tracking pathophysiological processes in Alzheimer's disease: an updated hypothetical model of dynamic biomarkers. The Lancet Neurology. 2013;12(2):207-16.

Jack CR, Jr., Knopman DS, Weigand SD, Wiste HJ, Vemuri P, Lowe V, et al. An operational approach to National Institute on Aging-Alzheimer's Association criteria for preclinical Alzheimer disease. Annals of neurology. 2012;71(6):765-75.

Kemppainen NM, Scheinin NM, Koivunen J, Johansson J, Toivonen JT, Nagren K, et al. Five-year follow-up of 11C-PIB uptake in Alzheimer's disease and MCI. European journal of nuclear medicine and molecular imaging. 2014;41(2):283-9.

Knopman DS, Jack CR, Jr., Lundt ES, Wiste HJ, Weigand SD, Vemuri P, et al. Role of beta-Amyloidosis and Neurodegeneration in Subsequent Imaging Changes in Mild Cognitive Impairment. JAMA neurology. 2015:1-9.

Koivunen J, Scheinin N, Virta JR, Aalto S, Vahlberg T, Nagren K, et al. Amyloid PET imaging in patients with mild cognitive impairment: a 2-year follow-up study. Neurology. 2011;76(12):1085-90.

Landau SM, Mintun MA, Joshi AD, Koeppe RA, Petersen RC, Aisen PS, et al. Amyloid deposition, hypometabolism, and longitudinal cognitive decline. Annals of neurology. 2012;72(4):578-86.

Mathotaarachchi S, Wang S, Shin M, Pascoal TA, Benedet AL, Kang MS, et al. VoxelStats: A MATLAB package for multi-modal voxel-wise brain image analysis. Frontiers in Neuroinformatics. 2016;10.

Morris JC, Price JL. Pathologic correlates of nondemented aging, mild cognitive impairment, and early-stage Alzheimer's disease. Journal of molecular neuroscience : MN. 2001;17(2):101-18.

Nelson PT, Schmitt FA, Lin Y, Abner EL, Jicha GA, Patel E, et al. Hippocampal sclerosis in advanced age: clinical and pathological features. Brain : a journal of neurology. 2011;134(Pt 5):1506-18.

Olsson A, Vanderstichele H, Andreasen N, De Meyer G, Wallin A, Holmberg B, et al. Simultaneous measurement of beta-amyloid(1-42), total tau, and phosphorylated tau (Thr181) in cerebrospinal fluid by the xMAP technology. Clinical chemistry. 2005;51(2):336-45.

Ossenkoppele R, van der Flier WM, Verfaillie SC, Vrenken H, Versteeg A, van Schijndel RA, et al. Long-term effects of amyloid, hypometabolism, and atrophy on neuropsychological functions. Neurology. 2014;82(20):1768-75.

Pascoal TA, Mathotaarachchi S, Mohades S, Benedet AL, Chung CO, Shin M, et al. Amyloid-beta and hyperphosphorylated tau synergy drives metabolic decline in preclinical Alzheimer's disease. Mol Psychiatry. 2016.

Petersen RC. Mild cognitive impairment: Aging to Alzheimer's disease: Oxford University Press; 2003.

Petersen RC, Aisen P, Boeve BF, Geda YE, Ivnik RJ, Knopman DS, et al. Mild cognitive impairment due to Alzheimer disease in the community. Annals of neurology. 2013;74(2):199-208.

Schreiber S, Landau SM, Fero A, Schreiber F, Jagust WJ, Alzheimer's Disease Neuroimaging I. Comparison of Visual and Quantitative Florbetapir F 18 Positron Emission Tomography Analysis in Predicting Mild Cognitive Impairment Outcomes. JAMA neurology. 2015.

Schroeter ML, Stein T, Maslowski N, Neumann J. Neural correlates of Alzheimer's disease and mild cognitive impairment: a systematic and quantitative meta-analysis involving 1351 patients. NeuroImage. 2009;47(4):1196-206.

Selkoe DJ. Defining molecular targets to prevent Alzheimer disease. Archives of neurology. 2005;62(2):192-5.

Shaw LM, Vanderstichele H, Knapik-Czajka M, Clark CM, Aisen PS, Petersen RC, et al. Cerebrospinal fluid biomarker signature in Alzheimer's disease neuroimaging initiative subjects. Annals of neurology. 2009;65(4):403-13.

Sperling R, Mormino E, Johnson K. The evolution of preclinical Alzheimer's disease: implications for prevention trials. Neuron. 2014;84(3):608-22.

Spix C, Berthold F, Hero B, Michaelis J, Schilling FH. Correction factors for self-selection when evaluating screening programmes. Journal of medical screening. 2015.

Toledo JB, Xie SX, Trojanowski JQ, Shaw LM. Longitudinal change in CSF Tau and Abeta biomarkers for up to 48 months in ADNI. Acta neuropathologica. 2013;126(5):659-70.

Villemagne VL, Pike KE, Chetelat G, Ellis KA, Mulligan RS, Bourgeat P, et al. Longitudinal assessment of Abeta and cognition in aging and Alzheimer disease. Annals of neurology. 2011;69(1):181-92.

Vos SJ, Xiong C, Visser PJ, Jasielec MS, Hassenstab J, Grant EA, et al. Preclinical Alzheimer's disease and its outcome: a longitudinal cohort study. The Lancet Neurology. 2013;12(10):957-65.

Vossel KA, Xu JC, Fomenko V, Miyamoto T, Suberbielle E, Knox JA, et al. Tau reduction prevents Abeta-induced axonal transport deficits by blocking activation of GSK3beta. The Journal of cell biology. 2015;209(3):419-33.

Vossel KA, Zhang K, Brodbeck J, Daub AC, Sharma P, Finkbeiner S, et al. Tau reduction prevents Abeta-induced defects in axonal transport. Science. 2010;330(6001):198.

Wisse LE, Butala N, Das SR, Davatzikos C, Dickerson BC, Vaishnavi SN, et al. Suspected non-AD pathology in mild cognitive impairment. Neurobiology of aging. 2015.

Worsley K. Developments in random field theory. Human brain function. 2003;2:881-6.

Chapter 5: Aβ-induced vulnerability propagates via the brain's default mode network

Tharick A. Pascoal MD[1, 2], Sulantha Mathotaarachchi MSc[1], Min Su Kang BSc[1, 2], Sara Mohaddes MSc[1], Monica Shin MSc[1], Ah Yeon Park, PhD[3], Maxime J. Parent PhD[1, 2], Andrea L. Benedet MSc[1], Mira Chamoun PhD [1], Joseph Therriault BSc[1], Heungsun Hwang PhD[4], A. Claudio Cuello, MD, FRSC[5, 6], Bratislav Misic, PhD[2], Jean-Paul Soucy MD, MSc[2], John A. D. Aston, PhD[3], Serge Gauthier MD, FRCPC[6], and Pedro Rosa-Neto MD, PhD[*1,2,5,6] for the Alzheimer's Disease Neuroimaging Initiative[**]

[1]Translational Neuroimaging Laboratory, The McGill University Research Centre for Studies in Aging, H4H 1R3, Montreal, Canada. [2]Montreal Neurological Institute, H3A 2B4, Montreal, Canada. [3] Statistical Laboratory, University of Cambridge, CB3 0WB, Cambridge, UK. [4] Department of Psychology, McGill University. [5]Department of Pharmacology and Therapeutics, McGill University, H3A 2T5. Montreal, Canada. [6]Alzheimer's Disease Research Unit, The McGill University Research Centre for Studies in Aging, H4H 1R3, Montreal, Canada.

5.1 Preface

In the previous chapters, we demonstrated the associations between amyloid-β and tau in the progression of AD. These studies have shown that synergistic interactions between these proteinopathies are associated with disease progression. However, current literature suggests an association between fibrillar amyloid-β and neurodegeneration, even in the absence of tau pathology (Tsai *et al.*, 2004). Indeed, compelling evidence has indicated that patients on the AD pathway show the coexistence of amyloid-β and metabolic dysfunction in the brain's DMN (Buckner *et al.*, 2005, Sperling *et al.*, 2009, Landau *et al.*, 2012, Mosconi, 2013). These observations support the notion that the deleterious effect of amyloid-β in this set of functionally connected brain regions impose subsequent dysfunctions in AD (Buckner *et al.*, 2005). At first glance, this fits in the sequential model of disease progression in which amyloid-β triggers overlapping DMN metabolic dysfunction, which subsequently leads to cognitive decline (Buckner *et al.*, 2005, Jack *et al.*, 2013). However, high levels of amyloid-β aggregation in the brain's DMN of cognitively intact individuals refute the idea that the sole presence of amyloid-β in these regions is a sufficient condition to dementia (Morris and Price, 2001, Altmann *et al.*, 2015). Since the coexistence of amyloid-β and metabolic dysfunction in the brain's DMN is highly associated with dementia but there is no clear regional correlation between these processes (Furst *et al.*, 2012, Altmann *et al.*, 2015), it is plausible to understand that complex interactions between amyloid-β and DMN metabolic dysfunction are implicated in AD progression. Therefore, in Chapter 5, we extended previous chapters and tested how amyloid-β and neurodegeneration interact to determine disease progression, independently of tau pathology. Specifically, we examined the association between amyloid-β and hypometabolism across the AD clinical spectrum, correcting for each individual's tau pathological levels. Furthermore, to ensure that the results of such associations were independent of tau, we tested these associations

in a transgenic rat model that shows amyloid-β pathology but does not express any other human brain proteinopathy, such as neurofibrillary tangles.

5.2 Abstract

The link between amyloid-β (Aβ), metabolism, and dementia symptoms remains a pressing question in Alzheimer's disease (AD). Using positron emission tomography with a novel analytical framework, we found that Aβ aggregation within the brain's default mode network leads to regional hypometabolism in distant but functionally connected brain regions. Moreover, we found that an interaction between this hypometabolism with overlapping Aβ aggregation is associated with subsequent cognitive decline. Notably, we replicated these results in transgenic Aβ rats that do not form neurofibrillary tangles, which support these findings as an independent mechanism of cognitive deterioration. These results suggest a model in which distant Aβ induces regional metabolic vulnerability, whereas the interaction between local Aβ with a vulnerable environment drives the clinical progression of dementia.

5.3 Introduction

The relationship between regional cerebral amyloid-β (Aβ) aggregation and hypometabolism has been a topic of significant debate in Alzheimer's disease (AD). Whereas some studies suggest an association (Engler *et al.*, 2006, Edison *et al.*, 2007, Lowe *et al.*, 2014), others refute that these pathological processes are directly related (Furst *et al.*, 2012, Altmann *et al.*, 2015). The lack of association between these pathologies has been supported by studies showing the absence of hypometabolism in some brain regions with high Aβ load as well as the presence of hypometabolism in other areas with low Aβ concentrations (Edison *et al.*, 2007, Li *et al.*, 2008,

Forster *et al.*, 2012). Notably, the lack of association between regional Aβ and hypometabolism contrasts with the idea of a direct deleterious effect of Aβ on disease progression as initially proposed in the Aβ hypothesis (Morris and Price, 2001, Furst *et al.*, 2012).

One possible explanation that links Aβ with disease progression and integrates the aforementioned conflicting observations is the idea that regional hypometabolism is caused by the toxic effects of Aβ aggregation from distant rather than topographically overlapping brain regions. Indeed, early observations using [^{18}F]fluorodeoxyglucose ([^{18}F]FDG) positron emission tomography (PET) support this notion, by showing that brain damage may lead to hypometabolism in remote, but metabolically connected cortical areas (Akiyama *et al.*, 1989, Nagasawa *et al.*, 1994, Meguro *et al.*, 1999). These results highlight the possibility of a direct deleterious effect of Aβ on distant hypometabolism, which might be being overlooked by the current biomarker studies.

Regardless of the presence of a regional correlation between Aβ and hypometabolism, it is well established that the topographic coexistence of these pathologies in some brain regions such as the posterior cingulate cortex constitutes a signature of forthcoming dementia symptoms (Buckner *et al.*, 2005, Sperling *et al.*, 2009, Landau *et al.*, 2012, Mosconi, 2013). Also, studies have shown that either Aβ or hypometabolism may be the first abnormality in these regions (Jack *et al.*, 2013), and that cognitive changes may be potentiated by an interactive effect between these processes (Mormino *et al.*, 2014). Together, these results indicate that although regional Aβ may not be the cause of its overlapping hypometabolism, progression to dementia may be the result of a local interaction between these pathologies.

Here, we tested a hypothesis in which distant Aβ aggregation determines the region's metabolic vulnerability, whereas the synergy between this regional vulnerability with co-localized concentrations of Aβ determines the progression to dementia. To test this hypothesis, we assessed preclinical, mild cognitive impairment (MCI), and AD dementia individuals based on the assumption that these associations are disease phase dependent. Also, we conducted the same analysis in transgenic rats that display Aβ single pathology to test this model in the absence of other brain human proteinopathies, such as neurofibrillary tangles, commonly observed in AD patients (Do Carmo and Cuello, 2013).

5.4 Results

Demographics and key characteristics of the human population are summarized in Table 5-1. Voxel-wise analysis of covariance showed that compared to cognitively normal (CN) individuals, MCIs had reduced gray matter density in the medial temporal cortex (Supplementary Fig. 1a), whereas AD patients had reductions in the precuneus, posterior cingulate, and temporal cortices (Supplementary Fig. 1d). MCI and AD individuals had reduced metabolism in the precuneus, posterior cingulate, inferior parietal, and temporal cortices (Supplementary Fig. 1b, e). MCI and AD individuals had widespread cortical Aβ deposition (Supplementary Fig. 1c, f).

Aβ is unrelated to overlapping hypometabolism

In Aβ positive individuals segregated by clinical diagnostics, voxel-wise models showed that Aβ was not locally associated with hypometabolism in CN, MCI, and AD. On the other hand, these models showed that global Aβ is associated with hypometabolism in the posterior cingulate,

precuneus, lateral temporal, and inferior parietal cortices in CN (Fig. 5-1a, d) and MCI (Fig. 5-1b, e). Additionally, a bootstrap-scheme supported that regional Aβ did not affect the stability of the global Aβ effects on hypometabolism in the models mentioned above (Supplementary Fig. 2). No significant associations were found between Aβ and hypometabolism in AD patients.

We further replicated the results found in humans using a cohort of 20 rats (10 homozygous McGill-R-Thy1-APP rats overexpressing human Aβ precursor protein and 10 wild-type Wistar rats). They were 11 months old, and the wild-type rats provided the means for determining that 11-month McGill-R-Thy1-APP transgenic rats presented mild cognitive symptoms, with a significant baseline genotype effect on the Morris Water Maze (MWM) (P = 0.03). In the transgenic Aβ rats, the voxel-wise regression supported that local Aβ and hypometabolism were unrelated to one another. On the other hand, the model revealed that global Aβ load was strongly associated with hypometabolism in the retrosplenial cortex (which corresponds to the posterior cingulate in humans (Lu *et al.*, 2012)), and medial and lateral temporal, and inferior parietal cortices (Fig. 5-1c, f).

Aβ determines distant hypometabolism in functionally connected regions

In Aβ positive individuals, metabolic connectivity analysis showed that the regions comprising the brain's DMN in the precuneus, posterior cingulate, lateral temporal, inferior parietal, and medial prefrontal cortices were highly correlated with each other (Fig. 5-2b). Partial correlation matrices revealed that Aβ is negatively associated with metabolism in distant but metabolically connected brain regions (Fig. 5-2c-h and Supplementary Movie 1). Notably, the elements of the glucose-glucose and glucose-Aβ matrices were highly negatively correlated with one another (r

= − 0.54, $P < 0.0001$), which reinforced the link between metabolic connectivity and Aβ effects. Furthermore, the lack of correlation between the glucose-Aβ matrix elements and the Euclidean distance between regions ($r = -0.0006$, $P = 0.9544$) supported that regions' proximity did not drive these correlations.

In Aβ positive individuals segregated by clinical diagnostics, voxel-wise network analysis showed that Aβ load in the precuneus, posterior cingulate, lateral temporal, inferior parietal, and medial prefrontal cortices is associated with distant but within-DMN hypometabolism in CN (Fig. 5-3) and MCI (Fig. 5-4). On the other hand, Aβ outside of the DMN either did not associate with hypometabolism or was associated with hypometabolism predominantly in regions comprising other brain networks, such as the Frontoparietal and Limbic networks. No significant associations were found between Aβ and hypometabolism in AD patients.

In the transgenic Aβ rats, the voxel-wise regression analysis confirmed that Aβ is associated with distant, rather than co-localized, hypometabolism (Fig. 5-5). As expected, there were no associations between Aβ and hypometabolism uptake in the wild-type control rats.

Synergy of Aβ with overlapping hypometabolism on cognitive decline

A voxel-wise interaction model showed that high local levels of Aβ and low local levels of glucose uptake in the precuneus, posterior cingulate, inferior parietal, and lateral temporal cortices synergistically determined subsequent cognitive decline up to 5.6 years in MCI Aβ positive individuals (Fig. 5-6a, c, Supplementary Fig. 3, and Supplementary Movie 2). This local interaction also shortened the time-to-progression from MCIs Aβ positive to dementia ($P <$

0.0001). In addition, a bootstrap analysis further confirmed that the effect of the local interaction between Aβ and metabolism on cognitive decline was not influenced by a global Aβ effect (Supplementary Fig. 4). Moreover, analysis of variance supported that the models with the interaction term best described the relationship between overlapping biomarkers and cognitive decline as compared to reduced models assessing: 1) only Aβ, 2) only metabolism, and 3) Aβ plus metabolism, with a $P < 0.0001$ in all three cases. In CN and AD Aβ positive individuals, the aforementioned interaction was not significantly associated with cognitive decline.

In the transgenic Aβ rats, a voxel-wise interaction model supported the synergy between Aβ and overlapping hypometabolism in the retrosplenial, inferior parietal, and mediolateral temporal cortices as a determinant of cognitive decline over 8 months (Fig. 5-6b, d). This interaction was absent in the wild-type control rats.

The distant and local Aβ effects on metabolism well describe AD progression

Structured equation model (SEM) showed that the construct in which Aβ occurring in distant regions drives hypometabolism, whereas the interaction between this hypometabolism and the co-localized Aβ determines cognitive decline fits the data well (Fig. 5-7). Notably, SEM testing the association between Aβ and hypometabolism on subsequent cognitive decline using a classical sequential model or a purely synergistic model fitted the data poorly (Supplementary Fig. 5).

5.5 Discussion

In summary, we have shown that Aβ is associated with vulnerability in distant brain regions functionally connected by the DMN, whereas the synergy between this vulnerability with local Aβ levels is related to the clinical progression to dementia (Fig. 5-8). Remarkably, similar results in transgenic Aβ rats, which do not form neurofibrillary tangles (Do Carmo and Cuello, 2013), supported this model as an independent mechanism of cognitive deterioration.

Our results indicate that the regional hypometabolism observed in AD may derive from distant Aβ effects within brain regions connected by the DMN. This observation is supported by early studies showing that lesions in remote brain regions are associated with DMN hypometabolism (Akiyama *et al.*, 1989, Nagasawa *et al.*, 1994, Meguro *et al.*, 1999). For instance, studies in non-human primates show that localized surgical lesions lead to hypometabolism in metabolically connected brain areas and that the severity of the inflicted lesion correlates with the degree of remote hypometabolism (Meguro *et al.*, 1999). These studies suggest that this occurs due to a synaptic disconnection between the damaged and the remote brain region (Meguro *et al.*, 1999). Based on these observations, one may argue that the regional patterns of hypometabolism in AD derive from a decreased synaptic input from distant but DMN connected brain areas affected by Aβ. Also, we have shown that global Aβ load, rather than local, is associated with regional DMN hypometabolism, which is in line with previous studies (Altmann *et al.*, 2015). Expanding upon these studies, our findings suggest that this might be explained by the fact that Aβ from several distant brain regions contributes to regional hypometabolism. Therefore, it seems reasonable that a global Aβ composite contemplating all distant brain regions shows a better association with regional hypometabolism than its local Aβ levels. Altogether, our results corroborate the toxic effects of Aβ on the DMN as previously suggested by the network neurodegeneration hypothesis

of AD (Buckner *et al.*, 2008, Seeley *et al.*, 2009, Sperling *et al.*, 2009), by showing that cortical Aβ leads to hypometabolism in distant regions interconnected by the brain's DMN, rather than merely locally, as inferred from the traditional view (Buckner *et al.*, 2008).

On the other hand, our results suggest a synergy between the local levels of Aβ and topographically overlapped DMN vulnerability as a driving force behind dementia symptoms. It is well known that individuals might respond differently to Aβ based on their capacity to compensate through the reconfiguration of pre-existent or recruitment of alternative synapses using the DMN (Buckner *et al.*, 2008, Elman *et al.*, 2014). Moreover, DMN hypometabolism has been repeatedly suggested to represent underlying network dysfunction (Landau *et al.*, 2012, Altmann *et al.*, 2015, Passow *et al.*, 2015) and metabolic connectivity has been shown to represent synaptic pathways in the human brain (Stern *et al.*, 2005, Lee *et al.*, 2008, Riedl *et al.*, 2016). Thus, the hypometabolism in our results may indicate the dysfunction of the DMN in recruiting alternative synapses in the face to the toxic effects of Aβ. As such, our model could be understood to mean that the toxic effects of Aβ and the underlying local levels of DMN dysfunction in handling these toxic effects synergistically determine the severity of the subsequent cognitive deterioration. Together, these findings support that regional vulnerability to Aβ plays an important role in the progression to AD and that this occurs through the decrease of the capacity of the DMN to compensate for the local deleterious effects of Aβ (Mattson and Magnus, 2006, Jackson, 2014, Walsh and Selkoe, 2016).

Although our results showed that regional metabolic vulnerability depends on distant Aβ, other factors may potentiate this vulnerability in AD. Determinants of such vulnerability might include

inflammatory agents and pathology related stressors that might lead to biochemical dysregulations, resulting in decreased synaptic exchanges and therefore hypometabolism (Mattson and Magnus, 2006, Kreisl *et al.*, 2013, Lesne *et al.*, 2013, Savas *et al.*, 2015). Other factors may include cerebral vascular diseases, systemic metabolic disorders, and allele variants implicated in brain plasticity and resilience (Mesulam, 1999, Ossenkoppele *et al.*, 2015, Pascoal *et al.*, 2016). Also, previous studies have suggested that *APOE ε4* may lead to hypometabolism independently of Aβ (de Leon *et al.*, 1987, Jagust *et al.*, 2012). Recently, it has been shown that astrocytes play an important role in [^{18}F]FDG signal (Zimmer *et al.*, 2017). Since astrocytes have been associated with numerous mechanisms involving neuronal plasticity and transmission (Volterra and Meldolesi, 2005), astrocytic dysfunction may be involved in the DMN vulnerability reported here.

As previously reported by our group and others, interactions between Aβ and tau proteins determine AD progression (Fortea *et al.*, 2014, Pascoal *et al.*, 2016, Pascoal *et al.*, 2016). Since glucose metabolism is proposed to be closely linked to tau pathology (Ossenkoppele *et al.*, 2015), the regional effects of hypometabolism in the present study could be merely inferred as a proxy of neurofibrillary tangles. Therefore, we used the McGill-R-Thy1-APP rats overexpressing human Aβ pathology to clarify our results. Remarkably, the similar results in our transgenic Aβ rats, which do not form tangles (Do Carmo and Cuello, 2013), supported the associations between Aβ and DMN vulnerability as a tau-independent mechanism of cognitive deterioration. It is worth to mention that, although independent, this model is likely to be highly potentiated by neurofibrillary tangles, which is supported by the more markedly cognitive deterioration found in humans as compared to the transgenic Aβ rats. Indeed, it is probable that

the Aβ induced metabolic vulnerability reported here will create a favorable environment also for neurofibrillary tangles to determine cognitive decline. Importantly, the DMN is suggested as an evolutionarily conserved feature involved in the integration of cognitive abilities in humans and rodents (Swanson, 1992, Lu *et al.*, 2012).

Methodological strengths of the present study include the use of continuous biomarkers analyzed with a robust voxel-wise approach, the large sample size, and the use of an animal model in a controlled experimental setting, which permitted assessing the effects of Aβ on metabolism independent of possible confounding factors such as neurofibrillary tangles. This study has methodological limitations. Our studied population represents a self-selected group of elderly individuals motivated to participate in an AD study. Therefore, these individuals may not represent a general elderly population. In addition, it would be highly desirable to study the models proposed here also in a younger population. In a heterogeneous population such as MCIs, some individuals have early Aβ deposition and may present a positive association between Aβ and metabolism (Ashraf *et al.*, 2015), while others in later disease stages may present a negative association. Thus, these opposing phenomena in the same population may obscure the regional association between these biomarkers. Although patients with AD dementia had both high levels of Aβ deposition and DMN hypometabolism, the interaction between these pathologies was not associated with subsequent cognitive deteriorations. One might argue that this could be explained by the well reported *"ceiling effect"* of Aβ pathology in late disease phases (Jack *et al.*, 2013). Although we restricted our analyses to Aβ positive individuals and adjusted the models for p-tau levels, we cannot exclude that other pathological processes than Aβ - such as tau aggregates, neuroinflammation, cholinergic depletion, cerebrovascular disease, α-synuclein,

and TDP-43 – have influenced the interpretation of the present results (Jicha *et al.*, 2006). McGill-R-Thy1-APP rats develop Aβ plaque and oligomeric species (Leon *et al.*, 2010). Since regional Aβ load is highly associated with regional oligomeric Aβ (Lesne *et al.*, 2013), the deleterious effects of Aβ on metabolism reported here might reflect oligomers rather than fibrillar conformations. Also, there are large pathophysiological differences between human AD and transgenic models overexpressing Aβ. However, it is important to mention that the less aggressive progression of Aβ in rats, compared to mice, makes this model more similar to the insidious disease progression of elderlies with sporadic AD. For instance, McGill-R-Thy1-APP mice and rats express exactly the same mutations, but rats present plaques at 6–9 months while mice do as early as at 4 months (Do Carmo and Cuello, 2013). Importantly, the much larger brain size of rats (approximately 5 times bigger than mice) makes the identification of specific brain structures using techniques with low spatial resolution, such as PET, possible to be performed in this study (Zimmer *et al.*, 2014).

To conclude, our results suggest that within the brain's DMN; regional vulnerability is associated with distant Aβ, while the interaction between this vulnerability with local Aβ is associated with dementia.

5.6 Material and Methods

Human subjects

Data used in the preparation of this article were obtained from the Alzheimer's Disease Neuroimaging Initiative (ADNI) database, phases GO and 2 (adni.loni.usc.edu). ADNI was launched in 2003 as a public-private partnership, led by Principal Investigator Michael W.

Weiner, MD. The primary goal of ADNI has been to test whether serial magnetic resonance imaging (MRI), PET, other biological markers, and clinical and neuropsychological assessments can be combined to measure the progression of MCI and early AD. ADNI study was approved by the ethics committees of each participating site, and a written informed consent was obtained from all participants. For the present study, we selected participants who underwent [^{18}F]FDG PET, [^{18}F]florbetapir PET, MRI, and cerebrospinal fluid (CSF) p-tau at baseline, as well as cognitive assessments at baseline and follow-up. Cognition was assessed with Mini-Mental State Examination (MMSE), Rey Auditory Verbal Learning Test 30-min delayed recall, Trail Making Test Part A and B, and Boston Naming Test. Control individuals had MMSE scores of 24 or higher and a clinical dementia rating (CDR) of 0. MCIs had MMSE scores equal to or greater than 24, a CDR of 0.5, subjective and objective memory impairments, and essentially normal activities of daily living. AD dementia patients had MMSE scores lower than or equal to 26, CDR higher than 0.5, and met the National Institute of Neurological and Communicative Disorders and Stroke–Alzheimer's Disease and Related Disorders Association criteria for probable AD (McKhann *et al.*, 1984). Individuals did not present other neuropsychiatric disorders (Further information about ADNI cognitive tests and inclusion/exclusion criteria may be found at www.adni-info.org).

Animal use

We imaged and cognitively assessed 20 rats, 10 homozygous McGill-R-Thy1-APP rats overexpressing human Aβ precursor protein (Do Carmo and Cuello, 2013) with the Swedish double mutation (K670N, M671L (Mullan *et al.*, 1992)) and the Indiana mutation (V717F (Murrell *et al.*, 1991)), along with 10 wild-type Wistar rats. Half of the rats in each group were

males. The rats performed MRI, [^{18}F]FDG PET, and [^{18}F]NAV4694 PET at baseline (11 months old (SD 0.14)), as well as the MWM test at baseline and at 8 months follow-up. The MWM was performed with four trials per day, over four consecutive days. The rats were placed on the platform if they failed to find it within 90 s, and we assumed a maximum trial length of 90 s (Morris, 1984). The time to find the platform was measured with overhead camera tracking using ANY-maze software (*Stoelting Co.*). One probe trial (no platform) and one visible platform trial were also conducted at the end of the fourth day. All rats were kept in ventilated cages in groups of two in environmentally controlled conditions: 12 hours light/dark cycle at 21 °C with access to food and water ad libitum. All procedures involving rats were performed in accordance to the Guide to the Care and Use of Experimental Animals of the Canadian Council on Animal Care and the National Institutes of Health (NIH) and were approved by the McGill Animal Care Ethics Committee.

Human imaging methods

MRI and PET acquisitions followed ADNI protocols (http://adni.loni.usc.edu/methods). T1-weighted MRIs were corrected for field distortions, non-uniformity corrected, brain masked, segmented, and non-linearly transformed to the MNI reference space using the CIVET pipeline (Zijdenbos *et al.*, 2002). Subsequently, gray matter density was computed using voxel-wise morphometry. PET scans used [^{18}F]florbetapir tracer for imaging Aβ and [^{18}F]FDG tracer for imaging glucose metabolism. Briefly, PET images were non-linearly registered to the MNI space using the individual's PET/T1-weighted native MRI registration and the non-linear MRI transformation to the MNI space. PET images were spatially smoothed to achieve a final 8-mm full-width at half maximum resolution and corrected for partial volume effects using region-

based voxel-wise (RBV) method (Thomas *et al.*, 2011). [^{18}F]Florbetapir and [^{18}F]FDG SUVR images were obtained using the cerebellum gray matter and the pons as reference regions, respectively. A global [^{18}F]florbetapir SUVR value was obtained using the precuneus, posterior and anterior cingulate, inferior and superior parietal, medial prefrontal, lateral temporal, and orbitofrontal cortices. Individuals were Aβ positive if [^{18}F]florbetapir SUVR > 1.15 (Pascoal *et al.*, 2018). Further information and the schematic representation of the human imaging methods pipeline may be found elsewhere (Pascoal *et al.*, 2016) and in the Supplementary Figure 6.

Rat imaging methods

MRIs were acquired using a Bruker 7T BioSpec 70/30 USR animal dedicated. First, the rats were anesthetized with 5% isoflurane/medical air, which was then maintained at 1-2% after placing the animals in the scanner, with the breathing at 20-30 breaths per min. We used a 37°C constant airflow to maintain the rats warm. The structural images were generated using the 7T Bruker standard 3D-True Fast Imaging with Steady State Precession (FISP) pulse sequence (Oppelt *et al.*, 1986). Gray matter density was computed using voxel-wise morphometry. PET images were acquired using a CTI Concorde R4 microPET for rodents (Siemens). PET scans used [^{18}F]NAV4694 tracer for imaging Aβ and [^{18}F]FDG tracer for imaging glucose metabolism. In preparation for the scans, rats received anesthesia using 5% isoflurane, which was then maintained at 2% throughout the procedure. The animals underwent a 9-min transmission scan using a rotating ^{57}Co point source before each PET image acquisition. For [^{18}F]NAV4694, a 60-min dynamic emission scan began concomitantly with the bolus injection of the radiotracer via the tail vein. For [^{18}F]FDG, after fasting for 12 hours, the animals received the radiotracer injection during the awake state via the tail vein. Then, a 20-min dynamic emission scan at 50

min post-injection was performed. PET images were reconstructed using a Maximum a posteriori algorithm and corrected for scattering, dead time, and decay. [^{18}F]NAV4694 non-displaceable Binding Potential (BP_{ND}) parametric images were generated using the Simplified Reference Tissue Method with the cerebellar gray matter as reference (Gunn *et al.*, 1997). [^{18}F]FDG SUVR images were generated using the pons as the reference region. PET images were co-registered to the animal's MRI and non-linearly transformed to a standardized rat brain space created based on the wild-type rats MRIs. PET images were spatially smoothed using a Gaussian kernel with a full-width at half-maximum of 2.4 mm. Further information and the schematic representation of the rat imaging methods pipeline may be found elsewhere (Zimmer *et al.*, 2014) and in Supplementary Figure 7.

Human CSF analysis

CSF p-tau at threonine 181 was measured using a multiplex xMAP Luminex platform (Luminex Corp, Austin, TX) with INNO-BIA AlzBio3 immunoassay kit-based reagents (Innogenetics, Ghent, Belgium) (Shaw *et al.*, 2009, Toledo *et al.*, 2013). Details about CSF acquisition and quantification can be found at www.adni-info.org.

Statistical analysis

Regressions were performed using R Statistical Software Package version 3.1.2 (http://www.r-project.org/) to test for significant associations between biomarkers and also demographic differences between groups for continuous variables, whereas a contingency chi-square was used for categorical variables. The voxel-wise analyses were performed using MATLAB software version 9.2 (http://www.mathworks.com) with a computational framework developed to perform

complex voxel-wise statistical operations, such as interaction models, using multiple imaging modalities in humans and rats (Fig. 5-9) (Mathotaarachchi *et al.*, 2016).

In humans, we evaluated the brain abnormalities associated with the clinical diagnosis using a voxel-wise analysis of variance in which the signal intensity of the imaging modality was used as the dependent variable, while the diagnosis was used as the independent variable.

Subsequently, voxel-wise regression models, taking into consideration voxel and global Aβ concentrations, tested the association between Aβ deposition and glucose metabolism in humans and rats. In humans, we also considered age, gender, education, APOE *ε4* status, p-tau, and gray matter density in the models, whereas in rats age, gender, and gray matter density were considered.

Then, connectivity analysis was performed using eight regions-of-interest used to assess the global PET Aβ value in the precuneus, posterior and anterior cingulate, inferior and superior parietal, medial prefrontal, lateral temporal, and orbitofrontal cortices as well as two additional regions in the insular and occipital cortices, using coordinates in the MNI ICBM atlas (Mazziotta *et al.*, 2001). The edge values were assumed to be the correlation coefficients between regions, which were used as the matrix elements. Interregional correlation coefficients were computed using Pearson partial correlation analysis controlling for age, gender, education, *APOE ε4* status, and p-tau. Metabolic connectivity was assessed with a symmetric matrix showing the strength of the correlation of glucose uptake between regions. An asymmetric matrix assessed the associations of Aβ deposition and hypometabolism between regions-of-interest. The matrices

were corrected for multiple comparisons using Bonferroni at $P < 0.05$. FDG-FDG and FDG-Aβ matrix elements were further correlated using Pearson's correlation. We also tested the correlation between the matrix elements and the Euclidean distance between nodes (mm) to ensure that the results were not driven by regions' proximity.

In humans, we further performed a voxel-wise connectivity analysis using Aβ values within the 10 regions-of-interest mentioned above as independent predictors and glucose metabolism at every voxel as the outcome accounting for age, gender, education, *APOE ε4* status, p-tau, and gray matter density. In addition, a network atlas provided the means to assess regional overlap between results and brain networks (Visual, Somatomotor, Dorsal and Ventral attention, Limbic, Frontoparietal, and Default Mode networks (Yeo *et al.*, 2011)). In rats, a voxel-wise connectivity analysis was performed using Aβ values within 8 regions-of-interest, based on previous literature, in retrosplenial, medial temporal, lateral temporal, inferior parietal, frontoparietal, olfactory bulb, cerebellar, and somatosensory cortices as independent predictors and glucose metabolism at every voxel as the outcome accounting for age, gender, and gray matter density (Swanson, 1992, Lu *et al.*, 2012).

The association between image biomarkers and cognitive changes was tested in humans with a voxel-wise model using the slope of change in cognitive performance as the dependent variable and the main and interactive effects of [^{18}F]florbetapir SUVR and [^{18}F]FDG SUVR at every voxel as independent predictors. The slope of change in cognitive performance was defined using all available MMSE evaluations for each subject with a mean of 4 (SD 0.96) evaluations spanning up to 5.6 years (mean of 3.4 years (SD 1.02)). The analysis was adjusted for global Aβ,

age, gender, education, *APOE ε4* status, p-tau, gray matter density, and follow-up duration. The voxel-wise interaction model was built as follows:

$$\Delta MMSE = \beta 0 + \beta 1(Florbetapir\ SUVR) + \beta 2\ (FDG\ SUVR) + \beta 3\ (Florbetapir\ SUVR * FDG\ SUVR) + covariates + error$$

In rats, we built the same voxel-wise model performed in humans using the slope of change in the MWM as the dependent variable and the main and interactive effects of [^{18}F]NAV4694 BP_{ND} and [^{18}F]FDG SUVR as independent predictors. A slope of change in cognitive performance was defined for each rat using the MWM changes in average (four trials) latency to find the platform over 8 months. The model was adjusted for global Aβ, age, gender, and gray matter density. The voxel-wise interaction model was built as follows:

$$\Delta MWM = \beta 0 + \beta 1(\text{NAV4694}\ BP_{ND}) + \beta 2\ (FDG\ SUVR) + \beta 3\ (\text{NAV4694}\ BP_{ND} * FDG\ SUVR) + covariates + error$$

Statistical parametric maps were corrected for multiple comparisons and the statistical significance was defined using a family-wise error rate (FWER) threshold of $P < 0.05$.

The presence of collinearity between regional and global Aβ PET values could inflate the variance of estimates, potentially leading to incorrect statistical results of significance when both effects are used in the same model. To assess whether such case occurred in our analysis, we investigated the stability of estimates by measuring the variance based on a resampling scheme

repeated 10,000 times. Additionally, the adequacy of the models with the interaction term was further assessed with an analysis of variance comparing the interaction model with each reduced model: 1) Aβ, 2) metabolism, and 3) Aβ plus metabolism.

The relationship between Aβ, metabolism, and the longitudinal cognitive decline was further assessed via SEM using the R package Lavaan (MacCallum and Austin, 2000). SEM was built to test the specific hypotheses demonstrated in each figure's meta-model (Schermelleh-Engel *et al.*, 2003). SEM was classified as satisfactory whether: comparative fit index (CFI) > 0.95 and standardized root mean square residual (SRMR) < 0.1 (Kievit *et al.*, 2014).

5.7 Tables and Figure

Table 5-1. Demographics and key characteristics of the population.

	Control	MCI	AD	*P*-values
Number of subjects	152	304	51	-
Age, y, mean (SD)	74.8 (6.8) [b]	72.1 (7.5)	74.7 (8.4) [b]	<0.001
Male, no. (%)	71 (47)	167 (55) [a]	30 (59)	0.169
APOE ε4, no. (%)	40 (26)	135 (44) [a]	34 (67) [a,b]	<0.001
Education, y, mean (SD)	16.4 (2.6)	16.2 (2.6)	15.9 (2.7)	0.389
MMSE, score, mean (SD)	29 (1.2)	28.1 (1.7) [a]	22.9 (2.2) [a,b]	<0.001
MMSE, slope of change, y, mean (SD)	−0.09 (0.5)	−0.59 (1.3) [a]	−2.21 (3.4) [a,b]	<0.001
Follow-up, y, mean (SD)	3.44 (1.0)	3.47 (0.9)	2.74 (1.1) [a,b]	<0.001
Visits, no. (SD)	4.35 (0.9)	3.93 (0.9) [a]	3.38 (0.7) [a,b]	<0.001
[^{18}F]Florbetapir, mean SUVR (SD)	1.15 (0.13)	1.23 (0.16) [a]	1.4 (0.14) [a,b]	<0.001
[^{18}F]Florbetapir positive, no. (%)	53 (35)	170 (56) [a]	46 (90) [a,b]	<0.001
[^{18}F]FDG, mean SUVR (SD)	1.41 (0.04)	1.38 (0.05) [a]	1.34 (0.05) [a,b]	<0.001

P values indicate the values assessed with analyses of variance for each variable, except for gender, APOE ε4 status, and [^{18}F]florbetapir positivity where a contingency chi-square was

performed. Post-hoc analysis provided significant differences between groups from: [a] control and [b] MCI.

Figure 5-1. Global rather than local Aβ is associated with DMN hypometabolism.

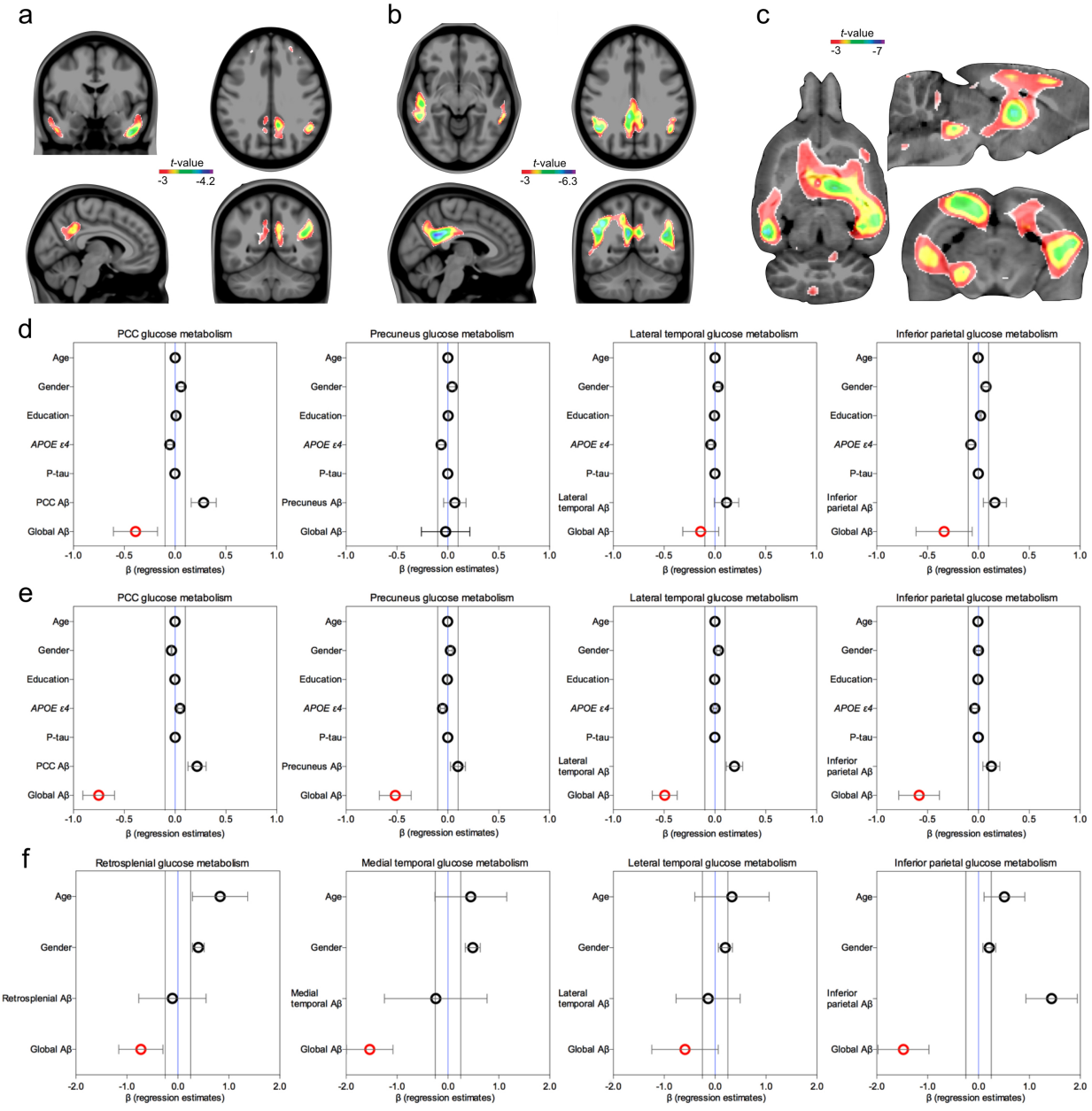

Voxel-wise models, taking voxel and global Aβ values into consideration, showed that global Aβ is associated with hypometabolism in (**a**) CN Aβ positive (n = 53) and in (**b**) MCI Aβ positive (n = 170) individuals in the posterior cingulate, precuneus, lateral temporal, and inferior parietal cortices, and in (**c**) transgenic Aβ rats (n = 10) in the retrosplenial, medial and lateral temporal,

and inferior parietal cortices. The effects of regional Aβ values on its overlapping hypometabolism were negligible in the voxel-wise models. There were no associations between Aβ and hypometabolism in AD Aβ positive (n = 46) individuals. Parametric images were FWER corrected at $P < 0.05$ and adjusted for age, gender, education, APOE ε4 status, p-tau, and gray matter density in humans, and age, gender, and gray matter density in rats. Regression models performed in (**d**) CN Aβ positive and in (**e**) MCI Aβ positive individuals within anatomically segregated regions further supported that the effects of local Aβ on hypometabolism (i.e., in the same region) were negligible. Similarly, inside segregated clusters, local Aβ effects on hypometabolism were negligible in (**f**) transgenic Aβ rats. In figures **d-f**, the dots and bars represent β estimates and standard error, respectively, of the independent variables used in the models.

Figure 5-2. Aβ is associated with hypometabolism in distant but functionally connected brain regions.

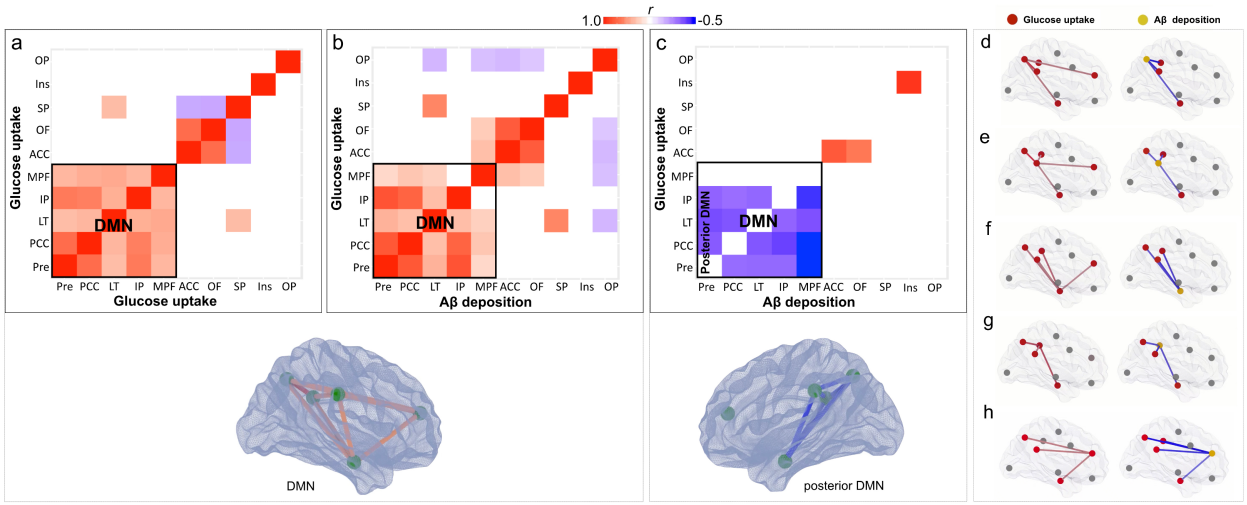

Metabolic connectivity analysis between eight regions-of-interest used to assess the global Aβ value in the precuneus (Pre), posterior (PCC) and anterior (ACC) cingulate, inferior (IP) and superior parietal (SP), medial prefrontal (MPF), lateral temporal (LT), orbitofrontal (OF), as well as two additional regions in the insular (Ins) and occipital pole (OP) cortices demonstrated that regions comprising the DMN were highly correlated with each other in (**a**) CN Aβ negative (n = 99) as well as in (**b**) all Aβ positive individuals (n = 269). (**c**) Partial correlation analysis showed that Aβ within the DMN was associated with distant but within-network hypometabolism in Aβ positive individuals. Note that Aβ and its overlapping glucose metabolism showed positive or non-correlation. Correlation maps displayed in 3D brain surfaces show the correlations of glucose-glucose and glucose-Aβ in the (**d**) Pre, (**e**) PCC, (**f**) LT, (**g**) IP, and (**h**) MPF cortices. The matrices are presented with Pearson partial correlation coefficients (r) controlled for age, gender, education, *APOE ε4* status, p-tau, and Bonferroni-corrected at $P < 0.05$.

Figure 5-3. Voxel-wise analysis showed that Aβ in DMN is predominantly associated with distant within-network hypometabolism in CN Aβ positive individuals.

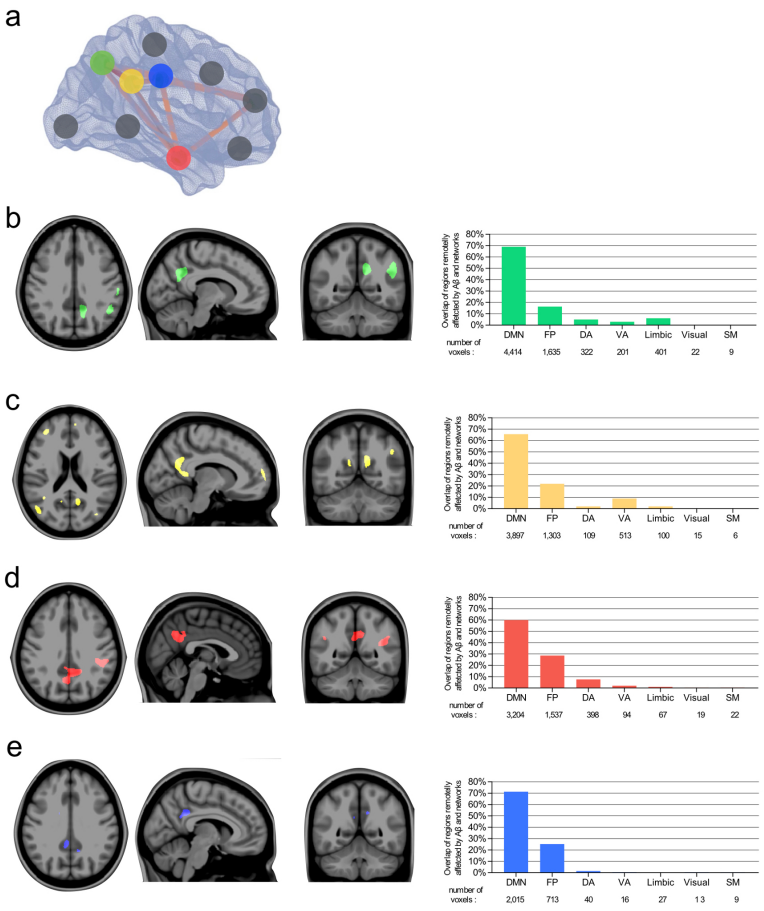

(**a**) 3D brain representation of the regions-of-interest in which the Aβ values were obtained. Statistical parametric maps, overlaid on a structural MRI template, show the brains regions where glucose metabolism was negatively associated with Aβ load in the (**b**) precuneus, (**c**) posterior cingulate, (**d**) lateral temporal, and (**e**) inferior parietal cortices in CN Aβ positive (n = 53) individuals. Aβ in medial prefrontal, anterior cingulate, orbitofrontal, superior parietal, insular, and occipital pole cortices (gray) did not associate with hypometabolism. Parametric images were FWER corrected at $P < 0.05$ and adjusted for age, gender, education, APOE ε4 status, p-tau, and gray matter density.

Figure 5-4. Voxel-wise analysis showed that Aβ in DMN is predominantly associated with distant within-network hypometabolism in MCI Aβ positive individuals.

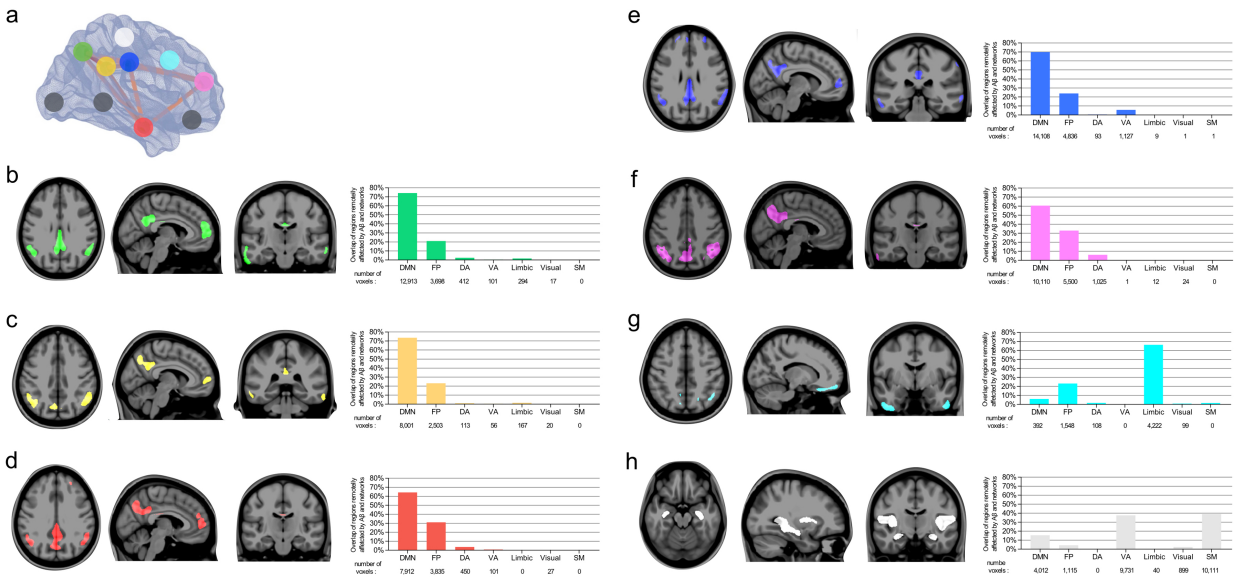

(**a**) 3D brain representation of the regions-of-interest in which the Aβ values were obtained. Statistical parametric maps, overlaid on a structural MRI template, show the brains regions where glucose metabolism was negatively associated with Aβ load in the (**b**) precuneus, (**c**) posterior cingulate, (**d**) lateral temporal, (**e**) inferior parietal, (**f**) medial prefrontal, (**g**) anterior cingulate, and (**h**) superior parietal cortices in MCI Aβ positive (n = 170) individuals. Aβ in the orbitofrontal, insular, and occipital pole cortices (gray) did not associate with hypometabolism. Parametric images were FWER corrected at $P < 0.05$ and adjusted for age, gender, education, APOE ε4 status, p-tau, and gray matter density.

Figure 5-5. Voxel-wise analysis showed that Aβ is associated with distant within-network hypometabolism in transgenic Aβ rats.

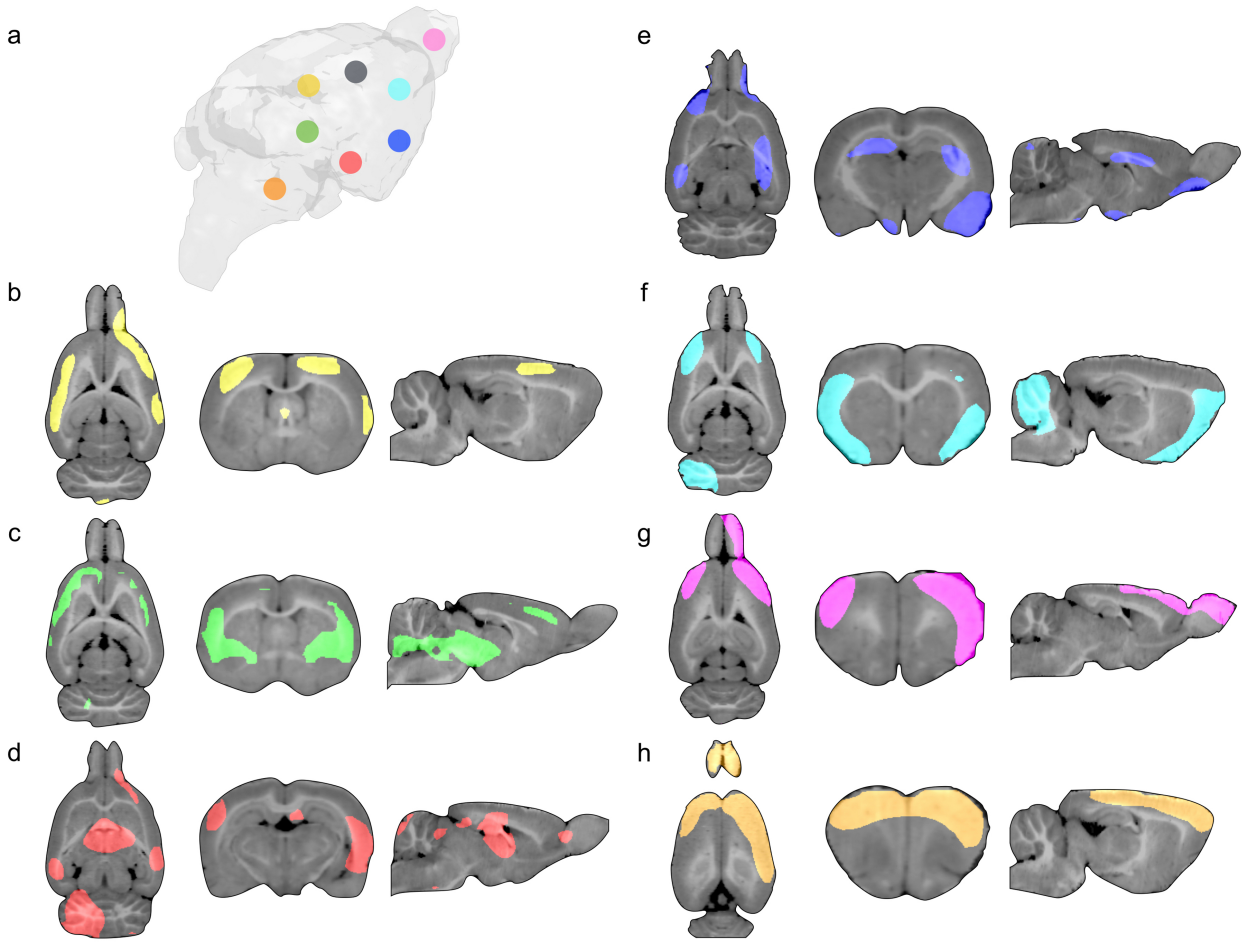

(**a**) 3D brain representation of the regions-of-interest in which the Aβ values were obtained. Statistical parametric maps, overlaid on a structural MRI template, show the brains regions where glucose metabolism was negatively associated with Aβ load in the (**b**) retrosplenial, (**c**) medial temporal, (**d**) lateral temporal, (**e**) inferior parietal, (**f**) frontoparietal, (**g**) olfactory bulb, and (**h**) cerebellar cortices in transgenic Aβ rats (n = 10). Aβ in the somatosensory cortex (gray) did not associate with hypometabolism. Parametric images were FWER corrected at $P < 0.05$ and adjusted for age, gender, and gray matter density.

Figure 5-6. The synergy of Aβ with overlapping hypometabolism drives cognitive decline.

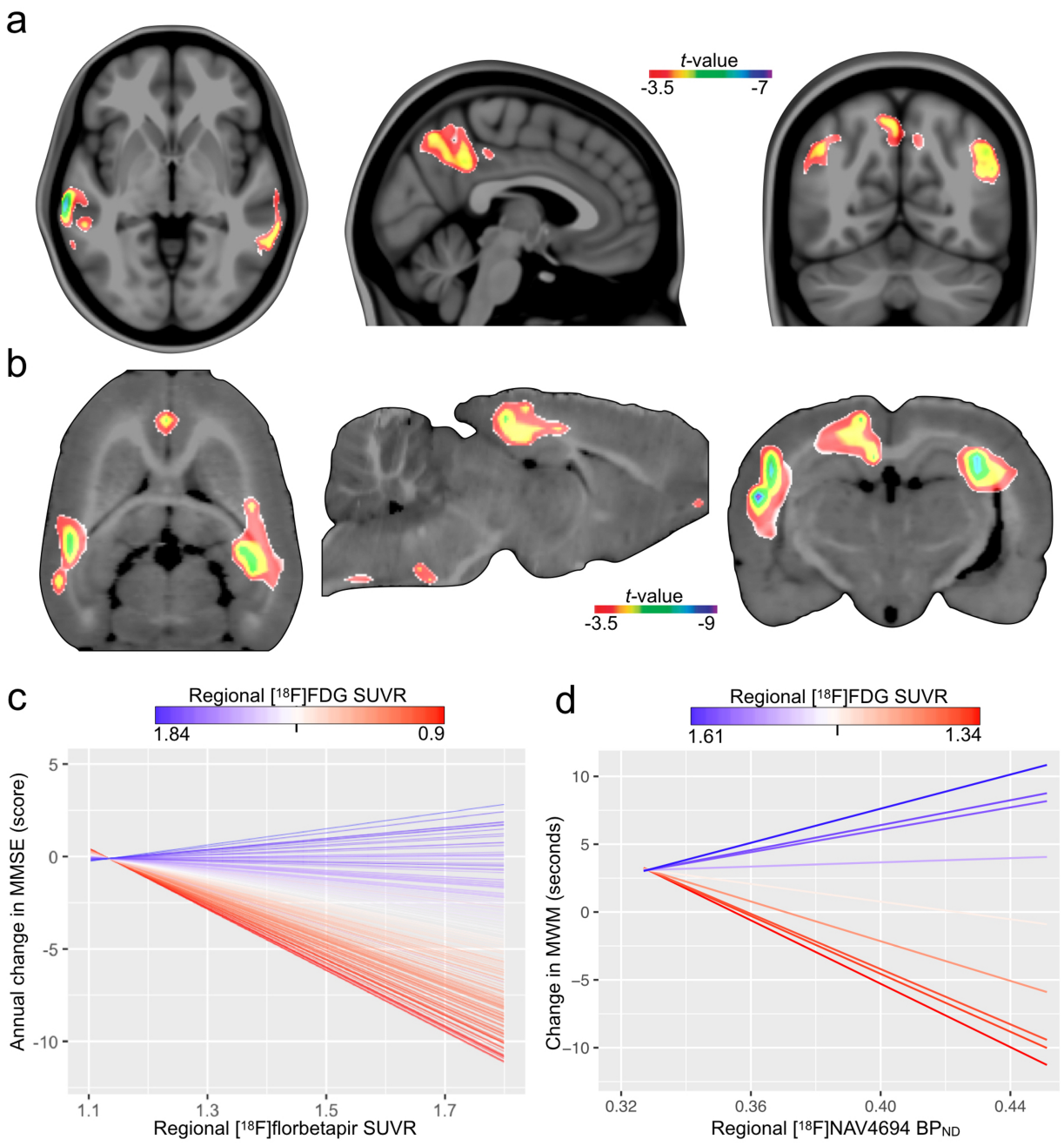

(**a**) The parametric map shows significant interactive effects at a voxel level between Aβ and glucose uptake on MMSE worsening over up to 5.6 years in the precuneus, posterior cingulate, inferior parietal, and lateral temporal cortices in MCIs Aβ positive (n = 170). (**b**) In transgenic Aβ rats, significant voxel-wise interactive effects between Aβ and glucose uptake on MWM worsening over 8 months were found in the retrosplenial cortex, which corresponds to the posterior cingulate in humans, inferior parietal, mediobasal and lateral temporal cortices. The plots show the graphical representation of the interaction in (**c**) MCIs Aβ positive and in (**d**) transgenic Aβ rats, where each parallel line represents a single subject. Parametric images were

FWER corrected at $P < 0.05$ and adjusted for global Aβ, age, gender, education, *APOE ε4* status, p-tau, gray matter density, and follow-up duration in humans, and adjusted for global Aβ, age, gender, and gray matter density in rats. For longitudinal changes in MMSE and MWM, lower values indicate greater impairment.

Figure 5-7. Structured equation modeling showed that the distant and local Aβ effects on hypometabolism well describe AD progression.

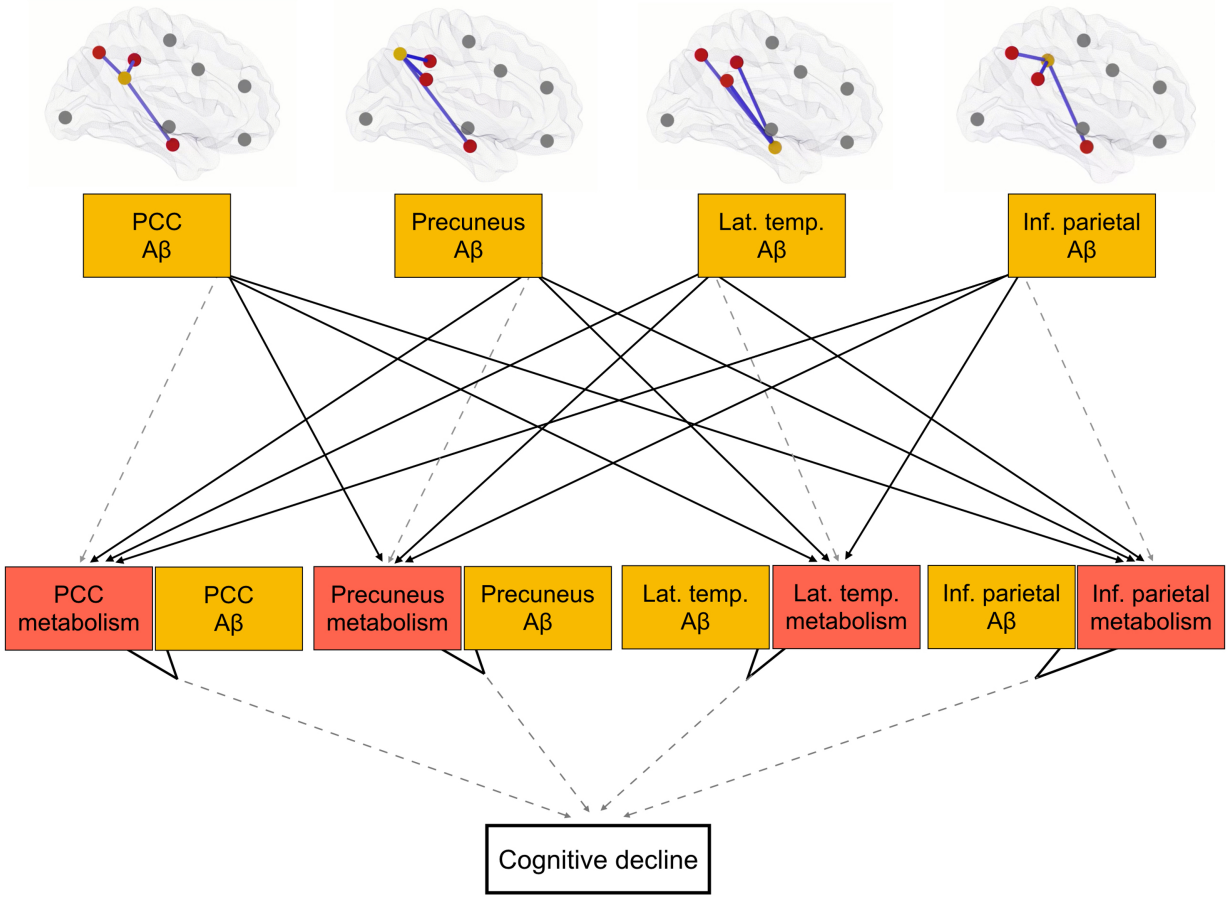

This model represents the hypothesis that distant and local Aβ effects on posterior DMN hypometabolism are associated with cognitive decline. The model used all Aβ individuals and the associations were corrected for age, gender, education, APOE ε4 status, and p-tau. Negative associations are shown in solid lines, whereas dashed lines show positive associations. In the SEM model, Aβ showed positive association with its overlapping metabolism but negative associations with distant metabolism. The hypothesized model fitted the data well (N= 269, X^2=83, degrees of freedom = 23, $P < 0.01$, standardized root mean square residual (SRMR) = 0.077, Comparative Fit Index (CFI) = 0.972, and Tucker-Lewis Index (TLI) = 0.908).

Figure 5-8. Schematic representation of the distant and local Aβ effects on metabolism.

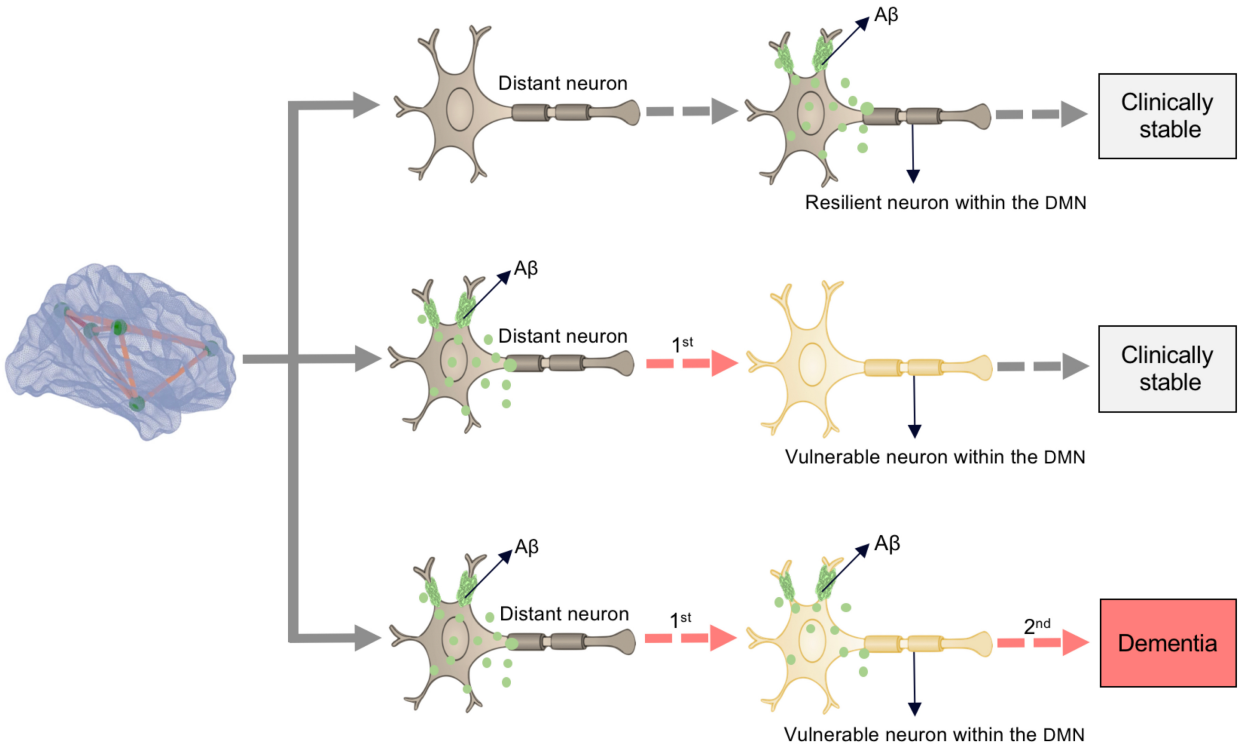

Aβ from distant brain regions leads to regional metabolic vulnerability, whereas the synergy between this vulnerability with local Aβ effects drives the clinical progression of dementia. Importantly, either Aβ or metabolic vulnerability as a single abnormality is insufficient to determine dementia.

Figure 5-9. Multimodal analytical operations performed at every brain voxel.

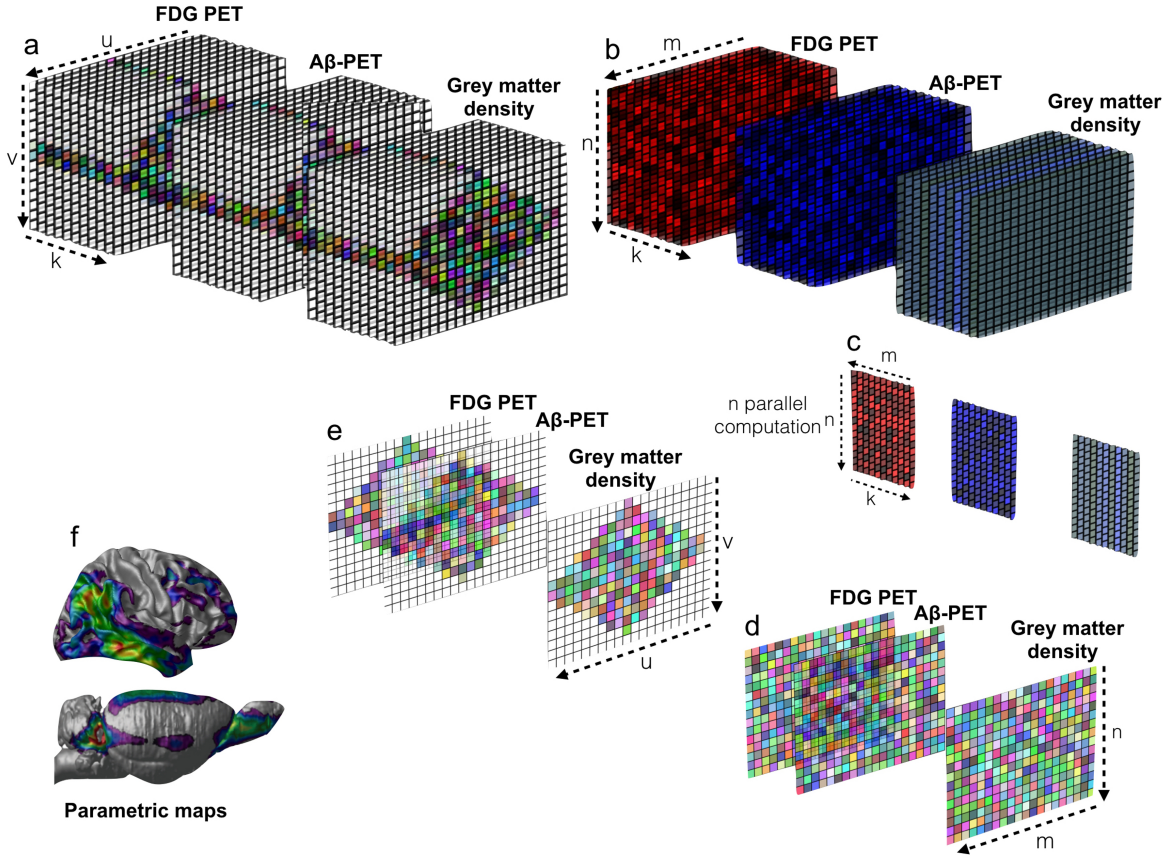

The illustration shows the analytical model developed to perform statistical operations on multiple scalar variables and with multiple imaging modalities at every brain voxel in humans and rats. Briefly, (**a**) the brain image data were retrieved from a 3D image space and converted to a 2D matrix in the image space for each subject. (**b**) Then, the image data were transformed to the processing space using artificial parcellation. (**c**) In the computational phase, the statistical modeling was performed in every brain voxel accounting for voxel and global PET uptake values, as well as voxel gray matter density and covariates. (**d**) Subsequently, statistical matrices were generated from the results and (**e**) transformed back to the 3D image space. (**f**) Finally, 3D parametric maps displaying the results of the regression models were generated. k = subjects; u = image slice; v = slice elements; m = artificial parcellation; n = elements in each parcellation.

5.8 Acknowledgments

This work was supported by the Canadian Institutes of Health Research (CIHR) (MOP-11-51-31, PR-N), Weston Brain Institute (P.R-N), the Canadian Institutes of Health Research (MOP-11-51-

31, P.R-N), the Alzheimer's Association (NIRG-12- 92090 and NIRP-12-259245, P.R-N), the Alzheimer Society Research Program and the Canadian Consortium on Neurodegeneration in Aging (CCNA) (T.A.P). A.C.C. has been supported by the CIHR. A.C.C., S.G. and P.R-N. are members of the CIHR/CCNA. Data collection and sharing for this project was funded by the Alzheimer's Disease Neuroimaging Initiative (ADNI; National Institutes of Health Grant U01 AG024904) and DOD ADNI (Department of Defense award number W81XWH-12-2-0012). ADNI is funded by the National Institute on Aging, the National Institute of Biomedical Imaging and Bioengineering and through generous contributions from the following: AbbVie, Alzheimer's Association; Alzheimer's Drug Discovery Foundation; Araclon Biotech; BioClinica; Biogen; Bristol–Myers Squibb Company; CereSpir; Eisai Inc.; Elan Pharmaceuticals; Eli Lilly and Company; EuroImmun; F. Hoffmann-La Roche and its affiliated company Genentech; Fujirebio; GE Healthcare; IXICO; Janssen Alzheimer Immunotherapy Research & Development; Johnson & Johnson Pharmaceutical Research & Development; Lumosity; Lundbeck; Merck; Meso Scale Diagnostics; NeuroRx Research; Neurotrack Technologies; Novartis Pharmaceuticals Corporation; Pfizer; Piramal Imaging; Servier; Takeda Pharmaceutical Company; and Transition Therapeutics. The Canadian Institutes of Health Research is providing funds to support ADNI clinical sites in Canada. Private sector contributions are facilitated by the Foundation for the National Institutes of Health (www.fnih.org). The grantee organization is the Northern California Institute for Research and Education, and the study is coordinated by the Alzheimer's Disease Cooperative Study at the University of California, San Diego. ADNI data are disseminated by the Laboratory for Neuro Imaging at the University of Southern California.

5.9 Supplementary Material

Supplementary Figure 1. Local diagnostic effect on gray matter density, glucose metabolism, and Aβ deposition across the AD clinical spectrum.

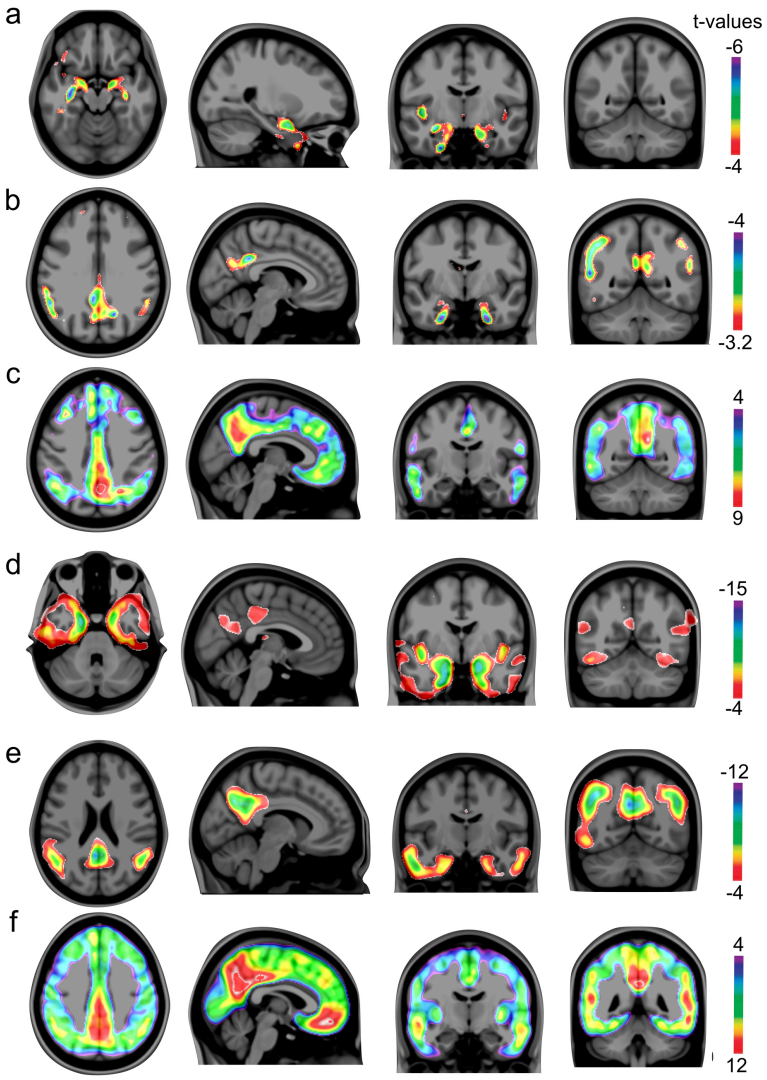

Statistical parametric maps, FWER corrected at $P < 0.05$, revealed areas with reduced gray matter density in (**a**) MCIs ($n = 304$) and (**d**) AD patients ($n = 51$); hypometabolism in (**b**) MCIs and (**e**) AD patients; and areas with increased Aβ deposition in (**c**) MCIs and (**f**) AD patients as compared to CN ($n = 152$) individuals.

Supplementary Figure 2. Regional Aβ did not affect the negative association between global Aβ and metabolism.

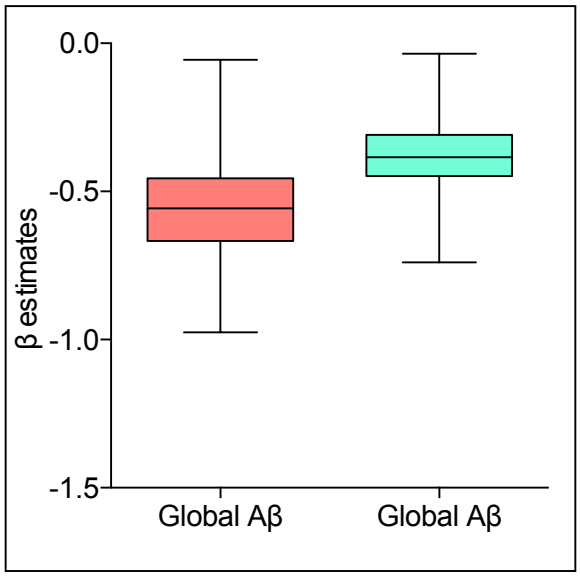

The figure shows the bootstrap-based estimates of the global [^{18}F]florbetapir effect on precuneus [^{18}F]FDG with (red box) and without (green box) precuneus [^{18}F]florbetapir effect in the models in MCIs Aβ positive (n = 170). The models were also adjusted for age, gender, education, *APOE ε4* status, and p-tau. Resampling with replacement was iterated 10,000 times and sampling distributions of resulting estimates are presented as box plots. In the plots, the lower and upper boundaries show the 25th and 75th percentiles, respectively, the horizontal line indicates the median and the error bars show the minimum and maximum estimate values. The results suggest that the presence of regional [^{18}F]florbetapir did not cause significant instability in the model since the estimates that resulted from the models with and without regional [^{18}F]florbetapir effects showed similar association between global [^{18}F]florbetapir and regional [^{18}F]FDG. Notably, all 10,000 bootstrap-based estimates showed a negative association between global [^{18}F]florbetapir and regional [^{18}F]FDG. Results were similar for PCC, lateral temporal, and inferior parietal cortices.

Supplementary Figure 3. The synergy of Aβ with overlapping hypometabolism on cognitive decline in MCIs Aβ positive.

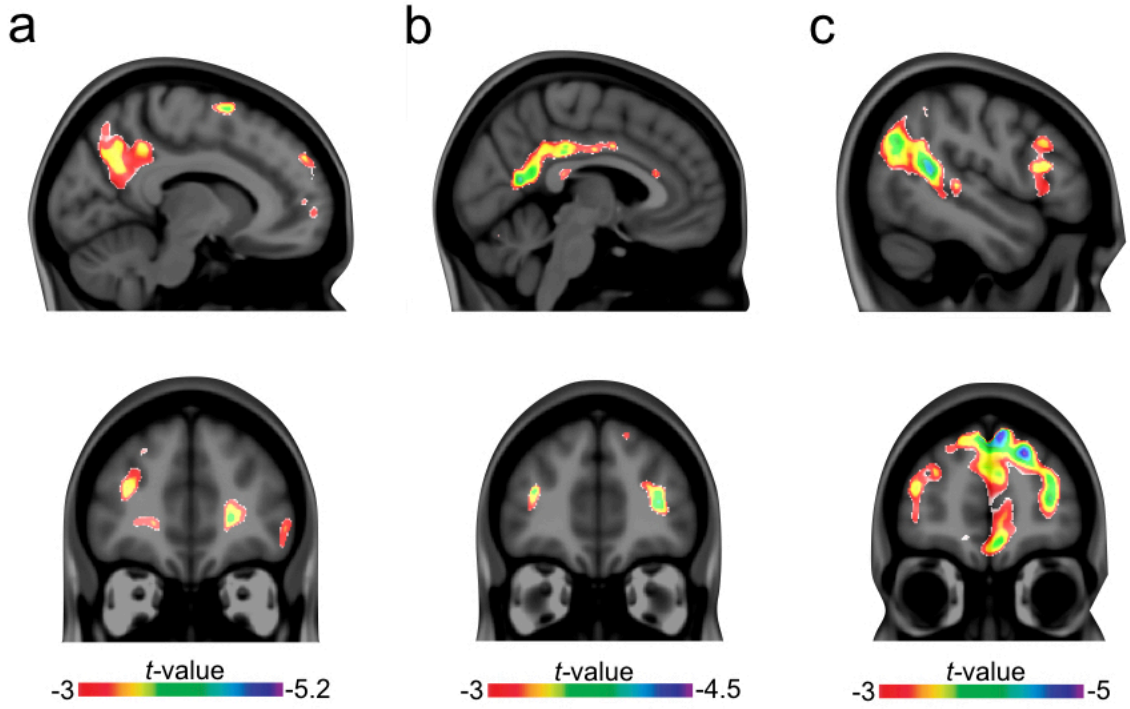

Statistical parametric maps, FWER corrected at $P < 0.05$, show regions with a significant interactive effect between Aβ and glucose uptake on worsening in (**a**) Trail Making Test Part A, (**b**) Trail Making Test Part B, and (**c**) Boston Naming Test over 2 years in MCIs Aβ positive (n = 170). Aβ and glucose metabolism interaction did not significantly associate with changes in the Rey Auditory Verbal Learning Test 30-min delayed recall. There were no significant associations between the above-mentioned interaction and cognitive tests in CN and AD individuals. Trail Making Test Part A assessed psychomotor speed processing, whereas Part B executive function. Boston Naming Test was used to test language and the Rey Auditory Verbal Learning Test assessed 30-min delayed recall memory.

Supplementary Figure 4. Global Aβ values did not affect the stability of the local interaction between Aβ and hypometabolism.

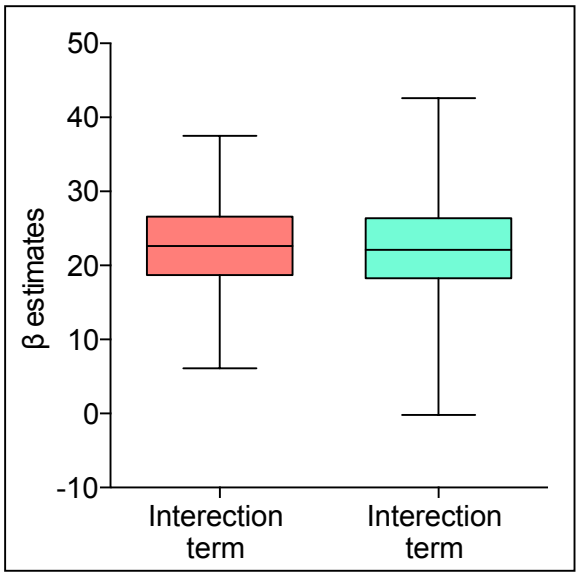

The figure shows the bootstrap-based estimates of the interactive effect of regional [^{18}F]florbetapir and [^{18}F]FDG on changes in cognition (MMSE) with (red box) and without (green box) global [^{18}F]florbetapir effect in MCIs Aβ positive (n = 170). The models were also adjusted for age, gender, education, *APOE ε4* status, and p-tau. Resampling with replacement was iterated 10,000 times and sampling distributions of resulting estimates are presented as box plots. In the plots, the lower and upper boundaries show the 25th and 75th percentiles, respectively, the horizontal line indicates the median and the error bars show the minimum and maximum estimate values. Regional PET values used in the models were the mean of the average voxels presented in figure 6a. The results suggest that the presence of global [^{18}F]florbetapir did not cause instability in the model since the estimates that resulted from the models with global [^{18}F]florbetapir effects were similar to the ones that resulted from the models without global [^{18}F]florbetapir effects.

Supplementary Figure 5. Structured equation meta-models representing a sequential and a synergistic models of AD progression.

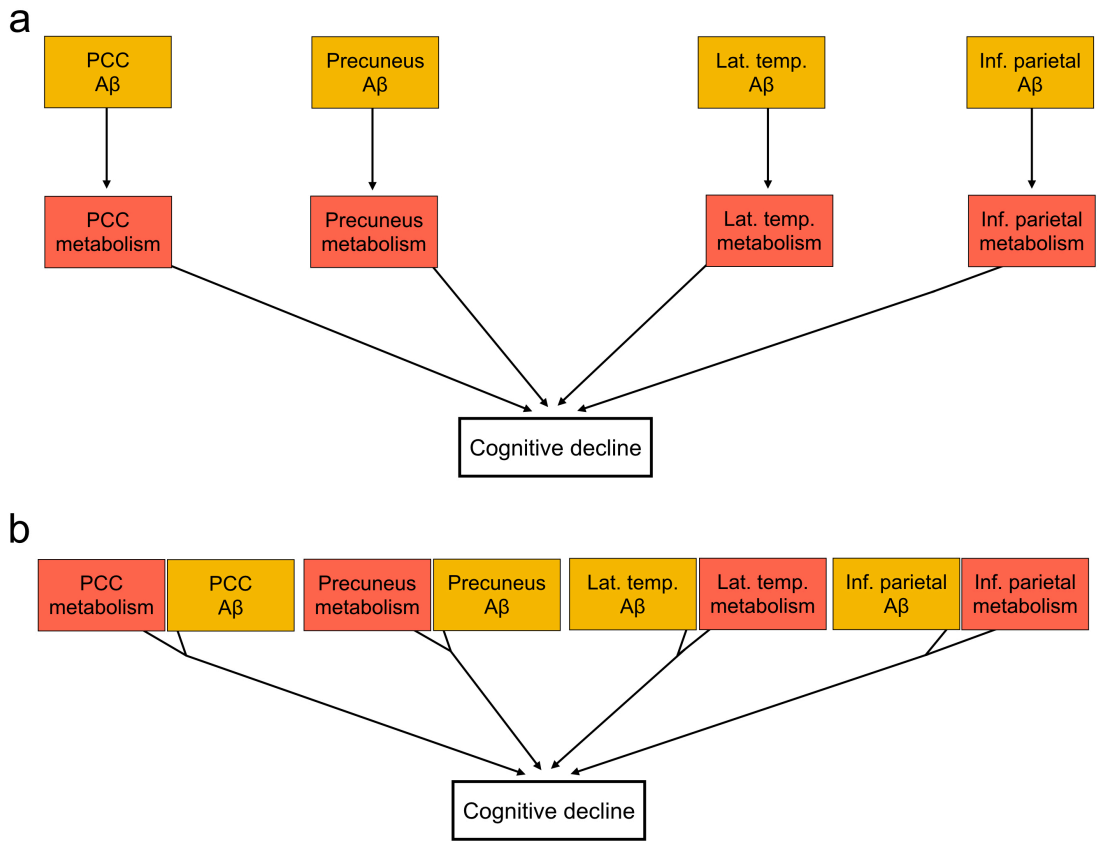

(**a**) This meta-model represents a sequential model of AD progression, and its respective SEM fitted the data poorly (N = 269, X^2 = 742, degrees of freedom = 37, $P < 0.001$, SRMR = 0.189, CFI = 0.675, and TLI = 0.341). (**b**) This meta-model represents a purely synergistic model of AD progression, and its respective SEM fitted the data poorly (N = 269, X^2 = 894, degrees of freedom = 57, $P < 0.001$, SRMR = 0.237, CFI = 0.614, and TLI = 0.492).

Supplementary Figure 6. Schematic representation of the human image pipeline.

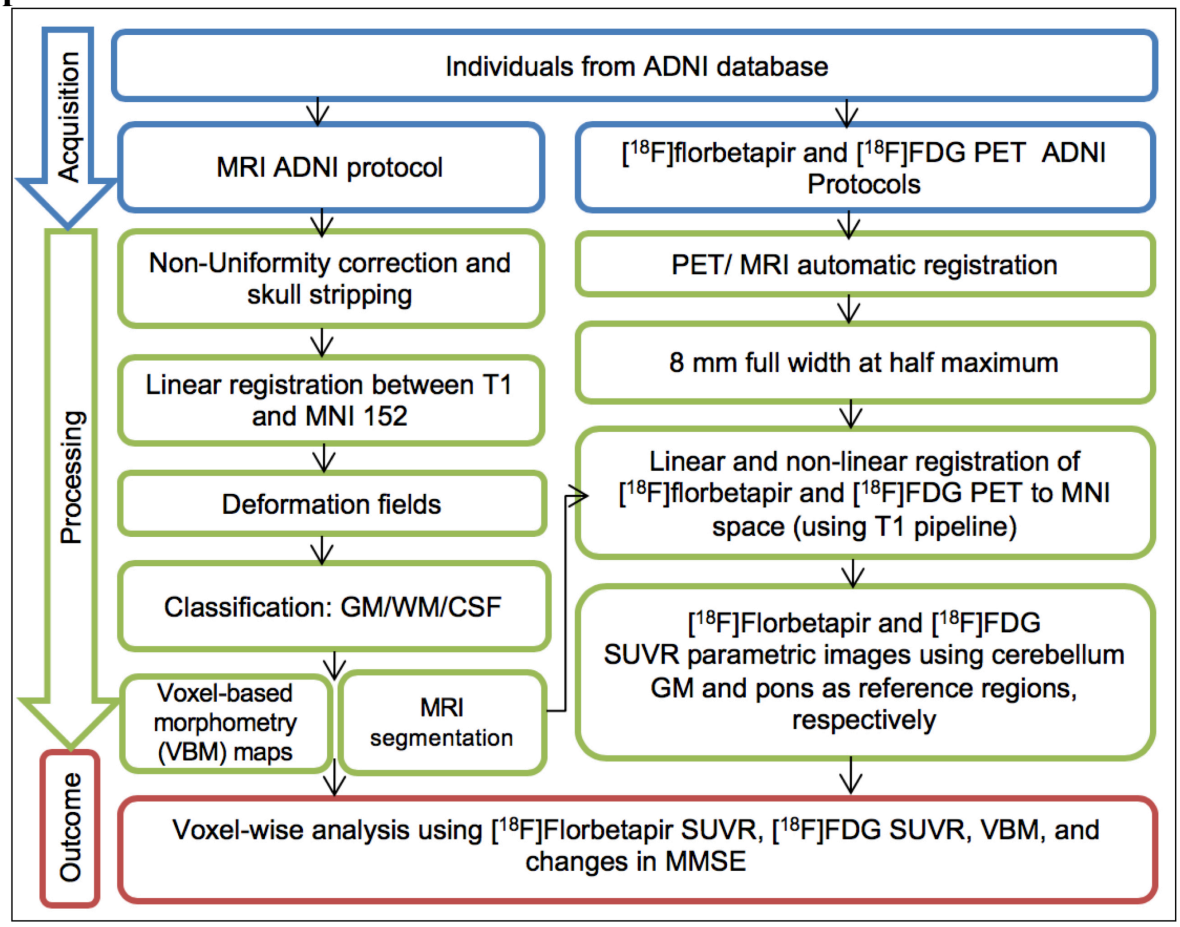

GM = gray matter; WM = white matter.

Supplementary Figure 7. Schematic representation of the rat image pipeline.

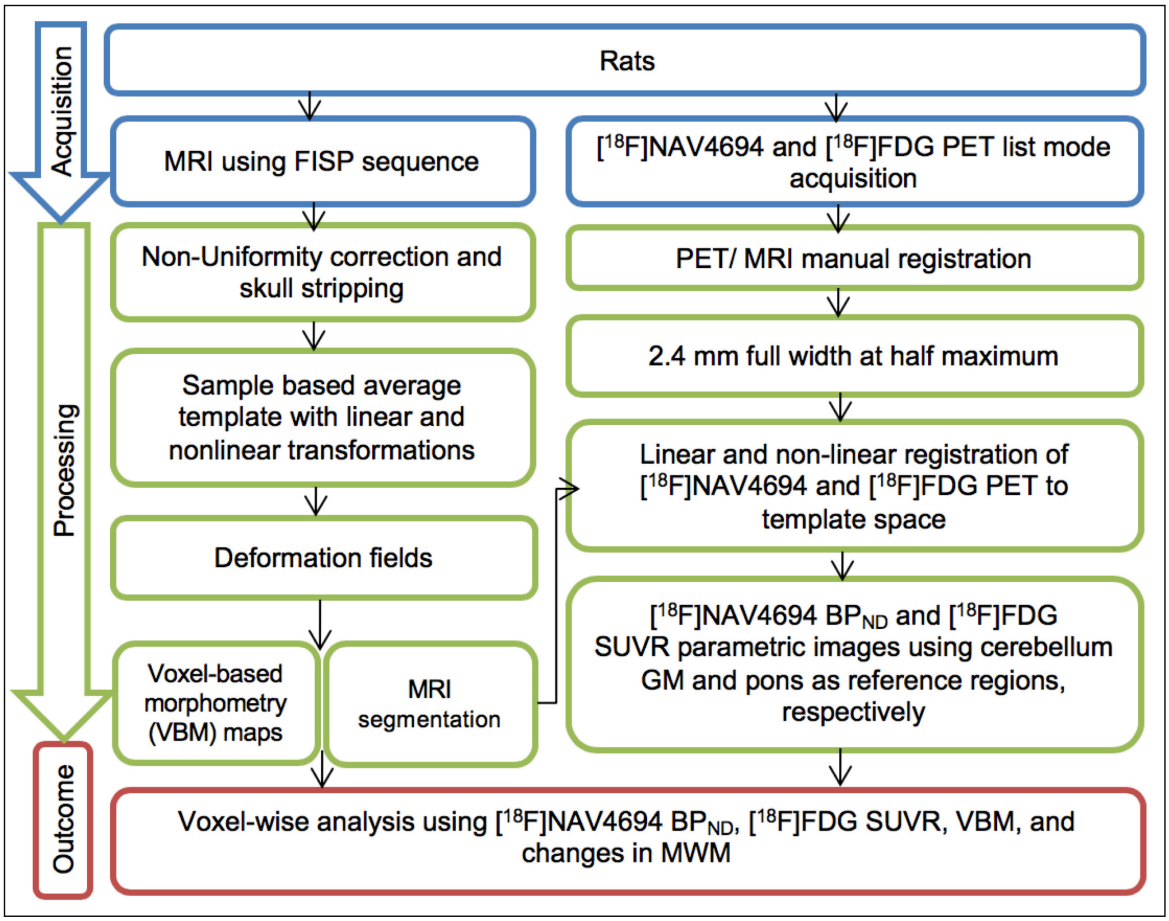

FISP = Fast Imaging with Steady State Precession.

5.10 References

Akiyama H, Harrop R, McGeer P, Peppard R, McGeer E. Crossed cerebellar and uncrossed basal ganglia and thalarnic diaschisis in Alzheimer's disease. Neurology. 1989;39(4):541-.

Altmann A, Ng B, Landau SM, Jagust WJ, Greicius MD, Alzheimer's Disease Neuroimaging I. Regional brain hypometabolism is unrelated to regional amyloid plaque burden. Brain : a journal of neurology. 2015;138(Pt 12):3734-46.

Ashraf A, Fan Z, Brooks DJ, Edison P. Cortical hypermetabolism in MCI subjects: a compensatory mechanism? European journal of nuclear medicine and molecular imaging. 2015;42(3):447-58.

Buckner RL, Andrews‐Hanna JR, Schacter DL. The brain's default network. Annals of the New York Academy of Sciences. 2008;1124(1):1-38.

Buckner RL, Snyder AZ, Shannon BJ, LaRossa G, Sachs R, Fotenos AF, et al. Molecular, structural, and functional characterization of Alzheimer's disease: evidence for a relationship between default activity, amyloid, and memory. The Journal of neuroscience : the official journal of the Society for Neuroscience. 2005;25(34):7709-17.

de Leon MJ, George AE, Tomanelli J, Christman D, Kluger A, Miller J, et al. Positron emission tomography studies of normal aging: a replication of PET III and 18-FDG using PET VI and 11-CDG. Neurobiology of aging. 1987;8(4):319-23.

Do Carmo S, Cuello AC. Modeling Alzheimer's disease in transgenic rats. Mol Neurodegener. 2013;8:37.

Edison P, Archer HA, Hinz R, Hammers A, Pavese N, Tai YF, et al. Amyloid, hypometabolism, and cognition in Alzheimer disease: an [11C]PIB and [18F]FDG PET study. Neurology. 2007;68(7):501-8.

Elman JA, Oh H, Madison CM, Baker SL, Vogel JW, Marks SM, et al. Neural compensation in older people with brain amyloid-[beta] deposition. Nature neuroscience. 2014;17(10):1316-8.

Engler H, Forsberg A, Almkvist O, Blomquist G, Larsson E, Savitcheva I, et al. Two-year follow-up of amyloid deposition in patients with Alzheimer's disease. Brain : a journal of neurology. 2006;129(Pt 11):2856-66.

Forster S, Grimmer T, Miederer I, Henriksen G, Yousefi BH, Graner P, et al. Regional expansion of hypometabolism in Alzheimer's disease follows amyloid deposition with temporal delay. Biol Psychiatry. 2012;71(9):792-7.

Fortea J, Vilaplana E, Alcolea D, Carmona-Iragui M, Sanchez-Saudinos MB, Sala I, et al. Cerebrospinal fluid beta-amyloid and phospho-tau biomarker interactions affecting brain structure in preclinical Alzheimer disease. Annals of neurology. 2014;76(2):223-30.

Furst AJ, Rabinovici GD, Rostomian AH, Steed T, Alkalay A, Racine C, et al. Cognition, glucose metabolism and amyloid burden in Alzheimer's disease. Neurobiology of aging. 2012;33(2):215-25.

Gunn RN, Lammertsma AA, Hume SP, Cunningham VJ. Parametric imaging of ligand-receptor binding in PET using a simplified reference region model. NeuroImage. 1997;6(4):279-87.

Jack CR, Jr., Knopman DS, Jagust WJ, Petersen RC, Weiner MW, Aisen PS, et al. Tracking pathophysiological processes in Alzheimer's disease: an updated hypothetical model of dynamic biomarkers. The Lancet Neurology. 2013;12(2):207-16.

Jack CR, Jr., Wiste HJ, Weigand SD, Knopman DS, Lowe V, Vemuri P, et al. Amyloid-first and neurodegeneration-first profiles characterize incident amyloid PET positivity. Neurology. 2013;81(20):1732-40.

Jackson WS. Selective vulnerability to neurodegenerative disease: the curious case of Prion Protein. Disease Models and Mechanisms. 2014;7(1):21-9.

Jagust WJ, Landau SM, Alzheimer's Disease Neuroimaging I. Apolipoprotein E, not fibrillar beta-amyloid, reduces cerebral glucose metabolism in normal aging. The Journal of neuroscience : the official journal of the Society for Neuroscience. 2012;32(50):18227-33.

Jicha GA, Parisi JE, Dickson DW, Johnson K, Cha R, Ivnik RJ, et al. Neuropathologic outcome of mild cognitive impairment following progression to clinical dementia. Archives of neurology. 2006;63(5):674-81.

Kievit RA, Davis SW, Mitchell DJ, Taylor JR, Duncan J, Cam CANRT, et al. Distinct aspects of frontal lobe structure mediate age-related differences in fluid intelligence and multitasking. Nat Commun. 2014;5:5658.

Kreisl WC, Lyoo CH, McGwier M, Snow J, Jenko KJ, Kimura N, et al. In vivo radioligand binding to translocator protein correlates with severity of Alzheimer's disease. Brain : a journal of neurology. 2013;136(Pt 7):2228-38.

Landau SM, Mintun MA, Joshi AD, Koeppe RA, Petersen RC, Aisen PS, et al. Amyloid deposition, hypometabolism, and longitudinal cognitive decline. Annals of neurology. 2012;72(4):578-86.

Lee DS, Kang H, Kim H, Park H, Oh JS, Lee JS, et al. Metabolic connectivity by interregional correlation analysis using statistical parametric mapping (SPM) and FDG brain PET; methodological development and patterns of metabolic connectivity in adults. Eur J Nucl Med Mol Imaging. 2008;35(9):1681-91.

Leon WC, Canneva F, Partridge V, Allard S, Ferretti MT, DeWilde A, et al. A novel transgenic rat model with a full Alzheimer's-like amyloid pathology displays pre-plaque intracellular amyloid-beta-associated cognitive impairment. Journal of Alzheimer's disease : JAD. 2010;20(1):113-26.

Lesne SE, Sherman MA, Grant M, Kuskowski M, Schneider JA, Bennett DA, et al. Brain amyloid-beta oligomers in ageing and Alzheimer's disease. Brain : a journal of neurology. 2013;136(Pt 5):1383-98.

Li Y, Rinne JO, Mosconi L, Pirraglia E, Rusinek H, DeSanti S, et al. Regional analysis of FDG and PIB-PET images in normal aging, mild cognitive impairment, and Alzheimer's disease. European journal of nuclear medicine and molecular imaging. 2008;35(12):2169-81.

Lowe VJ, Weigand SD, Senjem ML, Vemuri P, Jordan L, Kantarci K, et al. Association of hypometabolism and amyloid levels in aging, normal subjects. Neurology. 2014;82(22):1959-67.

Lu H, Zou Q, Gu H, Raichle ME, Stein EA, Yang Y. Rat brains also have a default mode network. Proceedings of the National Academy of Sciences of the United States of America. 2012;109(10):3979-84.

MacCallum RC, Austin JT. Applications of structural equation modeling in psychological research. Annu Rev Psychol. 2000;51:201-26.

Mathotaarachchi S, Wang S, Shin M, Pascoal TA, Benedet AL, Kang MS, et al. VoxelStats: A MATLAB Package for Multi-Modal Voxel-Wise Brain Image Analysis. Front Neuroinform. 2016;10:20.

Mattson MP, Magnus T. Ageing and neuronal vulnerability. Nat Rev Neurosci. 2006;7(4):278-94.

Mazziotta J, Toga A, Evans A, Fox P, Lancaster J, Zilles K, et al. A probabilistic atlas and reference system for the human brain: International Consortium for Brain Mapping (ICBM). Philos Trans R Soc Lond B Biol Sci. 2001;356(1412):1293-322.

McKhann G, Drachman D, Folstein M, Katzman R, Price D, Stadlan EM. Clinical diagnosis of Alzheimer's disease: report of the NINCDS-ADRDA Work Group under the auspices of Department of Health and Human Services Task Force on Alzheimer's Disease. Neurology. 1984;34(7):939-44.

Meguro K, Blaizot X, Kondoh Y, Le Mestric C, Baron J, Chavoix C. Neocortical and hippocampal glucose hypometabolism following neurotoxic lesions of the entorhinal and perirhinal cortices in the non-human primate as shown by PET. Brain : a journal of neurology. 1999;122(8):1519-31.

Mesulam MM. Neuroplasticity failure in Alzheimer's disease: bridging the gap between plaques and tangles. Neuron. 1999;24(3):521-9.

Mormino EC, Betensky RA, Hedden T, Schultz AP, Amariglio RE, Rentz DM, et al. Synergistic effect of beta-amyloid and neurodegeneration on cognitive decline in clinically normal individuals. JAMA neurology. 2014;71(11):1379-85.

Morris JC, Price JL. Pathologic correlates of nondemented aging, mild cognitive impairment, and early-stage Alzheimer's disease. Journal of molecular neuroscience : MN. 2001;17(2):101-18.

Morris R. Developments of a water-maze procedure for studying spatial learning in the rat. J Neurosci Methods. 1984;11(1):47-60.

Mosconi L. Glucose metabolism in normal aging and Alzheimer's disease: Methodological and physiological considerations for PET studies. Clin Transl Imaging. 2013;1(4).

Mullan M, Crawford F, Axelman K, Houlden H, Lilius L, Winblad B, et al. A pathogenic mutation for probable Alzheimer's disease in the APP gene at the N-terminus of beta-amyloid. Nat Genet. 1992;1(5):345-7.

Murrell J, Farlow M, Ghetti B, Benson MD. A mutation in the amyloid precursor protein associated with hereditary Alzheimer's disease. Science. 1991;254(5028):97-9.

Nagasawa H, Kogure K, Fujiwara T, Itoh M, Ido T. Metabolic disturbances in exo-focal brain areas after cortical stroke studied by positron emission tomography. Journal of the neurological sciences. 1994;123(1):147-53.

Oppelt A, Graumann R, Barfuss H, Fischer H, Hartl W, Schajor W. FISP—a new fast MRI sequence. Electromedica. 1986;54(1):15-8.

Ossenkoppele R, Schonhaut DR, Baker SL, O'Neil JP, Janabi M, Ghosh PM, et al. Tau, amyloid, and hypometabolism in a patient with posterior cortical atrophy. Annals of neurology. 2015;77(2):338-42.

Pascoal TA, Mathotaarachchi S, Mohades S, Benedet AL, Chung CO, Shin M, et al. Amyloid-beta and hyperphosphorylated tau synergy drives metabolic decline in preclinical Alzheimer's disease. Mol Psychiatry. 2016.

Pascoal TA, Mathotaarachchi S, Shin M, Benedet AL, Mohades S, Wang S, et al. Synergistic interaction between amyloid and tau predicts the progression to dementia. Alzheimer's & dementia : the journal of the Alzheimer's Association. 2016.

Pascoal TA, Mathotaarachchi S, Shin M, Park AY, Mohades S, Benedet AL, et al. Amyloid and tau signatures of brain metabolic decline in preclinical Alzheimer's disease. European journal of nuclear medicine and molecular imaging. 2018;45(6):1021-30.

Passow S, Specht K, Adamsen TC, Biermann M, Brekke N, Craven AR, et al. Default‐mode network functional connectivity is closely related to metabolic activity. Human brain mapping. 2015;36(6):2027-38.

Riedl V, Utz L, Castrillon G, Grimmer T, Rauschecker JP, Ploner M, et al. Metabolic connectivity mapping reveals effective connectivity in the resting human brain. Proceedings of the National Academy of Sciences of the United States of America. 2016;113(2):428-33.

Savas JN, Ribeiro LF, Wierda KD, Wright R, DeNardo-Wilke LA, Rice HC, et al. The Sorting Receptor SorCS1 Regulates Trafficking of Neurexin and AMPA Receptors. Neuron. 2015;87(4):764-80.

Schermelleh-Engel K, Moosbrugger H, Müller H. Evaluating the Fit of Structural Equation Models: Tests of Significance and Descriptive Goodness-of-Fit Measures; 2003.

Seeley WW, Crawford RK, Zhou J, Miller BL, Greicius MD. Neurodegenerative diseases target large-scale human brain networks. Neuron. 2009;62(1):42-52.

Shaw LM, Vanderstichele H, Knapik-Czajka M, Clark CM, Aisen PS, Petersen RC, et al. Cerebrospinal fluid biomarker signature in Alzheimer's disease neuroimaging initiative subjects. Annals of neurology. 2009;65(4):403-13.

Sperling RA, Laviolette PS, O'Keefe K, O'Brien J, Rentz DM, Pihlajamaki M, et al. Amyloid deposition is associated with impaired default network function in older persons without dementia. Neuron. 2009;63(2):178-88.

Stern Y, Habeck C, Moeller J, Scarmeas N, Anderson KE, Hilton HJ, et al. Brain networks associated with cognitive reserve in healthy young and old adults. Cereb Cortex. 2005;15(4):394-402.

Swanson L. Brain Maps: Structure of the Rat Brain (2nd edn). Nature. 1992;363:347-50.

Thomas BA, Erlandsson K, Modat M, Thurfjell L, Vandenberghe R, Ourselin S, et al. The importance of appropriate partial volume correction for PET quantification in Alzheimer's disease. European journal of nuclear medicine and molecular imaging. 2011;38(6):1104-19.

Toledo JB, Xie SX, Trojanowski JQ, Shaw LM. Longitudinal change in CSF Tau and Abeta biomarkers for up to 48 months in ADNI. Acta neuropathologica. 2013;126(5):659-70.

Tsai J, Grutzendler J, Duff K, Gan WB. Fibrillar amyloid deposition leads to local synaptic abnormalities and breakage of neuronal branches. Nature neuroscience. 2004;7(11):1181-3.

Volterra A, Meldolesi J. Astrocytes, from brain glue to communication elements: the revolution continues. Nat Rev Neurosci. 2005;6(8):626-40.

Walsh DM, Selkoe DJ. A critical appraisal of the pathogenic protein spread hypothesis of neurodegeneration. Nat Rev Neurosci. 2016;17(4):251-60.

Yeo BT, Krienen FM, Sepulcre J, Sabuncu MR, Lashkari D, Hollinshead M, et al. The organization of the human cerebral cortex estimated by intrinsic functional connectivity. J Neurophysiol. 2011;106(3):1125-65.

Zijdenbos AP, Forghani R, Evans AC. Automatic "pipeline" analysis of 3-D MRI data for clinical trials: application to multiple sclerosis. IEEE Trans Med Imaging. 2002;21(10):1280-91.

Zimmer ER, Parent MJ, Cuello AC, Gauthier S, Rosa-Neto P. MicroPET imaging and transgenic models: a blueprint for Alzheimer's disease clinical research. Trends Neurosci. 2014;37(11):629-41.

Zimmer ER, Parent MJ, Souza DG, Leuzy A, Lecrux C, Kim HI, et al. [18F]FDG PET signal is driven by astroglial glutamate transport. Nature neuroscience. 2017.

Chapter 6: *In vivo* quantification of neurofibrillary tangles with [^{18}F]MK-6240

Tharick A. Pascoal MD[1,2], Monica Shin MSc[1], Min Su Kang BSc[1,2], Mira Chamoun PhD[2], Daniel Chartrand MD[2], Sulantha Mathotaarachchi MSc[1,2], Idriss Bennacef PhD[3], Joseph Therriault BSc[1], Kok Pin Ng MRCP[1], Robert Hopewell PhD[2], Reda Bouhachi BSc[2], Hung-Hsin Hsiao BSc[2], Andrea L. Benedet MSc[1], Jean-Paul Soucy MD, MSc[2], Gassan Massarweh PhD[2], Serge Gauthier MD, FRCPC[1], and Pedro Rosa-Neto MD, PhD[1,2*]

[1]Translational Neuroimaging Laboratory, The McGill University Research Centre for Studies in Aging, H4H 1R3, 6825 LaSalle Boulevard Verdun, Quebec, Canada. [2]Montreal Neurological Institute, H3A 2B4, 3801, University Street, Montreal, Quebec, Canada. [3]Translational Biomarkers, Merck & Co., Inc., PA 19486, 770 Sumneytown Pike, West Point, Pennsylvania, USA.

Published in Alzheimer's Research & Therapy. 2018 Jul 31;10(1):74 (PMID: 30064520).

6.1 Preface

In order to test whether epigenetic modifications are a biological link between AD-related brain processes and dementia, which will be described in detail in Chapter 7, it was necessary to measure brain concentrations of neurofibrillary tangles *in vivo*. However, in a study conducted in our laboratory, we learned that the tau PET tracer that would be used in this study ([^{18}F]THK5351) displays brain uptake of MAO-B, rather than the desired tau protein (Figure 6-1).

Figure 6-1. The MAO-B inhibitor, selegiline, reduces the [^{18}F]THK5351uptake in the human brain.

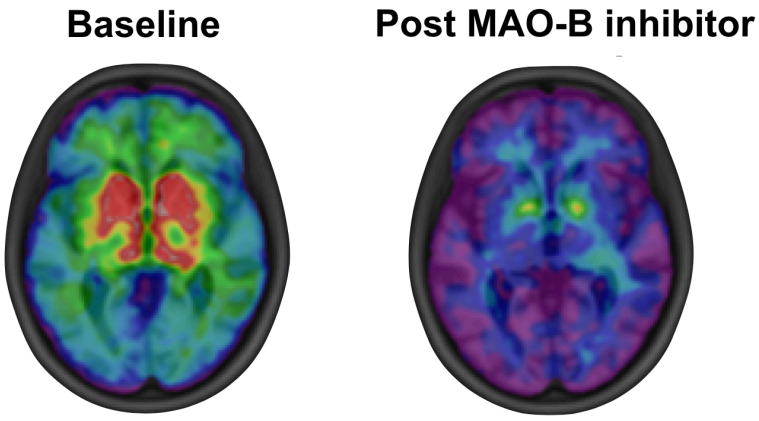

Standardized maps overlaid on a structural MRI show baseline and 1 h post-selegiline scans in a representative MCI individual. The MAO-B inhibitor, selegiline, significantly reduced the [^{18}F]THK5351 binding, suggesting that MAO-B highly influences the tracer signal. Adapted from Ng, at al (Ng *et al.*, 2017).

Moreover, previous studies have suggested that the uptakes of the other first-generation tau tracers are also heavily influenced by other pathophysiological processes, rather than tangles (Hostetler *et al.*, 2016, Koga *et al.*, 2017). As a result, second-generation tau tracers, such as [^{18}F]MK-6240, have recently gained attention. Preclinical results suggest that [^{18}F]MK-6240 exhibits high selectivity for tangles (Hostetler *et al.*, 2016). Therefore, in Chapter 6, using gold

standard methods with full dynamic scans and plasma input function, we validated the use of simplified methodologies to circumvent the need of arterial sampling and long scan durations for the use of [^{18}F]MK-6240 in large populations.

6.2 Abstract

Background: Imaging agents capable of quantifying the brain's tau aggregates will allow a more precise staging of Alzheimer's disease (AD). The aim of the present study was to examine the *in vitro* properties as well as the *in vivo* kinetics, using gold standard methods, of the novel positron emission tomography (PET) tau imaging agent [^{18}F]MK-6240.

Methods: *In vitro* properties of [^{18}F]MK-6240 were estimated with autoradiography in postmortem brain tissues of 14 subjects (7 AD and 7 age-matched controls). *In vivo* quantification of [^{18}F]MK-6240 binding was performed in 16 subjects (4 AD, 3 mild cognitive impairment, 6 healthy elderly, and 3 healthy young) who underwent 180-min dynamic scans; 6 had an arterial sampling for metabolite correction. Simplified approaches for [^{18}F]MK-6240 quantification were validated using full kinetic modeling with metabolite-corrected arterial input function. All participants also underwent amyloid-PET and structural magnetic resonance imaging.

Results: *In vitro* [^{18}F]MK-6240 uptake was higher in AD than in age-matched controls in brain regions expected to contain tangles such as the hippocampus, whereas no difference was found in the cerebellar gray matter. *In vivo*, [^{18}F]MK-6240 displayed favorable kinetics with rapid brain delivery and washout. The cerebellar gray matter had low binding across individuals, showing

the potential to be used as a reference region. A reversible two-tissue compartment model well described the time–activity curves across individuals and brain regions. Distribution volume ratios (DVRs) using the plasma input and standardized uptake value ratios (SUVRs) calculated after the binding approached the equilibrium (90 min) were correlated and higher in MCI or AD dementia than controls. Reliability analysis revealed robust SUVRs calculated from 90 to 110 min, while earlier time points provided inaccurate estimates.

Conclusions: This evaluation shows an [^{18}F]MK-6240 distribution in concordance with postmortem studies and that simplified quantitative approaches such as SUVR offer valid estimates of neurofibrillary tangles load 90 min post-injection. [^{18}F]MK-6240 is a promising tau tracer with the potential to be applied in the disease diagnosis and assessment of therapeutic interventions.

6.3 Background

In vivo quantification of neurofibrillary tangles constitutes a new challenge in the field of Alzheimer's disease (AD) imaging research. It is expected that reliable imaging agents that are able to accurately quantify tangles in the human brain will complement the information provided by the existing amyloid-β tracers, allowing a more precise staging of AD. In addition, these imaging agents may prove to be crucial for the enrichment of clinical trial populations with tau-positive individuals and for monitoring the efficacy of disease-modifying interventions.

Over the last few years, three classes of tau tracers have appeared as candidates to selectively measure neurofibrillary tangles in the living human brain. The derivative of pyrido-indole

([^{18}F]AV-1451) (Chien *et al.*, 2013, Xia *et al.*, 2013), the derivatives of aryquinoline ([^{18}F]THK5117, [^{18}F]THK5317, and [^{18}F]THK5351) (Harada *et al.*, 2015, Stepanov *et al.*, 2017), and the derivative of phenyl/pyridinyl-butadienyl-benzothiazoles/benzothiazolium ([^{11}C]PBB3) (Hashimoto *et al.*, 2014). Although these tracers have shown affinity to neurofibrillary tangles, compelling evidence suggests that off-target binding heavily influences the signal of some of them, even in cortical brain regions that are considered as a target for AD. For example, in a recent *in vivo* study, we have shown that the binding of [^{18}F]THK5351 in regions including the cingulate, temporal, and inferior parietal cortices is strongly driven by MAO-B availability (Ng *et al.*, 2017). Similarly, *in vitro* evidence suggest that MAO-A may influence the signal of [^{18}F]AV-1451 (Hostetler *et al.*, 2016) and that [^{11}C]PBB3 may bind to α-synuclein pathology (Koga *et al.*, 2017). Furthermore, most of these tracers have shown high binding in the striatum, which is not a region where the histopathological studies show a high density of tangles in AD (Braak and Braak, 1991). Thus, a tau-imaging agent with a low brain off-target binding remains as an unmet need in the field of AD research.

The pyrrolopyridinyl isoquinoline amine derivative [^{18}F]MK-6240 has been recently developed by Merck. [^{18}F]MK-6240 is a tracer with a sub-nanomolar affinity and high selectivity for neurofibrillary tangles that showed excellent physicochemical properties in a preclinical observation (Hostetler *et al.*, 2016). [^{18}F]MK-6240 has shown characteristics with the potential to fulfill the criteria for a promising new generation tau tracer, such as reduced brain off-target binding, fast brain penetration and kinetics, and the absence of brain permeable metabolite. Here, we aim to quantify [^{18}F]MK-6240 using gold standard methods with metabolite-corrected arterial input function. In addition, we aim to validate simplified methodologies that are capable of

bypassing the need for invasive arterial sampling in young and elderly cognitively healthy (CN), mild cognitive impairment (MCI), and AD.

6.4 Material and Methods

[^{18}F]MK-6240 autoradiography

In vitro autoradiography with [^{18}F]MK-6240 was conducted in postmortem brain samples of patients with antemortem diagnosis of AD (Consortium to Establish a Registry for Alzheimer Disease (CERAD) positive) (Mirra *et al.*, 1991)) and CN (CERAD negative) obtained from the Douglas-Bell Canada Brain Bank with the approval of the Brain Bank's scientific review and Douglas Institute's research ethics boards. A total of 7 AD and 7 CN individuals were studied. 6 AD and 6 CN had the cerebellum, hippocampus, and prefrontal regions assessed (1 AD and 1 CN did not have viable hippocampal sections.). 1 AD and 1 CN had the whole hemisphere sections assessed. The postmortem delay ranged from 8.5 to 18.25 h and 17.25 to 21.25 h in AD and CN, respectively. Briefly, flash-frozen tissues were cut in 20 μm thick sections and thawed on coated microscope slides using a freezing sliding microtome (Leica CM3050 S) at -15 ºC. The samples were then air-dried, warmed-up to room temperature, and preincubated with 1% bovine serum albumin in a phosphate-buffered saline solution (pH 7.4) for 10 min to remove endogenous ligands. These samples were then once more air-dried and incubated with 20.4 MBq of [^{18}F]MK-6240 in 600 mL of phosphate-buffered saline solution for additional 150 min. Subsequently, the tissues were dipped three times in the phosphate-buffered solution and, subsequently, dipped in distilled water at 4 °C and dried under a stream of cool air. Finally, the samples were exposed to a radioluminographic imaging plate (Fujifilm BA SMS2025) for 20 min, and the activity in photostimulated luminescence unit per mm^2 was calculated using the

ImageGauge software 4.0 (Fujifilm Medical Systems, Inc.). The activity in each individual's brain region was measured in three equidistant regions-of-interest (ROIs) placed by an experimenter blind to clinical diagnosis. Then, an averaged value of these ROIs was used as the final region uptake. In order to correct for background noise and nonspecific activity, this uptake was normalized to the individual's cerebellar gray matter uptake. T-test assessed the difference in uptake across diagnostic groups. Further details regarding the *in vitro* autoradiography methods may be found elsewhere (Parent *et al.*, 2013).

Participants

AD and MCI patients, young and aged CN individuals were recruited after extensive clinical assessments at the McGill University Research Centre for Studies in Aging. All participants underwent a detailed neuropsychological evaluation including Clinical Dementia Rating (CDR) scale and Mini-Mental State Examination (MMSE), an amyloid-PET scans with [^{18}F]AZD4694 in order to assess the presence of brain AD pathophysiology, and a tau PET with [^{18}F]MK-6240. CN had no subjective or objective cognitive impairment and a CDR of 0. MCI had a CDR of 0.5, subjective and objective memory impairments, and essentially normal activities of daily living. AD dementia patients had CDR equal to or greater than 1 and met the National Institute on Aging and the Alzheimer's Association criteria for probable AD (McKhann *et al.*, 2011). None of the individuals met the criteria for other neuropsychiatric disorders.

Radiosynthesis

[^{18}F]Fluoride was produced via the ^{18}O(p,n)^{18}F reaction in a water target. The target filling was transferred with a steady stream of argon into a septum-closed vial inside a hot cell, where the

synthesis of [^{18}F]MK-6240 took place. After the delivery of the radioactivity, the module transferred the fluoride anion onto a quaternary methyl amine (QMA) cartridge where it was retained, and the target water was transferred into a collection vial for recycling. [^{18}F]Fluoride was then eluted off the QMA cartridge and into the reactor with a solution of 1.35 mL of acetonitrile containing 15 ± 1 mg TEA (tetraethyl ammonium). The solution was then evaporated to dryness repeatedly with additional acetonitrile at a temperature of 95 ºC, a stream of nitrogen, and reduced pressure. After 15 min, a solution of 1-2 mg of the MK-6240 precursor in 0.7 mL DMSO (dimethyl sulfoxide) was added to the reactor and was heated stepwise to 150-155ºC for about 20 min. During this step, the de-protected final product [^{18}F]MK-6240 was formed. The reactor was then cooled to 70ºC, and 1.5 mL of high-pressure liquid chromatography (HPLC) solvent (10mM sodium acetate/ethanol, 75/25) was added. The resulting mixture was transferred into the injector loop of the HPLC system and purified on a Gemini C6-Phenyl 250 x 10 mm 5 µM HPLC column (Phenomenex Inc.), with a flow of 5 mL/min. The desired product eluted at a retention time of about 26-28 min. The product peak was collected with a 30-ml syringe containing 15 mL of water and 50 µL of ascorbic acid. The solution was passed through a C18 Sep-Pak cartridge (Waters Corp.). The cartridge was washed with an additional 10 mL of water. The product was then eluted from the cartridge into a round flask with 5 mL of ethanol. The flask was sealed off with a vacuum piece attached to a vacuum pump, and a water bath was raised to insert the flask into hot water. The HPLC solvent was evaporated to dryness under reduced pressure, and approximately 5 mL of ethanol was added to the flask via a three-way stopcock and a line attached to the vacuum piece. The ethanol was evaporated to dryness, and if any solvent remained visible, another 5 mL of ethanol USP (United States Pharmacopeia) was added and evaporated again. The dried [^{18}F]MK-6240 was then dissolved in 9.5 mL of sterile

phosphate buffer and 0.5 mL of ethanol, then transferred into a 10-mL syringe with an attached needle. The needle was then removed and the syringe was inserted into the female Luer lock of a sterile filter, which is part of a pre-assembled bulk vial. Finally, the [^{18}F]MK-6240 was sterile filtered into the product vial. [^{18}F]MK-6240 had an averaged injected dose of 241 (standard deviation (SD)=23) MBq with a specific activity at the time of injection of 629 (standard deviation (SD)=330) GBq/μmol. [^{18}F]AZD4694 was synthesized according to the previously published literature (Cselenyi *et al.*, 2012), with an averaged injected dose of 237 MBq (SD=19) μg and an averaged specific activity at the time of injection of 325 (SD=480) GBq/μmol.

PET acquisitions

PET scans were performed using the Siemens High Resolution Research Tomograph (HRRT) PET scanner. [^{18}F]MK-6240 images were acquired dynamically and uninterruptedly in list mode files between 0–180 min after the intravenous bolus injection of the tracer. [^{18}F]MK-6240 scans were reconstructed using an Ordered-Subsets Expectation Maximization (OSEM) algorithm on a 4D volume with 52 frames (12 x 6s, 6 x 18s, 4 x 30s, 5 x 60s, 5 x 120s, 8 x 300s, and 12 x 600s) (Hudson and Larkin, 1994). [^{18}F]AZD4694 images were acquired at 40–70 min after the intravenous bolus injection of the tracer, and the scans were reconstructed with the same OSEM algorithm on a 4D volume with 3 frames (3 x 600s). A 6-min transmission scan was conducted with a rotating ^{137}Cs point source at the end of each dynamic acquisition for attenuation correction. All images were subsequently corrected for dead time, decay, and both random and scattered coincidences. A head holder was used to reduce head motion during the scan time. In addition, possible movements during the scanning procedure were corrected using a co-

registration based method that performs frames' realignment and compensates for emission-transmission mismatches (Costes *et al.*, 2009).

Image processing

All participants had an anatomical 3D T1-weighted magnetic resonance imaging (MRI, 3T Siemens). The image analyses were performed using the Medical Image NetCDF software toolbox (www.bic.mni.mcgill.ca/ServicesSoftware/MINC). In brief, the T1-weighted images were corrected for field distortions, segmented, non-uniformity corrected, and processed using the CIVET pipeline (Zijdenbos *et al.*, 2002). Subsequently, the T1-weighted images were linearly registered to the MNI reference template space (Mazziotta *et al.*, 1995), whereas the PET images were automatically co-registered to the individual's MRI space. Then, the final PET linear registration was performed using the transformations obtained from the MRI to MNI linear template and the PET to T1-weighted native image. PET images were then spatially smoothed to achieve a final resolution of 8-mm full-width at half maximum. ROIs were obtained from the MNI non-linear ICBM atlas and subsequently reoriented to the individual's linear space (Mazziotta *et al.*, 2001). The ROIs were tailored from the frontal, medial prefrontal, orbitofrontal, precuneus, anterior (ACC) and posterior cingulate (PCC), lateral and mediobasal temporal, inferior parietal, parahippocampus, hippocampus, insula, occipitotemporal, occipital pole, and cerebellar cortices as well as from the striatum, pons, and the telencephalon white matter (cerebellar white matter not included). Subsequently, the ROIs were applied to the dynamic PET frames to obtain the time–activity curve data. The parametric images and the ROIs standardized uptake value ratios (SUVRs) were measured for multiple different scan time frames and were generated using the cerebellar gray matter as the reference. Amyloid-PET positivity

was determined visually by two raters blind to clinical diagnosis. Further information regarding the imaging methods pipeline may be found elsewhere (Pascoal *et al.*, 2017, Pascoal *et al.*, 2017).

[^{18}F]MK-6240 metabolism

During the [^{18}F]MK-6240 scans, arterial blood samples were collected with an automatic blood sampling system (Swisstrace GmbH) throughout the full scanning procedure with a pump flow rate of 5 mL/min between 0 – 10 min and 0.65 mL/min between 11 – 180 min. Additional 5 mL samples for metabolite correction were collected manually at 5, 10, 20, 40, 60, 90, 120, and 180 min. A cross-calibrated gamma well counter (Caprac, Inc.) was used to measure the radioactivity in the whole blood and in the plasma. Briefly, the manual samples were collected with a 5-mL heparinized syringe and centrifuged at 4000 rpm for 5 min at 4 °C. Then, the plasma was separated from the blood cells, and 1 mL was diluted with 1 mL of acetonitrile. The samples were vortexed and once more centrifuged at 4000 rpm for 5 min at 4 °C. Then, the supernatant was separated and filtered using a Millipore GV 13 mm diameter filter. This supernatant plasma was injected into the HPLC system (Waters 1525 Binary HPLC pump, Waters Corp.), connected to a UV/visible detector (Waters 2489 UV/Visible Detector) and a coincidence detector (Bioscan, Inc.), with a flow rate of 1 mL/min. This dedicated radio-HPLC system used an isocratic method with a C18 analytical column (XTerra MS C18 Column, 5 μm, 4.6 mm X 250 mm) and a mobile phase consisting of 55% sodium acetate and 45% acetonitrile in order to provide the parent-to-metabolite ratio. The radioactivity estimated with the radio-HPLC system was denoised to reduce the instability generated by its low levels in the later time frames. After background correction and cross-calibration with the PET scanner, the blood activity was

multiplied by both the plasma-to-whole blood and the parent compound fractions in order to derive the metabolite-corrected plasma input function.

[^{18}F]MK-6240 kinetic modeling

The kinetic modeling was performed using the KinFit (version 1.7) and PMOD (version 3.8) software. Using the metabolite-corrected plasma input function, the kinetic parameters of [^{18}F]MK-6240 were initially quantified using a reversible two-tissue compartment model with 4 parameters (2T-CM4k), assuming rapid kinetics between free and nonspecifically bound tracer. For the 2T-CM4k, the total distribution volume (V_T) was measured as K_1/k_2 $(1+k_3/k_4)$ (mL/cm^3), and the binding potential (BP) was directly measured as k_3/k_4. In this equation, K_1 (mL/cm^3/min) and k_2 (1/min) represent the transport rates for the influx and efflux of the tracer across the blood-brain-barrier, and the rate constants k_3 (1/min) and k_4 (1/min) represent the exchange from the non-displaceable (ND; free and nonspecific tracer) to the specific binding compartment and in return, respectively (Gunn *et al.*, 2001). In addition, a one-tissue compartment model (1T-CM), irreversible 2T-CM with 3 fitted parameters (2T-CM3k), and Logan linear graphical method were performed (Logan *et al.*, 1990). The distribution volume ratio (DVR) was calculated by dividing the V_T from a target region by the distribution volume of a region assumed to contain only free and nonspecifically bound tracer ($V_{ND;}$ cerebellar gray matter). We assumed a fractional tissue blood volume of 5% for the aforementioned models. The simplified reference tissue model (SRTM) and the reference Logan methods both using the cerebellar gray matter as the reference were also fitted in order to obtain DVRs (BP_{ND} + 1) (Lammertsma and Hume, 1996, Logan *et al.*, 1996, Wu and Carson, 2002). A k_2' value was estimated for each individual with the SRTM and used in the reference Logan. The model's goodness-of-fit was

assessed with R-squared and F-test, while the Akaike information criterion (AIC) was used to compare the models (Akaike, 1974). T-test compared AIC values from different quantification methods. We tested the similarity between models with regression analysis based on all ROIs.

Determination of the optimal time window for the SUVR calculation

[^{18}F]MK-6240 secular and peak equilibria were used to guide the determination of the first time point used for the SUVR calculation. The shortest scan duration without compromising reliability was determined by analyzing the stability of SUVRs calculated using different time durations. Finally, we validated SUVR estimates against the gold standard 2T-CM4k with metabolite-corrected plasma input function.

The time to reach the secular equilibrium was assumed as the point in which the curves representing the ratio of the target-to-reference region reached a plateau (Farde *et al.*, 1989). Similarly, the peak equilibrium was calculated using specific binding curves estimated as the difference between the target and the reference regions (Cselenyi *et al.*, 2012), where the equilibrium was defined when dCb(specific binding)/d(t) = 0. The target region used in the analyses was a composite value from the regions with the highest ligand uptake (precuneus, posterior cingulate, inferior parietal, and lateral temporal cortices), whereas the reference region was the cerebellum gray matter. The time-activity curves were normalized for injected tracer dose and the individual's weight.

In order to assess the optimal scan duration, we tested the stability of the coefficient of variation (CV) and the intraclass correlation coefficient (ICC) in SUVRs obtained with progressive longer

durations (10, 20, 30, 40, 50, and 60 min) (Bartko, 1966, Quan and Shih, 1996). 95% confidence interval (CI) determined the absence of change in the CV and the ICC among the different SUVR durations. For each SUVR time duration, a subject's CV was determined as the average of CVs obtained within each ROI. ICCs were determined between SUVR time durations using all individuals' ROIs. In addition, ICCs were calculated between SUVR and 2T-CM4k DVR and BP (k_3/k_4) estimates.

Finally, we estimated the slope, intercept, and R^2 between 2T-CM4k and SUVRs measured over the 52 reconstructed time frames in order to ascertain the points with an optimal equivalence between these two methods.

6.5 Results

In vitro [^{18}F]MK-6240 autoradiography was performed in postmortem brain tissues from 7 AD (mean age of death = 72.5 (SD=10), 3 males) and 7 CN (mean age of death = 70 (SD=13), 3 males). The total brain mass was 24% lower in AD (mean = 977 (SD=195) g) than CN (mean = 1,221 (SD=112) g) (P = 0.03). Autoradiographs showed greater [^{18}F]MK-6240 uptake in AD than in CN in brain regions that were expected to contain tangles such as prefrontal and hippocampal cortices, whereas similar uptake was found in the cerebellar gray matter (P = 0.2) (Fig. 6-2).

In vivo dynamic [^{18}F]MK-6240 acquisitions were performed in sixteen individuals (4 AD, 3 MCI, 6 elderly CN, and 3 young CN). The demographics and key characteristics of the *in vivo* population are summarized in Table 6-1.

Time-activity curves revealed that the radioactivity appeared rapidly in the brain with an SUV peak between 2 and 5 min after the [^{18}F]MK-6240 injection. In young and elderly CN, the time–activity curves had a uniform rapid washout and were similar in target and reference regions. In AD and MCI, the radioactivity showed a slower clearance in the regions that were expected to contain high concentrations of neurofibrillary tangles. Regional time-activity curves from selected brain regions of all individuals of the population are presented in Figure 6-3.

Plasma analysis revealed that [^{18}F]MK-6240 has rapid clearance from the blood. The radio-metabolite analysis suggested only one metabolite, which is more polar than the parent compound. The metabolite peak was identified in the plasma eluting with a retention time of 4 min, whereas the parent compound appeared at 8 min. After 10 min, approximately 70% of the parent compound was metabolized (Fig. 6-4A).

The time-activity curves were well described by the 2T-CM4k across individuals and brain regions (Fig. 6-4B). 2T-CM4k (AIC mean = 11.39 (SD=33)) provided a better fit than the 2T-CM3k (AIC mean = 69.98 (SD=45)) visually and statistically across subjects and regions ($P <$ 0.0001, t-test). The kinetic parameters derived from the preferred 2T-CM4k are presented in Table 6-2. The cerebellar gray matter fitted the 2T-CM4k better, whereas the pons showed no difference in AIC between the fits with the 2T-CM4k and 1T-CM. The Logan graphical model became linear approximately 80 min after the tracer injection in high binding regions (Fig. 6-4C).

The stabilization of specific binding (the difference between target and reference region) and total/ND binding (the ratio between target and reference region) were observed in 60 and 90 min for symptomatic individuals, respectively. In young and elderly CN, specific binding and total/ND estimates were low, and the stabilization was reached earlier (Fig. 6-5).

The CV and ICC analyses performed after the total/ND binding reached equilibrium indicated that scan acquisitions from 90 to 110 min offer reliable measurements for the [^{18}F]MK-6240 SUVR calculation (Fig. 6-6). Additionally, ICCs between SUVRs measured from 90 to 110 min ($SUVR_{90\text{-}110}$) and 2T-CM4k DVRs and BPs (k_3/k_4) were 0.993 (95% CI 0.99-0.995) and 0.791 (95% CI 0.7-0.857), respectively.

Using the cerebellar gray matter as the reference, the association between SUVR and 2T-CM4k showed progressively better goodness-of-fit and these quantification methods showed progressively more similar estimates using progressively later time frames for the SUVR calculation, essentially approaching a plateau around 90 min (Fig. 6-7).

In addition, 2T-CM4k DVRs were highly associated with DVRs from the Logan (slope = 0.9872, R^2 = 0.9953, Fig.6-8A), reference Logan (slope = 0.8879, R^2 = 0.9864; Fig. 6-8B), and SRTM (slope = 0.8658, R^2 = 0.9846; Fig. 6-8C). Moreover, DVRs using the reference Logan (slope = 1.113, R^2 = 0.9915) and SRTM (slope = 1.126, R^2 = 0.9807) were highly correlated with $SUVR_{90\text{-}110}$ (Fig. 6-8D & E).

2T-CM4k and Logan V_T estimates in the cerebellum gray matter and pons were the lowest and had the lowest variance between individuals and across diagnostic groups (Fig. 6-9A). DVR and SUVR $_{90\text{-}110}$ estimates showed a clear differentiation between MCI and AD from CN (Fig. 6-9B & C). AD and MCI patients showed the highest binding in the PCC and the precuneus, where the binding in MCI and AD participants were on average around 4 and 3 times higher than elderly CN, respectively. [^{18}F]MK-6240 and [^{18}F]AZD4694 SUVR parametric images from all individuals of the population are presented in Figure 6-10.

6.6 Discussion

We have described here the first human evaluation of the novel PET ligand for neurofibrillary tangles [^{18}F]MK-6240 using full kinetic modeling and long scan acquisition duration. In this early observation, [^{18}F]MK-6240 was able to differentiate CN from individuals with MCI or AD, and valid binding estimates were obtained with simplified methods using a reference region such as SUVR.

[^{18}F]MK-6240 showed fast brain penetration and kinetics after the injection, and one metabolite more polar than the parent compound was found. There were no clinically detectable side effects attributed to the [^{18}F]MK-6240 injection in our population. The fact that V_T values stabilized during the scan acquisition in humans, together with a previous preclinical observation, indirectly supports the notion that there is no radioactive metabolite gradually entering the brain at significant levels (Hostetler *et al.*, 2016).

The time-activity curves were well described with 2T-CM4k, and the 2T-CM4k and Logan graphical method using the plasma input function had similar estimates to the reference Logan, SRTM, and SUVR. Moreover, reference region methods were highly correlated with each other. Together, these results further suggest that simplified reference methods offer valid estimates for the quantification of neurofibrillary tangles in the human brain using [^{18}F]MK-6240. Importantly, in our analysis, the estimates from reference methods underestimated 2T-CM4k. Underestimation of 2T-CM by reference methods have been observed in several other PET ligands such as [^{11}C]PIB, [^{18}F]AZD4694, and D2 receptor ligands, and the reasons suggested as underpinnings of this underestimation vary across ligands (Carson *et al.*, 1993, Gunn *et al.*, 1997, Yaqub *et al.*, 2008, Cselenyi *et al.*, 2012, Zhou *et al.*, 2012).

V_T values were the lowest in the cerebellar gray matter, pons, striatum, and white matter. The lowest variance between cognitively healthy and demented individuals was found in the cerebellar gray matter and pons, suggesting these two regions to have the highest potential to be used as reference. Importantly, these regions are reported to be relatively unaffected by neurofibrillary tangles in histopathological AD studies (Braak and Braak, 1991). Since the time-activity curves in the cerebellar gray matter were more stable across subjects, which is expected since it is a larger region, this region was chosen as the reference region. In our analysis, the cerebellar gray matter fitted the 2T-CM4k. Similarly, the fact that more than one compartment is needed to describe a reference region has already been observed with other imaging agents for protein aggregates (Price *et al.*, 2005, Cselenyi *et al.*, 2012). In the case of [^{18}F]MK-6240, it is unclear whether the uptake in the cerebellar meninges may contribute to this finding. Although the BP (k_3/k_4) values of the cerebellar gray matter overlapped across the diagnostic groups for

some of the individuals, symptomatic individuals had a slightly higher V_T than CN, suggesting that future studies should assess the [^{18}F]MK-6240 binding in the reference regions.

The moment in which the specific binding peaks and the moment that the target-to-reference region ratio approaches the plateau have been designated as the peak equilibrium (Cselenyi *et al.*, 2012) and transient (Carson *et al.*, 1993) or secular (Farde *et al.*, 1989) equilibrium, respectively. Both of these parameters of equilibrium have been used for previous PET studies (Olsson and Farde, 2001, Wong *et al.*, 2010, Cselenyi *et al.*, 2012). In the present study, averaged [^{18}F]MK-6240 cortical-to-cerebellar gray matter ratio curves showed a constant relative increase, reaching an asymptote after 90 min. Therefore, this parameter suggested 90 min as the earliest time point for the SUVR calculation, while the SUVRs' stability analysis suggested that there is no benefit in acquisitions longer than 20 min for scans starting 90 min post-injection. Taking these observations together, we determined scans performed at 90 to 110 min post-injection to have an optimal trade-off between duration and reliability.

As a sub-nanomolar affinity tracer, [^{18}F]MK-6240 reached equilibrium earlier (60 min) in low as compared with medium and high binding regions, where the ratio between the total/ND binding stabilized after 90 min. Therefore, SUVRs calculated with frames obtained earlier than 90 min leads to a progressively higher underestimation of tau pathology among low, medium, and high load regions. As a consequence, it is expected that SUVRs estimated earlier than 90 min will underestimate the rate of tau accumulation over time. In the context of anti-tau clinical trials, SUVRs obtained before 90 min will reduce the drug effect size since pre-treatment estimates will present a higher underestimation than post-treatment estimates. Studies in other sub-nanomolar

affinity tracers, such as the D2 receptor ligands, have already shown the pitfalls of using early time windows for binding estimation in tracers with distinct times to reach the equilibrium in regions with low- and high-density receptors (Olsson and Farde, 2001).

MCI and AD patients showed [^{18}F]MK-6240 uptake across the whole brain cortex, with the highest binding in the PCC, precuneus, inferior parietal, and lateral temporal cortices. Regional [^{18}F]MK-6240 bindings measured with arterial input function and simplified reference methods were able to distinguish MCI and AD from CN. *In vitro* autoradiography further supported greater contrast of [^{18}F]MK-6240 uptake in AD than age-matched CN across the aforementioned regions. This regional uptake is consistent with the pattern of neurofibrillary tangle deposition that was previously described in post-mortem studies of AD and supports [^{18}F]MK-6240 as a promising ligand for measuring neurofibrillary tangles in the human brain (Braak and Braak, 1991).

Apparent differences in binding sites between [^{18}F]MK-6240 and the other available tau tracers were observed in this evaluation. For example, in contrast to the other ligands for neurofibrillary tangles, [^{18}F]MK-6240 had minimum uptake in the striatum, which despite being known as a region with low tangles concentration, is one of the major binding sites of the other available tau tracers (Saint-Aubert *et al.*, 2017). Moreover, the time-activity curves and quantification methods suggested similarities in [^{18}F]MK-6240 retention between young and elderly CN individuals within the associative neocortical brain regions that are expected to contain low tangle density in these populations. Together, these initial results support [^{18}F]MK-6240 as a ligand with high brain selectivity to neurofibrillary tangles. It is important to mention that

possible off-target binding of [^{18}F]MK6240 was observed in regions including the retina, ethmoid sinus, substantia nigra, and dura mater. However, since some of these findings were not consistent among participants, these observations require further validation.

This study has methodological limitations. The absence of confirmation of the presence of neurofibrillary tangles with specific antibodies is a limitation of our *in vitro* study. The small sample size is a limitation of our *in vivo* study. However, the subjects studied here had a wide range of dynamic [^{18}F]MK-6240 uptake, which allowed the evaluation of the tracer kinetics in individuals with low and high binding. Future studies should address the test-retest reliability of [^{18}F]MK-6240 and definitively confirm whether the [^{18}F]MK-6240 radioactive metabolite does not appear in the brain in a significant amount. Since the HPLC has limited sensitivity in detecting low radioactivity counts (Price *et al.*, 2005), a further study using a more sensitive method of measuring the parent fraction is underway to completely define the limitations of quantifying [^{18}F]MK-6240 using simplified methods. [^{18}F]MK-6240 had the highest uptake in the precuneus and PCC. Previous postmortem observations did not relate these brain regions with the neurofibrillary tangles patterns typically found in AD (Braak and Braak, 1991). In contrast, a recent PET study has shown that neurofibrillary tangles accumulation in the PCC is highly associated with AD pathophysiology (Jack *et al.*, 2018). This study highlights that the PCC may have been overlooked by postmortem observations that do not traditionally assess neurofibrillary tangles in this region (Jack *et al.*, 2018). Although we have focused on PCC for some of our kinetic analysis, it is important to emphasize the importance of other brain regions such as the medial temporal cortex to the AD pathophysiological process. In addition, although our results suggest [^{18}F]MK-6240 binding as an indicator of AD-related tangles, it is important to

mention that the association of this binding with the clinical staging and natural history of AD can be determined only by larger longitudinal studies. Since our population was limited to controls and individuals across the AD spectrum, more studies are needed to determine [^{18}F]MK-6240 binding properties associated with other non-AD tauopathies.

6.7 Conclusions

To conclude, [^{18}F]MK-6240 displayed favorable pharmacokinetics with rapid brain penetration and washout. In this early observation, [^{18}F]MK-6240 discriminated MCI and AD from controls using methods with plasma input function or simplified SUVR estimates. [^{18}F]MK-6240 is a promising new generation tau radiotracer with the potential to be employed in the evaluation of disease-modifying therapies and future diagnostic use.

6.8 Tables and Figures

Table 6-1. Demographics and key characteristics of the *in vivo* population.

	Young CN	Elderly CN	MCI	AD
No.	3	6	3	4
Age, y, mean (SD)	22.3 (1.5)	67.8 (8.5)	69 (3,4)	60.7 (6)
Male, no. (%)	2 (67)	5 (83)	2 (67)	3 (75)
MMSE, mean (SD)	30 (0)	29.5 (0.5)	25 (2.6)	17.3 (5.8)
APOE ε4, no. (%)	0 (0)	4 (67)	1 (33)	2 (50)
Amyloid-PET +, no. (%)	0 (0)	1 (17)	3 (100)	4 (100)

AD, Alzheimer's disease; CN, cognitively healthy; MCI, mild cognitive impairment; MMSE, mini-mental state examination; PET, positron emission tomography; SD, standard deviation; y, years.

Table 6-2. Kinetic parameters obtained with the 2T-CM4k.

	Region	K_1	k_2	k_3	k_4	V_T	K_1/k_2	k_3/k_4	AIC	R^2
Asymptomatic individuals										
	Cer GM	0.327 (0.08)	0.235 (0.00)	0.025 (0.03)	0.046 (0.04)	2 (0.1)	1.39 (0.36)	0.41 (0.3)	- 11 (2.8)	0.99 (0.00)
	PCC	0.343 (0.03)	0.237 (0.04)	0.021 (0.01)	0.044 (0.01)	2.2 (0.1)	1.48 (0.42)	0.56 (0.52)	- 33.7 (4.3)	0.99 (0.00)
Symptomatic individuals										
	Cer GM	0.230 (0.02)	0.125 (0.02)	0.009 (0.01)	0.01 (0.00)	3.4 (0.8)	1.88 (0.37)	0.86 (0.5)	- 2.0 (55)	0.99 (0.00)
	PCC	0.246 (0.08)	0.099 (0.01)	0.052 (0.03)	0.01 (0.00)	14.2 (5.6)	2.45 (0.56)	5.11 (2.6)	- 3.7 (17)	0.99 (0.00)

Mean and standard deviation of the kinetic parameter obtained with the reversible two-tissue compartment model (2T-CM4k) in the cerebellar grey matter (Cer GM) and posterior cingulate cortex (PCC) of asymptomatic (young and elderly cognitively healthy) and symptomatic (mild cognitive impairment and Alzheimer's disease) individuals who underwent arterial sampling.

Figure 6-2. [^{18}F]MK-6240 autoradiographs of post-mortem brain tissues of AD and CN individuals.

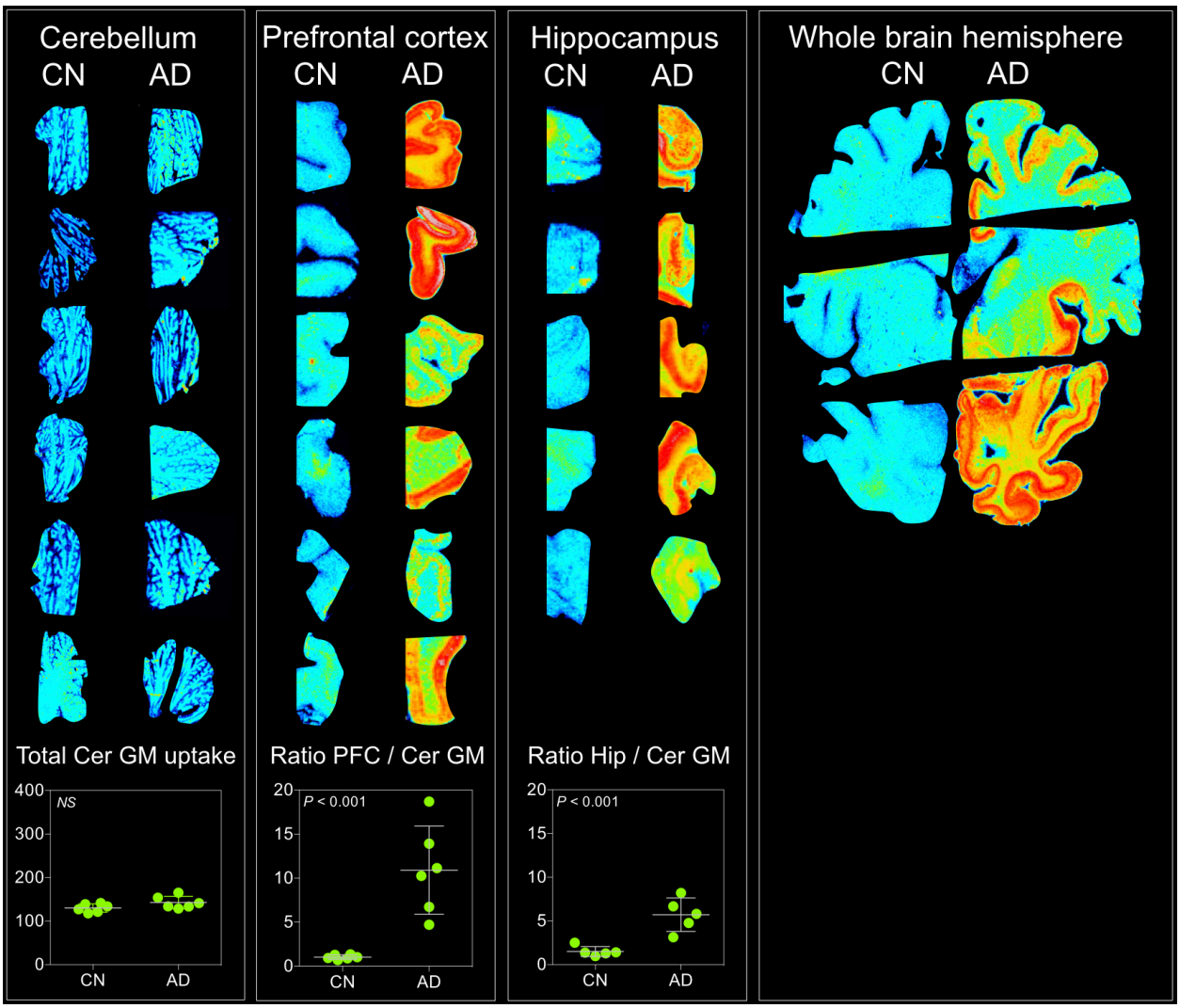

The figure shows *in vitro* autoradiography of postmortem brain tissue from the prefrontal (PFC) and the hippocampal (Hip) cortices, as well as from the cerebellum and the whole hemisphere of Alzheimer's disease (AD) and cognitively healthy (CN) individuals. Similar total uptake was found in the cerebellar gray matter (Cer GM) of CN and AD (P = 0.2). AD individuals had higher relative uptake (ratio with the Cer GM) than the CN in the PFC and Hip cortices (P < 0.001). Total uptake was measured with photostimulated luminescence unit per mm^2.

Figure 6-3. Regional time-activity curves from selected brain regions for all individuals of the population.

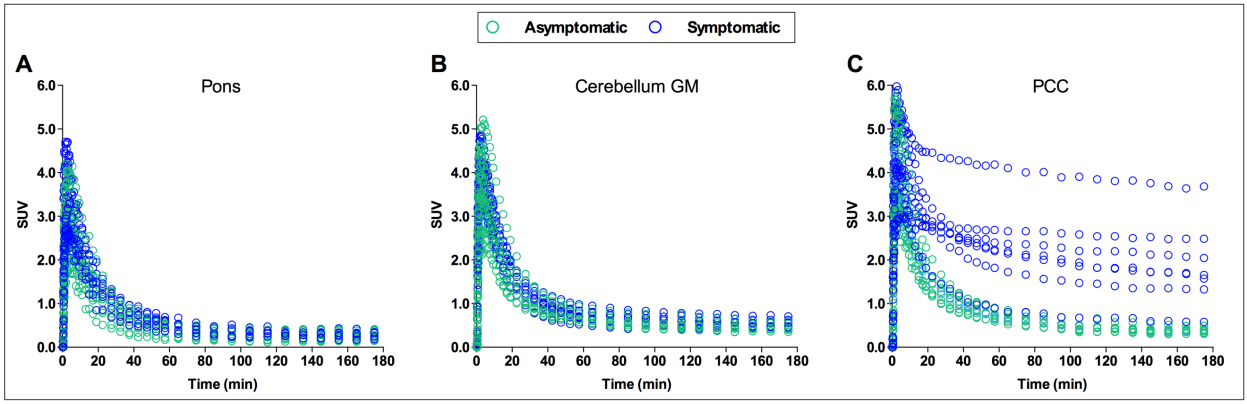

Regional standardized uptake value (SUV) time–activity curves of [^{18}F]MK-6240 in the pons (A), cerebellar gray matter (GM) (B), and posterior cingulate cortex (PCC) (C) for all participants. The green dots represent young and elderly cognitively healthy, whereas the blue dots represent mild cognitive impairment and Alzheimer's disease individuals.

Figure 6-4. Chromatography, model compartmentalization, and data fit of [^{18}F]MK-6240.

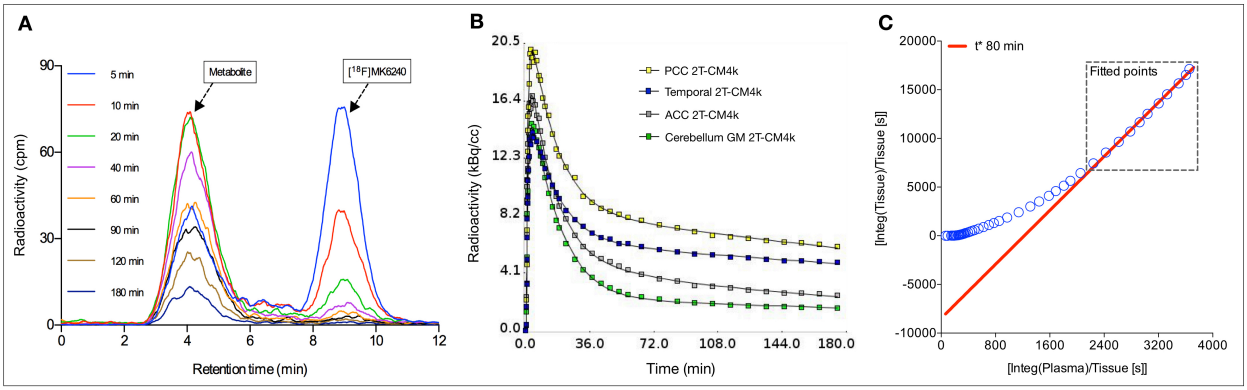

(A) Chromatogram showing the parent compound and the metabolite of [^{18}F]MK-6240 in counts per minute (cpm) in a representative AD participant. (B) Reversible two-tissue compartment model (2T-CM4k) fit in time-activity curves from the posterior cingulate (PCC), temporal, and anterior cingulate (ACC) cortices, as well as cerebellar gray matter (GM) of a representative mild cognitive impairment (MCI) individual. (C) The Logan graphical plot became linear approximately 80 min after the injection in the PCC of the representative MCI individual.

Figure 6-5. [^{18}F]MK-6240 uptake reaches equilibrium during the scan time.

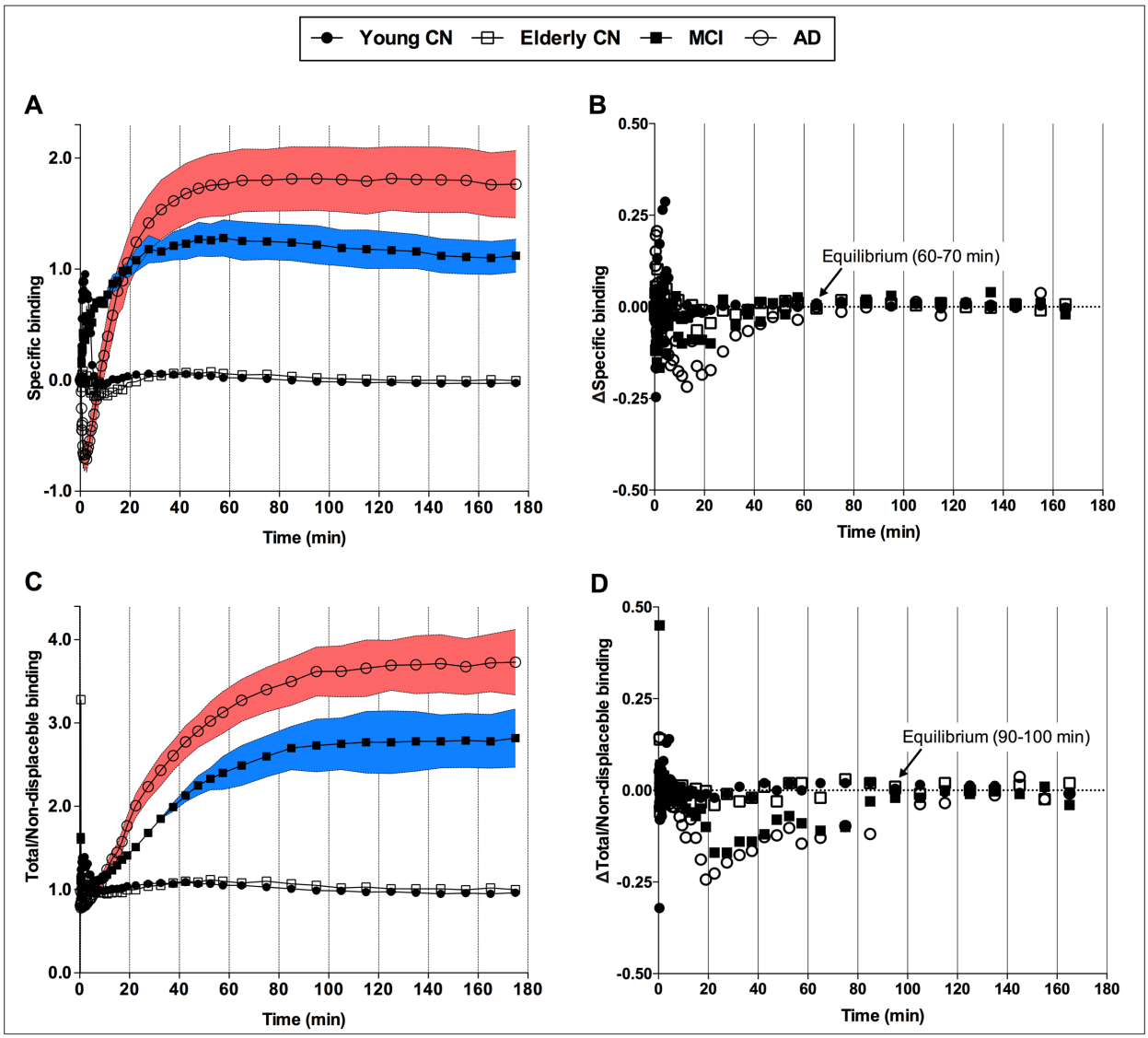

The curves show the mean of specific (A) and total/non-displaceable (ND) (C) binding across diagnostic groups over different scan acquisition time points and the area between the bars represents the standard error of the mean. The variation (Δ) of specific (B) and total/ND (D) binding was calculated as the difference between the averaged uptake value in a given time point to the averaged uptake value in the subsequent time point. The variation of specific and total/ND binding approached zero in frames starting in 60 and 90 min for both mild cognitive impairment (MCI) and Alzheimer's disease (AD) subjects, respectively. Elderly and young cognitively healthy subjects (CN) reached the aforementioned equilibria earlier. The target and ND regions assumed in the curves were a composite value from the regions with the highest ligand uptake (precuneus, posterior cingulate, inferior parietal, and lateral temporal cortices) and the cerebellum gray matter, respectively.

Figure 6-6. SUVRs measured from 90 to 110 min provide reliable [^{18}F]MK-6240 estimates.

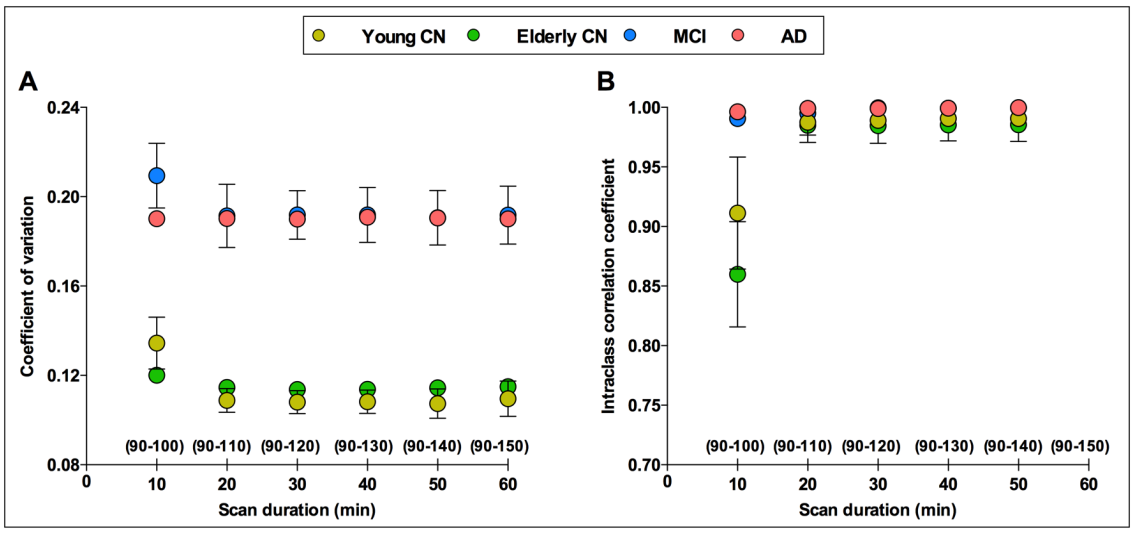

(A) The dots and bars represent the coefficient of variation (CV) and the 95% confidence interval (CI), respectively, assessed for each individual's regions-of-interest (ROIs) and averaged within groups using standardized uptake value ratios (SUVRs) measured with different durations after the tracer reached equilibrium (90 min, see Fig. 4). (B) The dots and bars represent the intraclass correlation coefficient (ICC) and the 95% CI, respectively, performed between SUVRs calculated using progressively longer frames. The 95% CI analyses suggested no differences in SUVR estimates measured using acquisitions equal to or longer than 20 min for [^{18}F]MK-6240 scans starting 90 min post-injection.

Figure 6-7. SUVRs measured in later time frames had progressively more similar estimates than the compartmental analysis.

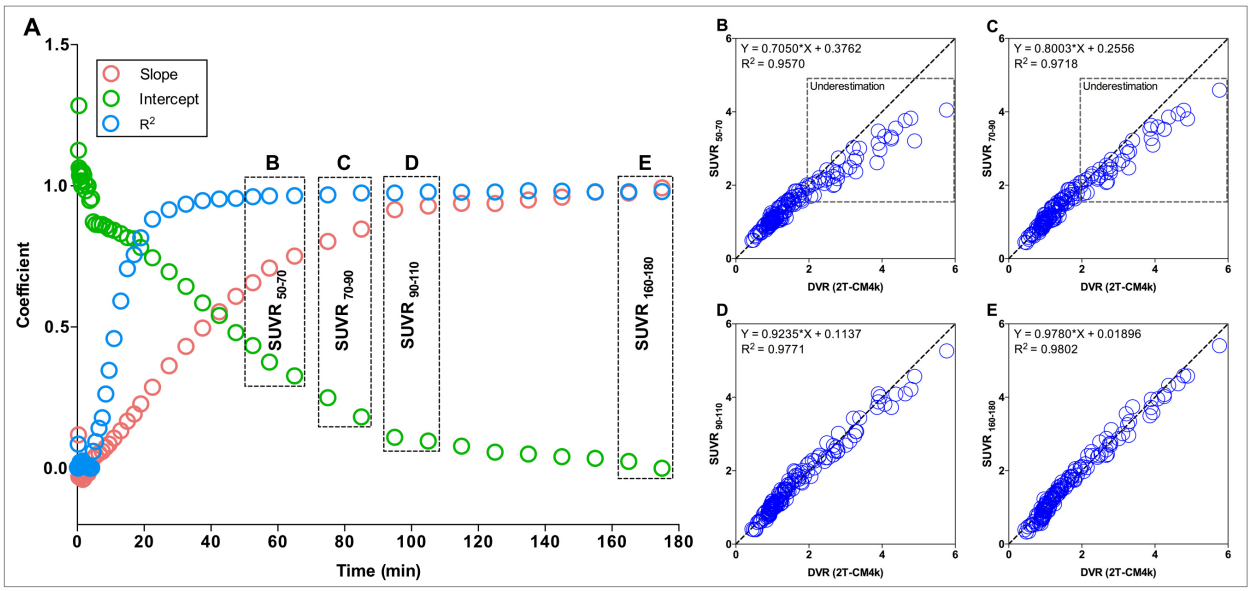

(A) The dots represent the results of regressions between standardized uptake value ratios (SUVRs) obtained from different scan acquisition times and the distribution volume ratio (DVR) obtained with the reversible two-tissue comportment model (2T-CM4k) across subjects and brain regions. The association between SUVR and 2T-CM4k showed progressively better goodness-of-fit (R^2) and these quantification methods showed progressively more similar estimates (slope closer to 1 and intercept closer to 0) when using progressively later time frames for the SUVR calculation. Although the strength of the relationship showed a constant increase until the end of the experiment, it approached the asymptote of the curve in 90 min post-injection. The scatter plots show the association between 2T-CM4k DVRs and SUVRs calculated from (B) 50-70, (C) 70-90, (D) 90-110, and (E) 160-180 min. SUVRs calculated before 90 min post-injection underestimated 2T-CM4k in regions with moderate and high binding, but not in low binding regions.

Figure 6-8. Comparisons between different quantification methods for [^{18}F]MK-6240.

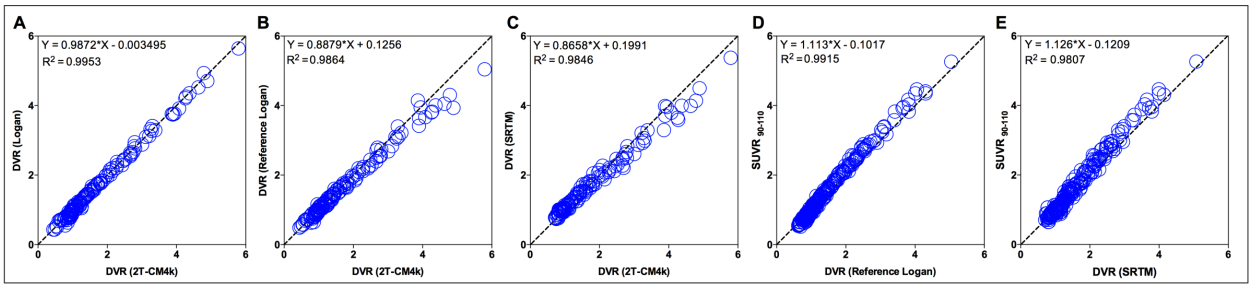

The scatter plots show regressions performed across individuals and brain regions between the (A) Logan vs. reversible two-tissue compartment model (2T-CM4k), (B) reference Logan vs. 2T-CM4k, (C) simplified reference tissue model (SRTM) vs. 2T-CM4k, (D) SUVR $_{90\text{-}110}$ vs. reference Logan, and (E) SUVR $_{90\text{-}110}$ vs. SRTM. Figures A-C include the individuals who underwent arterial blood sampling, whereas D and E include all participants.

Figure 6-9. Quantification estimates across clinical diagnosis and brain regions.

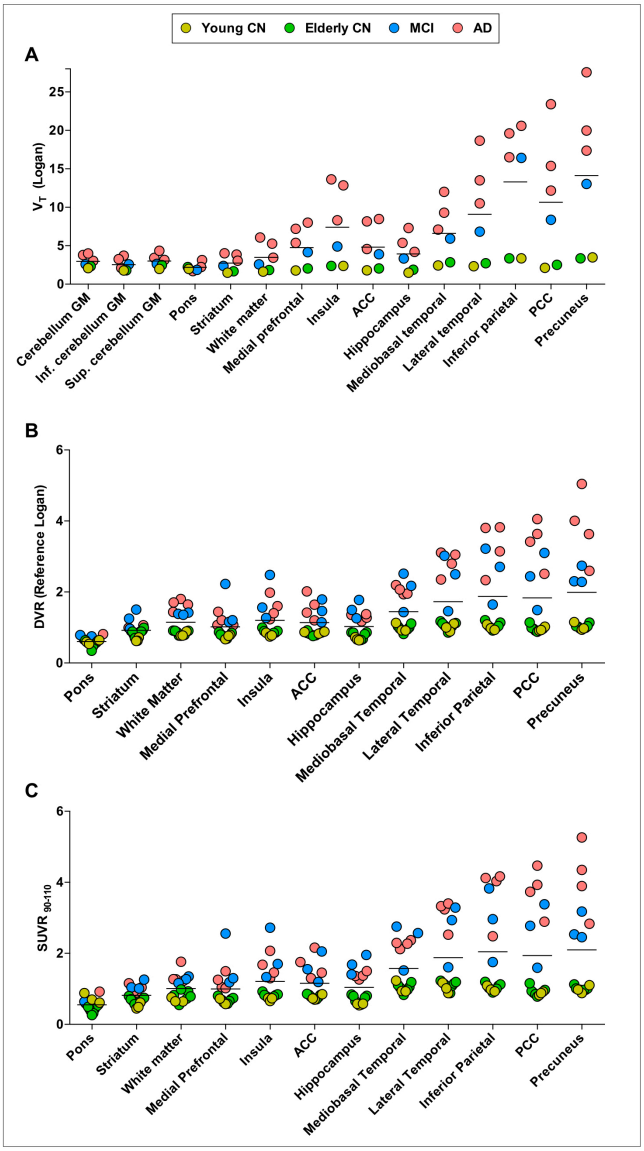

The horizontal bar in the plots represents the mean. (A) The plots show the total volume of distribution (V_T; mL/cm^3) values obtained with the Logan graphical method using the plasma input function in individuals who underwent arterial blood sampling. (B) The plots show distribution volume ratio (DVR) values obtained with the reference Logan and (C) the standardized uptake value ratio values measured between 90 and 110 min ($SUVR_{90-110}$) in all individuals of the population, both using the cerebellar gray matter as the reference region.

Figure 6-10. [^{18}F]MK-6240 SUVR parametric images of all participants.

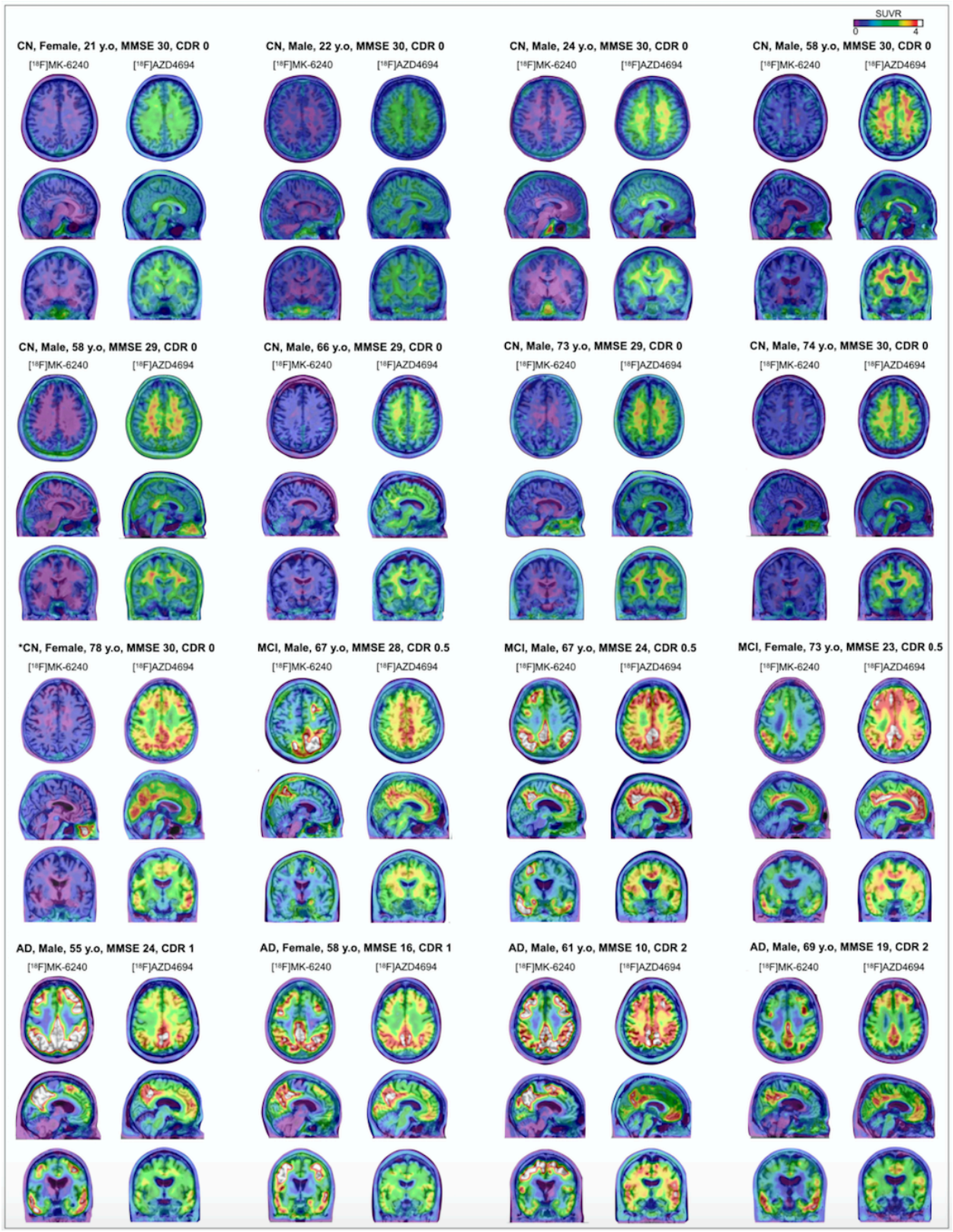

The figure shows [^{18}F]MK-6240 standardized uptake value ratio (SUVR) averaged between 90 to 110 min and [^{18}F]AZD4694 SUVR maps**,** overlaid on the individuals' structural magnetic resonance imaging, of all individuals of the population. [^{18}F]MK-6240 images show clear visual differentiation between symptomatic (mild cognitive impairment (MCI) and Alzheimer's disease (AD)) and asymptomatic (cognitively healthy controls (CN)) participants. All AD and MCIs, as well as 1 CN (*) were amyloid-β positive. CDR, Clinical Dementia Rating; MMSE, mini-mental state examination; y.o, years old.

6.9 Acknowledgments

This work was supported by the Weston Brain Institute, Canadian Institutes of Health Research (CIHR; MOP-11-51-31, PR-N), the Alzheimer's Association (NIRG-12- 92090, NIRP-12-259245, PR-N), Alzheimer Society Research Program (ASRP) and Canadian Consortium on Neurodegeneration in Aging (CCNA) scholarship (TAP), Fonds de Recherche du Québec – Santé (FRQS; Chercheur Boursier, PR-N). S.G. and P.R-N. are members of the CIHR-CCNA Canadian Consortium of Neurodegeneration in Aging. The authors thank Alexey Kostikov, Dean Jolly, Karen Ross, Mehdi Boudjemeline, Sandy Li, and Monica Samoila-Lactatus for the radiochemistry production.

6.10 References

Akaike H. A new look at the statistical model identification. IEEE Transactions on Automatic Control. 1974;19(6):716-23.

Bartko JJ. The intraclass correlation coefficient as a measure of reliability. Psychol Rep. 1966;19(1):3-11.

Braak H, Braak E. Neuropathological stageing of Alzheimer-related changes. Acta neuropathologica. 1991;82(4):239-59.

Carson RE, Channing MA, Blasberg RG, Dunn BB, Cohen RM, Rice KC, et al. Comparison of bolus and infusion methods for receptor quantitation: application to [18F]cyclofoxy and positron emission tomography. Journal of cerebral blood flow and metabolism : official journal of the International Society of Cerebral Blood Flow and Metabolism. 1993;13(1):24-42.

Chien DT, Bahri S, Szardenings AK, Walsh JC, Mu F, Su MY, et al. Early clinical PET imaging results with the novel PHF-tau radioligand [F-18]-T807. Journal of Alzheimer's disease : JAD. 2013;34(2):457-68.

Costes N, Dagher A, Larcher K, Evans AC, Collins DL, Reilhac A. Motion correction of multi-frame PET data in neuroreceptor mapping: simulation based validation. NeuroImage. 2009;47(4):1496-505.

Cselenyi Z, Jonhagen ME, Forsberg A, Halldin C, Julin P, Schou M, et al. Clinical validation of 18F-AZD4694, an amyloid-beta-specific PET radioligand. Journal of nuclear medicine : official publication, Society of Nuclear Medicine. 2012;53(3):415-24.

Farde L, Eriksson L, Blomquist G, Halldin C. Kinetic analysis of central [11C]raclopride binding to D2-dopamine receptors studied by PET--a comparison to the equilibrium analysis. Journal of cerebral blood flow and metabolism : official journal of the International Society of Cerebral Blood Flow and Metabolism. 1989;9(5):696-708.

Gunn RN, Gunn SR, Cunningham VJ. Positron emission tomography compartmental models. Journal of cerebral blood flow and metabolism : official journal of the International Society of Cerebral Blood Flow and Metabolism. 2001;21(6):635-52.

Gunn RN, Lammertsma AA, Hume SP, Cunningham VJ. Parametric imaging of ligand-receptor binding in PET using a simplified reference region model. NeuroImage. 1997;6(4):279-87.

Harada R, Okamura N, Furumoto S, Furukawa K, Ishiki A, Tomita N, et al. [(18)F]THK-5117 PET for assessing neurofibrillary pathology in Alzheimer's disease. European journal of nuclear medicine and molecular imaging. 2015;42(7):1052-61.

Hashimoto H, Kawamura K, Igarashi N, Takei M, Fujishiro T, Aihara Y, et al. Radiosynthesis, photoisomerization, biodistribution, and metabolite analysis of 11C-PBB3 as a clinically useful PET probe for imaging of tau pathology. Journal of nuclear medicine : official publication, Society of Nuclear Medicine. 2014;55(9):1532-8.

Hostetler ED, Walji AM, Zeng Z, Miller P, Bennacef I, Salinas C, et al. Preclinical Characterization of 18F-MK-6240, a Promising PET Tracer for In Vivo Quantification of Human Neurofibrillary Tangles. Journal of nuclear medicine : official publication, Society of Nuclear Medicine. 2016;57(10):1599-606.

Hudson HM, Larkin RS. Accelerated image reconstruction using ordered subsets of projection data. IEEE Trans Med Imaging. 1994;13(4):601-9.

Jack CR, Jr., Wiste HJ, Schwarz CG, Lowe VJ, Senjem ML, Vemuri P, et al. Longitudinal tau PET in ageing and Alzheimer's disease. Brain : a journal of neurology. 2018;141(5):1517-28.

Koga S, Ono M, Sahara N, Higuchi M, Dickson DW. Fluorescence and autoradiographic evaluation of tau PET ligand PBB3 to alpha-synuclein pathology. Mov Disord. 2017;32(6):884-92.

Lammertsma AA, Hume SP. Simplified reference tissue model for PET receptor studies. NeuroImage. 1996;4(3 Pt 1):153-8.

Logan J, Fowler JS, Volkow ND, Wang GJ, Ding YS, Alexoff DL. Distribution volume ratios without blood sampling from graphical analysis of PET data. Journal of cerebral blood flow and

metabolism : official journal of the International Society of Cerebral Blood Flow and Metabolism. 1996;16(5):834-40.

Logan J, Fowler JS, Volkow ND, Wolf AP, Dewey SL, Schlyer DJ, et al. Graphical analysis of reversible radioligand binding from time-activity measurements applied to [N-11C-methyl]-(-)-cocaine PET studies in human subjects. Journal of cerebral blood flow and metabolism : official journal of the International Society of Cerebral Blood Flow and Metabolism. 1990;10(5):740-7.

Mazziotta J, Toga A, Evans A, Fox P, Lancaster J, Zilles K, et al. A probabilistic atlas and reference system for the human brain: International Consortium for Brain Mapping (ICBM). Philos Trans R Soc Lond B Biol Sci. 2001;356(1412):1293-322.

Mazziotta JC, Toga AW, Evans A, Fox P, Lancaster J. A probabilistic atlas of the human brain: theory and rationale for its development. The International Consortium for Brain Mapping (ICBM). NeuroImage. 1995;2(2):89-101.

McKhann GM, Knopman DS, Chertkow H, Hyman BT, Jack CR, Jr., Kawas CH, et al. The diagnosis of dementia due to Alzheimer's disease: recommendations from the National Institute on Aging-Alzheimer's Association workgroups on diagnostic guidelines for Alzheimer's disease. Alzheimer's & dementia : the journal of the Alzheimer's Association. 2011;7(3):263-9.

Mirra SS, Heyman A, McKeel D, Sumi SM, Crain BJ, Brownlee LM, et al. The Consortium to Establish a Registry for Alzheimer's Disease (CERAD). Part II. Standardization of the neuropathologic assessment of Alzheimer's disease. Neurology. 1991;41(4):479-86.

Ng KP, Pascoal TA, Mathotaarachchi S, Therriault J, Kang MS, Shin M, et al. Monoamine oxidase B inhibitor, selegiline, reduces 18F-THK5351 uptake in the human brain. Alzheimer's research & therapy. 2017;9(1):25.

Olsson H, Farde L. Potentials and pitfalls using high affinity radioligands in PET and SPET determinations on regional drug induced D2 receptor occupancy--a simulation study based on experimental data. NeuroImage. 2001;14(4):936-45.

Parent MJ, Bedard MA, Aliaga A, Minuzzi L, Mechawar N, Soucy JP, et al. Cholinergic Depletion in Alzheimer's Disease Shown by [(18) F]FEOBV Autoradiography. Int J Mol Imaging. 2013;2013:205045.

Pascoal TA, Mathotaarachchi S, Mohades S, Benedet AL, Chung CO, Shin M, et al. Amyloid-beta and hyperphosphorylated tau synergy drives metabolic decline in preclinical Alzheimer's disease. Mol Psychiatry. 2017;22(2):306-11.

Pascoal TA, Mathotaarachchi S, Shin M, Benedet AL, Mohades S, Wang S, et al. Synergistic interaction between amyloid and tau predicts the progression to dementia. Alzheimer's & dementia : the journal of the Alzheimer's Association. 2017;13(6):644-53.

Price JC, Klunk WE, Lopresti BJ, Lu X, Hoge JA, Ziolko SK, et al. Kinetic modeling of amyloid binding in humans using PET imaging and Pittsburgh Compound-B. Journal of cerebral blood flow and metabolism : official journal of the International Society of Cerebral Blood Flow and Metabolism. 2005;25(11):1528-47.

Quan H, Shih WJ. Assessing reproducibility by the within-subject coefficient of variation with random effects models. Biometrics. 1996;52(4):1195-203.

Saint-Aubert L, Lemoine L, Chiotis K, Leuzy A, Rodriguez-Vieitez E, Nordberg A. Tau PET imaging: present and future directions. Mol Neurodegener. 2017;12(1):19.

Stepanov V, Svedberg M, Jia Z, Krasikova R, Lemoine L, Okamura N, et al. Development of [11C]/[3H]THK-5351 - A potential novel carbon-11 tau imaging PET radioligand. Nucl Med Biol. 2017;46:50-3.

Wong DF, Rosenberg PB, Zhou Y, Kumar A, Raymont V, Ravert HT, et al. In vivo imaging of amyloid deposition in Alzheimer disease using the radioligand 18F-AV-45 (florbetapir [corrected] F 18). Journal of nuclear medicine : official publication, Society of Nuclear Medicine. 2010;51(6):913-20.

Wu Y, Carson RE. Noise reduction in the simplified reference tissue model for neuroreceptor functional imaging. Journal of cerebral blood flow and metabolism : official journal of the International Society of Cerebral Blood Flow and Metabolism. 2002;22(12):1440-52.

Xia CF, Arteaga J, Chen G, Gangadharmath U, Gomez LF, Kasi D, et al. [(18)F]T807, a novel tau positron emission tomography imaging agent for Alzheimer's disease. Alzheimer's & dementia : the journal of the Alzheimer's Association. 2013;9(6):666-76.

Yaqub M, Tolboom N, Boellaard R, van Berckel BN, van Tilburg EW, Luurtsema G, et al. Simplified parametric methods for [11C]PIB studies. NeuroImage. 2008;42(1):76-86.

Zhou Y, Sojkova J, Resnick SM, Wong DF. Relative equilibrium plot improves graphical analysis and allows bias correction of standardized uptake value ratio in quantitative 11C-PiB PET studies. Journal of nuclear medicine : official publication, Society of Nuclear Medicine. 2012;53(4):622-8.

Zijdenbos AP, Forghani R, Evans AC. Automatic "pipeline" analysis of 3-D MRI data for clinical trials: application to multiple sclerosis. IEEE Trans Med Imaging. 2002;21(10):1280-91.

Chapter 7: Class I HDAC reduction links amyloid-β and tau with dementia in living patients with Alzheimer's disease

Tharick A. Pascoal MD [1,2], Mira Chamoun PhD [1], Elad Lax PhD [3], Hsiao-Ying Wey PhD [4], Monica Shin MSc [1], Kok Pin Ng MD, MRCP [1], Min Su Kang BSc [1,2], Sulantha Mathotaarachchi MSc [1], Andrea L. Benedet MSc [1], Joseph Therriault BSc [1], Frederick A. Schroeder PhD [4], Jonathan M. DuBois PhD [4], Baileigh G. Hightower BA [4], Tonya M. Gilbert PhD [4], Nicole R. Zürcher PhD [4], Changning Wang PhD [4], Robert Hopewell PhD [2], Mallar Chakravarty PhD [5], Melissa Savard MSc [1], Emilie Thomas PhD [1], Sara Mohaddes MSc [1], Sarah Farzin BSc [5], Alyssa Salaciak BSc [5], Stephanie Tullo MSc [5], A. Claudio Cuello MD, FRSC [3], Jean-Paul Soucy MD, MSc [2], Gassan Massarweh PhD [2], Heungsun Hwang PhD [6], Eliane Kobayashi [2], Bradley T. Hyman MD, PhD [7], Bradford C. Dickerson MD [4,7], Moshe Szyf PhD [3], Serge Gauthier MD, FRCPC [1], Jacob M. Hooker PhD [4], and Pedro Rosa-Neto MD, PhD [1,2].

[1]Translational Neuroimaging Laboratory, The McGill University Research Centre for Studies in Aging, Department of Neurology and Neurosurgery, Faculty of Medicine, McGill University, Montreal, QC, Canada. [2] Montreal Neurological Institute, McGill University, Montreal, QC, Canada. [3]Department of Pharmacology and Therapeutics, McGill University, Montreal, QC, Canada. [4]Athinoula A. Martinos Center for Biomedical Imaging, Department of Radiology, Massachusetts General Hospital, Harvard Medical School, Charlestown, MA, USA. [5]Departments of Biological and Biomedical Engineering and Psychiatry, Douglas Mental Health University Institute, Brain Imaging Centre, Montreal, QC, Canada. [6]Department of Psychology, McGill University, Montreal, QC, Canada. [7]Department of Neurology, Massachusetts General Hospital, Harvard Medical School, Boston, MA, USA.

7.1 Preface

In previous chapters, we characterized interactions between amyloid-β, tau, and neurodegeneration as drivers of AD. However, these studies were based on phenomenological observations without focusing on a biological mechanism by which these pathologies interact to drive the disease. A growing body of evidence suggests that changes in the brain environment due to processes associated with AD may present at the epigenetic level where gene expression is regulated (Xu *et al.*, 2011, Anderson *et al.*, 2015, Nativio *et al.*, 2018). An important epigenetic mechanism for controlling gene expression is the modulation of chromatin density by histone modifications (Grunstein, 1997). Histone modifications, regulated by HDACs I, have been separately linked to amyloid-β, tau, neurodegeneration, and dementia (Sananbenesi and Fischer, 2009, Graff *et al.*, 2012, Bie *et al.*, 2014, Zhu *et al.*, 2017, Mahady *et al.*, 2018). Thus, in Chapter 7, we extended the findings of previous chapters and tested whether HDACs I modification may be a biological mechanism linking the aforementioned processes with dementia. Specifically, we designed a study in which living patients simultaneously underwent brain imaging of amyloid-β, tau, neurodegeneration, and HDACs I biomarkers to test the associations between these processes at tissue level.

7.2 Abstract

BACKGROUND

The rationale for clinical trials using class I histone deacetylases (HDACs I) inhibitors in Alzheimer's disease (AD) patients stems from experimental disease models showing HDACs I upregulation as well as cognitive improvement following HDACs I inhibition. However, this framework derives exclusively from studies using animal models that develop partial disease

phenotypes and post-mortem human studies using a small subset of brain regions affected by AD.

METHODS

To test this framework in living humans, we studied controls and patients across the AD clinical spectrum using a novel positron emission tomography (PET) agent selective for HDACs I (isoforms 1-3), amyloid-β PET, tau PET, magnetic resonance, and cognitive and genetic assessments. Also, we measured HDAC1-3 expressions using Western blotting in post-mortem brain tissues from AD patients and controls and two transgenic rat models.

RESULTS

We found that HDACs I availability is reduced in living AD patients in brain regions vulnerable to amyloid-β and tau pathologies. Structural equation modeling revealed that HDACs I reduction mediates the deleterious effects of amyloid-β and tau on brain atrophy and cognitive impairment. Post-mortem analysis confirmed that HDAC I isoforms 1-3 are reduced in AD patients in the same brain regions identified *in vivo*. Also, we found HDAC1 and HDAC2 reductions in rats expressing amyloid-β and tau, contrasting with normal levels in rats expressing single amyloid-β pathology.

CONCLUSIONS

Apart from refuting that HDAC I upregulation is a key element underlying AD pathophysiology, these results suggest that pharmacological HDAC I inhibition may accelerate symptoms if administered in AD patients.

7.3 Introduction

Alzheimer's disease (AD) is characterized by the brain accumulation of amyloid-β and tau proteins (Jack *et al.*, 2013). However, the mechanisms by which these proteinopathies interact to determine downstream neurodegeneration and cognitive impairment are poorly understood. It has been proposed that the progressive accumulation of protein aggregates imposes neuroepigenetic modifications determining the patient's vulnerability to dementia (Graff *et al.*, 2012, Graff and Tsai, 2013). Epigenetic regulation of gene expression is essential for maintaining mammalian cognitive function (Dulac, 2010). Among the epigenetic regulators, histone acetylation has been frequently associated with AD and other pathological processes in recent studies (Graff *et al.*, 2012, Graff and Tsai, 2013, Kandel and Kandel, 2014). Acetylation of histones, which are proteins that DNA wraps around, reduces the electrostatic affinity between adjacent histones and DNA to configure an open-chromatin structure, allowing gene transcription (Grunstein, 1997). Increased histone acetylation due to a reduction of class I histone deacetylases (HDACs I) has been shown to improve learning and memory in rodents (Fischer *et al.*, 2007, Sweatt, 2007, Guan *et al.*, 2009, Peleg *et al.*, 2010, Lattal and Wood, 2013, Falkenberg and Johnstone, 2014). Based on these observations, increased HDACs I level has been hypothesized to impair cognition in neurodegenerative conditions (Sweatt, 2007, Jakovcevski and Akbarian, 2012, Falkenberg and Johnstone, 2014). Indeed, subsequent studies confirmed HDACs I increase within selected brain regions in multiple animal models of AD and post-mortem human brain tissue (Graff *et al.*, 2012, Bie *et al.*, 2014, Gonzalez-Zuniga *et al.*, 2014, Yamakawa *et al.*, 2017, Zhu *et al.*, 2017, Mahady *et al.*, 2018). In some of these models, increased levels of HDAC I isoform 1 are associated with tau pathology (Mahady *et al.*, 2018), while increased levels of HDAC I isoforms 2 and 3 are associated with amyloid-β pathology (Bie

et al., 2014, Zhu *et al.*, 2017). Also, HDAC I inhibitors improve cognition in several mouse models of AD (Fischer *et al.*, 2007, Kilgore *et al.*, 2010, Cuadrado-Tejedor *et al.*, 2017). Together, these observations corroborate a framework proposing that AD-related cognitive decline results from aberrantly increased HDACs I levels (Xu *et al.*, 2011, Graff *et al.*, 2012, Graff and Tsai, 2013, Falkenberg and Johnstone, 2014, Yang *et al.*, 2017), which has been used as justification for ongoing clinical trials testing HDAC I inhibitors in AD patients (Cummings *et al.*, 2018).

The present study was designed to test the hypothesis that HDAC I upregulation is a key element underlying AD - for the first time - in living patients. We also assessed the magnitude of change in HDACs I level across the AD clinical spectrum and its association with amyloid-β and tau concentrations.

7.4 Methods

HUMAN PARTICIPANTS

A total of 94 participants aged 18 to 91 years were evaluated (Table 1). The study participants were from the community or outpatients at the McGill University Research Centre for Studies in Aging (MCSA) and Massachusetts General Hospital (MGH), Harvard Medical School. In order to ensure external validity, both sites conducted concomitant but entirely independent studies on design and analysis. At the end of both studies, the two sites presented their final results blind to each other's findings and these results are the ones presented in this study. MCSA participants had detailed clinical assessments including Mini-Mental State Examination (MMSE), Clinical Dementia Rating (CDR), and cerebrovascular disease risk with the Hachinski Ischemic scale.

Cognitively normal (CN) individuals had no objective cognitive impairment and a CDR score of 0. Mild cognitive impairment (MCI) individuals had subjective and objective cognitive impairments, essentially preserved activities of daily living, and a CDR score of 0.5. Mild-to-moderate AD dementia patients had a CDR score between 1 and 2, met the National Institute on Aging and the Alzheimer's Association criteria for probable AD determined by a licensed physician, and had amyloid-β and tau abnormalities. MGH participants had detailed clinical assessments including MMSE and CDR. CN individuals had no objective cognitive impairment and a CDR score of 0. Mild AD dementia patients had a CDR score between 0.5 and 1 and a clinical diagnostic of AD dementia determined by a licensed physician/nurse practitioner. In both MCSA and MGH sites, participants were excluded if they had active substance abuse or inadequately treated comorbid psychiatric conditions, recent head trauma or major surgery, or if they presented any magnetic resonance imaging (MRI) / positron emission tomography (PET) safety contraindication. AD patients did not have to discontinue any medication for this study. Both studies were approved by the appropriate institutional ethics committees (The Douglas Mental Health University Institute Research Ethics Board, Montreal Neurological Instituted PET working committee, the Partners HealthCare Institutional Review Board, and the Massachusetts General Hospital Radioactive Drug Research Committee) and a written informed consent was obtained from all participants; a surrogate consent was obtained for those patients who did not have the capacity to consent themselves.

HUMAN MATERIAL

Frozen brain tissues from the posterior cingulate and prefrontal cortices of six patients with ante- and post-mortem diagnosis of AD (65-80 years old, Consortium to Establish a Registry for

Alzheimer Disease (CERAD) positive (Mirra *et al.*, 1991)) and nine age-matched CN (CERAD negative) were obtained from the Douglas-Bell Canada Brain Bank with the approval of the Brain Bank's and Douglas Institute's ethic boards.

ANIMAL USE

All rat work was performed in accordance to the National Institutes of Health and to the Guide to the Care and Use of Experimental Animals of the Canadian Council on Animal Care following the approval by the McGill Animal Care Ethics Committee. The rats were kept in ventilated cages in pairs with environmentally controlled conditions: 12-hours light/dark cycle at 21 °C with access to food and water ad libitum. Four transgenic McGill-R-Thy1-APP rats (14-16 months old) (Do Carmo and Cuello, 2013), presenting the Swedish double (K670N, M671L) and the Indiana (V717F) mutations, and their respective control littermates were used for this study. McGill-R-Thy1-APP rats present human amyloid-β pathology and cognitive impairment at as early as 6 months, and they do not form neurofibrillary tangles during their lifetime (Do Carmo and Cuello, 2013). Five transgenic TgF344-AD rats (10-12 months old) (Cohen *et al.*, 2013), presenting presenilin 1 (PS1ΔE9) and amyloid-β protein precursor Swedish mutations, and their respective control littermates were also assessed. TgF344-AD rats manifest human amyloid-β pathology, downstream neurofibrillary tangles, and cognitive impairment at as early as 6 months (Cohen *et al.*, 2013). We studied male and female rats and the groups were matched for sex. Rats were sacrificed by decapitation while anesthetized, and the brains were rapidly removed, frozen in liquid nitrogen-isopentanol solution, and stored at -80˚C. The prefrontal cortex and the posterior portion of the cingulate cortex (retrosplenial) were dissected and used for this study.

RADIOSYNTHESIS

[^{11}C]Martinostat (Wey *et al.*, 2016), [^{18}F]MK-6240 (Pascoal *et al.*, 2018), and [^{18}F]AZD4694 (Cselenyi *et al.*, 2012) were synthesized as previously described.

IMAGE METHODS

At the MCSA site, participants had a 3T MRI (Siemens) and PET scans were acquired with a brain-dedicated Siemens High Resolution Research Tomograph. [^{11}C]Martinostat images for quantifying HDACs I (isoform 1,2, and 3) were acquired at 60–90 min after the intravenous bolus injection of the tracer (Wey *et al.*, 2016). [^{18}F]MK-6240 images for quantifying tau neurofibrillary tangles were acquired at 90–110 min after the intravenous bolus injection of the tracer (Pascoal *et al.*, 2018). [^{18}F]AZD4694 images for quantifying amyloid-β were acquired at 40–70 min after the intravenous bolus injection of the tracer (Cselenyi *et al.*, 2012). PET images were reconstructed using an ordered subset expectation–maximization (OSEM) algorithm on 4D volumes. At the end of each PET acquisition, a 6-min transmission scan was conducted with a rotating ^{137}Cs point source for attenuation correction. PET images were additionally corrected for motion, dead time, decay, and random and scattered coincidences. The image analysis was performed using the Medical Image NetCDF software toolbox version 2.2 (www.bic.mni.mcgill.ca/ServicesSoftware/MINC). Gray matter density was computed using the T1-weighted images with voxel-based morphometry. [^{11}C]Martinostat standardized uptake value ratio (SUVR) images used the telencephalon white matter (Wey *et al.*, 2016), whereas [^{18}F]MK-6240 and [^{18}F]AZD4694 SUVRs used the cerebellum gray matter as reference region (Cselenyi *et al.*, 2012, Pascoal *et al.*, 2018). Regions-of-interest were tailored using the MNI ICBM atlas. At the MGH site, MR and PET images were simultaneously acquired on a 3T Siemens TIM Trio

containing a BrainPET insert. Motion correction was implemented with the MCFLIRT tool. [^{11}C]Martinostat images were acquired at 60–90 min post-radiotracer injection. MR-based attenuation correction was applied using Statistical Parametric Mapping–based, pseudo–computed tomography methodology. PET data were binned and reconstructed using the 3D ordinary Poisson OSEM algorithm. [^{11}C]Martinostat SUVR images used the telencephalon white matter. At both sites, PET images were spatially smoothed to achieve a final 8-mm full-width at half maximum resolution. Although both sites used brain-dedicated PET scanners with high spatial resolution, which makes the images less susceptible to partial volume effects, we confirmed all the results using partial volume corrected data (Thomas *et al.*, 2011).

APOLIPOPROTEIN E (APOE) GENOTYPING

APOE genotyping was performed using polymerase chain reaction amplification technique, followed by restriction enzyme digestion, standard gel resolution, and visualization processes as described in detail elsewhere (Saykin *et al.*, 2015).

PROTEIN EXTRACTION AND IMMUNOBLOT

Human and rat brain sections were harvested and lysed in RIPA buffer (150mM NaCl, 0.1% SDS, 0.5% Deoxycholate, 50mM Tris pH 7.5, 1% NP-40) containing complete protease inhibitor (Roche, Laval, QC). Following centrifugation (10000 rpm, 10min, 4C), the total protein was collected from the upper phase. Cell lysates were subjected to gel electrophoresis on 4-12% precast SDS-polyacrylamide gel (SurePAGE™, Bis-Tris, 10x8, 4-12%, 12 wells Genscript, USA) in MOPS buffer. Separated proteins were transferred onto nitrocellulose membranes in a wet transfer tank (Bio-Rad) and then probed with antibodies against HDAC1 (ABCAM

ab19845), HDAC2 (ABCAM ab16032) and HDAC3 (ABCAM y415-ab32369) at a 1:1000 dilutions in all cases for one hour, followed by a secondary anti-rabbit IgG antibody at 1:5000 dilution for one hour. Whenever possible (i.e., for HDAC1 and HDAC2) knockout-validated antibodies were used. Beta-actin was used as a reference protein (1:5000) and was followed by a secondary anti-mouse IgG antibody at 1:5000. Blots were scanned and analyzed by ChemiDoc gel imaging system (Bio-Rad, Mississauga, ON).

STATISTICS AND REPRODUCIBILITY

Statistical analyses were performed using R Statistical software version 3.1.2. Voxel-wise statistics were performed using MATLAB software version 9.2 with VoxelStats package (Mathotaarachchi *et al.*, 2016). Biomarker abnormalities were assessed using analysis of covariance (ANCOVA) with post hoc multiple comparisons as well as two-tailed *t*-test, whereas associations between biomarkers were tested with regression and Pearson correlation. Regression models were adjusted for age, sex, *APOE ε4* status, years of formal education (model involving cognition), and two-tailed false discovery rate corrected for multiple comparisons at $P < 0.05$ (voxel-wise models). Patients' z-score parametric images were obtained anchored on the normative data of the elderly CN population. Voxel-wise receiver operating characteristic curve (ROC), contrasting elderly controls and AD individuals, provided the area under the curve for a diagnosis of AD. We evaluated the effects of HDACs I on AD using structural equation modeling with the R package lavaan (MacCallum and Austin, 2000). Meta-models were created based on expected and hypothesized connections to test the specific hypothesis demonstrated in each figure (Jack *et al.*, 2013). A bootstrap method tested the statistical significance of the model's chi-square value and parameter estimates.

7.5 Results

Remarkably, we found a consistent reduction in HDACs I availability in individuals with AD within large brain regions in the posterior cingulate, precuneus, inferior parietal, lateral temporal, and hippocampal cortices compared with elderly matched controls (Figure 7-11A, and Figs. S1 and S2 in the Supplementary Appendix). In addition, voxel-wise ROC analysis revealed that HDACs I level differentiated AD from elderly controls reaching 100% accuracy in the aforementioned regions (Figure 7-1B). The above-mentioned results were independently replicated at a separate enrolment site without previous knowledge of these outcomes (Figure 1C and 1D). There were no regions with a significant increase in HDACs I level in AD patients in both enrolment sites. MCI individuals showed intermediary levels of HDACs I between elderly control and AD individuals, with a significant reduction in inferior parietal and hippocampal cortices (Figure 7-1E). Voxel-wise z-score maps showed that the HDACs I reduction in MCIs was confined to the same set of brain regions showing downregulation in AD patients (Figure 7-1F-J).

Subsequently, we tested whether HDACs I level associated with the pathophysiological characteristics of the population. As expected, individuals with MCI and AD dementia had increased amyloid-β and tau burden and decreased grey matter density (Fig. S3 in the Supplementary Appendix). Voxel-wise regressions and correlation analysis inside anatomically segregated brain regions revealed that HDACs I level was independent of sex, *APOE ε4* status, education, and cerebrovascular disease risk (Fig. S4 in the Supplementary Appendix). Age was negatively correlated with HDACs I in the prefrontal, medial temporal, anterior cingulate, and orbitofrontal cortices (Figure 7-2A and 7-2B). In the posterior cingulate, precuneus, inferior

parietal, and lateral temporal cortices, HDACs I availability negatively correlated with brain amyloid-β and tau concentrations (Figure 7-2C-F), while it positively correlated with grey matter density and cognitive performance (Figure 7-2G-J). HDACs I level did not associate with the aforementioned pathophysiological processes or cognition in any other brain region.

We investigated whether HDACs I level mediates the deleterious effects of amyloid-β and tau on brain atrophy and cognitive impairment using a structural equation model. The model showed that HDACs I completely mediate the effect of amyloid-β and partially mediates the effect of tau on brain atrophy and cognitive impairment (Figure 7-3). Notably, this construct was able to explain 85.9% and 91% of the variance in brain atrophy and cognitive impairment, respectively (Figure 7-3). This analysis inferred no direct association between brain atrophy and cognitive impairment, suggesting that the strong correlation between these two variables is due to the fact that the same pathological pathways affect both. The model testing the classical sequential construct of AD progression without using HDACs I level explained 66.8% and 80.1% of the brain atrophy and cognitive impairment variance, respectively (Fig. S5 in the Supplementary Appendix) (Jack *et al.*, 2013).

Next, to assess the individual levels of HDAC I isoforms, we compared the abundance of the HDAC I isoforms 1, 2, and 3 in post-mortem brain tissues from patients with ante and post-mortem diagnosis of sporadic AD and age-matched controls in regions with and without HDACs I changes in AD based on *in vivo* results. Consistent with PET imaging, we found that HDAC1-3 were reduced in the posterior cingulate cortex of AD patients, whereas no significant differences were found in the prefrontal cortex (Figure 7-4A and 7-4B, and Fig. S6 in the Supplementary

Appendix). To clarify whether HDACs I reduction is associated with the concomitance of amyloid-β aggregates and tau pathology in the form of neurofibrillary tangles, which are the two hallmark pathological features of AD, we measured HDACs I in a rat model that develops only human amyloid-β pathology (Do Carmo and Cuello, 2013) and for the first time in a rat model that develops both human amyloid-β and downstream neurofibrillary tangles (Cohen *et al.*, 2013). We found that the amyloid-β plus tau rat model had a significant reduction in HDAC1 and HDAC2 (Figure 7-4C, and Fig. S6 in the Supplementary Appendix), whereas the single amyloid-β rat model had normal HDACs I level (Figure 7-4D, and Fig. S6 in the Supplementary Appendix).

7.6 Discussion

The results presented in this study reveal that HDACs I reduction mediates neurodegeneration and cognitive decline in AD patients, which is in stark contrast to the HDACs I upregulation described in several previous studies (Graff *et al.*, 2012, Bie *et al.*, 2014, Zhu *et al.*, 2017). Thus, contradicting the predictions of the mainstream notion (Sweatt, 2007, Falkenberg and Johnstone, 2014, Yang *et al.*, 2017), our results raise concerns that HDAC I inhibitors might result in harm, rather than benefit for AD patients.

Supporting our findings, a study showed that p25/Cdk5, a kinase complex involved in AD, inhibits HDAC1 leading to neuronal cell death (Kim *et al.*, 2008). Also, HDAC1-3 levels have shown to play a role in maintaining neuronal plasticity and function (Akhtar *et al.*, 2009, Montgomery *et al.*, 2009, Jiang and Hsieh, 2014) and the HDAC I inhibitor valproate has been associated with faster brain atrophy and cognitive decline in patients with AD (Fleisher *et al.*,

2011). Although previous post-mortem observations have shown increased HDAC I levels in AD patients (Graff *et al.*, 2012), these studies exclusively assessed the prefrontal and medial temporal cortices (Graff *et al.*, 2012, Mahady *et al.*, 2018), which are not brain regions concomitantly affected by high levels of both amyloid-β and tau in early AD stages (Braak and Braak, 1991). While the medial temporal cortex has low concentrations of amyloid-β, the prefrontal cortex has low levels of tau pathology (Braak and Braak, 1991). HDACs I reduction in human brain regions with high amyloid-β and tau load as well as in a rat model of amyloid-β plus tau support an epigenetic signature associated with the presence of both amyloid-β and tau pathologies (Pascoal *et al.*, 2017).

Although it is well-established that amyloid-β and tau play a central role in AD (Jack *et al.*, 2013), HDACs I reduction may underscore a mechanism by which these pathologies interact to drive disease progression, which is one of the most important unanswered questions in AD. The fact that HDAC I is associated with DNA repair and neuronal plasticity brings hope that the combination of an HDAC I agonist with the existing anti-protein aggregate therapies has the potential to rectify underlying epigenetic dysregulations and restore, at least in part, cognitive functioning in patients with AD (Kim *et al.*, 2008, Akhtar *et al.*, 2009, Montgomery *et al.*, 2009, Wang *et al.*, 2013). Understanding the entire complexity of epigenetic interactions in humans is imperative to interpreting the results from experimental models before testing epigenetic therapies in patients with complex brain disorders.

7.7 Tables and Figures

Table 7-1. Demographics of the human subjects in each study site.

	Young CN		Elderly CN		MCI	AD	
	MCSA	**MGH**	**MCSA**	**MGH**	**MCSA**	**MCSA**	**MGH**
Number of subjects (*n*)	2	23	15	13	15	16	10
Age, y, mean (SD)	23 (1.4)	27.2 (5.3)	67.4 (8.3)	63.2 (7.8)	72 (7)	69.7 (11.7)	66.9 (8.9)
Male, *n*. (%)	1 (50)	11 (48)	6 (40)	7 (54)	9 (60)	9 (56)	8 (80)
***APOE ε4*, *n*. (%)**	0 (0)	-	5 (33)	-	4 (27)	8 (50)	-
Education, y, mean (SD)	17.5 (0.7)	-	17.4 (4)	-	15.2 (4.8)	14 (4.6)	-
MMSE score, mean (SD)	30 (0)	-	29.5 (0.5)	29.1 (0.9)	27 (2.3)	14.4 (6.8)	19.9 (6.2)
CDR score, mean (SD)	0 (0)	-	0 (0)	0 (0)	0.5 (0)	1.4 (0.5)	0.8 (0.34)

Demographic breakdown by study site. MCSA; McGill University Research Centre for Studies in Aging. MGH; Massachusetts General Hospital.

Figure 7-1. HDACs I level is reduced in patients with Alzheimer's disease.

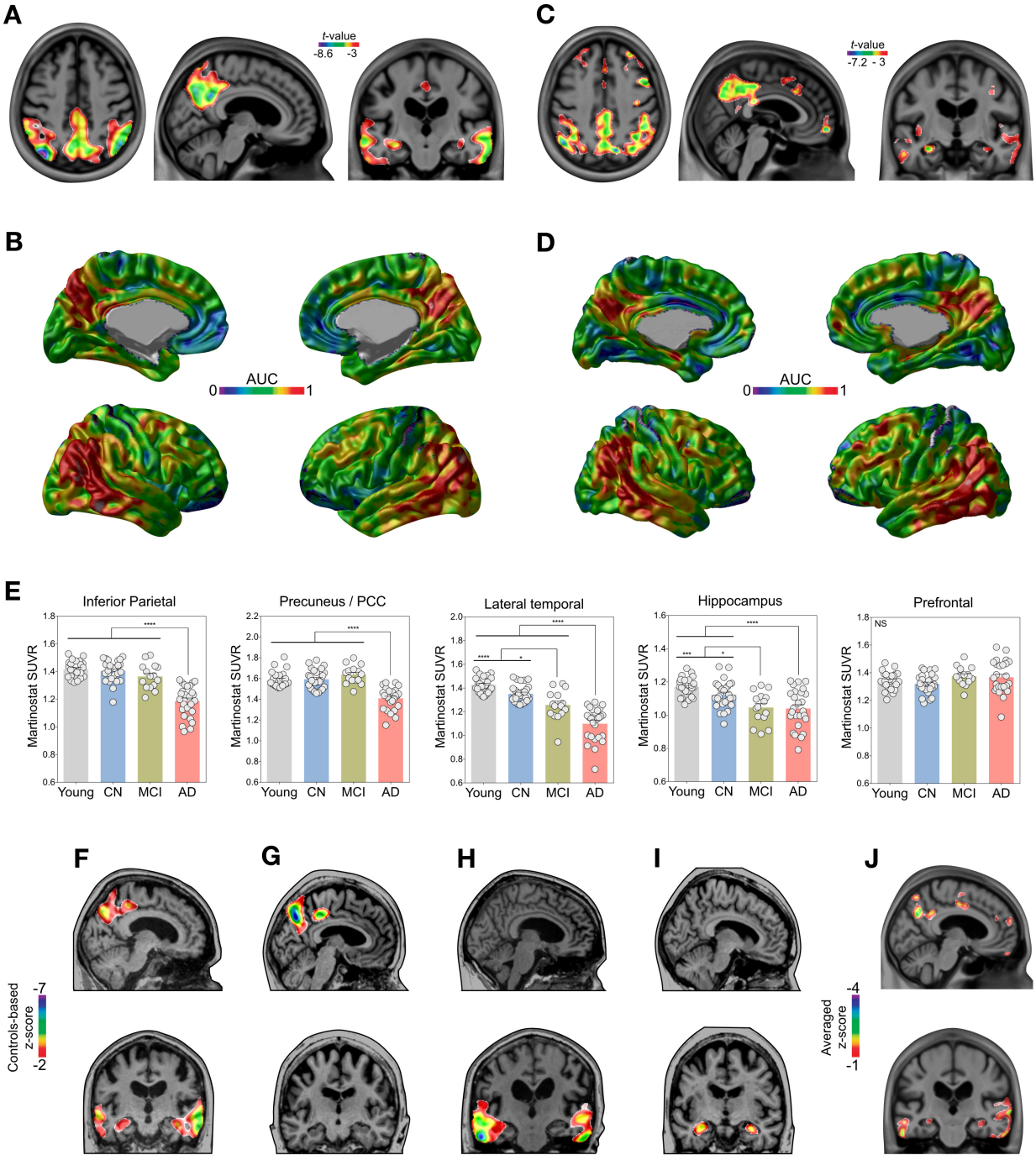

(**A**) T-statistical parametric map (two-tailed false discovery rate corrected for multiple comparisons at $P < 0.05$), overlaid on a structural MRI template, shows the regions where HDACs I level was significantly reduced in patients with AD ($n = 16$) compared to elderly CN ($n = 15$). (**B**) Voxel-wise ROC analysis revealed that HDACs I reduction differentiated AD from elderly controls reaching 100% accuracy in clusters in the posterior cingulate, precuneus, inferior parietal, and lateral temporal cortices. (**C** and **D**) Replication study confirmed HDACs I

reduction in patients with AD (n = 10) compared to elderly CN (n = 13) in the same set of brain regions described above (two-tailed false discovery rate correction at $P < 0.05$). Importantly, there was no significant increase in HDACs I level in AD patients in both datasets. **e,** ANCOVA and post hoc analyses among young (n = 25) and elderly (n = 28) CN, MCI (n = 15), and AD (n = 26) individuals in selected brain regions confirmed that HDACs I level is reduced in AD and showed a significant reduction in MCIs in the inferior parietal and hippocampal cortices, values are mean ± s.e.m. Voxel-wise z-score maps anchored in the elderly CN population, overlaid on each individual's structural MRI, showed the patterns of HDACs I reduction in representative individuals: (**F**) AD (Clinical Dementia Rating (CDR) = 1) and (**G** to **I**) MCIs (CDR = 0.5). (**J**) Averaged voxel-wise z-score map of all individuals with MCI, overlaid on a structural MRI template.

Figure 7-2. HDACs I level associates with Alzheimer's disease pathophysiological processes.

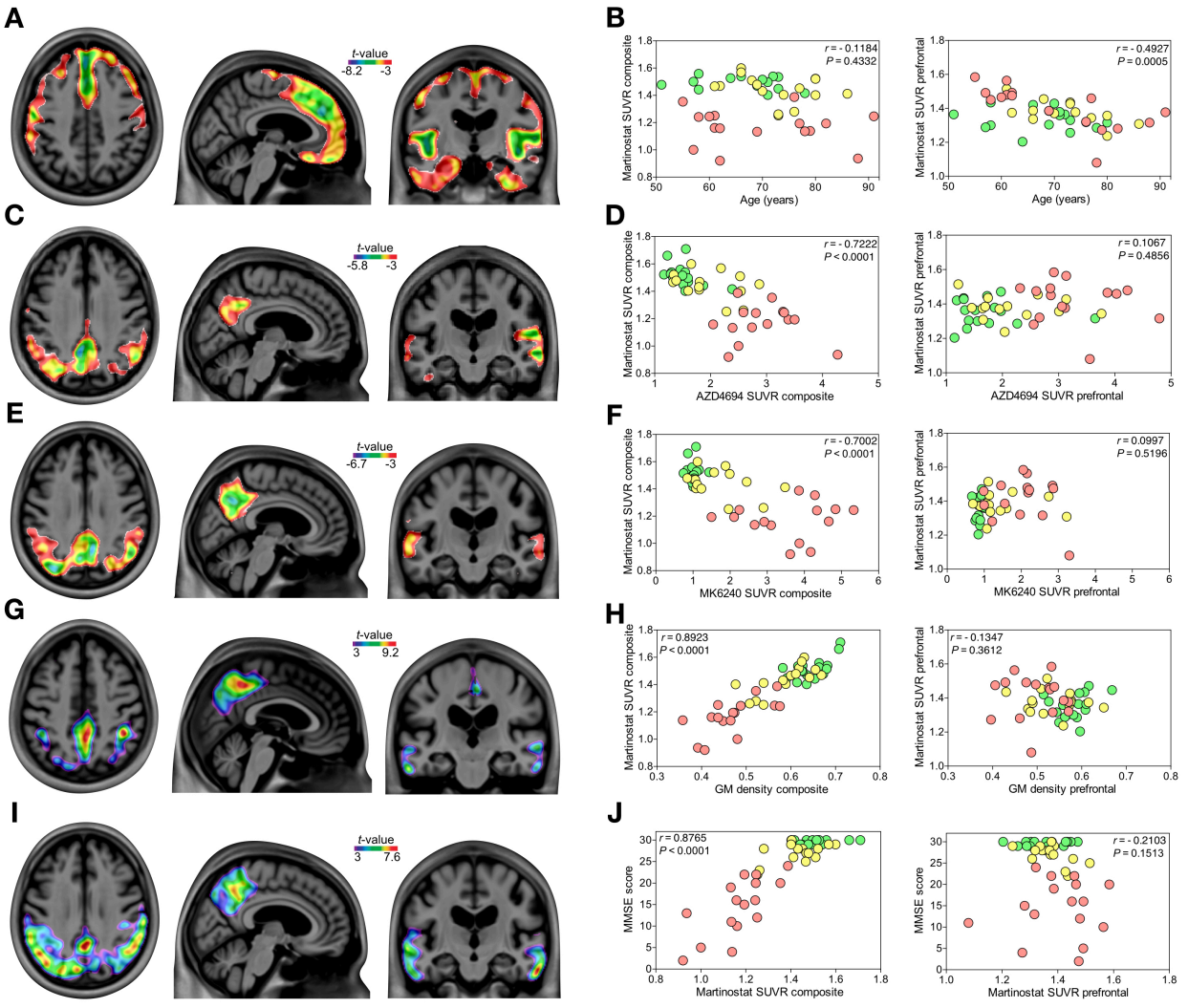

T-statistical parametric maps (two-tailed false discovery rate corrected for multiple comparisons at $P < 0.05$) of regressions performed at every brain voxel (left side), as well as scatter plots showing two-tailed Pearson correlation inside selected brain regions (right side) show the association between HDAC I with: (**A** and **B**) age ($n = 46$). (**C** and **D**) amyloid-β ($n = 45$). (**E** and **F**) neurofibrillary tangles ($n = 44$). (**G** and **H**) grey matter (GM) density ($n = 48$). (**I** and **J**) and cognition as measured with MMSE score ($n = 48$) in individuals who underwent amyloid-β or tau PET biomarkers. Green, yellow, and red dots represent CN, MCI, and AD individuals, respectively. The composite value in the scatter plots includes the brain regions with significant HDACs I reduction in AD (see Figure 1A)

Figure 7-3. HDACs I level mediates the effects of amyloid-β and tau pathologies on cognitive impairment.

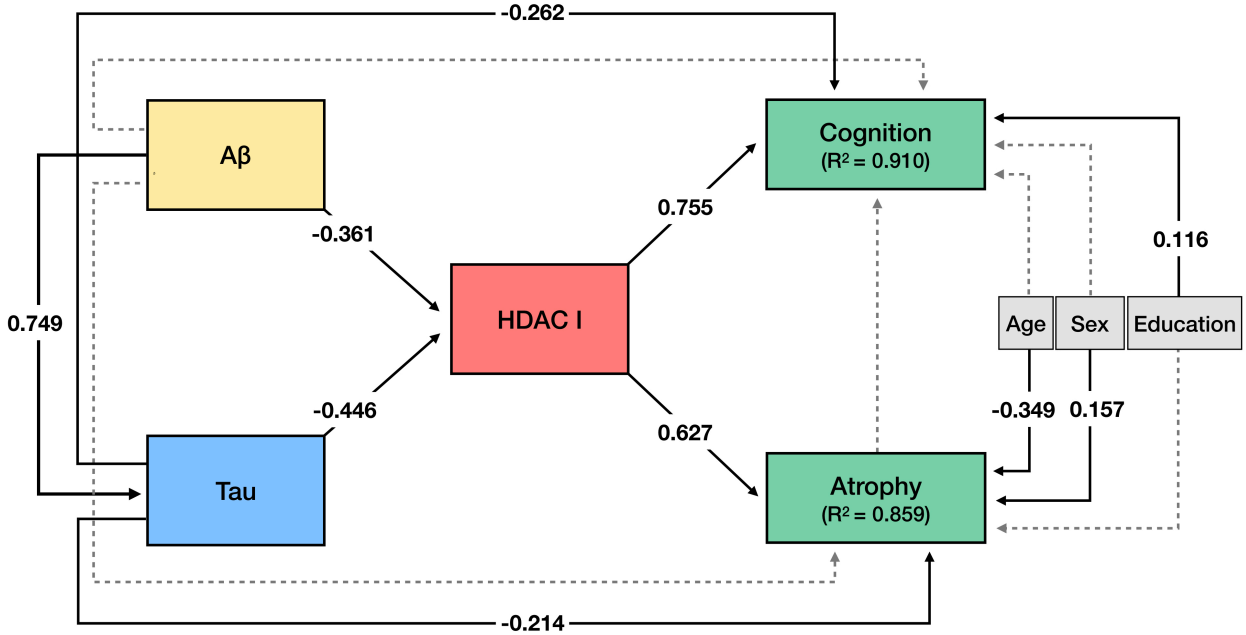

The path coefficient values presented in the figure are standardized. Solid arrows represent significant effects, whereas dashed lines represent non-significant effects. The hypothesized model fits the data well ($n = 44$, $X^2 = 1.818$, degrees of freedom = 6, $P = 0.936$, the root mean square error of approximation (RMSEA) = 0.000 (90% confidence interval [0.000-0.049]), standardized root mean square residual (SRMR) = 0.029, comparative fit index (CFI) = 1.000, Akaike information criterion (AIC) = 871.632, and Bayesian information criterion (BIC) = 907.316). The imaging biomarker values were extracted from a composite of brain regions with significant HDACs I reduction in AD (see Figure 1A). PET biomarker values were adjusted for age. Grey matter density and Mini-Mental State Examination (MMSE) represented brain atrophy and cognition, respectively.

Figure 7-4. Post-mortem analysis shows HDACs I reduction in vulnerable brain regions in Alzheimer's disease patients and rats overexpressing human amyloid-β and tau pathology.

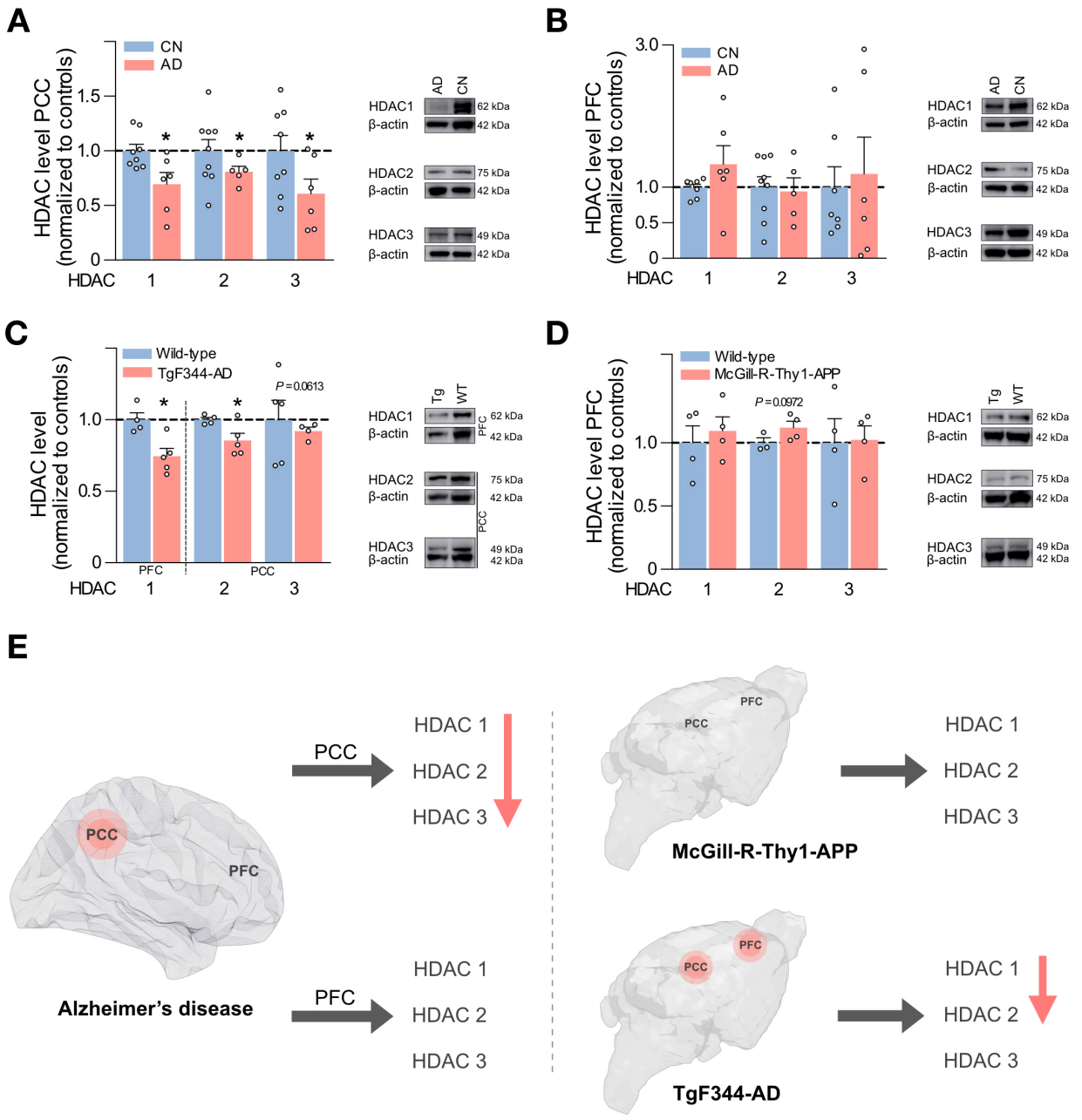

Quantification and representative western blots from brain lysate showed downregulation of HDAC1-3 in (**A**) the posterior cingulate cortex (PCC) of patients with AD, whereas no significant difference was found in (**B**) the prefrontal cortex (PFC) (CN, n = 7-9 individuals; AD, n = 5-6 patients). (**C**) TgF344-AD rats (n = 4-5 rats each), which express human amyloid-β plus neurofibrillary tangles, showed a significant reduction in HDAC1 and HDAC2. (**D**) McGill-R-Thy1-APP rats (n = 3-4 rats each), which express human amyloid-β without developing neurofibrillary tangles, showed normal HDACs I level. (**E**) Summary of the western blot results.

See Figure S6 for entire western blot results. * $P < 0.05$ (two-tailed), one-sample *t*-test; values are mean ± s.e.m. HDAC1-3 levels were normalized to beta-actin as a loading control.

7.8 Acknowledgments

The authors thank all participants of the study and staff of the MCSA, Athinoula A. Martinos Center for Biomedical Imaging, and MGH that supported this project. The MCSA group thanks Dean Jolly, Alexey Kostikov, Monica Samoila-Lactatus, Karen Ross, Mehdi Boudjemeline, and Sandy Li for assist in the radiochemistry production. We also thank Richard Strauss, Edith Strauss, Guylaine Gagne, Carley Mayhew, Tasha Vinet-Celluci, Karen Wan, Sarah Sbeiti, Jenna Stevenson, Meong Jin Joung, Miloudza Olmand, Rim Nazar, Hung-Hsin Hsiao, Reda Bouhachi, and Arturo Aliaga for consenting subjects and/or helping with data acquisition. We thank the Cerveau Technologies for providing the MK-6240 precursor. The Martinos Center/MGH group thanks A. Kendall, M. Wentworth, O. Johnson-Akeju, M. Albers, and N. Nortelus for consenting subjects and/or medical coverage; J. Sore and the radiopharmacy team for radiotracer synthesis; G. Arabasz, S. Hsu, and R. Butterfield for assistance with MR-PET imaging; D. Chonde and C. Catana for advice in PET image reconstruction. This work was supported by the Weston Brain Institute (P.R-N.), the Canadian Institutes of Health Research (MOP-11-51-31, P.R-N.), the Alzheimer's Association (NIRG-12-92090 and NIRP-12-259245, P.R-N.), the Alzheimer Society Research Program, the Canadian Consortium on Neurodegeneration in Aging (T.A.P.) and the Richard and Edith Strauss Canada Fund Postdoctoral Fellowship in Medicine (E.L.). This research also received funding from the National Institute on Aging of the NIH (R21AG051931 to J.M.H.), the American Federation for Aging Research (AFAR) New Investigator Award in Alzheimer’s Disease (H-Y.W.), Alzheimer's Drug Discovery Foundation Biomarker Development grant (J.M.H.), and MGH Research Scholar’s Program (J.M.H.), and NIDCD R01

DC014296 (B.C.D.). The development of the [^{11}C]Martinostat radiotracer was supported by the National Institute of Drug Abuse (NIDA) of the National Institutes of Health under grant numbers R01DA030321 (J.M.H.). Part of this research was carried out at the Athinoula A. Martinos Center for Biomedical Imaging at MGH, using resources provided by the Center for Functional Neuroimaging Technologies, P41EB015896, a P41 Biotechnology Resource Grant supported by the National Institute of Biomedical Imaging and Bioengineering of the NIH. This work also involved the use of instrumentation supported by the NIH Shared Instrumentation Grant Program; specifically, S10RR017208, S10RR026666, S10RR022976, S10RR019933, and S10RR023401.

7.9 Supplementary Material

Figure S1. Voxel-wise HDACs I level across diagnostic groups.

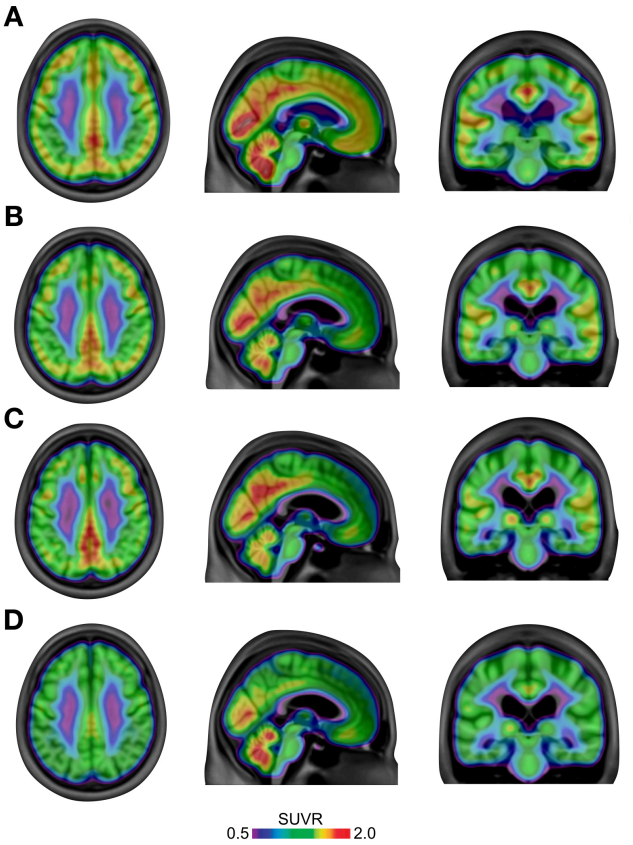

[^{11}C]Martinostat SUVR parametric images averaged among (**A**) young (n = 25) and (**B**) elderly (n = 28) CN, (**C**) MCI (n = 15), and (**D**) AD (n = 26) individuals. [^{11}C]Martinostat uptake is visually reduced in patients with AD in posterior cingulate, precuneus, inferior parietal, and lateral temporal cortices.

Figure S2. Voxel-wise HDACs I reduction after correction for partial volume effects.

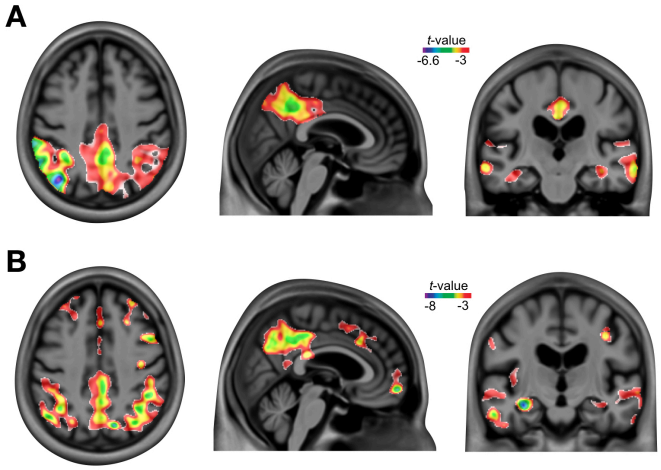

T-statistical parametric map, overlaid on a structural MRI template, shows the regions where HDACs I level was significantly reduced in patients with AD (n = 16) compared to elderly CN (n = 15) at (**A**) the MCSA site, and significantly reduced in patients with AD (n = 10) compared to elderly CN (n = 13) at (**B**) MGH site, after two-tailed false discovery rate correction for multiple comparisons at $P < 0.05$ and partial

Figure S3. Regional diagnostic effects on amyloid-β, tau, and gray matter density.

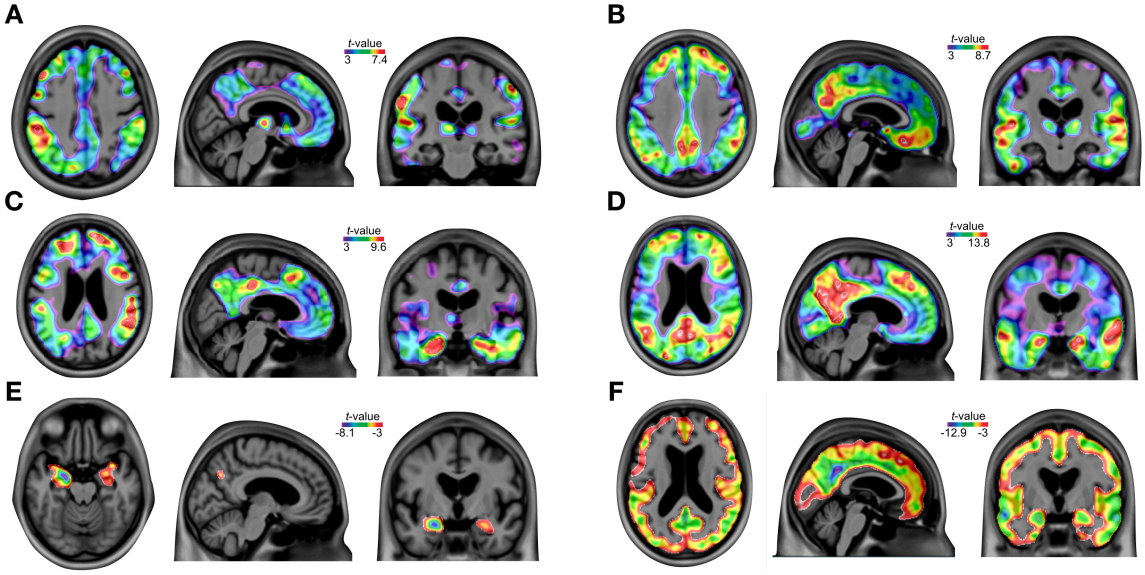

T-statistical parametric maps (two-tailed false discovery rate corrected at $P < 0.05$) revealed areas with increased amyloid-β deposition in (**A**) MCIs ($n = 14$) and (**B**) AD patients ($n = 15$); neurofibrillary tangles accumulation in (**C**) MCIs ($n = 14$) and (**D**) AD patients ($n = 15$); and decreased gray matter density in (**E**) MCIs ($n = 15$) and (**F**) AD patients ($n = 16$) as compared to elderly CN.

Figure S4. HDACs I level does not associate with sex, *APOE* ε4 status, education, or cerebrovascular disease risk.

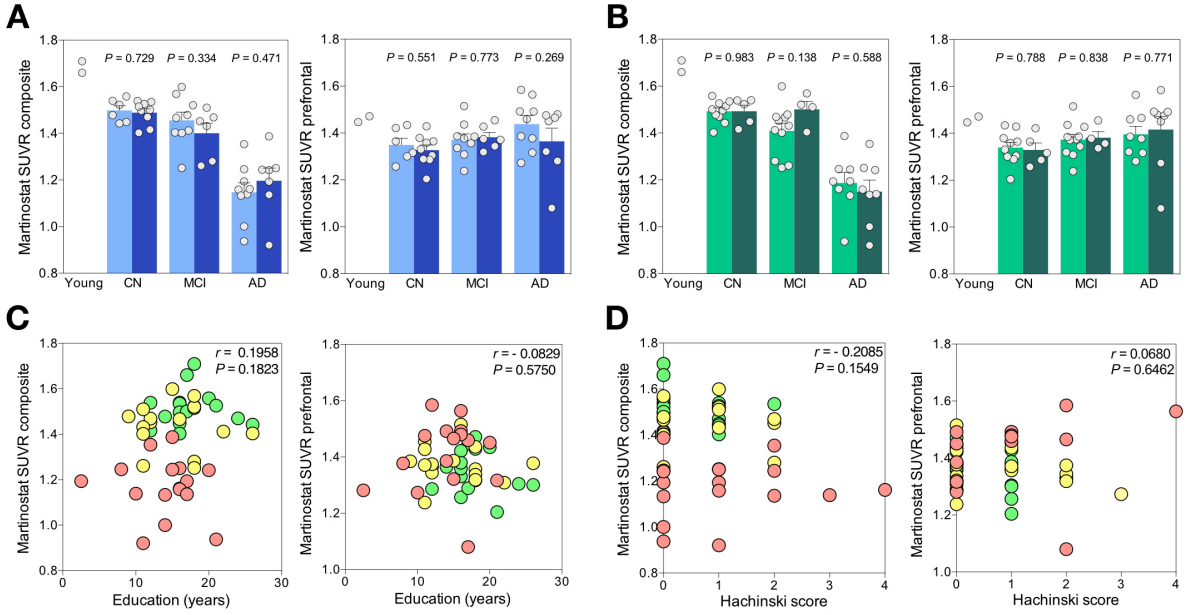

The bar plots show no significant difference in HDACs I availability between (**A**) males (light blue) and females (dark blue) and (**B**) *APOE ε4* non-carriers (light green) and carriers (dark

green) in individuals who underwent amyloid-β or tau PET biomarkers, values are mean ± s.e.m. *P* values represent the results of a two-tailed *t*-test performed inside each diagnostic group. The scatter plots show no association between HDACs I availability and (**C**) years of education or (**D**) cerebrovascular disease risk assessed with the Hachinski ischemic score. *P* values represent the results of two-tailed Pearson correlation. Green, yellow, and red dots represent CN (n = 15), MCI (n = 15), and AD (n = 16) individuals, respectively. The composite value in the plots includes the brain regions with significant HDACs I reduction in AD (see Figure 1A).

Figure S5. Structural equation model representing the classical sequential model of AD progression.

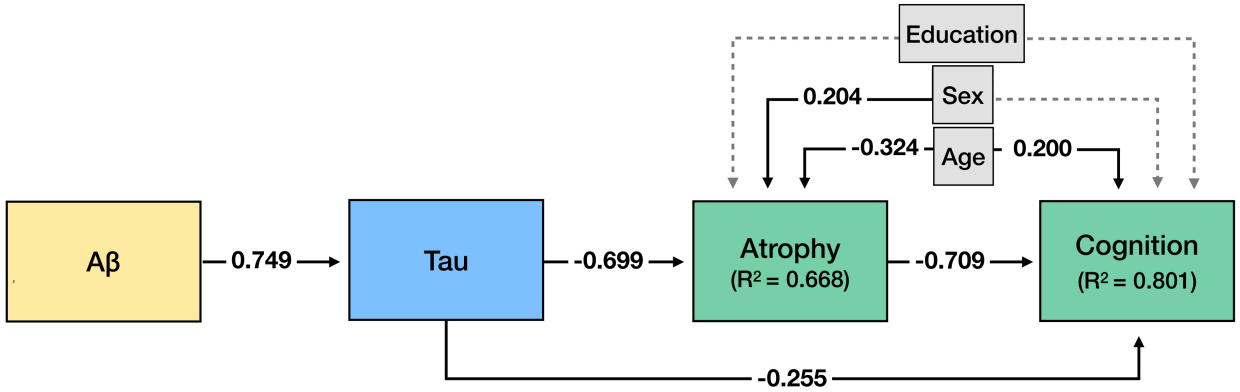

The path coefficient values presented in the figure are standardized. Solid and dashed lines represent significant and non-significant effects, respectively. The classical sequential model of AD progression fits the data well (n = 44, X^2 = 5.680, degrees of freedom = 5, P = 0.339, RMSEA = 0.056 (90% confidence interval, [0.000-0.223]), SRMR = 0.037, CFI = 0.995, AIC = 998.189, and BIC = 1021.383). The imaging biomarker values were extracted from a composite of brain regions with significant HDACs I reduction in AD (see Figure 1A). PET biomarker values were adjusted for age. Grey matter density and MMSE represented brain atrophy and cognition, respectively.

Figure S6. Western blots of HDACs in humans and rats.

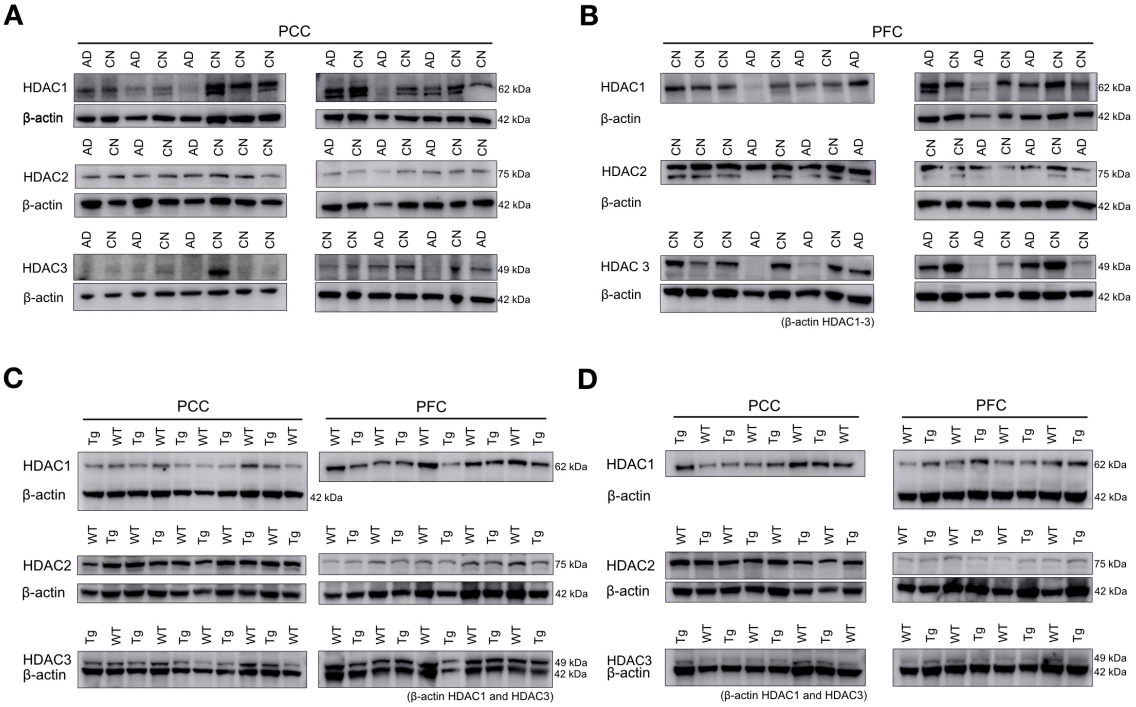

Western blots in the (**A**) posterior cingulate (PCC) and (**B**) prefrontal cortex (PFC) performed in CN (n = 9) and AD patients (n = 6), as well as wild-type (WT) and transgenic (Tg) (**C**) TgF344-AD (n = 5 each) and (**D**) McGill-R-Thy1-APP (n = 4 each) rats. In some of the human PFC samples (left), we used the same membrane to probe HDAC1-3 (first column). Similarly, in the PCC of McGill-R-Thy1-APP rats and the PFC of TgF344-AD rats, HDAC1 and HDAC3 were probed on the same membrane. In these cases, the same β-actin blot within the membrane was used as a loading control.

7.10 References

Akhtar MW, Raingo J, Nelson ED, Montgomery RL, Olson EN, Kavalali ET, et al. Histone deacetylases 1 and 2 form a developmental switch that controls excitatory synapse maturation and function. The Journal of neuroscience : the official journal of the Society for Neuroscience. 2009;29(25):8288-97.

Anderson KW, Chen J, Wang M, Mast N, Pikuleva IA, Turko IV. Quantification of histone deacetylase isoforms in human frontal cortex, human retina, and mouse brain. PloS one. 2015;10(5):e0126592.

Bie B, Wu J, Yang H, Xu JJ, Brown DL, Naguib M. Epigenetic suppression of neuroligin 1 underlies amyloid-induced memory deficiency. Nature neuroscience. 2014;17(2):223-31.

Braak H, Braak E. Neuropathological stageing of Alzheimer-related changes. Acta neuropathologica. 1991;82(4):239-59.

Cohen RM, Rezai-Zadeh K, Weitz TM, Rentsendorj A, Gate D, Spivak I, et al. A transgenic Alzheimer rat with plaques, tau pathology, behavioral impairment, oligomeric abeta, and frank neuronal loss. The Journal of neuroscience : the official journal of the Society for Neuroscience. 2013;33(15):6245-56.

Cselenyi Z, Jonhagen ME, Forsberg A, Halldin C, Julin P, Schou M, et al. Clinical validation of 18F-AZD4694, an amyloid-beta-specific PET radioligand. Journal of nuclear medicine : official publication, Society of Nuclear Medicine. 2012;53(3):415-24.

Cuadrado-Tejedor M, Garcia-Barroso C, Sanchez-Arias JA, Rabal O, Perez-Gonzalez M, Mederos S, et al. A First-in-Class Small-Molecule that Acts as a Dual Inhibitor of HDAC and PDE5 and that Rescues Hippocampal Synaptic Impairment in Alzheimer's Disease Mice. Neuropsychopharmacology : official publication of the American College of Neuropsychopharmacology. 2017;42(2):524-39.

Cummings J, Lee G, Ritter A, Zhong K. Alzheimer's disease drug development pipeline: 2018. Alzheimers Dement (N Y). 2018;4:195-214.

Do Carmo S, Cuello AC. Modeling Alzheimer's disease in transgenic rats. Mol Neurodegener. 2013;8:37.

Dulac C. Brain function and chromatin plasticity. Nature. 2010;465(7299):728-35.

Falkenberg KJ, Johnstone RW. Histone deacetylases and their inhibitors in cancer, neurological diseases and immune disorders. Nat Rev Drug Discov. 2014;13(9):673-91.

Fischer A, Sananbenesi F, Wang X, Dobbin M, Tsai LH. Recovery of learning and memory is associated with chromatin remodelling. Nature. 2007;447(7141):178-82.

Fleisher AS, Truran D, Mai JT, Langbaum JB, Aisen PS, Cummings JL, et al. Chronic divalproex sodium use and brain atrophy in Alzheimer disease. Neurology. 2011;77(13):1263-71.

Gonzalez-Zuniga M, Contreras PS, Estrada LD, Chamorro D, Villagra A, Zanlungo S, et al. c-Abl stabilizes HDAC2 levels by tyrosine phosphorylation repressing neuronal gene expression in Alzheimer's disease. Mol Cell. 2014;56(1):163-73.

Graff J, Rei D, Guan JS, Wang WY, Seo J, Hennig KM, et al. An epigenetic blockade of cognitive functions in the neurodegenerating brain. Nature. 2012;483(7388):222-6.

Graff J, Tsai LH. Histone acetylation: molecular mnemonics on the chromatin. Nat Rev Neurosci. 2013;14(2):97-111.

Grunstein M. Histone acetylation in chromatin structure and transcription. Nature. 1997;389(6649):349-52.

Guan JS, Haggarty SJ, Giacometti E, Dannenberg JH, Joseph N, Gao J, et al. HDAC2 negatively regulates memory formation and synaptic plasticity. Nature. 2009;459(7243):55-60.

Jack CR, Jr., Knopman DS, Jagust WJ, Petersen RC, Weiner MW, Aisen PS, et al. Tracking pathophysiological processes in Alzheimer's disease: an updated hypothetical model of dynamic biomarkers. The Lancet Neurology. 2013;12(2):207-16.

Jakovcevski M, Akbarian S. Epigenetic mechanisms in neurological disease. Nature medicine. 2012;18(8):1194-204.

Jiang Y, Hsieh J. HDAC3 controls gap 2/mitosis progression in adult neural stem/progenitor cells by regulating CDK1 levels. Proceedings of the National Academy of Sciences of the United States of America. 2014;111(37):13541-6.

Kandel DB, Kandel ER. A molecular basis for nicotine as a gateway drug. The New England journal of medicine. 2014;371(21):2038-9.

Kilgore M, Miller CA, Fass DM, Hennig KM, Haggarty SJ, Sweatt JD, et al. Inhibitors of class 1 histone deacetylases reverse contextual memory deficits in a mouse model of Alzheimer's disease. Neuropsychopharmacology : official publication of the American College of Neuropsychopharmacology. 2010;35(4):870-80.

Kim D, Frank CL, Dobbin MM, Tsunemoto RK, Tu W, Peng PL, et al. Deregulation of HDAC1 by p25/Cdk5 in neurotoxicity. Neuron. 2008;60(5):803-17.

Lattal KM, Wood MA. Epigenetics and persistent memory: implications for reconsolidation and silent extinction beyond the zero. Nature neuroscience. 2013;16(2):124-9.

MacCallum RC, Austin JT. Applications of structural equation modeling in psychological research. Annu Rev Psychol. 2000;51:201-26.

Mahady L, Nadeem M, Malek-Ahmadi M, Chen K, Perez SE, Mufson EJ. Frontal Cortex Epigenetic Dysregulation During the Progression of Alzheimer's Disease. Journal of Alzheimer's disease : JAD. 2018;62(1):115-31.

Mathotaarachchi S, Wang S, Shin M, Pascoal TA, Benedet AL, Kang MS, et al. VoxelStats: A MATLAB Package for Multi-Modal Voxel-Wise Brain Image Analysis. Front Neuroinform. 2016;10:20.

Mirra SS, Heyman A, McKeel D, Sumi SM, Crain BJ, Brownlee LM, et al. The Consortium to Establish a Registry for Alzheimer's Disease (CERAD). Part II. Standardization of the neuropathologic assessment of Alzheimer's disease. Neurology. 1991;41(4):479-86.

Montgomery RL, Hsieh J, Barbosa AC, Richardson JA, Olson EN. Histone deacetylases 1 and 2 control the progression of neural precursors to neurons during brain development. Proceedings of the National Academy of Sciences of the United States of America. 2009;106(19):7876-81.

Nativio R, Donahue G, Berson A, Lan Y, Amlie-Wolf A, Tuzer F, et al. Dysregulation of the epigenetic landscape of normal aging in Alzheimer's disease. Nature neuroscience. 2018.

Pascoal TA, Mathotaarachchi S, Mohades S, Benedet AL, Chung CO, Shin M, et al. Amyloid-beta and hyperphosphorylated tau synergy drives metabolic decline in preclinical Alzheimer's disease. Mol Psychiatry. 2017;22(2):306-11.

Pascoal TA, Shin M, Kang MS, Chamoun M, Chartrand D, Mathotaarachchi S, et al. In vivo quantification of neurofibrillary tangles with [(18)F]MK-6240. Alzheimer's research & therapy. 2018;10(1):74.

Peleg S, Sananbenesi F, Zovoilis A, Burkhardt S, Bahari-Javan S, Agis-Balboa RC, et al. Altered histone acetylation is associated with age-dependent memory impairment in mice. Science. 2010;328(5979):753-6.

Sananbenesi F, Fischer A. The epigenetic bottleneck of neurodegenerative and psychiatric diseases. Biol Chem. 2009;390(11):1145-53.

Saykin AJ, Shen L, Yao X, Kim S, Nho K, Risacher SL, et al. Genetic studies of quantitative MCI and AD phenotypes in ADNI: Progress, opportunities, and plans. Alzheimer's & dementia : the journal of the Alzheimer's Association. 2015;11(7):792-814.

Sweatt JD. Behavioural neuroscience: Down memory lane. Nature. 2007;447(7141):151-2.

Thomas BA, Erlandsson K, Modat M, Thurfjell L, Vandenberghe R, Ourselin S, et al. The importance of appropriate partial volume correction for PET quantification in Alzheimer's disease. European journal of nuclear medicine and molecular imaging. 2011;38(6):1104-19.

Wang WY, Pan L, Su SC, Quinn EJ, Sasaki M, Jimenez JC, et al. Interaction of FUS and HDAC1 regulates DNA damage response and repair in neurons. Nature neuroscience. 2013;16(10):1383-91.

Wey HY, Gilbert TM, Zurcher NR, She A, Bhanot A, Taillon BD, et al. Insights into neuroepigenetics through human histone deacetylase PET imaging. Sci Transl Med. 2016;8(351):351ra106.

Xu K, Dai XL, Huang HC, Jiang ZF. Targeting HDACs: a promising therapy for Alzheimer's disease. Oxid Med Cell Longev. 2011;2011:143269.

Yamakawa H, Cheng J, Penney J, Gao F, Rueda R, Wang J, et al. The Transcription Factor Sp3 Cooperates with HDAC2 to Regulate Synaptic Function and Plasticity in Neurons. Cell Rep. 2017;20(6):1319-34.

Yang SS, Zhang R, Wang G, Zhang YF. The development prospection of HDAC inhibitors as a potential therapeutic direction in Alzheimer's disease. Transl Neurodegener. 2017;6:19.

Zhu X, Wang S, Yu L, Jin J, Ye X, Liu Y, et al. HDAC3 negatively regulates spatial memory in a mouse model of Alzheimer's disease. Aging Cell. 2017;16(5):1073-82.

Chapter 8: Discussion

This thesis is composed of six studies and two main parts. The studies in Chapters 2 to 5 present evidence supporting a synergistic model of biomarkers progression in AD. This synergistic model challenges the dominant sequential model of biomarkers progression. On the other hand, the studies in Chapters 6 and 7 were part of the efforts to uncover epigenetic mechanisms behind these interactions.

8.1 Summary of results

8.1.1 Synergistic model of Alzheimer's disease progression

In **Chapter 2**, we showed that a synergistic interaction between amyloid-β and tau better describes metabolic decline in preclinical AD compared to sequential or additive effects between these pathologies. In **Chapter 3**, we determined the biomarker thresholds responsible for triggering the above-mentioned synergy. Complementing these findings, we demonstrate in **Chapter 4** that the synergy between amyloid-β and tau is also a determinant of the clinical progression to dementia. In **Chapter 5**, we showed that the synergy between amyloid-β and hypometabolism is associated with cognitive deterioration and dementia.

8.1.2 Epigenetics link Alzheimer's disease pathophysiology and cognitive symptoms

In **Chapter 6**, we described that the new PET tracer [^{18}F]MK-6240 has high sensitivity and specificity for neurofibrillary tangles. In **Chapter 7**, we demonstrated that HDACs I reduction links brain concentrations of amyloid-β and tau with degeneration and cognitive impairment in AD.

8.2 Discussion and future directions

8.2.1 Synergistic model of Alzheimer's disease progression

The synergistic model supported here integrates models predicting that amyloid-β, tau, and neurodegeneration sequentially or in parallel drive AD (Jack *et al.*, 2013, Jack *et al.*, 2018), suggesting that these pathologies may arise at least partially independently and when they topographically converge at certain levels, they synergistically determine dementia (Duyckaerts, 2011, Sperling *et al.*, 2014).

Although amyloid-β has a clear link with AD, the lack of strong association between amyloid-β and AD-related neurological insults or cognitive decline has been interpreted as evidence against its deleterious effect, as initially proposed by the amyloid-β hypothesis (Hardy and Selkoe, 2002, Jagust, 2016). Thus, one of the most important unanswered questions in AD is how amyloid-β is related to tau and neuronal injury and how these processes relate to each other to determine forthcoming dementia (Jagust, 2016). The synergistic construct supported in this thesis suggests a direct effect of amyloid-β on AD-related processes through its synergy with tau and neurodegeneration (Figure 8-1). Therefore, this construct strongly links amyloid-β with AD progression, as initially proposed by the amyloid-β hypothesis, shedding light on one of the most important unanswered questions in the field of AD.

Figure 8-1. Graphical representation of the synergistic interactions in Alzheimer's disease.

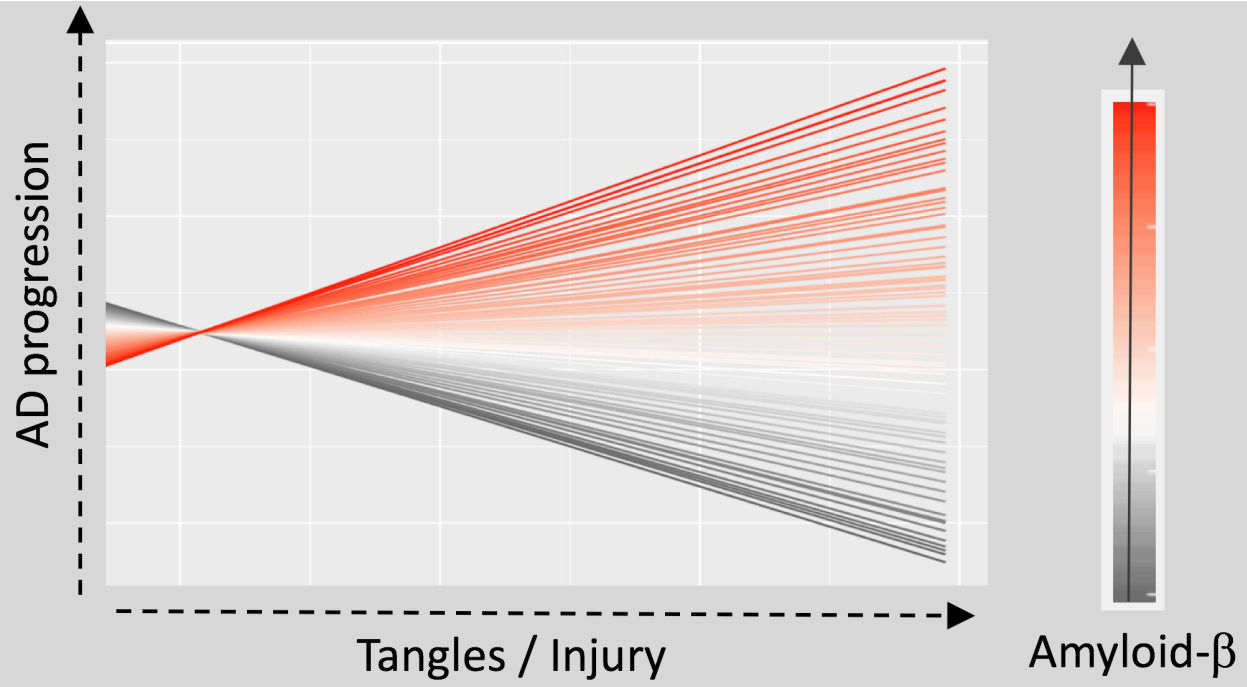

The plot shows the representation of the synergistic interactions found in this thesis, where each parallel line represents a single subject. Progressively higher levels of amyloid-β pathology in association with progressively higher levels of neurofibrillary tangles or neuronal injury lead to progressively higher rates of disease progression in a dose-dependent manner. Notably, either amyloid-β or tangles / injury as a single abnormality is insufficient to determine disease progression.

Indeed, subsequent human results support this model, showing evidence of interactions between amyloid-β, tau, and neurodegeneration leading to brain structural and functional abnormalities in preclinical AD (Kulic and Unschuld, 2016, Illan-Gala *et al.*, 2017, Bilgel *et al.*, 2018, Cummings, 2018, d'Oleire Uquillas *et al.*, 2018, Tardif *et al.*, 2018). Also, previous studies have proposed that mediobasal temporal atrophy occurs as a function of an interaction between CSF amyloid-β and p-tau (Desikan *et al.*, 2011, Fortea *et al.*, 2014) and that the association between CSF amyloid-β and cognition depends on an abnormal p-tau status (Desikan *et al.*, 2012). Additionally, studies have shown that either amyloid-β or neurodegeneration may be the first

biomarker abnormality in preclinical AD (Jack *et al.*, 2013) and that cognitive decline in these individuals is associated with an interaction between amyloid-β and neurodegeneration (Mormino *et al.*, 2014). A combined effect of amyloid-β and tau, leading to downstream neurotoxicity, has also been reported in experimental models of AD (Rhein *et al.*, 2009, Ittner *et al.*, 2010, Ittner and Gotz, 2011, Miller *et al.*, 2011, Shipton *et al.*, 2011, Guo *et al.*, 2013, Chabrier *et al.*, 2014, Khan *et al.*, 2014). These studies showed that tau pathology potentiates the deleterious effects of amyloid-β (Quintanilla *et al.*, 2014), and that reduction in tau levels alleviates amyloid-induced toxicity (Roberson *et al.*, 2007, Vossel *et al.*, 2010, Vossel *et al.*, 2015). Likewise, molecular interactions between amyloid-β and tau have shown to enhance synaptic dysfunction and damage in AD (Manczak and Reddy, 2013). Interestingly, interactions have already been described in Lewy body disease and frontotemporal lobar degeneration (Clinton *et al.*, 2010, Freibaum *et al.*, 2010, Wang *et al.*, 2014).

The presence of a synergy between amyloid-β and tau on AD progression has direct clinical implications in predicting possible therapeutic outcomes of anti-amyloid and anti-tau therapies (Sevigny *et al.*, 2016, Congdon and Sigurdsson, 2018). For instance, based on the synergistic model, one can expect that therapies targeting either amyloid-β or tau may similarly attenuate AD progression. In addition, the existence of such synergy suggests that better results can be achieved using a combined therapeutic approach targeting both proteinopathies simultaneously. Thus, the synergistic model may serve as the rationale for future combined therapeutic strategies in AD, similar to what already occurs in other diseases such as tuberculosis and human immunodeficiency virus infection (Tomaszewski *et al.*, 2016). The presence of a synergy between amyloid-β and tau has immediate implications also for the enrichment of clinical trial

populations. For instance, if amyloid-β and tau merely add their effects on cognitive decline, patients presenting both proteinopathies would lead to a reduced therapeutic effect of interventions targeting a single proteinopathy (amyloid-β or tau), given the remaining effect of the untreated proteinopathy on disease progression. On the other hand, if amyloid-β and tau determine dementia synergistically, clinical trial populations composed of individuals presenting both proteinopathies would increase the rates of disease progression without loss of therapeutic effect. Therefore, the synergistic model predicts that disease-modifying clinical trials should enrich their populations with carriers of both pathologies rather than focusing only on amyloid-β status (Sevigny *et al.*, 2016) in order to increase the rates of progression of participants and studies' statistical power.

In addition, the presence of a synergistic interaction between pathologies has a direct implication on the biomarker thresholds used to select individuals with the highest probability of disease progression. For instance, we proposed in this thesis - for the first time - the concept of amyloid-β and tau thresholds of imminent neurodegeneration. We have shown that these thresholds are higher than the standard thresholds used to determine biomarkers abnormality and that they provide a valuable asset for the enrichment of clinical trials. Specifically, we showed that a clinical trial using amyloid-β and tau thresholds associated with the triggering of their synergy would require as little as 174 CN individuals for testing a hypothetical 25% drug effect on temporal metabolic decline, in contrast to 832 individuals for a trial using standard thresholds. This is particularly important because although preclinical AD has become the focus of therapeutic clinical trials given the possibility of achieving better results before the onset of cognitive symptoms (Dubois *et al.*, 2016), studies in this population using current frameworks

need prohibitively large sample sizes (Gauthier *et al.*, 2016). For example, a recent study has proposed that preclinical AD individuals defined using standard amyloid-β and tau thresholds would require more than 2,000 individuals to test a hypothetical 25% drug effect on changes in cognition or brain atrophy (Holland *et al.*, 2012). We have also shown in this thesis that the progression from MCI to dementia is associated with a synergistic effect between amyloid-β and tau in a quantitative dose-response manner. Thus, based on this synergy, it is expected that, similarly to what we found in CN, the use of progressively more conservative thresholds leads to progressively higher rates of progression from MCI to dementia (Figure 8-2). Together, these results show the implications of the synergy between pathologies in the selection of biomarker thresholds for clinical trials using preclinical AD and MCIs.

Figure 8-2. Amyloid-β positive plus tau positive groups segregated using progressively higher thresholds show progressively higher rate of progression to Alzheimer's dementia.

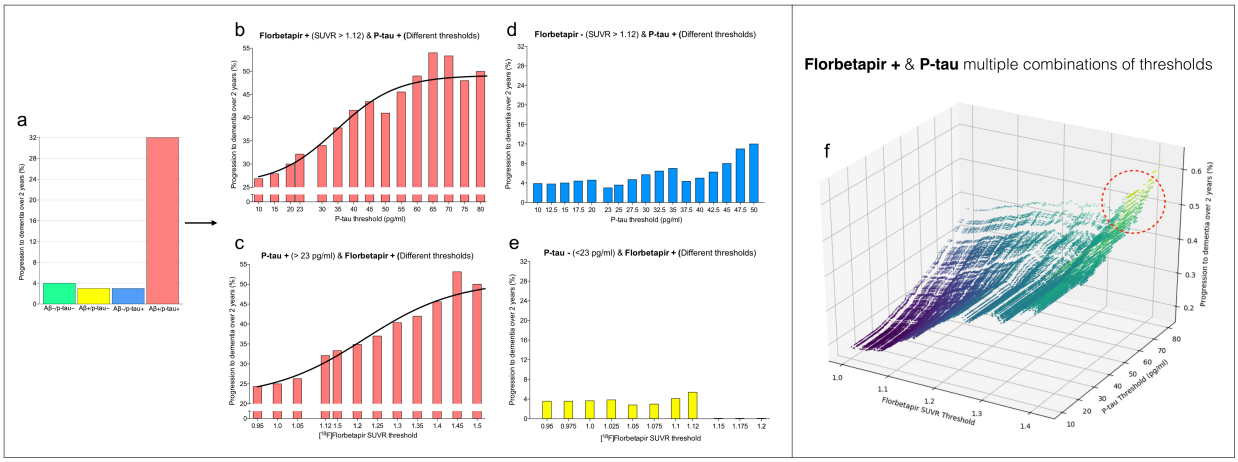

Figure (a) shows the Rate of progression to dementia over 2 years in 314 individuals, 47 biomarker negative (amyloid-β (Aβ)−/p-tau−), 37 only [^{18}F]florbetapir positive (Aβ+/p-tau−), 62 only p-tau positive (Aβ−/p-tau+), and 168 [^{18}F]florbetapir plus p-tau positive (Aβ+/p-tau+). Figures (b), (c), (d), and (e) show the rate of progression to dementia as a function of different threshold values for [^{18}F]florbetapir or CSF p-tau. Figure (f) shows a plot with 75,044 possible combinations of thresholds for [^{18}F]florbetapir and p-tau as a function of progression to dementia over 2 years (Adapted from the results of the study detailed in Chapter 4 of this thesis).

We have also shown that the interactions between amyloid-β and neurodegeneration are associated with dementia. Specifically, we have demonstrated evidence suggesting that early on in the disease process, amyloid-β leads to the vulnerability in distant brain regions that are functionally connected but not in the same region, and subsequently, an interaction between this vulnerability and overlapping amyloid-β is associated with cognitive decline. This dual effect of amyloid-β, leading first to tissue vulnerability in distant brain regions and after to cognitive decline, has important therapeutic implications supporting the use of anti-amyloid therapies early on in the disease process, even with evidence showing no regional association between amyloid-β and brain insult (Rabinovici *et al.*, 2010, Altmann *et al.*, 2015). Although our results indicate that this vulnerability is caused by remote effects of amyloid-β, other elements likely potentiate this vulnerability, such as other brain proteinopathies, age- and genetic-related factors (Mattson and Magnus, 2006, Kreisl *et al.*, 2013, Lesne *et al.*, 2013, Savas *et al.*, 2015) (Figure 8-3).

Figure 8-3. The topographic overlap of amyloid-β and metabolic vulnerability is associated with dementia symptoms.

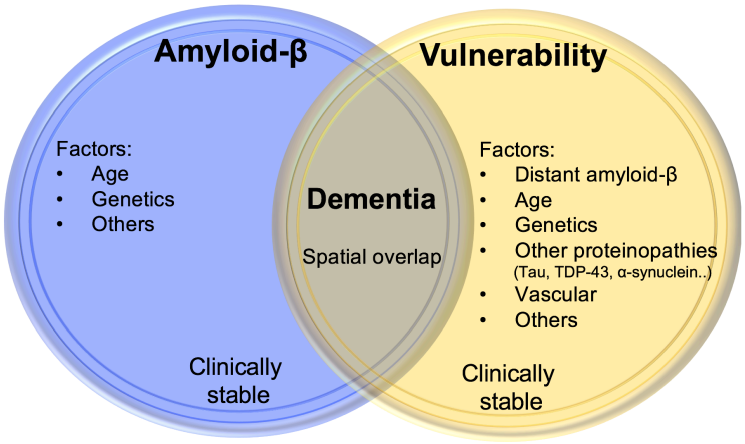

The regional interaction between amyloid-β aggregation and neuronal vulnerability is associated with dementia. The illustration shows the factors that contribute to the increase of amyloid-β aggregation and vulnerability.

It is important to mention that the results presented in this thesis supporting a synergy between pathologies leading to AD have important limitations. First, diseases biomarkers are proxies rather than direct measures of brain pathology; therefore, biomarker measurements are highly subject to analytical and methodological idiosyncrasies. The results were generated with ADNI subjects; a multicenter study of self-selected individuals who were willing to participate in a dementia study. The multicentric character of ADNI imposes important methodological limitations on the analysis of biomarkers, since different enrollment sites use different equipment and methodology, whereas self-selection may lead to samples that do not represent a general population. Also, we used CSF p-tau as a proxy of the brain's neurofibrillary tangles. Thus, the lack of tau PET is a limitation of the aforementioned results. Notably, evidence supporting amyloid-β leading to tau pathology and the presence of cognitive impairment in non-AD tauopathies (independent of amyloid-β) seemingly challenges a synergistic model for AD progression. However, deleterious interactions between other peptide aggregates have already been described in non-AD proteinopathies (Clinton *et al.*, 2010, Wang *et al.*, 2014). Also, it is important to note that the synergy between amyloid-β and tau leading to downstream disease progression does not exclude the possibility that these proteinopathies may arise sequentially (e.g., amyloid-β triggering the spreading of tau over the neocortex early on in the disease progression (Sperling *et al.*, 2014)).

Future human studies should use combined long-term sequential measurements of AD-related biomarkers at multiple time points to better assess their temporal relationships and to better differentiate between sequential and synergistic effects. Also, future work could test the presence of a synergy between pathologies using an experimental longitudinal approach with transgenic

animal models. In a controlled environment, these studies could test whether an animal model expressing amyloid-β and tau pathologies shows greater cognitive deterioration than the sum of the deteriorations of models expressing single amyloid-β or tau pathology.

Overall, these results have increased our understanding of the complex pathophysiological interactions involved in the progression of AD, which we believe to be an essential step in the development of more effective therapeutic strategies for AD.

8.2.2 Epigenetics link Alzheimer's disease pathophysiology and cognitive symptoms

The evidence that other pathophysiological processes (Hostetler *et al.*, 2016, Koga *et al.*, 2017, Ng *et al.*, 2017), rather than neurofibrillary tangles, strongly influence the brain signal of the first-generation tau tracers has motivated us to carry out the methodological validation of a new second-generation tau tracer before starting the last study of this thesis. In this validation, we showed that [^{18}F]MK-6240 has favorable pharmacokinetics, distinguishes cognitively impaired from unimpaired individuals, and that simplified methods such as SUVR provide estimates similar to those obtained with golden standard methods using plasma input function. Most importantly, [^{18}F]MK-6240 showed a deposition pattern similar to that reported by histopathological studies of neurofibrillary tangles, along with negligible brain off-target binding. For instance, [^{18}F]MK-6240 showed low binding in the striatum, which despite having been shown to have low levels of tangles in postmortem studies, is one of the most important binding sites of the first-generation tau tracers (Saint-Aubert *et al.*, 2017). In this study, we determined that [^{18}F]MK-6240 shows apparently high selectivity for neurofibrillary tangles and

is a viable biomarker to be practiced in large cohorts using simplified quantification approaches without the need for arterial lines and long scan durations.

The existing framework proposing epigenetic mechanisms in the diathesis of AD states that HDACs I upregulation drives cognitive decline. This framework is unanimously supported by several preclinical studies (Fischer *et al.*, 2007, Sweatt, 2007, Kilgore *et al.*, 2010, Xu *et al.*, 2011, Graff *et al.*, 2012, Konsoula and Barile, 2012, Zhang and Schluesener, 2013, Bie *et al.*, 2014, Falkenberg and Johnstone, 2014, Gonzalez-Zuniga *et al.*, 2014, Cuadrado-Tejedor *et al.*, 2017, Yamakawa *et al.*, 2017, Yang *et al.*, 2017, Zhu *et al.*, 2017, Cao *et al.*, 2018) and provides the rationale for ongoing clinical trials using HDACs I inhibitors as AD therapeutics (Cummings *et al.*, 2018). However, one of the limitations of this construct comes from the fact that it is derived exclusively from studies using animal models that develop incomplete disease phenotypes (e.g., models that express human amyloid-β but not downstream tau pathology) or human postmortem studies using the prefrontal and mediobasal temporal cortices (Graff *et al.*, 2012, Mahady *et al.*, 2018). Notably, these regions are not concomitantly affected in early disease stages by high pathological levels of the two hallmark features of AD, amyloid-β and tau (Braak and Braak, 1991). In fact, little is known about HDACs I concentrations in the majority of brain regions vulnerable to AD such as the precuneus, posterior cingulate, and inferior parietal cortices. Thus, the link between AD pathophysiology and HDACs I could be better investigated using brain imaging techniques in living patients. Although, until recently, this remained technically challenging due to the absence of *in vivo* brain HDAC biomarkers, recent progress in radiochemistry enabled the production of a PET molecular imaging agent capable of quantifying HDACs I in living people. This PET agent ([^{11}C]Martinostat(Wey *et al.*, 2015, Wey *et al.*,

2016)) allows unprecedented investigation of the associations between brain concentrations of HDACs I, amyloid-β, and tau across the entire brain, in particularly in those areas with known vulnerability to AD pathophysiology.

Using [^{11}C]Martinostat, we found that a reduction in HDACs I level mediates the effects of amyloid-β and tau on neurodegeneration and cognitive impairment in patients across the AD spectrum (Figure 8-4). Post-mortem analysis anatomically guided by the *in vivo* imaging confirmed the reduction of class I HDAC isoforms 1, 2, and 3 in brain regions affected by both amyloid-β and tau in AD patient. Additional validation conducted in two transgenic rat models corroborated that class I HDACs reduction is a tissue signature associated with the concomitance of the two pathological hallmarks of AD, amyloid-β and tau pathologies. As a whole, these findings refute the notion that HDACs I upregulation is part of the pathogenesis of AD, which is unanimously described in previous studies performed on experimental models of the disease (Graff *et al.*, 2012, Bie *et al.*, 2014, Zhu *et al.*, 2017). Several reasons may explain the discrepancies between our results and the current literature. Firstly, previous studies measured class I HDACs from a small subset of brain regions affected by AD and in a small subset of brain regions affected by AD and have extrapolated their findings to represent the entire brain disease process (Graff *et al.*, 2012). Secondly, previous post-mortem validations did not measure HDACs I in regions highly affected by both hallmark pathological features of AD, amyloid-β and tau (Mahady *et al.*, 2018). Finally, previous studies used mouse models that either did not express human amyloid-β or when expressed, did not develop downstream tau pathology (Graff *et al.*, 2012, Bie *et al.*, 2014, Gonzalez-Zuniga *et al.*, 2014, Yamakawa *et al.*, 2017, Zhu *et al.*, 2017, Mahady *et al.*, 2018). Altogether, these findings have important implications for numerous

drug-developing programs by alerting clinical trialists to the dangers of repurposing therapies form the cancer research to complex brain disorders such as AD without robust validation in patients or models that well-represent the diseases process.

Figure 8-4. Regions with high levels of amyloid-β and neurofibrillary tangles show reduction in HDACs I level.

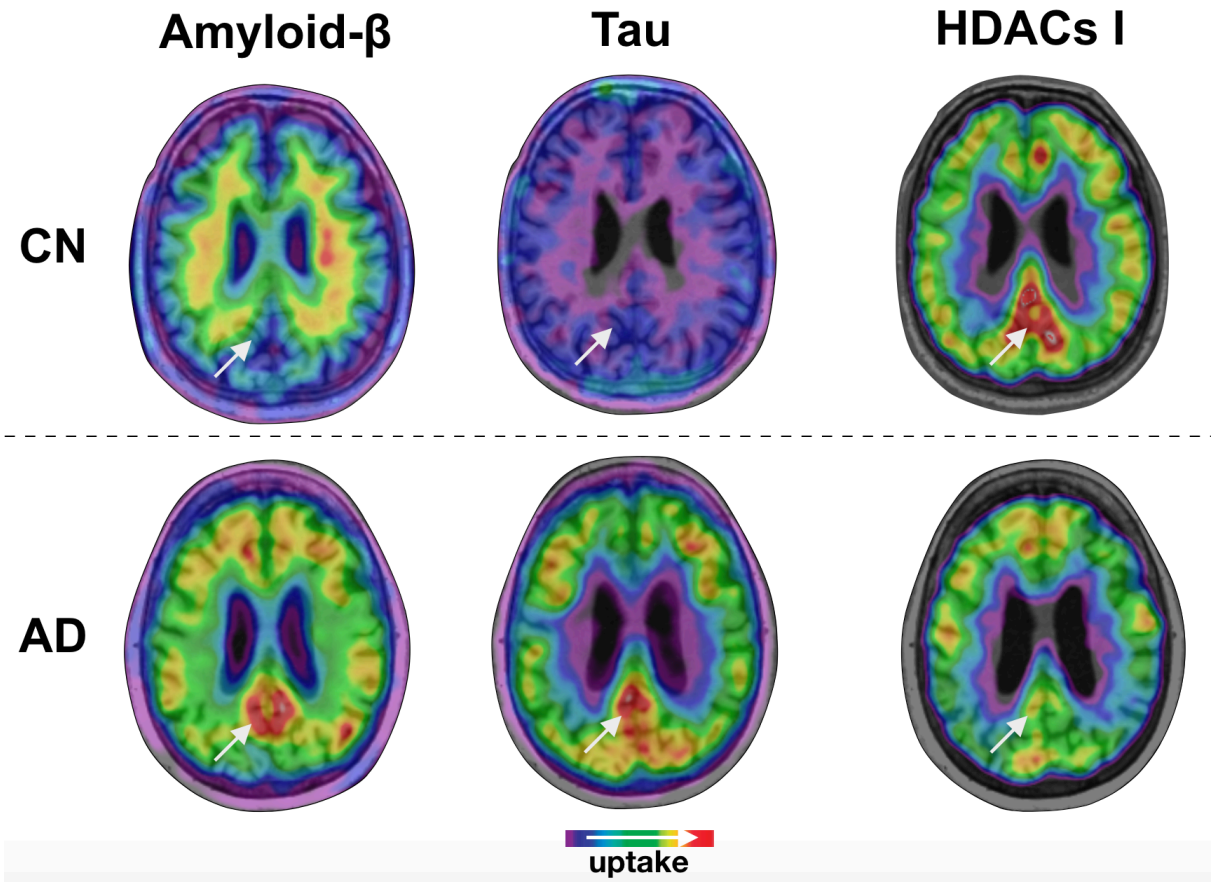

The figure shows two representative individuals from our cohort. The white arrow indicates that in AD, brain regions with high concentrations of both amyloid-β plaques ([^{18}F]NAV4694 PET) and neurofibrillary tangles ([^{18}F]MK6240 PET) show reduced levels of HDACs I ([^{11}C]Martinostat).

In addition, the results presented in this thesis, obtained from the analysis of the entire brain HDAC I concentrations in living people, support a novel conceptual framework in which increased amyloid-β and tau levels impose local suppression of HDACs I in the subjacent cortex,

which in turn leads to cognitive deterioration. Importantly, the fact that we found HDACs I downregulation exclusively in regions of the human brain showing high amyloid-β and tau levels and in a rat model of amyloid-β and tau pathologies, but not in a rat model of amyloid-β single pathology, supports this HDACs I reduction as an epigenetic signature associated with the coexistence of amyloid-β and tau (Pascoal *et al.*, 2017) (Figure 8-5).

Figure 8-5. The presence of amyloid-β plaques and neurofibrillary tangles dysregulates epigenetic landscape leading to neurodegeneration and dementia.

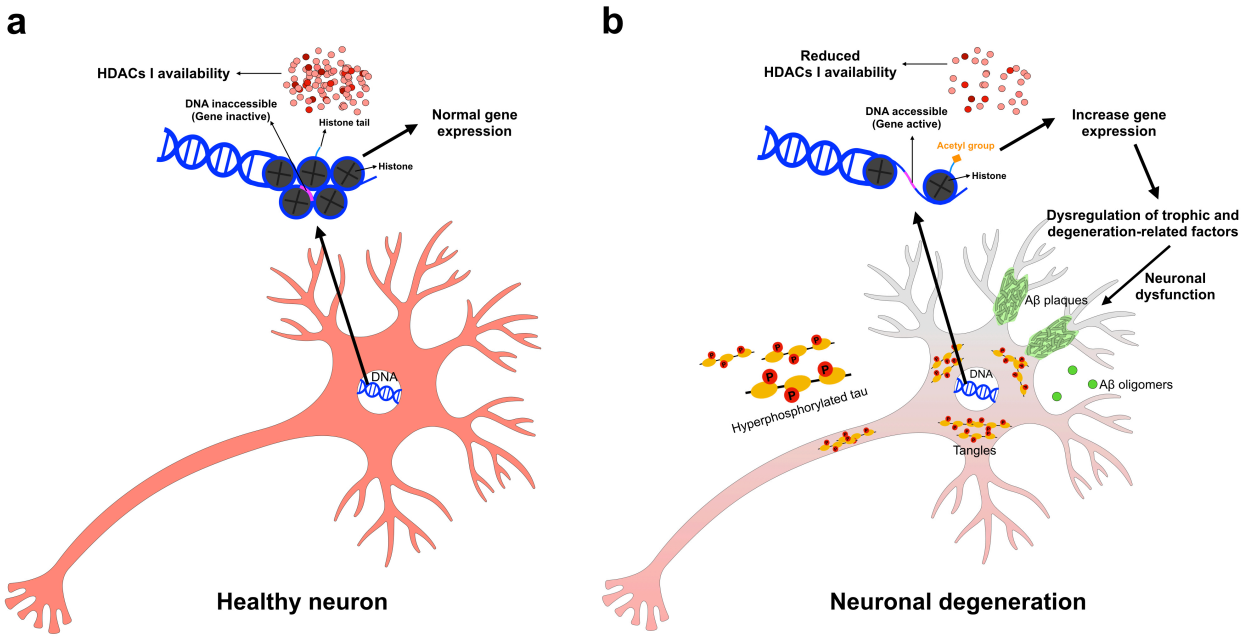

The co-occurrence of amyloid-β plaques and tau tangles in the brain tissue leads to a reduction in HDACs I, which increases histone tail acetylation, diminishes the electrostatic affinity between histones and DNA and configure an open-chromatin structure. This eventually leads to an abnormally increased gene expression and dysregulations of its downstream processes, including ribonucleic acid (RNA) signaling and protein' encoding.

From this new paradigm, one can predict that the rectification of abnormally reduced HDAC I tissue concentrations could mitigate AD progression. In addition, the fact that HDAC I is associated with neuronal plasticity (Kim *et al.*, 2008, Akhtar *et al.*, 2009, Montgomery *et al.*, 2009, Wang *et al.*, 2013) raises the hope that an HDAC I agonist can rectify the underlying

epigenetic dysregulations, restoring cognitive function in AD. Importantly, there are numerous available therapeutic agents capable of modulating the expression of HDACs I (e.g., Theophylline increases HDACs I level (Ito *et al.*, 2002)), which can potentially be tested in AD.

The conclusions derived from these results have limitations. For example, the lack of preclinical AD individual carriers of amyloid-β and tau pathologies imposes limitations to define the best window of opportunity for testing an HDACs I agonist in AD. Thus, in order to propose a disease-modifying intervention based on this novel target, it is crucial that future studies describe HDACs I reduction in preclinical AD. Also, the cross-section design of the study limits possible inferences about the causal relationships between HDACs I, amyloid-β, and tau. Therefore, future work showing the longitudinal dynamics of brain levels of HDACs I, amyloid-β, and tau would be highly desirable.

Together, our results refute the current framework derived from experimental disease models suggesting HDACs I upregulation as a key element involved in AD (Graff *et al.*, 2012) and, instead, suggest HDACs I downregulation as the mechanism linking the interactions between AD-related pathophysiological processes with dementia.

8.3 Conclusion

The studies detailed in this thesis shed light in the complex pathological interactions associated with AD. These studies support synergistic interactions between amyloid-β, tau, and neurodegeneration as driving forces behind disease progression. Importantly, rather than refuting amyloid-β as the key trigger of AD, the synergistic interaction model suggests the brain

convergence of pathological pathways as the crucial element leading to dementia. Therefore, this framework highlights that amyloid-β, rather than being a mere trigger, remains a crucial pathological process during the subsequent phases of AD progression. Specifically, we showed the synergy between amyloid-β and tau as a driving force leading to metabolic decline in brain regions related to AD in CN subjects (**Chapter 2**), and the existence of thresholds associated with this synergy that can provide important information to clinical trialists to select CN individuals who are more likely to progress pathophysiologically (**Chapter 3**). In later stages of the disease, we demonstrated that interactions between amyloid-β and tau (**Chapter 4**) as well as neurodegeneration (**Chapter 5**) play important and independent roles in the clinical progression from MCI to dementia. Finally, using amyloid-β PET, HDACs I PET, as well as the novel tau tracer [^{18}F]MK6240, which we showed to be highly specific for tangles (**Chapter 6**), we found evidence that epigenetic dysregulations imposed on brain tissue may be the key element linking the above-mentioned processes with dementia (**Chapter 7**). Characterizing the epigenetic mechanisms associated with the interaction between the multiple pathophysiological processes associated with AD has the potential to provide the key to fill the gaps in our understanding of the pathogenesis of AD and point to a cure.

Chapter 9: Bibliography

2018 Alzheimer's disease facts and figures. Alzheimer's & Dementia: The Journal of the Alzheimer's Association. 2018;14(3):367-429.

Aisen PS, Petersen RC, Donohue MC, Gamst A, Raman R, Thomas RG, et al. Clinical Core of the Alzheimer's Disease Neuroimaging Initiative: progress and plans. Alzheimer's & dementia : the journal of the Alzheimer's Association. 2010;6(3):239-46.

Akaike H. A new look at the statistical model identification. IEEE Transactions on Automatic Control. 1974;19(6):716-23.

Akhtar MW, Raingo J, Nelson ED, Montgomery RL, Olson EN, Kavalali ET, et al. Histone deacetylases 1 and 2 form a developmental switch that controls excitatory synapse maturation and function. The Journal of neuroscience : the official journal of the Society for Neuroscience. 2009;29(25):8288-97.

Akiyama H, Barger S, Barnum S, Bradt B, Bauer J, Cole GM, et al. Inflammation and Alzheimer's disease. Neurobiology of aging. 2000;21(3):383-421.

Akiyama H, Harrop R, McGeer P, Peppard R, McGeer E. Crossed cerebellar and uncrossed basal ganglia and thalarnic diaschisis in Alzheimer's disease. Neurology. 1989;39(4):541-.

Albert MS, DeKosky ST, Dickson D, Dubois B, Feldman HH, Fox NC, et al. The diagnosis of mild cognitive impairment due to Alzheimer's disease: recommendations from the National Institute on Aging-Alzheimer's Association workgroups on diagnostic guidelines for Alzheimer's disease. Alzheimer's & dementia : the journal of the Alzheimer's Association. 2011;7(3):270-9.

Altmann A, Ng B, Landau SM, Jagust WJ, Greicius MD, Alzheimer's Disease Neuroimaging I. Regional brain hypometabolism is unrelated to regional amyloid plaque burden. Brain : a journal of neurology. 2015;138(Pt 12):3734-46.

Alzheimer AJZfdgNuP. Über eigenartige Krankheitsfälle des späteren Alters. 1911;4(1):356.

Anderson KW, Chen J, Wang M, Mast N, Pikuleva IA, Turko IV. Quantification of histone deacetylase isoforms in human frontal cortex, human retina, and mouse brain. PloS one. 2015;10(5):e0126592.

Ashraf A, Fan Z, Brooks DJ, Edison P. Cortical hypermetabolism in MCI subjects: a compensatory mechanism? European journal of nuclear medicine and molecular imaging. 2015;42(3):447-58.

Association AP, Association AP. Diagnostic and statistical manual of mental disorders (revised 4th ed.). Washington, DC: Author. 2000.

Bacskai BJ, Frosch MP, Freeman SH, Raymond SB, Augustinack JC, Johnson KA, et al. Molecular imaging with Pittsburgh Compound B confirmed at autopsy: a case report. Archives of neurology. 2007;64(3):431-4.

Bamberger ME, Harris ME, McDonald DR, Husemann J, Landreth GE. A cell surface receptor complex for fibrillar beta-amyloid mediates microglial activation. The Journal of neuroscience : the official journal of the Society for Neuroscience. 2003;23(7):2665-74.

Bartko JJ. The intraclass correlation coefficient as a measure of reliability. Psychol Rep. 1966;19(1):3-11.

Beach TG, Wilson JR, Sue LI, Newell A, Poston M, Cisneros R, et al. Circle of Willis atherosclerosis: association with Alzheimer's disease, neuritic plaques and neurofibrillary tangles. Acta neuropathologica. 2007;113(1):13-21.

Beckett LA, Donohue MC, Wang C, Aisen P, Harvey DJ, Saito N, et al. The Alzheimer's Disease Neuroimaging Initiative phase 2: Increasing the length, breadth, and depth of our understanding. Alzheimer's & dementia : the journal of the Alzheimer's Association. 2015;11(7):823-31.

Benjamini Y, Hochberg Y. Controlling the false discovery rate: a practical and powerful approach to multiple testing. Journal of the royal statistical society Series B (Methodological). 1995:289-300.

Bennett DA, Schneider JA, Arvanitakis Z, Kelly JF, Aggarwal NT, Shah RC, et al. Neuropathology of older persons without cognitive impairment from two community-based studies. Neurology. 2006;66(12):1837-44.

Bergland AK, Dalen I, Larsen AI, Aarsland D, Soennesyn H. Effect of Vascular Risk Factors on the Progression of Mild Alzheimer's Disease and Lewy Body Dementia. Journal of Alzheimer's disease : JAD. 2017;56(2):575-84.

Betthauser TJ, Lao PJ, Murali D, Barnhart TE, Furumoto S, Okamura N, et al. In Vivo Comparison of Tau Radioligands (18)F-THK-5351 and (18)F-THK-5317. Journal of nuclear medicine : official publication, Society of Nuclear Medicine. 2017;58(6):996-1002.

Bie B, Wu J, Yang H, Xu JJ, Brown DL, Naguib M. Epigenetic suppression of neuroligin 1 underlies amyloid-induced memory deficiency. Nature neuroscience. 2014;17(2):223-31.

Bilgel M, An Y, Helphrey J, Elkins W, Gomez G, Wong DF, et al. Effects of amyloid pathology and neurodegeneration on cognitive change in cognitively normal adults. Brain : a journal of neurology. 2018.

Biomarkers Definitions Working G. Biomarkers and surrogate endpoints: preferred definitions and conceptual framework. Clin Pharmacol Ther. 2001;69(3):89-95.

Blennow K, Hampel H, Weiner M, Zetterberg H. Cerebrospinal fluid and plasma biomarkers in Alzheimer disease. Nature reviews Neurology. 2010;6(3):131-44.

Blennow K, Vanmechelen E. CSF markers for pathogenic processes in Alzheimer's disease: diagnostic implications and use in clinical neurochemistry. Brain Res Bull. 2003;61(3):235-42.

Blennow K, Zetterberg H. Understanding biomarkers of neurodegeneration: Ultrasensitive detection techniques pave the way for mechanistic understanding. Nature medicine. 2015;21(3):217-9.

Boche D, Nicoll JA. The role of the immune system in clearance of Abeta from the brain. Brain Pathol. 2008;18(2):267-78.

Boller F, Forbes MM. History of dementia and dementia in history: an overview. J Neurol Sci. 1998;158(2):125-33.

Bouras C, Hof PR, Morrison JH. Neurofibrillary tangle densities in the hippocampal formation in a non-demented population define subgroups of patients with differential early pathologic changes. Neuroscience letters. 1993;153(2):131-5.

Bousiges O, Vasconcelos AP, Neidl R, Cosquer B, Herbeaux K, Panteleeva I, et al. Spatial memory consolidation is associated with induction of several lysine-acetyltransferase (histone acetyltransferase) expression levels and H2B/H4 acetylation-dependent transcriptional events in the rat hippocampus. Neuropsychopharmacology : official publication of the American College of Neuropsychopharmacology. 2010;35(13):2521-37.

Braak H, Braak E. Neuropathological stageing of Alzheimer-related changes. Acta neuropathologica. 1991;82(4):239-59.

Braak H, Braak E. Staging of Alzheimer's disease-related neurofibrillary changes. Neurobiology of aging. 1995;16(3):271-8; discussion 8-84.

Braak H, Braak E. Staging of Alzheimer-related cortical destruction. Int Psychogeriatr. 1997;9 Suppl 1:257-61; discussion 69-72.

Braak HaB, E. Neuropathological stageing of Alzheimer-related changes. Acta Neuropathol. 1991;82:20.

Brandt R, Hundelt M, Shahani N. Tau alteration and neuronal degeneration in tauopathies: mechanisms and models. Biochimica et biophysica acta. 2005;1739(2-3):331-54.

Bredy TW, Barad M. The histone deacetylase inhibitor valproic acid enhances acquisition, extinction, and reconsolidation of conditioned fear. Learn Mem. 2008;15(1):39-45.

Bruck A, Virta JR, Koivunen J, Koikkalainen J, Scheinin NM, Helenius H, et al. [11C]PIB, [18F]FDG and MR imaging in patients with mild cognitive impairment. European journal of nuclear medicine and molecular imaging. 2013;40(10):1567-72.

Buckner RL, Andrews‐Hanna JR, Schacter DL. The brain's default network. Annals of the New York Academy of Sciences. 2008;1124(1):1-38.

Buckner RL, Snyder AZ, Shannon BJ, LaRossa G, Sachs R, Fotenos AF, et al. Molecular, structural, and functional characterization of Alzheimer's disease: evidence for a relationship between default activity, amyloid, and memory. The Journal of neuroscience : the official journal of the Society for Neuroscience. 2005;25(34):7709-17.

Buerger K, Ewers M, Andreasen N, Zinkowski R, Ishiguro K, Vanmechelen E, et al. Phosphorylated tau predicts rate of cognitive decline in MCI subjects: a comparative CSF study. Neurology. 2005;65(9):1502-3.

Buerger K, Ewers M, Pirttila T, Zinkowski R, Alafuzoff I, Teipel SJ, et al. CSF phosphorylated tau protein correlates with neocortical neurofibrillary pathology in Alzheimer's disease. Brain : a journal of neurology. 2006;129(Pt 11):3035-41.

Burns A, Byrne EJ, Maurer K. Alzheimer's disease. Lancet. 2002;360(9327):163-5.

Cao F, Zwinderman MRH, Dekker FJ. The Process and Strategy for Developing Selective Histone Deacetylase 3 Inhibitors. Molecules. 2018;23(3).

Caroli A, Prestia A, Galluzzi S, Ferrari C, van der Flier WM, Ossenkoppele R, et al. Mild cognitive impairment with suspected nonamyloid pathology (SNAP): Prediction of progression. Neurology. 2015;84(5):508-15.

Carson RE, Channing MA, Blasberg RG, Dunn BB, Cohen RM, Rice KC, et al. Comparison of bolus and infusion methods for receptor quantitation: application to [18F]cyclofoxy and positron emission tomography. Journal of cerebral blood flow and metabolism : official journal of the International Society of Cerebral Blood Flow and Metabolism. 1993;13(1):24-42.

Chabrier MA, Cheng D, Castello NA, Green KN, LaFerla FM. Synergistic effects of amyloid-beta and wild-type human tau on dendritic spine loss in a floxed double transgenic model of Alzheimer's disease. Neurobiology of disease. 2014;64:107-17.

Chetelat G, Villemagne VL, Pike KE, Ellis KA, Ames D, Masters CL, et al. Relationship between memory performance and beta-amyloid deposition at different stages of Alzheimer's disease. Neuro-degenerative diseases. 2012;10(1-4):141-4.

Chien DT, Bahri S, Szardenings AK, Walsh JC, Mu F, Su MY, et al. Early clinical PET imaging results with the novel PHF-tau radioligand [F-18]-T807. Journal of Alzheimer's disease : JAD. 2013;34(2):457-68.

Chow VW, Mattson MP, Wong PC, Gleichmann M. An overview of APP processing enzymes and products. Neuromolecular Med. 2010;12(1):1-12.

Cipriani G, Dolciotti C, Picchi L, Bonuccelli U. Alzheimer and his disease: a brief history. Neurol Sci. 2011;32(2):275-9.

Clinton LK, Blurton-Jones M, Myczek K, Trojanowski JQ, LaFerla FM. Synergistic Interactions between Abeta, tau, and alpha-synuclein: acceleration of neuropathology and cognitive decline. The Journal of neuroscience : the official journal of the Society for Neuroscience. 2010;30(21):7281-9.

Cohen RM, Rezai-Zadeh K, Weitz TM, Rentsendorj A, Gate D, Spivak I, et al. A transgenic Alzheimer rat with plaques, tau pathology, behavioral impairment, oligomeric abeta, and frank

neuronal loss. The Journal of neuroscience : the official journal of the Society for Neuroscience. 2013;33(15):6245-56.

Congdon EE, Sigurdsson EM. Tau-targeting therapies for Alzheimer disease. Nature reviews Neurology. 2018;14(7):399-415.

Costes N, Dagher A, Larcher K, Evans AC, Collins DL, Reilhac A. Motion correction of multi-frame PET data in neuroreceptor mapping: simulation based validation. NeuroImage. 2009;47(4):1496-505.

Cselenyi Z, Jonhagen ME, Forsberg A, Halldin C, Julin P, Schou M, et al. Clinical validation of 18F-AZD4694, an amyloid-beta-specific PET radioligand. Journal of nuclear medicine : official publication, Society of Nuclear Medicine. 2012;53(3):415-24.

Cuadrado-Tejedor M, Garcia-Barroso C, Sanchez-Arias JA, Rabal O, Perez-Gonzalez M, Mederos S, et al. A First-in-Class Small-Molecule that Acts as a Dual Inhibitor of HDAC and PDE5 and that Rescues Hippocampal Synaptic Impairment in Alzheimer's Disease Mice. Neuropsychopharmacology : official publication of the American College of Neuropsychopharmacology. 2017;42(2):524-39.

Cummings J. The National Institute on Aging-Alzheimer's Association Framework on Alzheimer's disease: Application to clinical trials. Alzheimer's & dementia : the journal of the Alzheimer's Association. 2018.

Cummings J, Lee G, Ritter A, Zhong K. Alzheimer's disease drug development pipeline: 2018. Alzheimers Dement (N Y). 2018;4:195-214.

d'Oleire Uquillas F, Jacobs HIL, Hanseeuw B, Marshall GA, Properzi M, Schultz AP, et al. Interactive versus additive relationships between regional cortical thinning and amyloid burden

in predicting clinical decline in mild AD and MCI individuals. NeuroImage Clinical. 2018;17:388-96.

de Leon MJ, George AE, Tomanelli J, Christman D, Kluger A, Miller J, et al. Positron emission tomography studies of normal aging: a replication of PET III and 18-FDG using PET VI and 11-CDG. Neurobiology of aging. 1987;8(4):319-23.

De Strooper B, Karran E. The Cellular Phase of Alzheimer's Disease. Cell. 2016;164(4):603-15.

DeCarli C. Mild cognitive impairment: prevalence, prognosis, aetiology, and treatment. The Lancet Neurology. 2003;2(1):15-21.

Delacourte A, David JP, Sergeant N, Buee L, Wattez A, Vermersch P, et al. The biochemical pathway of neurofibrillary degeneration in aging and Alzheimer's disease. Neurology. 1999;52(6):1158-65.

Desikan RS, McEvoy LK, Thompson WK, Holland D, Brewer JB, Aisen PS, et al. Amyloid-beta--associated clinical decline occurs only in the presence of elevated P-tau. Archives of neurology. 2012;69(6):709-13.

Desikan RS, McEvoy LK, Thompson WK, Holland D, Roddey JC, Blennow K, et al. Amyloid-beta associated volume loss occurs only in the presence of phospho-tau. Annals of neurology. 2011;70(4):657-61.

DiPatre PL, Gelman BBJJoN, Neurology E. Microglial cell activation in aging and Alzheimer disease: partial linkage with neurofibrillary tangle burden in the hippocampus. 1997;56(2):143-9.

Do Carmo S, Cuello AC. Modeling Alzheimer's disease in transgenic rats. Mol Neurodegener. 2013;8:37.

Dowling NM, Johnson SC, Gleason CE, Jagust WJ, Alzheimer's Disease Neuroimaging I. The mediational effects of FDG hypometabolism on the association between cerebrospinal fluid biomarkers and neurocognitive function. NeuroImage. 2015;105:357-68.

Dubois B, Feldman HH, Jacova C, Dekosky ST, Barberger-Gateau P, Cummings J, et al. Research criteria for the diagnosis of Alzheimer's disease: revising the NINCDS-ADRDA criteria. The Lancet Neurology. 2007;6(8):734-46.

Dubois B, Feldman HH, Jacova C, Hampel H, Molinuevo JL, Blennow K, et al. Advancing research diagnostic criteria for Alzheimer's disease: the IWG-2 criteria. The Lancet Neurology. 2014;13(6):614-29.

Dubois B, Hampel H, Feldman HH, Scheltens P, Aisen P, Andrieu S, et al. Preclinical Alzheimer's disease: Definition, natural history, and diagnostic criteria. Alzheimer's & dementia : the journal of the Alzheimer's Association. 2016;12(3):292-323.

Dulac C. Brain function and chromatin plasticity. Nature. 2010;465(7299):728-35.

Duyckaerts C. Tau pathology in children and young adults: can you still be unconditionally baptist? Acta neuropathologica. 2011;121(2):145-7.

Edison P, Archer HA, Hinz R, Hammers A, Pavese N, Tai YF, et al. Amyloid, hypometabolism, and cognition in Alzheimer disease: an [11C]PIB and [18F]FDG PET study. Neurology. 2007;68(7):501-8.

Egger G, Liang G, Aparicio A, Jones PA. Epigenetics in human disease and prospects for epigenetic therapy. Nature. 2004;429(6990):457-63.

Eikelenboom P, van Exel E, Hoozemans JJ, Veerhuis R, Rozemuller AJ, van Gool WA. Neuroinflammation - an early event in both the history and pathogenesis of Alzheimer's disease. Neuro-degenerative diseases. 2010;7(1-3):38-41.

Elman JA, Oh H, Madison CM, Baker SL, Vogel JW, Marks SM, et al. Neural compensation in older people with brain amyloid-[beta] deposition. Nature neuroscience. 2014;17(10):1316-8.

Engler H, Forsberg A, Almkvist O, Blomquist G, Larsson E, Savitcheva I, et al. Two-year follow-up of amyloid deposition in patients with Alzheimer's disease. Brain : a journal of neurology. 2006;129(Pt 11):2856-66.

Eskildsen SF, Coupe P, Fonov V, Manjon JV, Leung KK, Guizard N, et al. BEaST: brain extraction based on nonlocal segmentation technique. NeuroImage. 2012;59(3):2362-73.

Fagan AM, Mintun MA, Mach RH, Lee SY, Dence CS, Shah AR, et al. Inverse relation between in vivo amyloid imaging load and cerebrospinal fluid Abeta42 in humans. Annals of neurology. 2006;59(3):512-9.

Fagan AM, Mintun MA, Shah AR, Aldea P, Roe CM, Mach RH, et al. Cerebrospinal fluid tau and ptau(181) increase with cortical amyloid deposition in cognitively normal individuals: implications for future clinical trials of Alzheimer's disease. EMBO molecular medicine. 2009;1(8-9):371-80.

Falkenberg KJ, Johnstone RW. Histone deacetylases and their inhibitors in cancer, neurological diseases and immune disorders. Nat Rev Drug Discov. 2014;13(9):673-91.

Farde L, Eriksson L, Blomquist G, Halldin C. Kinetic analysis of central [11C]raclopride binding to D2-dopamine receptors studied by PET--a comparison to the equilibrium analysis. Journal of cerebral blood flow and metabolism : official journal of the International Society of Cerebral Blood Flow and Metabolism. 1989;9(5):696-708.

Feinberg AP. Phenotypic plasticity and the epigenetics of human disease. Nature. 2007;447(7143):433-40.

Fischer A, Sananbenesi F, Wang X, Dobbin M, Tsai LH. Recovery of learning and memory is associated with chromatin remodelling. Nature. 2007;447(7141):178-82.

Fleisher AS, Truran D, Mai JT, Langbaum JB, Aisen PS, Cummings JL, et al. Chronic divalproex sodium use and brain atrophy in Alzheimer disease. Neurology. 2011;77(13):1263-71.

Forsberg A, Engler H, Almkvist O, Blomquist G, Hagman G, Wall A, et al. PET imaging of amyloid deposition in patients with mild cognitive impairment. Neurobiology of aging. 2008;29(10):1456-65.

Forster S, Grimmer T, Miederer I, Henriksen G, Yousefi BH, Graner P, et al. Regional expansion of hypometabolism in Alzheimer's disease follows amyloid deposition with temporal delay. Biol Psychiatry. 2012;71(9):792-7.

Fortea J, Vilaplana E, Alcolea D, Carmona-Iragui M, Sanchez-Saudinos MB, Sala I, et al. Cerebrospinal fluid beta-amyloid and phospho-tau biomarker interactions affecting brain structure in preclinical Alzheimer disease. Annals of neurology. 2014;76(2):223-30.

Fouquet M, Desgranges B, Landeau B, Duchesnay E, Mezenge F, de la Sayette V, et al. Longitudinal brain metabolic changes from amnestic mild cognitive impairment to Alzheimer's disease. Brain : a journal of neurology. 2009;132(Pt 8):2058-67.

Fox NC, Cousens S, Scahill R, Harvey RJ, Rossor MN. Using serial registered brain magnetic resonance imaging to measure disease progression in Alzheimer disease: power calculations and estimates of sample size to detect treatment effects. Archives of neurology. 2000;57(3):339-44.

Freibaum BD, Chitta RK, High AA, Taylor JP. Global analysis of TDP-43 interacting proteins reveals strong association with RNA splicing and translation machinery. Journal of proteome research. 2010;9(2):1104-20.

Furst AJ, Rabinovici GD, Rostomian AH, Steed T, Alkalay A, Racine C, et al. Cognition, glucose metabolism and amyloid burden in Alzheimer's disease. Neurobiology of aging. 2012;33(2):215-25.

Ganai SA, Ramadoss M, Mahadevan V. Histone Deacetylase (HDAC) Inhibitors - emerging roles in neuronal memory, learning, synaptic plasticity and neural regeneration. Curr Neuropharmacol. 2015.

Gauthier S, Albert M, Fox N, Goedert M, Kivipelto M, Mestre-Ferrandiz J, et al. Why has therapy development for dementia failed in the last two decades? Alzheimer's & dementia : the journal of the Alzheimer's Association. 2016;12(1):60-4.

Gauthier S, Reisberg B, Zaudig M, Petersen RC, Ritchie K, Broich K, et al. Mild cognitive impairment. Lancet. 2006;367(9518):1262-70.

Gauthier S, Zhang H, Ng KP, Pascoal TA, Rosa-Neto P. Impact of the biological definition of Alzheimer's disease using amyloid, tau and neurodegeneration (ATN): what about the role of vascular changes, inflammation, Lewy body pathology? Transl Neurodegener. 2018;7:12.

Gomez-Isla T, Price JL, McKeel DW, Jr., Morris JC, Growdon JH, Hyman BT. Profound loss of layer II entorhinal cortex neurons occurs in very mild Alzheimer's disease. The Journal of neuroscience : the official journal of the Society for Neuroscience. 1996;16(14):4491-500.

Gonzalez-Zuniga M, Contreras PS, Estrada LD, Chamorro D, Villagra A, Zanlungo S, et al. c-Abl stabilizes HDAC2 levels by tyrosine phosphorylation repressing neuronal gene expression in Alzheimer's disease. Mol Cell. 2014;56(1):163-73.

Gotz J, Ittner LM. Animal models of Alzheimer's disease and frontotemporal dementia. Nat Rev Neurosci. 2008;9(7):532-44.

Gotz J, Streffer JR, David D, Schild A, Hoerndli F, Pennanen L, et al. Transgenic animal models of Alzheimer's disease and related disorders: histopathology, behavior and therapy. Mol Psychiatry. 2004;9(7):664-83.

Graff J, Rei D, Guan JS, Wang WY, Seo J, Hennig KM, et al. An epigenetic blockade of cognitive functions in the neurodegenerating brain. Nature. 2012;483(7388):222-6.

Graff J, Tsai LH. Histone acetylation: molecular mnemonics on the chromatin. Nat Rev Neurosci. 2013;14(2):97-111.

Grill JD, Di L, Lu PH, Lee C, Ringman J, Apostolova LG, et al. Estimating sample sizes for predementia Alzheimer's trials based on the Alzheimer's Disease Neuroimaging Initiative. Neurobiology of aging. 2013;34(1):62-72.

Grundke-Iqbal I, Iqbal K, Tung YC, Quinlan M, Wisniewski HM, Binder LI. Abnormal phosphorylation of the microtubule-associated protein tau (tau) in Alzheimer cytoskeletal pathology. Proceedings of the National Academy of Sciences of the United States of America. 1986;83(13):4913-7.

Grunstein M. Histone acetylation in chromatin structure and transcription. Nature. 1997;389(6649):349-52.

Guan JS, Haggarty SJ, Giacometti E, Dannenberg JH, Joseph N, Gao J, et al. HDAC2 negatively regulates memory formation and synaptic plasticity. Nature. 2009;459(7243):55-60.

Gunn RN, Gunn SR, Cunningham VJ. Positron emission tomography compartmental models. Journal of cerebral blood flow and metabolism : official journal of the International Society of Cerebral Blood Flow and Metabolism. 2001;21(6):635-52.

Gunn RN, Lammertsma AA, Hume SP, Cunningham VJ. Parametric imaging of ligand-receptor binding in PET using a simplified reference region model. NeuroImage. 1997;6(4):279-87.

Guo Q, Li H, Cole AL, Hur JY, Li Y, Zheng H. Modeling Alzheimer's disease in mouse without mutant protein overexpression: cooperative and independent effects of Abeta and tau. PloS one. 2013;8(11):e80706.

Guy M. McKhanna DSK, Howard Chertkowd, Bradley T. Hyman, Clifford R. Jack, Jr., Claudia H. Kawash, William E. Klunk, Walter J. Koroshetz, Jennifer J. Manlym, Richard Mayeuxm, Richard C. Mohs, John C. Morris, Martin N. Rossor, Philip Scheltens, Maria C. Carillo, Bill Thies, Sandra Weintraub, Creighton H. Phelps. The diagnosis of dementia due to Alzheimer's disease- Recommendations from the National Institute on Aging and the Alzheimer's Association workgroup. Alzheimer & Dementia. 2011.

Haettig J, Stefanko DP, Multani ML, Figueroa DX, McQuown SC, Wood MA. HDAC inhibition modulates hippocampus-dependent long-term memory for object location in a CBP-dependent manner. Learn Mem. 2011;18(2):71-9.

Hampel H, Blennow K, Shaw LM, Hoessler YC, Zetterberg H, Trojanowski JQ. Total and phosphorylated tau protein as biological markers of Alzheimer's disease. Experimental gerontology. 2010;45(1):30-40.

Hansson O, Zetterberg H, Buchhave P, Londos E, Blennow K, Minthon L. Association between CSF biomarkers and incipient Alzheimer's disease in patients with mild cognitive impairment: a follow-up study. The Lancet Neurology. 2006;5(3):228-34.

Harada R, Okamura N, Furumoto S, Furukawa K, Ishiki A, Tomita N, et al. [(18)F]THK-5117 PET for assessing neurofibrillary pathology in Alzheimer's disease. European journal of nuclear medicine and molecular imaging. 2015;42(7):1052-61.

Hardy J, Allsop D. Amyloid deposition as the central event in the aetiology of Alzheimer's disease. Trends Pharmacol Sci. 1991;12(10):383-8.

Hardy J, Selkoe DJ. The amyloid hypothesis of Alzheimer's disease: progress and problems on the road to therapeutics. Science. 2002;297(5580):353-6.

Hardy JA, Higgins GA. Alzheimer's disease: the amyloid cascade hypothesis. Science. 1992;256(5054):184-5.

Hashimoto H, Kawamura K, Igarashi N, Takei M, Fujishiro T, Aihara Y, et al. Radiosynthesis, photoisomerization, biodistribution, and metabolite analysis of 11C-PBB3 as a clinically useful PET probe for imaging of tau pathology. Journal of nuclear medicine : official publication, Society of Nuclear Medicine. 2014;55(9):1532-8.

Hatashita S, Yamasaki H, Suzuki Y, Tanaka K, Wakebe D, Hayakawa H. [18F]Flutemetamol amyloid-beta PET imaging compared with [11C]PIB across the spectrum of Alzheimer's disease. European journal of nuclear medicine and molecular imaging. 2014;41(2):290-300.

Heneka MT, Carson MJ, El Khoury J, Landreth GE, Brosseron F, Feinstein DL, et al. Neuroinflammation in Alzheimer's disease. 2015;14(4):388-405.

Hof PR, Bierer LM, Perl DP, Delacourte A, Buee L, Bouras C, et al. Evidence for early vulnerability of the medial and inferior aspects of the temporal lobe in an 82-year-old patient with preclinical signs of dementia. Regional and laminar distribution of neurofibrillary tangles and senile plaques. Archives of neurology. 1992;49(9):946-53.

Holland D, McEvoy LK, Desikan RS, Dale AM, Alzheimer's Disease Neuroimaging I. Enrichment and stratification for predementia Alzheimer disease clinical trials. PloS one. 2012;7(10):e47739.

Hostetler ED, Walji AM, Zeng Z, Miller P, Bennacef I, Salinas C, et al. Preclinical Characterization of 18F-MK-6240, a Promising PET Tracer for In Vivo Quantification of

Human Neurofibrillary Tangles. Journal of nuclear medicine : official publication, Society of Nuclear Medicine. 2016;57(10):1599-606.

Hubbard BM, Anderson JM. Age-related variations in the neuron content of the cerebral cortex in senile dementia of Alzheimer type. Neuropathol Appl Neurobiol. 1985;11(5):369-82.

Hubbard BM, Fenton GW, Anderson JM. A quantitative histological study of early clinical and preclinical Alzheimer's disease. Neuropathol Appl Neurobiol. 1990;16(2):111-21.

Hudson HM, Larkin RS. Accelerated image reconstruction using ordered subsets of projection data. IEEE Trans Med Imaging. 1994;13(4):601-9.

Hyman BT, Phelps CH, Beach TG, Bigio EH, Cairns NJ, Carrillo MC, et al. National Institute on Aging-Alzheimer's Association guidelines for the neuropathologic assessment of Alzheimer's disease. Alzheimer's & dementia : the journal of the Alzheimer's Association. 2012;8(1):1-13.

Ikonomovic MD, Klunk WE, Abrahamson EE, Mathis CA, Price JC, Tsopelas ND, et al. Post-mortem correlates of in vivo PiB-PET amyloid imaging in a typical case of Alzheimer's disease. Brain. 2008;131(Pt 6):1630-45.

Illan-Gala I, Vilaplana E, Pegueroles J, Montal V, Alcolea D, Blesa R, et al. The pitfalls of biomarker-based classification schemes. Alzheimer's & dementia : the journal of the Alzheimer's Association. 2017.

Ishii K. PET approaches for diagnosis of dementia. AJNR Am J Neuroradiol. 2014;35(11):2030-8.

Ito K, Lim S, Caramori G, Cosio B, Chung KF, Adcock IM, et al. A molecular mechanism of action of theophylline: Induction of histone deacetylase activity to decrease inflammatory gene expression. Proceedings of the National Academy of Sciences of the United States of America. 2002;99(13):8921-6.

Ittner LM, Gotz J. Amyloid-beta and tau--a toxic pas de deux in Alzheimer's disease. Nat Rev Neurosci. 2011;12(2):65-72.

Ittner LM, Ke YD, Delerue F, Bi M, Gladbach A, van Eersel J, et al. Dendritic function of tau mediates amyloid-beta toxicity in Alzheimer's disease mouse models. Cell. 2010;142(3):387-97.

Iwatsubo T, Odaka A, Suzuki N, Mizusawa H, Nukina N, Ihara Y. Visualization of A beta 42(43) and A beta 40 in senile plaques with end-specific A beta monoclonals: evidence that an initially deposited species is A beta 42(43). Neuron. 1994;13(1):45-53.

Jack CR, Jr., Bennett DA, Blennow K, Carrillo MC, Dunn B, Haeberlein SB, et al. NIA-AA Research Framework: Toward a biological definition of Alzheimer's disease. Alzheimer's & dementia : the journal of the Alzheimer's Association. 2018;14(4):535-62.

Jack CR, Jr., Bennett DA, Blennow K, Carrillo MC, Feldman HH, Frisoni GB, et al. A/T/N: An unbiased descriptive classification scheme for Alzheimer disease biomarkers. Neurology. 2016;87(5):539-47.

Jack CR, Jr., Dickson DW, Parisi JE, Xu YC, Cha RH, O'Brien PC, et al. Antemortem MRI findings correlate with hippocampal neuropathology in typical aging and dementia. Neurology. 2002;58(5):750-7.

Jack CR, Jr., Knopman DS, Chetelat G, Dickson D, Fagan AM, Frisoni GB, et al. Suspected non-Alzheimer disease pathophysiology - concept and controversy. Nature reviews Neurology. 2016;12(2):117-24.

Jack CR, Jr., Knopman DS, Jagust WJ, Petersen RC, Weiner MW, Aisen PS, et al. Tracking pathophysiological processes in Alzheimer's disease: an updated hypothetical model of dynamic biomarkers. The Lancet Neurology. 2013;12(2):207-16.

Jack CR, Jr., Knopman DS, Weigand SD, Wiste HJ, Vemuri P, Lowe V, et al. An operational approach to National Institute on Aging-Alzheimer's Association criteria for preclinical Alzheimer disease. Annals of neurology. 2012;71(6):765-75.

Jack CR, Jr., Wiste HJ, Knopman DS, Vemuri P, Mielke MM, Weigand SD, et al. Rates of beta-amyloid accumulation are independent of hippocampal neurodegeneration. Neurology. 2014;82(18):1605-12.

Jack CR, Jr., Wiste HJ, Schwarz CG, Lowe VJ, Senjem ML, Vemuri P, et al. Longitudinal tau PET in ageing and Alzheimer's disease. Brain : a journal of neurology. 2018;141(5):1517-28.

Jack CR, Jr., Wiste HJ, Weigand SD, Knopman DS, Lowe V, Vemuri P, et al. Amyloid-first and neurodegeneration-first profiles characterize incident amyloid PET positivity. Neurology. 2013;81(20):1732-40.

Jack CR, Knopman DS, Jagust WJ, Shaw LM, Aisen PS, Weiner MW, et al. Hypothetical model of dynamic biomarkers of the Alzheimer's pathological cascade. Lancet neurology. 2009;9(1):119-28.

Jackson WS. Selective vulnerability to neurodegenerative disease: the curious case of Prion Protein. Disease Models and Mechanisms. 2014;7(1):21-9.

Jagust W. Is amyloid-beta harmful to the brain? Insights from human imaging studies. Brain : a journal of neurology. 2016;139(Pt 1):23-30.

Jagust W, Reed B, Mungas D, Ellis W, Decarli C. What does fluorodeoxyglucose PET imaging add to a clinical diagnosis of dementia? Neurology. 2007;69(9):871-7.

Jagust W, Reed B, Mungas D, Ellis W, Decarli C. What does fluorodeoxyglucose PET imaging add to a clinical diagnosis of dementia? Neurology. 2007;69(9):871-7.

Jagust WJ. Amyloid imaging: coming to a PET scanner near you. Annals of neurology. 2010;68(3):277-8.

Jagust WJ, Bandy D, Chen K, Foster NL, Landau SM, Mathis CA, et al. The Alzheimer's Disease Neuroimaging Initiative positron emission tomography core. Alzheimer's & dementia : the journal of the Alzheimer's Association. 2010;6(3):221-9.

Jagust WJ, Landau SM, Alzheimer's Disease Neuroimaging I. Apolipoprotein E, not fibrillar beta-amyloid, reduces cerebral glucose metabolism in normal aging. The Journal of neuroscience : the official journal of the Society for Neuroscience. 2012;32(50):18227-33.

Jakovcevski M, Akbarian S. Epigenetic mechanisms in neurological disease. Nature medicine. 2012;18(8):1194-204.

Jarrett JT, Berger EP, Lansbury PT, Jr. The carboxy terminus of the beta amyloid protein is critical for the seeding of amyloid formation: implications for the pathogenesis of Alzheimer's disease. Biochemistry. 1993;32(18):4693-7.

Jiang Y, Hsieh J. HDAC3 controls gap 2/mitosis progression in adult neural stem/progenitor cells by regulating CDK1 levels. Proceedings of the National Academy of Sciences of the United States of America. 2014;111(37):13541-6.

Jicha GA, Parisi JE, Dickson DW, Johnson K, Cha R, Ivnik RJ, et al. Neuropathologic outcome of mild cognitive impairment following progression to clinical dementia. Archives of neurology. 2006;63(5):674-81.

Johnson KA, Schultz A, Betensky RA, Becker JA, Sepulcre J, Rentz D, et al. Tau positron emission tomographic imaging in aging and early Alzheimer disease. Annals of neurology. 2016;79(1):110-9.

Joshi AD, Pontecorvo MJ, Clark CM, Carpenter AP, Jennings DL, Sadowsky CH, et al. Performance characteristics of amyloid PET with florbetapir F 18 in patients with alzheimer's disease and cognitively normal subjects. Journal of nuclear medicine : official publication, Society of Nuclear Medicine. 2012;53(3):378-84.

Kandel DB, Kandel ER. A molecular basis for nicotine as a gateway drug. The New England journal of medicine. 2014;371(21):2038-9.

Kang J, Lemaire HG, Unterbeck A, Salbaum JM, Masters CL, Grzeschik KH, et al. The precursor of Alzheimer's disease amyloid A4 protein resembles a cell-surface receptor. Nature. 1987;325(6106):733-6.

Kayed R, Head E, Thompson JL, McIntire TM, Milton SC, Cotman CW, et al. Common structure of soluble amyloid oligomers implies common mechanism of pathogenesis. Science. 2003;300(5618):486-9.

Kemppainen NM, Scheinin NM, Koivunen J, Johansson J, Toivonen JT, Nagren K, et al. Five-year follow-up of 11C-PIB uptake in Alzheimer's disease and MCI. European journal of nuclear medicine and molecular imaging. 2014;41(2):283-9.

Kester MI, van der Vlies AE, Blankenstein MA, Pijnenburg YA, van Elk EJ, Scheltens P, et al. CSF biomarkers predict rate of cognitive decline in Alzheimer disease. Neurology. 2009;73(17):1353-8.

Khan UA, Liu L, Provenzano FA, Berman DE, Profaci CP, Sloan R, et al. Molecular drivers and cortical spread of lateral entorhinal cortex dysfunction in preclinical Alzheimer's disease. Nature neuroscience. 2014;17(2):304-11.

Kievit RA, Davis SW, Mitchell DJ, Taylor JR, Duncan J, Cam CANRT, et al. Distinct aspects of frontal lobe structure mediate age-related differences in fluid intelligence and multitasking. Nat Commun. 2014;5:5658.

Kilgore M, Miller CA, Fass DM, Hennig KM, Haggarty SJ, Sweatt JD, et al. Inhibitors of class 1 histone deacetylases reverse contextual memory deficits in a mouse model of Alzheimer's disease. Neuropsychopharmacology : official publication of the American College of Neuropsychopharmacology. 2010;35(4):870-80.

Kim D, Frank CL, Dobbin MM, Tsunemoto RK, Tu W, Peng PL, et al. Deregulation of HDAC1 by p25/Cdk5 in neurotoxicity. Neuron. 2008;60(5):803-17.

Kim HJ, Choe Y, Park S, San Lee J, Jang YK, Jang H, et al. IN VIVO BRAAK STAGING OF AMNESTIC MCI USING 18F-THK5351 PET IMAGING. 2017;13(7):P786-P7.

Kim J, Basak JM, Holtzman DM. The role of apolipoprotein E in Alzheimer's disease. Neuron. 2009;63(3):287-303.

Kim MS, Akhtar MW, Adachi M, Mahgoub M, Bassel-Duby R, Kavalali ET, et al. An essential role for histone deacetylase 4 in synaptic plasticity and memory formation. The Journal of neuroscience : the official journal of the Society for Neuroscience. 2012;32(32):10879-86.

Klunk WE, Engler H, Nordberg A, Wang Y, Blomqvist G, Holt DP, et al. Imaging brain amyloid in Alzheimer's disease with Pittsburgh Compound-B. Annals of neurology. 2004;55(3):306-19.

Knopman DS, Jack CR, Jr., Lundt ES, Wiste HJ, Weigand SD, Vemuri P, et al. Role of beta-Amyloidosis and Neurodegeneration in Subsequent Imaging Changes in Mild Cognitive Impairment. JAMA neurology. 2015:1-9.

Knopman DS, Jack CR, Jr., Wiste HJ, Weigand SD, Vemuri P, Lowe V, et al. Short-term clinical outcomes for stages of NIA-AA preclinical Alzheimer disease. Neurology. 2012;78(20):1576-82.

Knopman DS, Jack CR, Jr., Wiste HJ, Weigand SD, Vemuri P, Lowe VJ, et al. Selective worsening of brain injury biomarker abnormalities in cognitively normal elderly persons with beta-amyloidosis. JAMA neurology. 2013;70(8):1030-8.

Knopman DS, Parisi JE, Salviati A, Floriach-Robert M, Boeve BF, Ivnik RJ, et al. Neuropathology of cognitively normal elderly. Journal of neuropathology and experimental neurology. 2003;62(11):1087-95.

Koga S, Ono M, Sahara N, Higuchi M, Dickson DW. Fluorescence and autoradiographic evaluation of tau PET ligand PBB3 to alpha-synuclein pathology. Mov Disord. 2017;32(6):884-92.

Kohnken R, Buerger K, Zinkowski R, Miller C, Kerkman D, DeBernardis J, et al. Detection of tau phosphorylated at threonine 231 in cerebrospinal fluid of Alzheimer's disease patients. Neuroscience letters. 2000;287(3):187-90.

Koivunen J, Scheinin N, Virta JR, Aalto S, Vahlberg T, Nagren K, et al. Amyloid PET imaging in patients with mild cognitive impairment: a 2-year follow-up study. Neurology. 2011;76(12):1085-90.

Konsoula Z, Barile FA. Epigenetic histone acetylation and deacetylation mechanisms in experimental models of neurodegenerative disorders. J Pharmacol Toxicol Methods. 2012;66(3):215-20.

Kreisl WC, Lyoo CH, McGwier M, Snow J, Jenko KJ, Kimura N, et al. In vivo radioligand binding to translocator protein correlates with severity of Alzheimer's disease. Brain : a journal of neurology. 2013;136(Pt 7):2228-38.

Kuhl DE, Metter EJ, Riege WH, Hawkins RA. The effect of normal aging on patterns of local cerebral glucose utilization. Annals of neurology. 1984;15 Suppl:S133-7.

Kulic L, Unschuld PG. Recent advances in cerebrospinal fluid biomarkers for the detection of preclinical Alzheimer's disease. Curr Opin Neurol. 2016;29(6):749-55.

Lammertsma AA, Hume SP. Simplified reference tissue model for PET receptor studies. NeuroImage. 1996;4(3 Pt 1):153-8.

Landau SM, Fero A, Baker SL, Koeppe R, Mintun M, Chen K, et al. Measurement of longitudinal beta-amyloid change with 18F-florbetapir PET and standardized uptake value ratios. Journal of nuclear medicine : official publication, Society of Nuclear Medicine. 2015;56(4):567-74.

Landau SM, Mintun MA, Joshi AD, Koeppe RA, Petersen RC, Aisen PS, et al. Amyloid deposition, hypometabolism, and longitudinal cognitive decline. Annals of neurology. 2012;72(4):578-86.

Lattal KM, Wood MA. Epigenetics and persistent memory: implications for reconsolidation and silent extinction beyond the zero. Nature neuroscience. 2013;16(2):124-9.

Lee DS, Kang H, Kim H, Park H, Oh JS, Lee JS, et al. Metabolic connectivity by interregional correlation analysis using statistical parametric mapping (SPM) and FDG brain PET; methodological development and patterns of metabolic connectivity in adults. Eur J Nucl Med Mol Imaging. 2008;35(9):1681-91.

Lee S, Viqar F, Zimmerman ME, Narkhede A, Tosto G, Benzinger TL, et al. White matter hyperintensities are a core feature of Alzheimer's disease: Evidence from the dominantly inherited Alzheimer network. Annals of neurology. 2016;79(6):929-39.

Leenders KL, Perani D, Lammertsma AA, Heather JD, Buckingham P, Healy MJ, et al. Cerebral blood flow, blood volume and oxygen utilization. Normal values and effect of age. Brain : a journal of neurology. 1990;113 (Pt 1):27-47.

Leon WC, Canneva F, Partridge V, Allard S, Ferretti MT, DeWilde A, et al. A novel transgenic rat model with a full Alzheimer's-like amyloid pathology displays pre-plaque intracellular amyloid-beta-associated cognitive impairment. Journal of Alzheimer's disease : JAD. 2010;20(1):113-26.

Lesne SE, Sherman MA, Grant M, Kuskowski M, Schneider JA, Bennett DA, et al. Brain amyloid-beta oligomers in ageing and Alzheimer's disease. Brain : a journal of neurology. 2013;136(Pt 5):1383-98.

Leung KK, Clarkson MJ, Bartlett JW, Clegg S, Jack CR, Jr., Weiner MW, et al. Robust atrophy rate measurement in Alzheimer's disease using multi-site serial MRI: tissue-specific intensity normalization and parameter selection. NeuroImage. 2010;50(2):516-23.

Leuzy A, Carter SF, Chiotis K, Almkvist O, Wall A, Nordberg A. Concordance and Diagnostic Accuracy of [11C]PIB PET and Cerebrospinal Fluid Biomarkers in a Sample of Patients with Mild Cognitive Impairment and Alzheimer's Disease. Journal of Alzheimer's disease : JAD. 2015;45(4):1077-88.

Levenson JM, Sweatt JD. Epigenetic mechanisms in memory formation. Nat Rev Neurosci. 2005;6(2):108-18.

Li J, Wang YJ, Zhang M, Xu ZQ, Gao CY, Fang CQ, et al. Vascular risk factors promote conversion from mild cognitive impairment to Alzheimer disease. Neurology. 2011;76(17):1485-91.

Li Y, Rinne JO, Mosconi L, Pirraglia E, Rusinek H, DeSanti S, et al. Regional analysis of FDG and PIB-PET images in normal aging, mild cognitive impairment, and Alzheimer's disease. European journal of nuclear medicine and molecular imaging. 2008;35(12):2169-81.

Liu F, Gong CX. Tau exon 10 alternative splicing and tauopathies. Mol Neurodegener. 2008;3:8.

Logan J, Fowler JS, Volkow ND, Wang GJ, Ding YS, Alexoff DL. Distribution volume ratios without blood sampling from graphical analysis of PET data. Journal of cerebral blood flow and metabolism : official journal of the International Society of Cerebral Blood Flow and Metabolism. 1996;16(5):834-40.

Logan J, Fowler JS, Volkow ND, Wolf AP, Dewey SL, Schlyer DJ, et al. Graphical analysis of reversible radioligand binding from time-activity measurements applied to [N-11C-methyl]-(-)-cocaine PET studies in human subjects. Journal of cerebral blood flow and metabolism : official journal of the International Society of Cerebral Blood Flow and Metabolism. 1990;10(5):740-7.

Lopez-Atalaya JP, Barco A. Can changes in histone acetylation contribute to memory formation? Trends Genet. 2014;30(12):529-39.

Lowe VJ, Weigand SD, Senjem ML, Vemuri P, Jordan L, Kantarci K, et al. Association of hypometabolism and amyloid levels in aging, normal subjects. Neurology. 2014;82(22):1959-67.

Lu H, Zou Q, Gu H, Raichle ME, Stein EA, Yang Y. Rat brains also have a default mode network. Proceedings of the National Academy of Sciences of the United States of America. 2012;109(10):3979-84.

Lubin FD, Sweatt JD. The IkappaB kinase regulates chromatin structure during reconsolidation of conditioned fear memories. Neuron. 2007;55(6):942-57.

MacCallum RC, Austin JT. Applications of structural equation modeling in psychological research. Annu Rev Psychol. 2000;51:201-26.

Maddox SA, Schafe GE. Epigenetic alterations in the lateral amygdala are required for reconsolidation of a Pavlovian fear memory. Learn Mem. 2011;18(9):579-93.

Mahady L, Nadeem M, Malek-Ahmadi M, Chen K, Perez SE, Mufson EJ. Frontal Cortex Epigenetic Dysregulation During the Progression of Alzheimer's Disease. Journal of Alzheimer's disease : JAD. 2018;62(1):115-31.

Mahan AL, Mou L, Shah N, Hu JH, Worley PF, Ressler KJ. Epigenetic modulation of Homer1a transcription regulation in amygdala and hippocampus with pavlovian fear conditioning. The Journal of neuroscience : the official journal of the Society for Neuroscience. 2012;32(13):4651-9.

Malvaez M, McQuown SC, Rogge GA, Astarabadi M, Jacques V, Carreiro S, et al. HDAC3-selective inhibitor enhances extinction of cocaine-seeking behavior in a persistent manner. Proceedings of the National Academy of Sciences of the United States of America. 2013;110(7):2647-52.

Manczak M, Reddy PH. Abnormal interaction of oligomeric amyloid-beta with phosphorylated tau: implications to synaptic dysfunction and neuronal damage. Journal of Alzheimer's disease : JAD. 2013;36(2):285-95.

Mandrekar S, Jiang Q, Lee CY, Koenigsknecht-Talboo J, Holtzman DM, Landreth GE. Microglia mediate the clearance of soluble Abeta through fluid phase macropinocytosis. The Journal of neuroscience : the official journal of the Society for Neuroscience. 2009;29(13):4252-62.

Masters CL, Bateman R, Blennow K, Rowe CC, Sperling RA, Cummings JL. Alzheimer's disease. Nat Rev Dis Primers. 2015;1:15056.

Masters CL, Cappai R, Barnham KJ, Villemagne VL. Molecular mechanisms for Alzheimer's disease: implications for neuroimaging and therapeutics. Journal of neurochemistry. 2006;97(6):1700-25.

Mathotaarachchi S, Wang S, Shin M, Pascoal TA, Benedet AL, Kang MS, et al. VoxelStats: A MATLAB package for multi-modal voxel-wise brain image analysis. Frontiers in Neuroinformatics. 2016;10.

Mathotaarachchi S, Wang S, Shin M, Pascoal TA, Benedet AL, Kang MS, et al. VoxelStats: A MATLAB Package for Multi-Modal Voxel-Wise Brain Image Analysis. Front Neuroinform. 2016;10:20.

Mattson MP, Magnus T. Ageing and neuronal vulnerability. Nat Rev Neurosci. 2006;7(4):278-94.

Mattsson N, Insel PS, Donohue M, Landau S, Jagust WJ, Shaw LM, et al. Independent information from cerebrospinal fluid amyloid-beta and florbetapir imaging in Alzheimer's disease. Brain : a journal of neurology. 2015;138(Pt 3):772-83.

Maurer K, Volk S, Gerbaldo H. Auguste D and Alzheimer's disease. Lancet. 1997;349(9064):1546-9.

Mazziotta J, Toga A, Evans A, Fox P, Lancaster J, Zilles K, et al. A probabilistic atlas and reference system for the human brain: International Consortium for Brain Mapping (ICBM). Philos Trans R Soc Lond B Biol Sci. 2001;356(1412):1293-322.

Mazziotta JC, Toga AW, Evans A, Fox P, Lancaster J. A probabilistic atlas of the human brain: theory and rationale for its development. The International Consortium for Brain Mapping (ICBM). NeuroImage. 1995;2(2):89-101.

McKhann G, Drachman D, Folstein M, Katzman R, Price D, Stadlan EM. Clinical diagnosis of Alzheimer's disease Report of the NINCDS‐ADRDA Work Group* under the auspices of Department of Health and Human Services Task Force on Alzheimer's Disease. Neurology. 1984;34(7):939-.

McKhann G, Drachman D, Folstein M, Katzman R, Price D, Stadlan EM. Clinical diagnosis of Alzheimer's disease: report of the NINCDS-ADRDA Work Group under the auspices of Department of Health and Human Services Task Force on Alzheimer's Disease. Neurology. 1984;34(7):939-44.

McKhann GM, Knopman DS, Chertkow H, Hyman BT, Jack CR, Jr., Kawas CH, et al. The diagnosis of dementia due to Alzheimer's disease: recommendations from the National Institute on Aging-Alzheimer's Association workgroups on diagnostic guidelines for Alzheimer's disease. Alzheimer's & dementia : the journal of the Alzheimer's Association. 2011;7(3):263-9.

Meguro K, Blaizot X, Kondoh Y, Le Mestric C, Baron J, Chavoix C. Neocortical and hippocampal glucose hypometabolism following neurotoxic lesions of the entorhinal and perirhinal cortices in the non-human primate as shown by PET. Brain : a journal of neurology. 1999;122(8):1519-31.

Mesulam MM. Neuroplasticity failure in Alzheimer's disease: bridging the gap between plaques and tangles. Neuron. 1999;24(3):521-9.

Miller Y, Ma B, Nussinov R. Synergistic interactions between repeats in tau protein and Abeta amyloids may be responsible for accelerated aggregation via polymorphic states. Biochemistry. 2011;50(23):5172-81.

Mirra SS, Heyman A, McKeel D, Sumi SM, Crain BJ, Brownlee LM, et al. The Consortium to Establish a Registry for Alzheimer's Disease (CERAD). Part II. Standardization of the neuropathologic assessment of Alzheimer's disease. Neurology. 1991;41(4):479-86.

Moeller JR, Ishikawa T, Dhawan V, Spetsieris P, Mandel F, Alexander GE, et al. The metabolic topography of normal aging. Journal of cerebral blood flow and metabolism : official journal of the International Society of Cerebral Blood Flow and Metabolism. 1996;16(3):385-98.

Montgomery RL, Hsieh J, Barbosa AC, Richardson JA, Olson EN. Histone deacetylases 1 and 2 control the progression of neural precursors to neurons during brain development. Proceedings of the National Academy of Sciences of the United States of America. 2009;106(19):7876-81.

Morbelli S, Bauckneht M, Arnaldi D, Picco A, Pardini M, Brugnolo A, et al. 18F-FDG PET diagnostic and prognostic patterns do not overlap in Alzheimer's disease (AD) patients at the mild cognitive impairment (MCI) stage. European journal of nuclear medicine and molecular imaging. 2017.

Mormino EC, Betensky RA, Hedden T, Schultz AP, Amariglio RE, Rentz DM, et al. Synergistic effect of beta-amyloid and neurodegeneration on cognitive decline in clinically normal individuals. JAMA neurology. 2014;71(11):1379-85.

Morris JC, Price JL. Pathologic correlates of nondemented aging, mild cognitive impairment, and early-stage Alzheimer's disease. Journal of molecular neuroscience : MN. 2001;17(2):101-18.

Morris R. Developments of a water-maze procedure for studying spatial learning in the rat. J Neurosci Methods. 1984;11(1):47-60.

Mosconi L. Glucose metabolism in normal aging and Alzheimer's disease: Methodological and physiological considerations for PET studies. Clin Transl Imaging. 2013;1(4).

Mosconi L, Mistur R, Switalski R, Brys M, Glodzik L, Rich K, et al. Declining brain glucose metabolism in normal individuals with a maternal history of Alzheimer disease. Neurology. 2009;72(6):513-20.

Motter R, Vigo-Pelfrey C, Kholodenko D, Barbour R, Johnson-Wood K, Galasko D, et al. Reduction of beta-amyloid peptide42 in the cerebrospinal fluid of patients with Alzheimer's disease. Annals of neurology. 1995;38(4):643-8.

Mullan M, Crawford F, Axelman K, Houlden H, Lilius L, Winblad B, et al. A pathogenic mutation for probable Alzheimer's disease in the APP gene at the N-terminus of beta-amyloid. Nat Genet. 1992;1(5):345-7.

Munoz-Moreno E, Tudela R, Lopez-Gil X, Soria G. Early brain connectivity alterations and cognitive impairment in a rat model of Alzheimer's disease. Alzheimer's research & therapy. 2018;10(1):16.

Murrell J, Farlow M, Ghetti B, Benson MD. A mutation in the amyloid precursor protein associated with hereditary Alzheimer's disease. Science. 1991;254(5028):97-9.

Nagasawa H, Kogure K, Fujiwara T, Itoh M, Ido T. Metabolic disturbances in exo-focal brain areas after cortical stroke studied by positron emission tomography. Journal of the neurological sciences. 1994;123(1):147-53.

Nativio R, Donahue G, Berson A, Lan Y, Amlie-Wolf A, Tuzer F, et al. Dysregulation of the epigenetic landscape of normal aging in Alzheimer's disease. Nature neuroscience. 2018.

Nelissen N, Van Laere K, Thurfjell L, Owenius R, Vandenbulcke M, Koole M, et al. Phase 1 study of the Pittsburgh compound B derivative 18F-flutemetamol in healthy volunteers and patients with probable Alzheimer disease. Journal of nuclear medicine : official publication, Society of Nuclear Medicine. 2009;50(8):1251-9.

Nelson PT, Schmitt FA, Lin Y, Abner EL, Jicha GA, Patel E, et al. Hippocampal sclerosis in advanced age: clinical and pathological features. Brain : a journal of neurology. 2011;134(Pt 5):1506-18.

Newberg AB, Arnold SE, Wintering N, Rovner BW, Alavi A. Initial clinical comparison of 18F-florbetapir and 18F-FDG PET in patients with Alzheimer disease and controls. Journal of nuclear medicine : official publication, Society of Nuclear Medicine. 2012;53(6):902-7.

Ng KP, Pascoal TA, Mathotaarachchi S, Therriault J, Kang MS, Shin M, et al. Monoamine oxidase B inhibitor, selegiline, reduces 18F-THK5351 uptake in the human brain. Alzheimer's research & therapy. 2017;9(1):25.

Nguyen HL, Thi Minh Thu T, Truong PM, Lan PD, Man VH, Nguyen PH, et al. Abeta41 Aggregates More Like Abeta40 than Like Abeta42: In Silico and in Vitro Study. J Phys Chem B. 2016;120(30):7371-9.

Okello A, Koivunen J, Edison P, Archer HA, Turkheimer FE, Nagren K, et al. Conversion of amyloid positive and negative MCI to AD over 3 years: an 11C-PIB PET study. Neurology. 2009;73(10):754-60.

Olson MI, Shaw C-M. PRESENILE DEMENTIA AND ALZHEIMER'S DISEASE IN MONGOLISM1. Brain : a journal of neurology. 1969;92(1):147-56.

Olsson A, Vanderstichele H, Andreasen N, De Meyer G, Wallin A, Holmberg B, et al. Simultaneous measurement of beta-amyloid(1-42), total tau, and phosphorylated tau (Thr181) in cerebrospinal fluid by the xMAP technology. Clinical chemistry. 2005;51(2):336-45.

Olsson H, Farde L. Potentials and pitfalls using high affinity radioligands in PET and SPET determinations on regional drug induced D2 receptor occupancy--a simulation study based on experimental data. NeuroImage. 2001;14(4):936-45.

Oppelt A, Graumann R, Barfuss H, Fischer H, Hartl W, Schajor W. FISP—a new fast MRI sequence. Electromedica. 1986;54(1):15-8.

Organization WH. Dementia: a public health priority: World Health Organization; 2012.

Ossenkoppele R, Schonhaut DR, Baker SL, O'Neil JP, Janabi M, Ghosh PM, et al. Tau, amyloid, and hypometabolism in a patient with posterior cortical atrophy. Annals of neurology. 2015;77(2):338-42.

Ossenkoppele R, Tolboom N, Foster-Dingley JC, Adriaanse SF, Boellaard R, Yaqub M, et al. Longitudinal imaging of Alzheimer pathology using [11C]PIB, [18F]FDDNP and [18F]FDG PET. European journal of nuclear medicine and molecular imaging. 2012;39(6):990-1000.

Ossenkoppele R, van der Flier WM, Verfaillie SC, Vrenken H, Versteeg A, van Schijndel RA, et al. Long-term effects of amyloid, hypometabolism, and atrophy on neuropsychological functions. Neurology. 2014;82(20):1768-75.

Parent MJ, Bedard MA, Aliaga A, Minuzzi L, Mechawar N, Soucy JP, et al. Cholinergic Depletion in Alzheimer's Disease Shown by [(18) F]FEOBV Autoradiography. Int J Mol Imaging. 2013;2013:205045.

Parent MJ, Zimmer ER, Shin M, Kang MS, Fonov VS, Mathieu A, et al. Multimodal Imaging in Rat Model Recapitulates Alzheimer's Disease Biomarkers Abnormalities. The Journal of neuroscience : the official journal of the Society for Neuroscience. 2017;37(50):12263-71.

Pascoal TA, Mathotaarachchi S, Mohades S, Benedet AL, Chung CO, Shin M, et al. Amyloid-beta and hyperphosphorylated tau synergy drives metabolic decline in preclinical Alzheimer's disease. Mol Psychiatry. 2016.

Pascoal TA, Mathotaarachchi S, Mohades S, Benedet AL, Chung CO, Shin M, et al. Amyloid-beta and hyperphosphorylated tau synergy drives metabolic decline in preclinical Alzheimer's disease. Mol Psychiatry. 2017;22(2):306-11.

Pascoal TA, Mathotaarachchi S, Shin M, Benedet AL, Mohades S, Wang S, et al. Synergistic interaction between amyloid and tau predicts the progression to dementia. Alzheimer's & dementia : the journal of the Alzheimer's Association. 2016.

Pascoal TA, Mathotaarachchi S, Shin M, Benedet AL, Mohades S, Wang S, et al. Synergistic interaction between amyloid and tau predicts the progression to dementia. Alzheimer's & dementia : the journal of the Alzheimer's Association. 2017;13(6):644-53.

Pascoal TA, Mathotaarachchi S, Shin M, Park AY, Mohades S, Benedet AL, et al. Amyloid and tau signatures of brain metabolic decline in preclinical Alzheimer's disease. European journal of nuclear medicine and molecular imaging. 2018;45(6):1021-30.

Pascoal TA, Shin M, Kang MS, Chamoun M, Chartrand D, Mathotaarachchi S, et al. In vivo quantification of neurofibrillary tangles with [(18)F]MK-6240. Alzheimer's research & therapy. 2018;10(1):74.

Passow S, Specht K, Adamsen TC, Biermann M, Brekke N, Craven AR, et al. Default‐mode network functional connectivity is closely related to metabolic activity. Human brain mapping. 2015;36(6):2027-38.

Peleg S, Sananbenesi F, Zovoilis A, Burkhardt S, Bahari-Javan S, Agis-Balboa RC, et al. Altered histone acetylation is associated with age-dependent memory impairment in mice. Science. 2010;328(5979):753-6.

Perusini GJHuHAJVGF. Über klinisch und histologisch eigenartige psychische Erkrankungen des späteren Lebensalters. 1909:297-351.

Petersen RC. Mild cognitive impairment: Aging to Alzheimer's disease: Oxford University Press; 2003.

Petersen RC, Aisen P, Boeve BF, Geda YE, Ivnik RJ, Knopman DS, et al. Mild cognitive impairment due to Alzheimer disease in the community. Annals of neurology. 2013;74(2):199-208.

Petersen RC, Parisi JE, Dickson DW, Johnson KA, Knopman DS, Boeve BF, et al. Neuropathologic features of amnestic mild cognitive impairment. Arch Neurol. 2006;63(5):665-72.

Price JC, Klunk WE, Lopresti BJ, Lu X, Hoge JA, Ziolko SK, et al. Kinetic modeling of amyloid binding in humans using PET imaging and Pittsburgh Compound-B. Journal of cerebral blood flow and metabolism : official journal of the International Society of Cerebral Blood Flow and Metabolism. 2005;25(11):1528-47.

Prince MJ, Comas-Herrera A, Knapp M, Guerchet MM, Karagiannidou M. World Alzheimer Report 2016 - Improving healthcare for people living with dementia: Coverage, quality and costs now and in the future. London: Alzheimer's Disease International; 2016.

Quan H, Shih WJ. Assessing reproducibility by the within-subject coefficient of variation with random effects models. Biometrics. 1996;52(4):1195-203.

Quintanilla RA, von Bernhardi R, Godoy JA, Inestrosa NC, Johnson GV. Phosphorylated tau potentiates Abeta-induced mitochondrial damage in mature neurons. Neurobiology of disease. 2014;71:260-9.

Rabinovici GD, Furst AJ, Alkalay A, Racine CA, O'Neil JP, Janabi M, et al. Increased metabolic vulnerability in early-onset Alzheimer's disease is not related to amyloid burden. Brain : a journal of neurology. 2010;133(Pt 2):512-28.

Raichle ME, Mintun MA. BRAIN WORK AND BRAIN IMAGING. Annu Rev Neurosci. 2006;29(1):449-76.

Reddy PH, Mani G, Park BS, Jacques J, Murdoch G, Whetsell W, Jr., et al. Differential loss of synaptic proteins in Alzheimer's disease: implications for synaptic dysfunction. Journal of Alzheimer's disease : JAD. 2005;7(2):103-17; discussion 73-80.

Rhein V, Song X, Wiesner A, Ittner LM, Baysang G, Meier F, et al. Amyloid-beta and tau synergistically impair the oxidative phosphorylation system in triple transgenic Alzheimer's disease mice. Proceedings of the National Academy of Sciences of the United States of America. 2009;106(47):20057-62.

Riedl V, Utz L, Castrillon G, Grimmer T, Rauschecker JP, Ploner M, et al. Metabolic connectivity mapping reveals effective connectivity in the resting human brain. Proceedings of the National Academy of Sciences of the United States of America. 2016;113(2):428-33.

Riley KP, Snowdon DA, Desrosiers MF, Markesbery WR. Early life linguistic ability, late life cognitive function, and neuropathology: findings from the Nun Study. Neurobiol Aging. 2005;26(3):341-7.

Roberson ED, Scearce-Levie K, Palop JJ, Yan F, Cheng IH, Wu T, et al. Reducing endogenous tau ameliorates amyloid beta-induced deficits in an Alzheimer's disease mouse model. Science. 2007;316(5825):750-4.

Roe CM, Fagan AM, Grant EA, Hassenstab J, Moulder KL, Maue Dreyfus D, et al. Amyloid imaging and CSF biomarkers in predicting cognitive impairment up to 7.5 years later. Neurology. 2013;80(19):1784-91.

Rowe CC, Pejoska S, Mulligan RS, Jones G, Chan JG, Svensson S, et al. Head-to-head comparison of 11C-PiB and 18F-AZD4694 (NAV4694) for beta-amyloid imaging in aging and dementia. Journal of nuclear medicine : official publication, Society of Nuclear Medicine. 2013;54(6):880-6.

Sabri O, Sabbagh MN, Seibyl J, Barthel H, Akatsu H, Ouchi Y, et al. Florbetaben PET imaging to detect amyloid beta plaques in Alzheimer's disease: phase 3 study. Alzheimer's & dementia : the journal of the Alzheimer's Association. 2015;11(8):964-74.

Saint-Aubert L, Lemoine L, Chiotis K, Leuzy A, Rodriguez-Vieitez E, Nordberg A. Tau PET imaging: present and future directions. Mol Neurodegener. 2017;12(1):19.

Sananbenesi F, Fischer A. The epigenetic bottleneck of neurodegenerative and psychiatric diseases. Biol Chem. 2009;390(11):1145-53.

Savas JN, Ribeiro LF, Wierda KD, Wright R, DeNardo-Wilke LA, Rice HC, et al. The Sorting Receptor SorCS1 Regulates Trafficking of Neurexin and AMPA Receptors. Neuron. 2015;87(4):764-80.

Savva GM, Wharton SB, Ince PG, Forster G, Matthews FE, Brayne C, et al. Age, neuropathology, and dementia. N Engl J Med. 2009;360(22):2302-9.

Saykin AJ, Shen L, Yao X, Kim S, Nho K, Risacher SL, et al. Genetic studies of quantitative MCI and AD phenotypes in ADNI: Progress, opportunities, and plans. Alzheimer's & dementia : the journal of the Alzheimer's Association. 2015;11(7):792-814.

Scahill RI, Schott JM, Stevens JM, Rossor MN, Fox NC. Mapping the evolution of regional atrophy in Alzheimer's disease: unbiased analysis of fluid-registered serial MRI. Proceedings of the National Academy of Sciences of the United States of America. 2002;99(7):4703-7.

Schermelleh-Engel K, Moosbrugger H, Müller H. Evaluating the Fit of Structural Equation Models: Tests of Significance and Descriptive Goodness-of-Fit Measures; 2003.

Schilling S, DeStefano AL, Sachdev PS, Choi SH, Mather KA, DeCarli CD, et al. APOE genotype and MRI markers of cerebrovascular disease: systematic review and meta-analysis. Neurology. 2013;81(3):292-300.

Schmitt FA, Davis DG, Wekstein DR, Smith CD, Ashford JW, Markesbery WR. "Preclinical" AD revisited: neuropathology of cognitively normal older adults. Neurology. 2000;55(3):370-6.

Schreiber S, Landau SM, Fero A, Schreiber F, Jagust WJ, Alzheimer's Disease Neuroimaging I. Comparison of Visual and Quantitative Florbetapir F 18 Positron Emission Tomography Analysis in Predicting Mild Cognitive Impairment Outcomes. JAMA neurology. 2015.

Schroeter ML, Stein T, Maslowski N, Neumann J. Neural correlates of Alzheimer's disease and mild cognitive impairment: a systematic and quantitative meta-analysis involving 1351 patients. NeuroImage. 2009;47(4):1196-206.

Schwarz AJ, Yu P, Miller BB, Shcherbinin S, Dickson J, Navitsky M, et al. Regional profiles of the candidate tau PET ligand 18F-AV-1451 recapitulate key features of Braak histopathological stages. Brain : a journal of neurology. 2016;139(Pt 5):1539-50.

Seeley WW, Crawford RK, Zhou J, Miller BL, Greicius MD. Neurodegenerative diseases target large-scale human brain networks. Neuron. 2009;62(1):42-52.

Selkoe DJ. The molecular pathology of Alzheimer's disease. Neuron. 1991;6(4):487-98.

Selkoe DJ. Defining molecular targets to prevent Alzheimer disease. Archives of neurology. 2005;62(2):192-5.

Sevigny J, Chiao P, Bussiere T, Weinreb PH, Williams L, Maier M, et al. The antibody aducanumab reduces Abeta plaques in Alzheimer's disease. Nature. 2016;537(7618):50-6.

Shaw LM, Vanderstichele H, Knapik-Czajka M, Clark CM, Aisen PS, Petersen RC, et al. Cerebrospinal fluid biomarker signature in Alzheimer's disease neuroimaging initiative subjects. Annals of neurology. 2009;65(4):403-13.

Shimizu S, Hirose D, Hatanaka H, Takenoshita N, Kaneko Y, Ogawa Y, et al. Role of Neuroimaging as a Biomarker for Neurodegenerative Diseases. Front Neurol. 2018;9:265.

Shipton OA, Leitz JR, Dworzak J, Acton CE, Tunbridge EM, Denk F, et al. Tau protein is required for amyloid {beta}-induced impairment of hippocampal long-term potentiation. The

Journal of neuroscience : the official journal of the Society for Neuroscience. 2011;31(5):1688-92.

Skillback T, Farahmand BY, Rosen C, Mattsson N, Nagga K, Kilander L, et al. Cerebrospinal fluid tau and amyloid-beta1-42 in patients with dementia. Brain : a journal of neurology. 2015;138(Pt 9):2716-31.

Slinker BK. The statistics of synergism. J Mol Cell Cardiol. 1998;30(4):723-31.

Small SA, Duff K. Linking Abeta and tau in late-onset Alzheimer's disease: a dual pathway hypothesis. Neuron. 2008;60(4):534-42.

Snowdon DA, Kemper SJ, Mortimer JA, Greiner LH, Wekstein DR, Markesbery WR. Linguistic ability in early life and cognitive function and Alzheimer's disease in late life. Findings from the Nun Study. JAMA. 1996;275(7):528-32.

Sonnen JA, Santa Cruz K, Hemmy LS, Woltjer R, Leverenz JB, Montine KS, et al. Ecology of the aging human brain. Archives of neurology. 2011;68(8):1049-56.

Sperling R, Mormino E, Johnson K. The evolution of preclinical Alzheimer's disease: implications for prevention trials. Neuron. 2014;84(3):608-22.

Sperling RA, Aisen PS, Beckett LA, Bennett DA, Craft S, Fagan AM, et al. Toward defining the preclinical stages of Alzheimer's disease: recommendations from the National Institute on Aging-Alzheimer's Association workgroups on diagnostic guidelines for Alzheimer's disease. Alzheimer's & dementia : the journal of the Alzheimer's Association. 2011;7(3):280-92.

Sperling RA, Laviolette PS, O'Keefe K, O'Brien J, Rentz DM, Pihlajamaki M, et al. Amyloid deposition is associated with impaired default network function in older persons without dementia. Neuron. 2009;63(2):178-88.

Spix C, Berthold F, Hero B, Michaelis J, Schilling FH. Correction factors for self-selection when evaluating screening programmes. Journal of medical screening. 2015.

Stefanko DP, Barrett RM, Ly AR, Reolon GK, Wood MA. Modulation of long-term memory for object recognition via HDAC inhibition. Proceedings of the National Academy of Sciences of the United States of America. 2009;106(23):9447-52.

Stepanov V, Svedberg M, Jia Z, Krasikova R, Lemoine L, Okamura N, et al. Development of [11C]/[3H]THK-5351 - A potential novel carbon-11 tau imaging PET radioligand. Nucl Med Biol. 2017;46:50-3.

Stern Y. Cognitive reserve in ageing and Alzheimer's disease. The Lancet Neurology. 2012;11(11):1006-12.

Stern Y, Habeck C, Moeller J, Scarmeas N, Anderson KE, Hilton HJ, et al. Brain networks associated with cognitive reserve in healthy young and old adults. Cereb Cortex. 2005;15(4):394-402.

Strozyk D, Blennow K, White LR, Launer LJ. CSF Abeta 42 levels correlate with amyloid-neuropathology in a population-based autopsy study. Neurology. 2003;60(4):652-6.

Swanson L. Brain Maps: Structure of the Rat Brain (2nd edn). Nature. 1992;363:347-50.

Sweatt JD. Behavioural neuroscience: Down memory lane. Nature. 2007;447(7141):151-2.

Tapiola T, Alafuzoff I, Herukka SK, Parkkinen L, Hartikainen P, Soininen H, et al. Cerebrospinal fluid {beta}-amyloid 42 and tau proteins as biomarkers of Alzheimer-type pathologic changes in the brain. Archives of neurology. 2009;66(3):382-9.

Tapiola T, Overmyer M, Lehtovirta M, Helisalmi S, Ramberg J, Alafuzoff I, et al. The level of cerebrospinal fluid tau correlates with neurofibrillary tangles in Alzheimer's disease. Neuroreport. 1997;8(18):3961-3.

Tardif CL, Devenyi GA, Amaral RSC, Pelleieux S, Poirier J, Rosa-Neto P, et al. Regionally specific changes in the hippocampal circuitry accompany progression of cerebrospinal fluid biomarkers in preclinical Alzheimer's disease. Hum Brain Mapp. 2018;39(2):971-84.

Terry RD, Masliah E, Salmon DP, Butters N, DeTeresa R, Hill R, et al. Physical basis of cognitive alterations in Alzheimer's disease: synapse loss is the major correlate of cognitive impairment. Ann Neurol. 1991;30(4):572-80.

Thal DR, Rub U, Orantes M, Braak H. Phases of A beta-deposition in the human brain and its relevance for the development of AD. Neurology. 2002;58(12):1791-800.

Thomas BA, Erlandsson K, Modat M, Thurfjell L, Vandenberghe R, Ourselin S, et al. The importance of appropriate partial volume correction for PET quantification in Alzheimer's disease. European journal of nuclear medicine and molecular imaging. 2011;38(6):1104-19.

Toledo JB, Xie SX, Trojanowski JQ, Shaw LM. Longitudinal change in CSF Tau and Abeta biomarkers for up to 48 months in ADNI. Acta neuropathologica. 2013;126(5):659-70.

Tomaszewski S, Gauthier S, Wimo A, Rosa-Neto P. Combination Therapy of Anti-Tau and Anti-Amyloid Drugs for Disease Modification in Early-stage Alzheimer's Disease: Socio-economic Considerations Modeled on Treatments for Tuberculosis, HIV/AIDS and Breast Cancer. J Prev Alzheimers Dis. 2016;3(3):164-72.

Torosyan N, Mason K, Dahlbom M, Silverman DHS, Alzheimer'sDisease Neuroimaging I. Value of FDG-PET scans of non-demented patients in predicting rates of future cognitive and functional decline. European journal of nuclear medicine and molecular imaging. 2017;44(8):1355-63.

Tosun D, Schuff N, Mathis CA, Jagust W, Weiner MW, Alzheimer's Disease NeuroImaging I. Spatial patterns of brain amyloid-beta burden and atrophy rate associations in mild cognitive impairment. Brain : a journal of neurology. 2011;134(Pt 4):1077-88.

Trojanowski JQ. Tauists, Baptists, Syners, Apostates, and new data. Annals of neurology. 2002;52(3):263-5.

Tsai J, Grutzendler J, Duff K, Gan WB. Fibrillar amyloid deposition leads to local synaptic abnormalities and breakage of neuronal branches. Nature neuroscience. 2004;7(11):1181-3.

Tyan SH, Shih AY, Walsh JJ, Maruyama H, Sarsoza F, Ku L, et al. Amyloid precursor protein (APP) regulates synaptic structure and function. Mol Cell Neurosci. 2012;51(1-2):43-52.

Vanmechelen E, Vanderstichele H, Davidsson P, Van Kerschaver E, Van Der Perre B, Sjogren M, et al. Quantification of tau phosphorylated at threonine 181 in human cerebrospinal fluid: a sandwich ELISA with a synthetic phosphopeptide for standardization. Neuroscience letters. 2000;285(1):49-52.

Verdone L, Agricola E, Caserta M, Di Mauro E. Histone acetylation in gene regulation. Brief Funct Genomic Proteomic. 2006;5(3):209-21.

Villemagne V, Dore V, Mulligan R, Lamb F, Bourgeat P, Salvado O, et al. Evaluation of 18F-PI-2620, a second-generation selective tau tracer for the assessment of Alzheimer’s and non-Alzheimer’s tauopathies. 2018;59(supplement 1):410-.

Villemagne VL, Pike KE, Chetelat G, Ellis KA, Mulligan RS, Bourgeat P, et al. Longitudinal assessment of Abeta and cognition in aging and Alzheimer disease. Annals of neurology. 2011;69(1):181-92.

Villeneuve S, Rabinovici GD, Cohn-Sheehy BI, Madison C, Ayakta N, Ghosh PM, et al. Existing Pittsburgh Compound-B positron emission tomography thresholds are too high: statistical and pathological evaluation. Brain : a journal of neurology. 2015.

Vingtdeux V, Sergeant N, Buee L. Potential contribution of exosomes to the prion-like propagation of lesions in Alzheimer's disease. Front Physiol. 2012;3:229.

Volterra A, Meldolesi J. Astrocytes, from brain glue to communication elements: the revolution continues. Nat Rev Neurosci. 2005;6(8):626-40.

Vos SJ, Xiong C, Visser PJ, Jasielec MS, Hassenstab J, Grant EA, et al. Preclinical Alzheimer's disease and its outcome: a longitudinal cohort study. The Lancet Neurology. 2013;12(10):957-65.

Vossel KA, Xu JC, Fomenko V, Miyamoto T, Suberbielle E, Knox JA, et al. Tau reduction prevents Abeta-induced axonal transport deficits by blocking activation of GSK3beta. The Journal of cell biology. 2015;209(3):419-33.

Vossel KA, Zhang K, Brodbeck J, Daub AC, Sharma P, Finkbeiner S, et al. Tau reduction prevents Abeta-induced defects in axonal transport. Science. 2010;330(6001):198.

Walsh DM, Selkoe DJ. A critical appraisal of the pathogenic protein spread hypothesis of neurodegeneration. Nat Rev Neurosci. 2016;17(4):251-60.

Wang J, Yan K, Wu ZQ, Zheng CY, Xu RX, Chen LH, et al. TDP-43 interaction with the intracellular domain of amyloid precursor protein induces p53-associated apoptosis. Neuroscience letters. 2014;569:131-6.

Wang WY, Pan L, Su SC, Quinn EJ, Sasaki M, Jimenez JC, et al. Interaction of FUS and HDAC1 regulates DNA damage response and repair in neurons. Nature neuroscience. 2013;16(10):1383-91.

Wei W, Liu X, Chen J, Gao S, Lu L, Zhang H, et al. Class I histone deacetylases are major histone decrotonylases: evidence for critical and broad function of histone crotonylation in transcription. Cell Res. 2017;27(7):898-915.

West MJ, Coleman PD, Flood DG, Troncoso JC. Differences in the pattern of hippocampal neuronal loss in normal ageing and Alzheimer's disease. Lancet. 1994;344(8925):769-72.

Wey H-Y, Gilbert TM, Zürcher NR, She A, Bhanot A, Taillon BD, et al. Insights into neuroepigenetics through human histone deacetylase PET imaging. Science Translational Medicine. 2016;8(351):351ra106-351ra106.

Wey H-Y, Wang C, Schroeder FA, Logan J, Price JC, Hooker JM. Kinetic Analysis and Quantification of [11C]Martinostat for in Vivo HDAC Imaging of the Brain. ACS chemical neuroscience. 2015;6(5):708-15.

Wey HY, Gilbert TM, Zurcher NR, She A, Bhanot A, Taillon BD, et al. Insights into neuroepigenetics through human histone deacetylase PET imaging. Sci Transl Med. 2016;8(351):351ra106.

Wilson RS, Leurgans SE, Boyle PA, Schneider JA, Bennett DA. Neurodegenerative basis of age-related cognitive decline. Neurology. 2010;75(12):1070-8.

Wisse LE, Butala N, Das SR, Davatzikos C, Dickerson BC, Vaishnavi SN, et al. Suspected non-AD pathology in mild cognitive impairment. Neurobiology of aging. 2015.

Wong DF, Comley R, Kuwabara H, Rosenberg PB, Resnick SM, Ostrowitzki S, et al. First in-human PET study of 3 novel tau radiopharmaceuticals: [(11)C]RO6924963, [(11)C]RO6931643, and [(18)F]RO6958948. Journal of nuclear medicine : official publication, Society of Nuclear Medicine. 2018.

Wong DF, Rosenberg PB, Zhou Y, Kumar A, Raymont V, Ravert HT, et al. In vivo imaging of amyloid deposition in Alzheimer disease using the radioligand 18F-AV-45 (florbetapir [corrected] F 18). Journal of nuclear medicine : official publication, Society of Nuclear Medicine. 2010;51(6):913-20.

Worsley K. Developments in random field theory. Human brain function. 2003;2:881-6.

Wu Y, Carson RE. Noise reduction in the simplified reference tissue model for neuroreceptor functional imaging. Journal of cerebral blood flow and metabolism : official journal of the International Society of Cerebral Blood Flow and Metabolism. 2002;22(12):1440-52.

Wyss-Coray T. Ageing, neurodegeneration and brain rejuvenation. Nature. 2016;539(7628):180-6.

Xia CF, Arteaga J, Chen G, Gangadharmath U, Gomez LF, Kasi D, et al. [(18)F]T807, a novel tau positron emission tomography imaging agent for Alzheimer's disease. Alzheimer's & dementia : the journal of the Alzheimer's Association. 2013;9(6):666-76.

Xu K, Dai XL, Huang HC, Jiang ZF. Targeting HDACs: a promising therapy for Alzheimer's disease. Oxid Med Cell Longev. 2011;2011:143269.

Yamakawa H, Cheng J, Penney J, Gao F, Rueda R, Wang J, et al. The Transcription Factor Sp3 Cooperates with HDAC2 to Regulate Synaptic Function and Plasticity in Neurons. Cell Rep. 2017;20(6):1319-34.

Yang SS, Zhang R, Wang G, Zhang YF. The development prospection of HDAC inhibitors as a potential therapeutic direction in Alzheimer's disease. Transl Neurodegener. 2017;6:19.

Yaqub M, Tolboom N, Boellaard R, van Berckel BN, van Tilburg EW, Luurtsema G, et al. Simplified parametric methods for [11C]PIB studies. NeuroImage. 2008;42(1):76-86.

Yarchoan M, Xie SX, Kling MA, Toledo JB, Wolk DA, Lee EB, et al. Cerebrovascular atherosclerosis correlates with Alzheimer pathology in neurodegenerative dementias. Brain : a journal of neurology. 2012;135(Pt 12):3749-56.

Yeo BT, Krienen FM, Sepulcre J, Sabuncu MR, Lashkari D, Hollinshead M, et al. The organization of the human cerebral cortex estimated by intrinsic functional connectivity. J Neurophysiol. 2011;106(3):1125-65.

Zhang ZY, Schluesener HJ. Oral administration of histone deacetylase inhibitor MS-275 ameliorates neuroinflammation and cerebral amyloidosis and improves behavior in a mouse model. Journal of neuropathology and experimental neurology. 2013;72(3):178-85.

Zhou Y, Sojkova J, Resnick SM, Wong DF. Relative equilibrium plot improves graphical analysis and allows bias correction of standardized uptake value ratio in quantitative 11C-PiB PET studies. Journal of nuclear medicine : official publication, Society of Nuclear Medicine. 2012;53(4):622-8.

Zhu X, Wang S, Yu L, Jin J, Ye X, Liu Y, et al. HDAC3 negatively regulates spatial memory in a mouse model of Alzheimer's disease. Aging Cell. 2017;16(5):1073-82.

Zijdenbos AP, Forghani R, Evans AC. Automatic "pipeline" analysis of 3-D MRI data for clinical trials: application to multiple sclerosis. IEEE Trans Med Imaging. 2002;21(10):1280-91.

Zimmer ER, Parent MJ, Cuello AC, Gauthier S, Rosa-Neto P. MicroPET imaging and transgenic models: a blueprint for Alzheimer's disease clinical research. Trends Neurosci. 2014;37(11):629-41.

Zimmer ER, Parent MJ, Souza DG, Leuzy A, Lecrux C, Kim HI, et al. [18F]FDG PET signal is driven by astroglial glutamate transport. Nature neuroscience. 2017.